frontiers | Research Topics

Vegetation resilience in ecological autocatalysis under climate change

Edited by
Virgil Alexandru Iordache and Samuel Kuria Kiboi

Published in
Frontiers in Plant Science

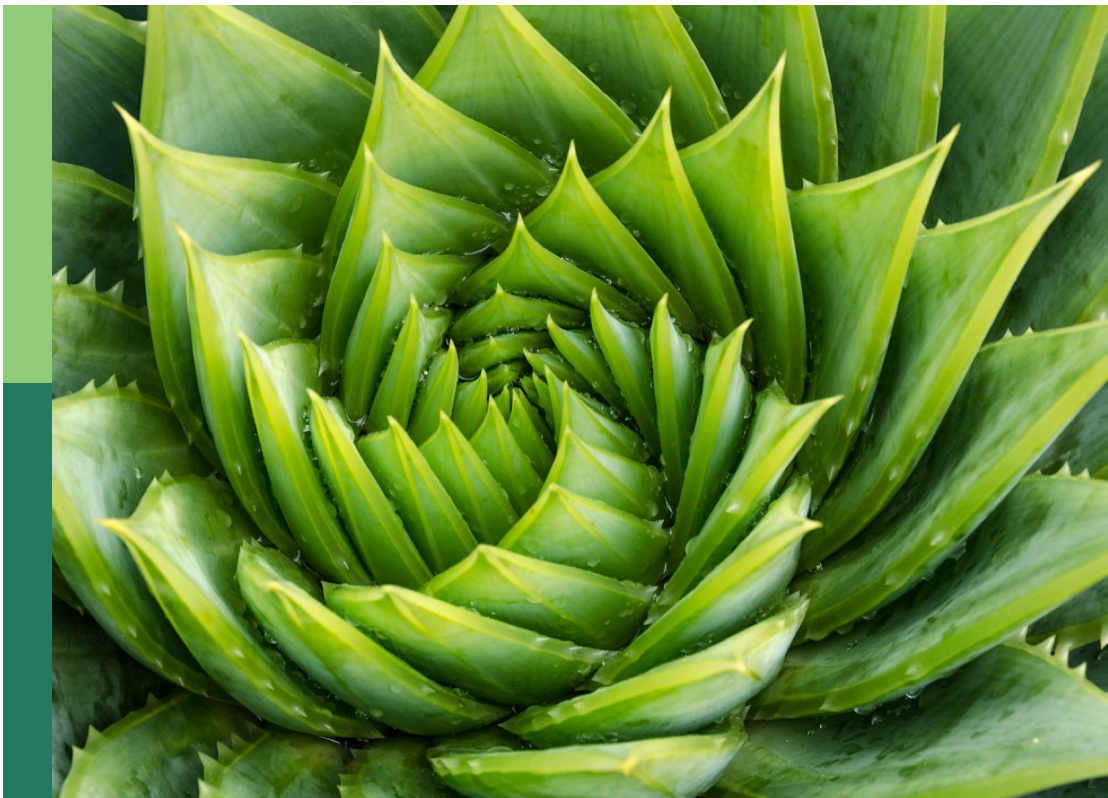

ISSN 1664-8714
ISBN 978-2-8325-7468-3
DOI 10.3389/978-2-8325-7468-3

Generative AI statement
Any alternative text (Alt text) provided alongside figures in the articles in this ebook has been generated by Frontiers with the support of artificial intelligence and reasonable efforts have been made to ensure accuracy, including review by the authors wherever possible. If you identify any issues, please contact us.

About Frontiers

Frontiers is more than just an open access publisher of scholarly articles: it is a pioneering approach to the world of academia, radically improving the way scholarly research is managed. The grand vision of Frontiers is a world where all people have an equal opportunity to seek, share and generate knowledge. Frontiers provides immediate and permanent online open access to all its publications, but this alone is not enough to realize our grand goals.

Frontiers journal series

The Frontiers journal series is a multi-tier and interdisciplinary set of open-access, online journals, promising a paradigm shift from the current review, selection and dissemination processes in academic publishing. All Frontiers journals are driven by researchers for researchers; therefore, they constitute a service to the scholarly community. At the same time, the *Frontiers journal series* operates on a revolutionary invention, the tiered publishing system, initially addressing specific communities of scholars, and gradually climbing up to broader public understanding, thus serving the interests of the lay society, too.

Dedication to quality

Each Frontiers article is a landmark of the highest quality, thanks to genuinely collaborative interactions between authors and review editors, who include some of the world's best academicians. Research must be certified by peers before entering a stream of knowledge that may eventually reach the public - and shape society; therefore, Frontiers only applies the most rigorous and unbiased reviews. Frontiers revolutionizes research publishing by freely delivering the most outstanding research, evaluated with no bias from both the academic and social point of view. By applying the most advanced information technologies, Frontiers is catapulting scholarly publishing into a new generation.

What are Frontiers Research Topics?

Frontiers Research Topics are very popular trademarks of the *Frontiers journals series*: they are collections of at least ten articles, all centered on a particular subject. With their unique mix of varied contributions from Original Research to Review Articles, Frontiers Research Topics unify the most influential researchers, the latest key findings and historical advances in a hot research area.

Find out more on how to host your own Frontiers Research Topic or contribute to one as an author by contacting the Frontiers editorial office: frontiersin.org/about/contact

Vegetation resilience in ecological autocatalysis under climate change

Topic editors

Virgil Alexandru Iordache — University of Bucharest, Romania

Samuel Kuria Kiboi — University of Nairobi, Kenya

Citation

Iordache, V. A., Kiboi, S. K., eds. (2026). *Vegetation resilience in ecological autocatalysis under climate change*. Lausanne: Frontiers Media SA.

doi: 10.3389/978-2-8325-7468-3

Table of contents

frontiers | Frontiers in Plant Science

TYPE Editorial
PUBLISHED 22 January 2026
DOI 10.3389/fpls.2025.1756384

OPEN ACCESS

EDITED AND REVIEWED BY
Sebastian Leuzinger,
Auckland University of Technology, New Zealand

*CORRESPONDENCE
Virgil Iordache
virgil.iordache@fulbrightmail.org
Samuel Kuria Kiboi
samuel.kiboi@uonbi.ac.ke

RECEIVED 28 November 2025
REVISED 17 December 2025
ACCEPTED 18 December 2025
PUBLISHED 22 January 2026

CITATION
Iordache V and Kiboi SK (2026) Editorial: Vegetation resilience in ecological autocatalysis under climate change. *Front. Plant Sci.* 16:1756384. doi: 10.3389/fpls.2025.1756384

Editorial: Vegetation resilience in ecological autocatalysis under climate change

Virgil Iordache[1]* and Samuel Kuria Kiboi[2]*

[1]Department of Systems Ecology and Sustainability, and "Dan Manoleli" Research Centre for Ecological Services—CESEC, University of Bucharest, Bucharest, Romania, [2]Department of Biology, University of Nairobi, Nairobi, Kenya

KEYWORDS

community resilience, ecological autocatalysis, ecosystem services, plant functional traits, systems ecology, vegetation resilience

Editorial on the Research Topic
Vegetation resilience in ecological autocatalysis under climate change

The concept of chemical autocatalysis was coined by Wilhelm Ostwald in 1980 (Peng, 2020). Its standard current definition refers to a chemical reaction in which one of the reaction's products acts as a catalyst. The concept was incorporated into origin-of-life theories in the 1970s and then was adapted by systems ecology to explain the self-organization and growth of ecosystems. There are three main strategies in this interdisciplinary field of research: 1) attempts to reduce the autocatalytic processes in the broad sense to chemical autocatalysis (the reductionist strategy, typical for those working on evolution and the origin of life); 2) investigating the formal mathematical structures (e.g., autocatalytic attractors) distilled from all types of autocatalytic processes (the structural strategy, typical of theoretical biology and ecology, but also applicable to the economy); and 3) approaching each subfield of life science or economics in terms of its specific networks with positive feedback (the autonomist strategy, such as in this Research Topic). We define ecological autocatalysis as a process by which organisms, populations, or communities self-reinforce through circular interactions with their immediate environment, and ecosystems develop circular interactions in which species promote each other, creating positive feedback loops that sustain the resilience of the productive ecological systems at all scales of complexity.

The topic of "Vegetation Resilience in Ecological Autocatalysis under Climate Change" concerns the roles of the autocatalytic processes depicted in Figure 1 in shaping vegetation resilience through plastic deformation and adaptability at the individual, population, and community levels and the consequences for ecosystem resilience. We use the term resilience to refer to four properties: resistance, elastic deformation, plastic deformation, and adaptability (Iordache and Neagoe, 2023). We split the environment of plant individuals, populations, and communities into two functional parts: the outer environment and the immediate environment as changed by the biological systems of different complexities, equating the latter with the "extended phenotypes *sensu lato*" (Diaz, 2025). We identify the roles of autocatalytic processes in vegetation resilience, as shown in Figure 1. These processes have lower complexity than the usual ecosystem

Property for measuring resilience	Relevant for levels	Involves autocatalysis
resistance (continuation with unchanged identity)	I, P, C	No
elastic deformation (rebound, restoration of reference identity)	I, P, C	No
plastic deformation with or without loss of functions and extension to new ones (extensibility, reconfiguration, state transition, recovery and extension of functions)	I, P, C, E	Yes
adaptability (transformability, evolution with change of identity)	P, C, E	Yes

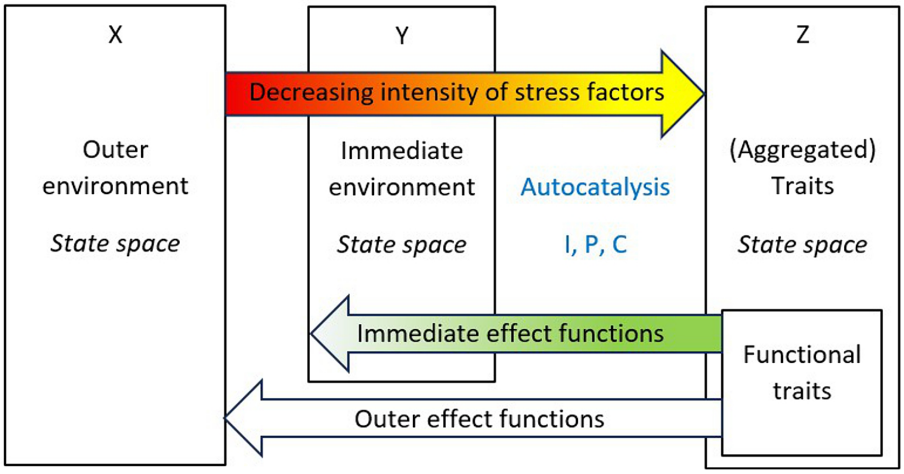

FIGURE 1
Methodological scheme describing autocatalytic processes relevant for vegetation resilience from individual (I) to population (P) to community (C) levels (adapted from Iordache and Neagoe, 2023). In a broad sense, all these autocatalytic processes are involved in ecological resilience; in a narrow sense, ecological resilience refers only to the resilience of ecosystems (E). We used the X, Y, and Z classes of variables to analyze the articles in this topic.

autocatalytic behavior conceptualized as species with specific functional traits or fluxes of energy and elements (Veldhuis et al., 2018; Jordan, 2022).

Three articles in the Research Topic causally link X variables (the outer environment) to Z variables (the trait's state space; Figure 1). Ge et al. examine the interactions among vegetation, surface water, and climate in the Bosten Lake Watershed, NW China, using EEMD to analyze multi-timescale dynamics, revealing significant correlations and the impacts of climate change. Li et al. assessed the effects of climate change on *Hovenia dulcis* habitats in China using the MaxEnt model, identified key environmental variables, and predicted future distribution shifts under different climate scenarios. Sinan et al. investigated the impact of drought on net primary productivity (NPP) in Inner Mongolia, using the CASA model and the SPEI index to analyze spatial and temporal trends and develop drought-loss rate curves. Such studies at regional and macroregional scales lay the groundwork for investigating vegetation resilience.

Two articles approached the same X-Z causation chain and explicitly assessed resilience in terms of resistance and elasticity. One study examined the stability and sensitivity of gross primary productivity (GPP) to climate variability in China from 1982 to 2019 (Xu et al.). The second one explored carbon sink stability in ecological restoration areas in China, driving mechanisms, and future predictions under different climate and human activity scenarios (Xu et al.). This kind of research enables the investigation of autocatalytic processes that support plastic deformation and the adaptability of vegetation.

Three articles used a Y (immediate environment, Figure 1) – Z causation chain. Jin et al. investigated the successional dynamics between alpine meadows and alpine steppes on the Qinghai-Tibet Plateau, focusing on species and functional diversity, community stability, and ecosystem multifunctionality. Ma et al. examined nonstructural carbohydrate allocation in *Spiraea* across Altai Mountain grasslands, highlighting the influence of environmental factors, including temperature, soil water content, and nitrogen, on carbohydrate concentrations and shrub adaptation strategies. Camel et al. investigated the mortality, structure, propagation, and microhabitat of *Haageocereus acranthus* in Peru's coastal lomas, highlighting human impacts, environmental factors, and conservation needs for this endemic cactus species. This kind of research covers the first part of the autocatalytic cycles depicted in Figure 1.

Zhou et al. used the longest causal chain (X to Z to Y) to investigate the effects of warming on leaf light-use efficiency and functional traits in alpine plants through a four-year field experiment, focusing on photosynthesis, leaf traits, and soil nutrients. Xin et al. also examined the effects of Z (independent variables) on Y (immediate environment). They investigated rainfall interception by sand-fixing vegetation and its impact on soil carbon and nitrogen distribution in sand-covered hilly areas, focusing on different vegetation types and their canopy structures. This kind of research covers the second part of the autocatalytic cycles (the immediate effect functions, Figure 1).

At the time of writing this editorial, there were 7830 articles with the terms "vegetation" and "resilience" in their titles, abstracts, or keywords in Web of Science; 207 also included the term "functional traits"; only one article had the terms "vegetation" and "autocatalysis". From 2023, the number of articles published by year increased sharply. An analysis of the citation networks among the 7830 articles using CiteSpace (Chen, 2005-2022) revealed 13 main clusters of literature. Two clusters of literature included the term "vegetation resilience" as a keyword, and one of these also included the term "trait".

To demonstrate the role of vegetation resilience in ecosystem resilience and its consequences for the production of ecosystem services, stronger cooperation between plant and environmental scientists is needed, combining structural and autonomist strategies to address autocatalytic processes. Such cooperation would be facilitated by a general theoretical background covering all autocatalytic processes relevant to resilience, from organisms to ecosystems, and by specific research infrastructures. Systems ecology is well-positioned to be reconceptualized to address this problem (Iordache, 2025), and successful long-term ecological research sites can provide institutional models for interdisciplinary research (Iordache and Groffman 2025). Specific information, such as the role of large organisms (Vasseur et al., 2025) and the modular structure of trait spaces (Carmona and Beccari 2025), allows the formulation of specific, tractable research hypotheses. The geographical coverage of continents with less intensive research is also a priority, as climate change manifests everywhere (Bedair et al., 2023). Plant scientists and botanists can increase collaboration with ecosystem ecologists and environmental and earth system scientists to address the complex challenges of vegetation resilience under climate change stress using plant functional traits.

Author contributions

VI: Writing – original draft, Writing – review & editing. SK: Writing – review & editing.

Funding

The author(s) declared that financial support was received for this work and/or its publication. The initiation of the research topic was supported by CNCS—UEFISCDI, project number PN-III-P4-ID-PCE-2020-0494, within PNCDI III (https://mettelflux.com). The conceptualization and writing of the editorial were supported by the Fulbright Romania Program, grant 867/2024 (https://fulbrightscholars.org/grantee/virgil-alexandru-iordache).

Acknowledgments

We thank Aurora Neagoe for her contribution to formulating the research topic and to David-Cristian Ciobanu for contributing to the innovative definition of ecological autocatalysis. The board of the Society of Ecological Restoration's Large-Scale Ecosystem Restoration provided the framework for the cooperation between the two editors. Sebastian Leuzinger significantly contributed to improving this editorial through constructive criticism.

Conflict of interest

The author(s) declared that this work was conducted in the absence of any commercial or financial relationships that could be construed as a potential conflict of interest.

Generative AI statement

The author(s) declared that generative AI was not used in the creation of this manuscript.

Any alternative text (alt text) provided alongside figures in this article has been generated by Frontiers with the support of artificial intelligence and reasonable efforts have been made to ensure accuracy, including review by the authors wherever possible. If you identify any issues, please contact us.

Publisher's note

References

Bedair, H., Alghariani, M. S., Omar, E., Anibaba, Q. A., Remon, M., Bornman, C., et al. (2023).Global Warming Status in the African Continent: Sources, Challenges, Policies, and Future Direction. *International Journal of Environmental Research*. 17. doi: 10.1007/s41742-023-00534-w

Carmona, C. P., and Beccari, E. (2025).The path toward a unified trait space: synthesizing plant functional diversity. *New Phytol*. 248, 2236–2242. doi: 10.1111/nph.70584).

Chen, C. (2015–2022). *How to use CiteSpace 6.1 R2*. (Leanpub).Available online at: https://leanpub.com/howtousecitespace (Accessed December 01, 2025).

Díaz, S. (2025).Plant functional traits and the entangled phenotype. *Functional Ecology*39, 1144–1159. doi: 10.1111/1365-2435.70017

Iordache, V. (2025).The Likens' problem: a journey in systems ecology. Presenting the Habilitation Thesis "Contributions to the development of theoretical biology and of interdisciplinary directions at the interface between life sciences and earth system science."*Zenodo*. doi: 10.5281/zenodo.14970079

Iordache, V., and Groffman, P. (2025). Increasing the resilience of long-term ecological research.. *2025 Annual Meeting of the Ecological Society of America - Ecology is Everywhere (ESA 2025)*. (Baltimore, Maryland: Zenodo). doi: 10.5281/zenodo.16809834

Iordache, V., and Neagoe, A. (2023). Conceptual methodological framework for the resilience of biogeochemical services to heavy metals stress. *J Environ Manage*. 325:116401. doi: 10.1016/j.jenvman.2022.116401

Jordan, C. F. (2022).*Evolution from a Thermodynamic Perspective: Implications for Species Conservation and Agricultural Sustainability*. (Springer).

Peng, Z., Paschek, K., and Xavier, J. C. (2022). What Wilhelm Ostwald meant by "Autokatalyse" and its significance to origins-of-life research: Facilitating the search for chemical pathways underlying abiogenesis by reviving Ostwald's thought that reactants may also be autocatalysts. *Bioessays* 44, e2200098. doi: 10.1002/bies.202200098

Vasseur, F., Mahaut, L., Enquist, B. J., and Violle, C. (2025). From organism traits to ecosystem processes: why size is so important. *Annu. Rev. Ecol. Evol. Syst.* 56, 145–170. doi: 10.1146/annurev-ecolsys-102723-054525

Veldhuis, M. P., Berg, M. P., Loreau, M., and Olff, H. (2018). Ecological autocatalysis: a central principle in ecosystem organization? *Ecol. Monogr.* 88, 304–319. doi: 10.1002/ecm.1292

frontiers | Frontiers in Plant Science

TYPE Original Research
PUBLISHED 19 March 2024
DOI 10.3389/fpls.2024.1353762

OPEN ACCESS

EDITED BY
Samuel Kuria Kiboi,
University of Nairobi, Kenya

REVIEWED BY
Shalik Ram Sigdel,
Institute of Tibetan Plateau Research, Chinese Academy of Sciences (CAS), China
Jalal Kassout,
National Institute for Agricultural Research, Morocco

*CORRESPONDENCE
Peixi Su
supx@lzb.ac.cn

RECEIVED 11 December 2023
ACCEPTED 27 February 2024
PUBLISHED 19 March 2024

CITATION
Zhou Z, Su P, Yang J, Shi R and Ding X (2024) Warming affects leaf light use efficiency and functional traits in alpine plants: evidence from a 4-year *in-situ* field experiment. *Front. Plant Sci.* 15:1353762. doi: 10.3389/fpls.2024.1353762

Warming affects leaf light use efficiency and functional traits in alpine plants: evidence from a 4-year *in-situ* field experiment

Zijuan Zhou[1], Peixi Su[1]*, Jianping Yang[1], Rui Shi[1] and Xinjing Ding[2]

[1]Key Laboratory of Land Surface Process and Climate Change in Cold and Arid Regions, Northwest Institute of Eco-Environment and Resources, Chinese Academy of Sciences, Lanzhou, China, [2]School of Geography, Liaoning Normal University, Dalian, China

Introduction: Light use efficiency (LUE) is a crucial determinant of plant productivity, while leaf functional traits directly affect ecosystem functions. However, it remains unclear how climate warming affects LUE and leaf functional traits of dominant species in alpine meadows.

Methods: We conducted a 4-year in-situ field warming experiment to investigate the eco-physiological characteristics for a dominant species (*Elymus nutans*) and a common species (*Potentilla anserina*) on the Tibetan Plateau. The leaf traits, photosynthesis and fluorescence characteristics were measured, along with the soil physical-chemical properties associated with the two species.

Results and discussions: Experimental warming increased the leaf LUE, maximum photochemical efficiency, non-photochemical quenching, relative water content and specific leaf area for both species. However, there was a decrease in leaf and soil element content. Different species exhibit varying adaptability to warming. Increasing temperature significantly increased the photosynthetic rate, stomatal conductance, transpiration rate, total water content, and specific leaf volume of *E. nutans*; however, all these traits exhibited an opposite trend in *P. anserina*. Warming has a direct negative impact on leaf LUE and an indirectly enhances LUE through its effects on leaf traits. The impact of warming on plant photosynthetic capacity is primarily mediated by soil nutrients and leaf traits. These results indicate that the two different species employ distinct adaptive strategies in response to climate change, which are related to their species-specific variations. Such changes can confer an adaptive advantage for plant to cope with environmental change and potentially lead to alterations to ecosystem structure and functioning.

KEYWORDS

photosynthesis, leaf traits, soil nutrients, climate change, alpine plants

1 Introduction

The global surface temperature has risen by approximately 1.09°C since the 1850s (Masson-Delmotte et al., 2021). Climate warming is recognized as a significant driver of global change and poses a substantial threat to ecological integrity and function (Hughes et al., 2018). In the alpine ecosystem, the temperature increase has been twice as high as the global average, with a rate of 0.3-0.4°C per decade, and this trend becomes more pronounced with increasing altitude (Fu et al., 2021). Temperature is widely recognized as a major limiting factor in alpine ecosystems, and alpine vegetation exhibits a high sensitivity to temperature (Duan et al., 2019). While warming partially meets the heat requirements of plants, it also alters the micro-climate environment of plant communities, directly or indirectly impacting the photosynthetic physiological processes and consequently influencing plant growth and development (Lee et al., 2020).

Plant physiological processes are extremely sensitive to temperature, and even slight temperature fluctuations leading to significant modifications in these processes (Atkin et al., 2005). Leaf photosynthetic properties can reflect plant responses to environmental changes and play a crucial role in plant growth, thereby impacting the structure and function of ecosystems (Zhang et al., 2022). Recent research indicates that gross primary productivity is affected by photosynthesis, rather than canopy structure (Li et al., 2024). Light use efficiency (LUE) is a crucial indicator of a plant's ability to convert absorbed light energy into chemical energy through photosynthesis (Medlyn, 1998). The strong solar radiation and long-term sunshine in the alpine region are conducive to the photosynthesis and LUE of alpine plants. However, low temperatures, significant temperature variations, short growth periods, and other factors impose limitations on plant growth and photosynthetic capacity. Warming can increase air and soil temperature, leading to a reduction in soil moisture, which in turn affects plant photosynthetic capacity and LUE (Forkel et al., 2016; Allison et al., 2018). Warming also caused a shift in plant functional traits, leading to an increase in acquisitive characteristics such as larger leaves, higher photosynthetic resource-use efficiency, thinner roots, and greater specific root length and nutrient concentrations (Wei et al., 2023). Yao et al. (2023) observed inconsistent responses in the net photosynthetic rate (P_n) of sedge, grass, and shrubs under future climate scenarios. Notably, grass exhibited the least sensitivity to future temperature and CO_2. Some studies have reported generally positive effects of climate change on plant photosynthesis, but there have also been reports of insignificant or even negative effects, which vary depending on the species-specific characteristics (Jassey and Signarbieux, 2019; Meng et al., 2023). However, it remains unclear how plant physiology will change as temperatures rise and how these changes will affect their LUE. To comprehend natural processes and ensure the long-term sustainability of alpine meadow development, it is essential to understand how physiological traits and photosynthetic capacity of alpine plants respond to climate warming.

In order to improve their survival fitness and competitive ability, plants modify their morphological and physiological characteristics in response to environmental changes and interactions with other organisms (Wang et al., 2021). A growing number of studies have demonstrated that leaf traits, such as leaf lifespan, leaf area, and leaf nutrient content, are highly sensitive to climate warming (Buzzard et al., 2019; Bjorkman et al., 2020). In both the alpine meadow and swamp ecosystems, Guittar et al. (2016) proposed that warming led to an increase in specific leaf area (SLA) for two dominant species, *E. nutans* and *C. scabrirostris*. The response of plants to climate change is also reflected in the trade-offs between resource availability and utilization. With increasing temperatures, a significant increase (Bai et al., 2013; Šímová et al., 2017) or decrease (Shen et al., 2022; Storkey and Macdonald, 2022) in leaf nitrogen content was observed. Leaf nitrogen content is consistently positively correlated with plant photosynthetic capacity due to the presence of photosynthetic enzymes and chlorophyll, which constitute a major portion of leaf nitrogen (Fu et al., 2015). The correlations between leaf traits and photosynthetic carbon assimilation are commonly employed for estimating primary production at various scales, ranging from individual leaves to global levels (Feng and Dietze, 2013).

Plant nutrient allocation reflects how plants respond to environmental changes, and the availability of soil nutrients determines the spatial and temporal patterns of leaf traits as well as plant resource utilization (Huang et al., 2021). Previous studies have indicated a close relationship between structural allocation trait (such as leaf area) and the functions of photosynthetic carbon capture, belowground nutrient acquisition, and resource transport (Kleyer et al., 2019). Changes in soil nutrients under climate warming can affect plant photosynthesis and physiological characteristics, which may further influence species composition by altering plant facilitation and competitive exclusion (Xu et al., 2022). According to Yang et al. (2022), experimental warming did not alter the content of soil organic carbon (SOC) during the growing season in an alpine meadow. Wei et al. (2023) demonstrated that plants exhibit consistent adaptive strategies in both above- and belowground traits, favoring more acquisitive traits in warmer environments. These changes could confer an adaptive advantage to plants in response to environmental change. Currently, the trade-offs between plant leaf traits and soil nutrients under climate change remain unclear, as well as the key factors that can have a greater impact on plant LUE.

Alpine meadows, as one of the typical grassland ecosystem types on the Qinghai-Tibetan Plateau (QTP), are highly sensitive to climate change (Immerzeel et al., 2020). A previous study demonstrated that the alpine meadow is becoming increasingly susceptible to the direct impacts of climate extremes, which affect ecosystem function and phenology by altering key traits of plant species (Knapp et al., 2020). The impact of global warming led to alterations in plant growth and soil nutrients in the alpine meadows. Due to low temperatures, significant diurnal temperature fluctuations, and short growth periods experienced by alpine plants, their LUE and productivity are generally very low. Therefore, gaining a better understanding of how alpine plants physiologically respond to environmental changes will greatly enhance predictions for vegetation productivity under climate change. In this study, we conducted warming experiment to investigate the effects of short-term (one year) and medium-term (four-year) warming on two alpine species in the eastern QTP. Our

hypothesis was that warming could induce changes in leaf traits, chlorophyll fluorescence, and soil nutrients, thereby altering the photosynthetic potential (photosynthesis and LUE) of these plants. The specific objectives of our study were to: 1) investigate the differential impacts of short-term and medium-term warming on the physiological performances of two alpine plants; 2) elucidate the key processes that contribute to changes in leaf photosynthetic capacity under warming conditions. This research is essential for enhancing our comprehension of the species-specific differences and the potential adaptation mechanisms employed by alpine plants in response to global warming.

2 Materials and methods

2.1 Study site

The research was carried out at the Zoige Alpine Wetland Ecosystem Research Station (3440 m, 33°51′52″N, 102°08′46″E) in the eastern Tibetan Plateau. The area has a typical plateau continental semi-humid climate with no frost-free period throughout the year. The annual average air temperature is 1.1°C, and there is around 600 mm of precipitation per year, mostly during the growing season from June to September.

Based on the categorization by the US Department of Agriculture, the soil type in the research area was identified as silt clay loam, consisting of 31.2% sand, 56.0% silt, and 12.8% clay in the top 30 cm of soil. *Elymus nutans* and *Kobresia setschwanensis* are the dominant species in the study area, while other associated species include *Potentilla anserina*, *Roegneria nutans*, *Poa pratensis*, *Plantago depressa*, *Leymus secalinus*, and *Ajania tenuifolia*, etc. We choose *E. nutans* and *P. anserina* as the focal species for investigating the impacts of warming on alpine plants. The two species representing two major plant functional groups (grasses and forbs) and naturally co-exist within our study site. *Elymus nutans* is the dominant perennial grass species in the alpine meadow. *Potentilla anserina* is a common companion species and is widely distributed in alpine meadows. Due to its wide ecological amplitude and vegetative reproduction ability, *P. anserina* is considered a prime species for ecological restoration in alpine regions (Wu et al., 2022). Our field investigation at the study site found that *E. nutans* and *P. anserina* together account for nearly 60% of the total vegetation coverage. *E. nutans* and *P. anserina* display distinct stratified structures. *E. nutans* predominantly occupies the upper part of the community and grow in full-sun conditions, while the leaves of *P. anserina* were restricted to the lower parts of the community close to soil surface. Consequently, they display distinct resource utilization patterns, particularly in terms of light and soil nutrients (Zhou et al., 2021). The upper leaf layer within the canopy typically absorbs light beyond its saturation point and dissipates excess energy through heat dissipation mechanisms. In contrast, lower layer leaves often face limitations due to insufficient available light.

2.2 Experimental design

In April 2015, we launched our in-situ warming experiment using open-top chambers (OTCs) to assess the impacts of warming on the alpine meadow ecosystem. The OTC had a 6.4 m^2 surface area, a height of 2 m, a bottom side length of 1.15 m, and a regular octagon form with an outside diameter of 3 m. Open areas (OAs) were developed as control regions with characteristics comparable to those of the OTCs. The detailed layout of the experimental design was mentioned in our previous articles (Zhou et al., 2021).

2.3 Environmental factors measurement

The ambient temperature (T_a, °C) and relative humidity (*RH*, %) were measured every 30 minutes by HOBO (U23-002, Pocasset, MA, USA), which was placed in the middle of the OTCs and OAs at a height of 1.5 m above the soil surface. Using an ECH_2O-TE sensor and EM50 data collecting system (Decagon Devices, Inc., USA), we automatically monitored soil temperature and soil moisture (volumetric soil moisture, V/V%) at a depth of 5 cm with 30-minute intervals during the experiment. Following four years of warming, the air temperature consistently increased year over year. In 2015–2018, the daily mean air temperature in the OTCs was 0.65°C, 0.74°C, 0.75°C, and 0.75°C higher than that in the OAs respectively. The average soil temperatures over the four-year period were recorded as 14.0°C in the OTCs and 13.2°C in the OAs. Warming led to a decline in soil moisture, with the OTCs experiencing reductions of 12.5%, 13.4%, 16.7%, and 10.1% during the growing seasons of 2015-2018. The lowest amount of precipitation during the growing season was recorded in 2015 (435 mm), while the highest amount was recorded in 2018 (669 mm) (see details in Supplementary Figure S1).

2.4 Gas exchange and chlorophyll fluorescence measurement

The gas exchange properties were measured using a portable photosynthetic system (LI-6400, LI-COR, Lincoln, USA). The experiments were conducted during the vigorous growth period (mid-July and mid-August) in each of the years spanning from 2015 to 2018. For comparative analysis, we selected 2015 (representing short-term warming) and 2018 (representing medium-term warming). The measurements were typically taken three times per month on clear days. Fully expanded and exposed leaves were selected, and measurements were taken from 09:00 to 13:00 with local time (which is 72 minutes later than Beijing time). For each replication, three individuals in a similar healthy state were selected. The following parameters were measured: net photosynthetic rate (P_n), transpiration rate (T_r), stomatal conductance (g_s), stomatal limitation (L_s), and intercellular CO_2 concentration (C_i). After that, the leaves were collected and their areas were scanned and precisely calculated using Image J software (version 1.47v, USA).

Leaf light use efficiency (LUE, mmol·CO_2·mol^{-1}·photons) was calculated based on the Equation 1:

$$LUE = P_n/PAR_i \quad (1)$$

Where PAR_i represents the incident photosynthetic active radiation (μmol·m^{-2}·s^{-1}).

A portable modulated chlorophyll fluorometer was used to assess the chlorophyll fluorescence characteristics immediately following photosynthesis measurements in the same plant (PAM-2100, Walz, Germany). The leaves were pre-adapted in the dark for 30 minutes before being measured hourly from 09:00-13:00 h. The maximal photochemical efficiency of PS II (F_v/F_m), photochemical quenching (*q*P), non-photochemical quenching (*q*N), and effective photochemical efficiency (*Yield*) of the chlorophyll fluorescence parameters were measured.

2.5 Leaf traits measurement

Fresh leaf samples were collected from the sunny side of each species, immediately weighed (fresh weight, FW), and then submerged in distilled water in the dark until saturated. After determining the saturated fresh weight (SW), the leaves were oven-dried at 70°C for 48 hours to estimate the dry weight (DW). The Equation 2 was used to obtain the relative water content (RWC, %) of the leaf:

$$RWC(\%) = [(FW - DW)/(SW - DW)] \times 100 \quad (2)$$

The leaf area of the fresh leaves was measured using Image J, and specific leaf area (SLA, cm^2·g^{-1}) was calculated as the ratio of one side's area of each leaf in each set to its dry mass (Perez-Harguindeguy et al., 2013). The drainage method was used to compute the specific leaf volume (SLV, cm^3·g^{-1}), which is the ratio of leaf volume to dry mass. Leaf dry matter content (LDMC, mg·g^{-1}) was computed as the ratio of leaf dry weight to leaf saturated fresh weight. In mid-July and mid-August, three repetitions of measurements were conducted for each leaf trait index of the two species.

2.6 Leaf stoichiometry

After sampling, the leaves were mixed to form composite samples from ten to fifteen different individuals. The materials were crushed, sieved through an 80-mesh screen, and then dried at 70°C for 24 hours before being packed in plastic bags for measurement. A Vario Macro Cube Elemental analyzer (Elementar, Hanau, Germany) was used to assess total contents of carbon and nitrogen. Total phosphorus contents were measured using a molybdenum antimony resistance colorimetric method. For each species, the measurements were repeated three times.

2.7 Soil respiration and soil nutrients

The LI-8100 automatic soil CO_2 flux system (LI-COR, Lincoln, USA) and its 20 cm survey chamber (8100-103) were used to assess soil respiration (R_s). The soil collars (8100-103) were positioned with their tops 2-3 cm above the soil surface and installed one day before the measurements. The litter in the collar was cleared before each measurement, and the above-ground of the plant was subtracted.

After 24 hours of equilibration, the soil respiration rate (R_s, μmol·m^{-2}·s^{-1}) returned to its initial level before collar insertion. Measurements were taken once per hour for two minutes between 9:00 to 13:00 with three repetitions. The R_s was computed based on the Equation 3:

$$Rs = \frac{V_C \times P \times \frac{\partial Cs}{\partial t}}{S_C \times (T + 273.15) \times R} \quad (3)$$

where S_C is the area of soil that the survey chamber covers (0.03 m^2). V_C (m^3) is computed as the sum of the volume of the 20 cm survey chamber (4.82×10^{-3} m^3) and the product of the chamber offset (the distance from the settled collar to the ground inside it) and the soil area (S_C), which represents the total volume of soil respiration system. $\frac{\partial C_s}{\partial t}$ is the rate of change in chamber CO_2 during soil respiration measurements (μmol CO_2 mol^{-1} s^{-1}), where *P* is the atmospheric pressure (P_a), *T* is chamber air temperature (°C), and *R* is the gas constant (8.314 Pa m^3 mol^{-1} K^{-1}).

The potassium dichromate oxidation titration was used to measure the content of soil organic carbon (SOC). The semi-trace Kjeldahl technique was used to measure the soil total nitrogen (TN), and the vanadium molybdate blue colorimetric method was employed to determine the soil total phosphorus (TP) (Xu et al., 2022). Alkaline hydrolysis was used to estimate soil available nitrogen (AN), and the molybdenum blue technique was employed to evaluate soil available phosphorus (AP) after extracting soil samples with sodium bicarbonate. After extraction with ammonium acetate, soil available potassium (AK) was measured using a flame photometric method. Using an autoanalyzer (SmartChem140, AMS Alliance, Italy), the content of soil NH_4^+-N was determined in extracts of 2 M KCl (1:4, soil: extractant).

2.8 Statistical analysis

The data was statistically analyzed using SPSS 20.0 (SPSS Inc., Chicago, USA), and the results were presented as means ± standard error (SE). Two-way ANOVA analysis was used to compare the photosynthetic physiological characteristics of two different species under varying warming treatments and years, followed by *post hoc* Duncan multiple comparison for further analysis. Principal component analysis (PCA) was employed to compare the variance in leaf traits among species and treatments over the course of four years. The plspm package in structural equation modeling (SEM) was utilized to investigate the influence of leaf functional traits and environmental factors on leaf photosynthetic capacity. The analyses were conducted using R program v3.4.4, and figures were generated with Origin Pro 2021 (OriginLab Corporation, United States).

3 Results

3.1 Leaf physiological and biochemical characteristics

3.1.1 Leaf photosynthesis and light use efficiency

Different warming years had significant impacts on the photosynthesis rate (P_n) and transpiration rate (T_r) of both species. Specifically, short-term warming in 2015 resulted in decreased P_n and T_r for *E. nutans*, while increasing P_n and T_r for *P. anserina*. Conversely, medium-term warming in 2018 led to increased P_n and T_r for *E. nutans* but decreased for *P. anserina* (Figures 1A, 2B). Significant differences in P_n and T_r were observed between the two species. When comparing the P_n of both species in 2015 and 2018 under warming conditions, it was found that the P_n of both species decreased with the prolonged duration of warming.

In short and medium-term warming, the stomatal conductance (g_s) of *P. anserina* was significantly higher than that of *E. nutans* (Figure 1C). There were significant differences in g_s between *E. nutans* and *P. anserina* across different years of warming. In 2015, both *E. nutans* and *P. anserina* experienced a reduction in g_s due to warming, while in 2018, the g_s of *E. nutans* increased while that of *P. anserina* decreased.

The LUE of *E. nutans* and *P. anserina* exhibited an increase with warming in the short and medium-terms (Figure 1D). In 2015, the LUE of *E. nutans* was measured at 4.64 and 4.49 mmol·CO_2·mol^{-1}·photons in the OTCs and OAs, respectively, while the LUE of *P. anserina* was recorded as 5.80 and 3.43 mmol·CO_2·mol^{-1}·photons in the OTCs and OAs. In 2018, warming increased the LUE of both *E. nutans* and *P. anserina*. However, there was no statistically significant difference in LUE between the two species ($p > 0.05$).

3.1.2 Chlorophyll fluorescence characteristics

In both 2015 and 2018, warming increased the F_v/F_m values of both species (Figure 2A). In 2015, the F_v/F_m values of *E. nutans* were 0.776 and 0.723 in OTCs and OAs, respectively, showing a statistically significant difference ($p< 0.05$). The F_v/F_m values of *P. anserina* also increased with warming, but the difference was not statistically significant ($p > 0.05$). In 2018, the F_v/F_m value of *P. anserina* was higher than that of *E. nutans*. The *yield* values of the two species exhibited opposite trends under short-term and medium-term warming, with *P. anserina* having a higher *yield* than *E. nutans*, and the *yield* values of the two plants exhibited significant differences (Figure 2B). Under short-term warming, the *yield* of *E. nutans* and *P. anserina* increased, while in medium-term warming, the *yield* of both species decreased.

The *qP* values of the two species exhibited significant differences across different warming years ($p< 0.05$). In 2015, warming increased the *qP* values of both species, with *E. nutans* exhibiting a higher value compared to *P. anserina* (Figure 2C). In 2018, warming increased the *qP* values of *E. nutans* and decreased those of *P. anserina*, but the difference was not statistically significant ($p > 0.05$). Short-term warming (2015) reduced the *qN* values of both *E. nutans* and *P. anserina*, while medium-term warming increased them (Figure 2D).

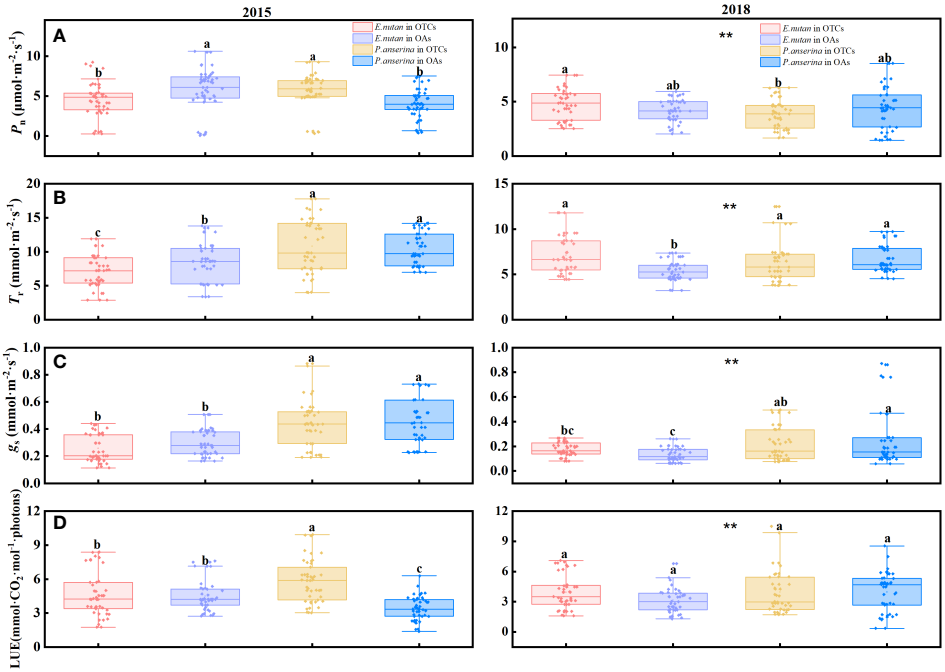

FIGURE 1
Effects of warming on photosynthesis and light use efficiency of *E nutans* and *P. anserina* in different years. The values are presented as means ± SE, with different letters indicating significant differences among species in the same year under warming at $p< 0.05$. ** indicates significant differences between different years. **(A)** net photosynthetic rate, **(B)** transpiration rate, **(C)** stomatal conductance, **(D)** light use efficiency. (The comparison of differences between species, treatments and years is shown in Supplementary Table S1).

10.3389/fpls.2024.1353762

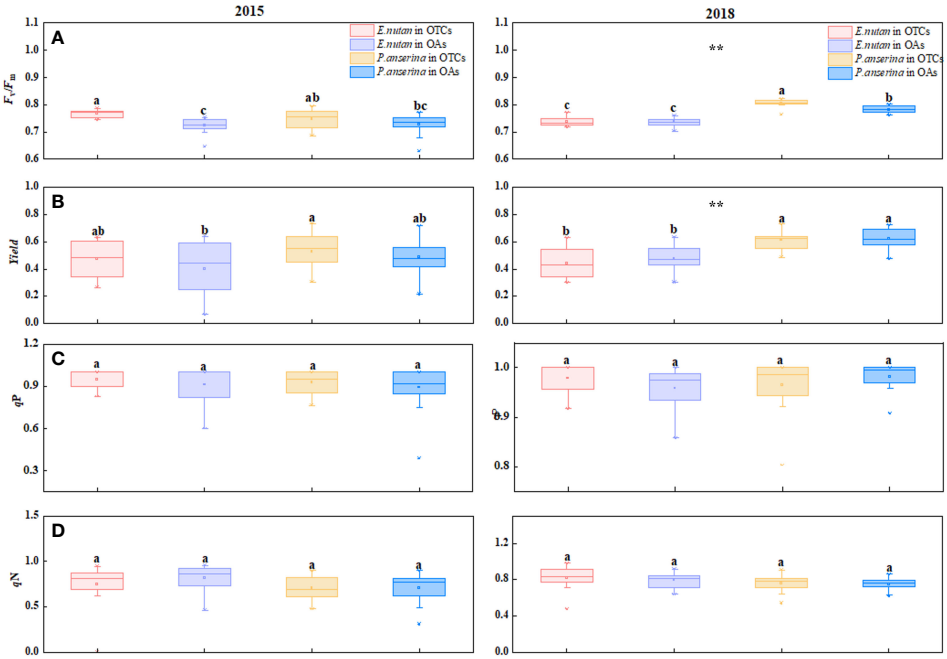

FIGURE 2
Effect of warming on chlorophyll fluorescence characteristics of *E nutans* and *P. anserina* in different years. The values are presented as means ± SE, with different letters indicating significant differences among species in the same year under warming at $p< 0.05$. ** indicates significant differences between different years. **(A)** maximum photochemical efficiency of PSII (F_v/F_m), **(B)** effective photochemical efficiency (*yield*), **(C)** photochemical quenching (*q*P), **(D)** non-photochemical quenching (*q*N). (The comparison of differences between species, treatments and years is shown in Supplementary Table S1).

3.1.3 Leaf physiological traits

Regarding the evaluated leaf physiological parameters, *E. nutans* and *P. anserina* responded differentially to in-situ warming (Table 1). *E. nutans* and *P. anserina* had significant differences in the contents of TWC, SLA, SLV, and LDMC under different warming treatments ($p< 0.05$). During the vigorous growth periods (July and August) in 2015, there were significant changes in the leaf physiological parameters of *P. anserina*, while those of *E. nutans* remained relatively stable. Warming increased the contents of TWC, SLA, and SLV in *E. nutans*, and reduced the contents of

TABLE 1 Changes in leaf traits of *E. nutans* and *P. anserina* under simulated warming in different years.

	species	experiments	TWC (%)	RWC (%)	LDMC ($mg·g^{-1}$)	SLA ($cm^2·g^{-1}$)	SLV ($cm^3·g^{-1}$)
2015	*E.nutans*	OTCs	60.9 ± 1.6 b	65.8 ± 4.3 b	294.6 ± 7.1 b	197.8 ± 4.4 a	5.26 ± 0.6 b
		OAs	60.8 ± 1.0 b	71.7 ± 3.1 ab	315.3 ± 7.6 b	189.5 ± 5.9 a	5.13 ± 0.3 b
	P. anserina	OTCs	60.9 ± 2.1 b	66.5 ± 5.7 b	294.0 ± 9.0 b	127.0 ± 7.2 b	5.11 ± 0.7 b
		OAs	69.1 ± 1.6 a	82.7 ± 2.1 a	269.8 ± 15.5 c	178.7 ± 4.8 a	7.35 ± 0.7 a
2018	*E.nutans*	OTCs	64.6 ± 2.0 a	81.7 ± 3.7 a	308.7 ± 21.1 b	187.1 ± 12.9 a	4.95 ± 0.3 a
		OAs	59.5 ± 4.4 a	79.9 ± 3.6 a	351.0 ± 34.6 a	179.9 ± 17.4 a	4.43 ± 0.4 a
	P. anserina	OTCs	60.5 ± 0.6 a	79.8 ± 3.9 a	341.3 ± 8.2 a	152.6 ± 14.7 b	4.47 ± 0.5 a
		OAs	62.9 ± 0.9 a	78.4 ± 1.3 a	316.1 ± 8.8 b	149.9 ± 11.5 b	5.38 ± 0.5 a
Significance	years		ns	**	**	ns	**
	species*years		ns	ns	ns	ns	ns
	years* treatments		ns	**	ns	ns	ns
	years*species* treatments		ns	ns	ns	ns	ns

Values are presented as means ± SE (n=6). Values with the same lowercase within columns indicate no significant differences among species in the same year under warming at $p< 0.05$. ** indicates significant differences among different years, species and treatments at the level of $p< 0.05$, and ns indicates not significant. TWC, the total water content; RWC, relative water content; LDMC, leaf dry matter content; SLA, specific leaf area; SLV, specific leaf volume.

10.3389/fpls.2024.1353762

TWC, RWC, SLA, and SLV in *P. anserina*. Different trends were observed in *E. nutans* and *P. anserina* under medium-term warming (2018). The TWC and SLV contents of *E. nutans* increased under in-situ warming, while decreased in *P. anserina*. Meanwhile, the RWC and SLA contents of *E. nutans* and *P. anserina* both increased. The content of LDMC decreased in *E. nutans* and increased in *P. anserina* in the OTCs.

3.1.4 Leaf element content

In both 2015 and 2018, *P. anserina* exhibited a higher total carbon (C) content compared to *E. nutans*, and there are significant differences between both two species ($p< 0.05$). In 2015, warming led to a decrease in the total carbon content of both species; however, in 2018, there was an increase in the total carbon content of *P. anserina* and a decrease in that of *E. nutans* (Figure 3A). Short-term warming decreased the total nitrogen (N) content of *E. nutans* while increased the total N content of *P. anserina*; however, the total N content of *E. nutans* was higher than that of *P. anserina* (Figure 3B). The total N content of the two species decreased under medium-term warming. The total phosphorus (P) content of the two species decreased significantly due to warming in the short and medium-terms (Figure 3C), while the leaf N:P ratio showed an opposite trend. The N:P ratios exhibited significant variations between the two species exposed to different warming treatments (Figure 3D). Under different treatments of short and medium-term warming, the N:P ratio of the two species experienced a remarkable increase. In 2015, the N:P ratios of *E. nutans* were 17.04 in OTCs and 14.42 in OAs, respectively, while those of *P. anserina* were 15.54 in OTCs and 10.46 in OAs. In 2018, the N:P ratios of *E. nutans* were 18.30 in OTCs and 13.75 in OAs, respectively, while those of *P. anserina* were 15.23 in OTCs and 12.57 in OAs.

3.2 Soil physicochemical properties

3.2.1 Soil respiration

It has been observed that the gradual increase in temperature has led to a slight rise in soil respiration (R_s) (Figure 4). In 2015, the R_s of OTCs and OAs were recorded as 1.06 and 0.97 $\mu mol \cdot m^{-2} \cdot s^{-1}$ respectively, while in 2018, the R_s of OTCs and OAs increased to 1.46 and 1.39 $\mu mol \cdot m^{-2} \cdot s^{-1}$ respectively. The impact of warming on R_s varied significantly across different years ($p< 0.05$), but there was minimal disparity between the various treatments (OTCs *vs.* OAs, $p > 0.05$).

3.2.2 Soil element content

Short-term and medium-term warming led to a decrease in the content of soil organic carbon (SOC), soil total nitrogen, soil total phosphorus, soil available phosphorus, soil available potassium, and soil NH_4^+-N (Table 2). In the short-term warming, there was a significant decline in soil available potassium and NH_4^+-N contents, while in the medium-term warming, there was a significant decrease in soil total phosphorus, and available phosphorus contents ($p< 0.05$). The total C content increased significantly in both 2015 and 2018 ($p< 0.05$).

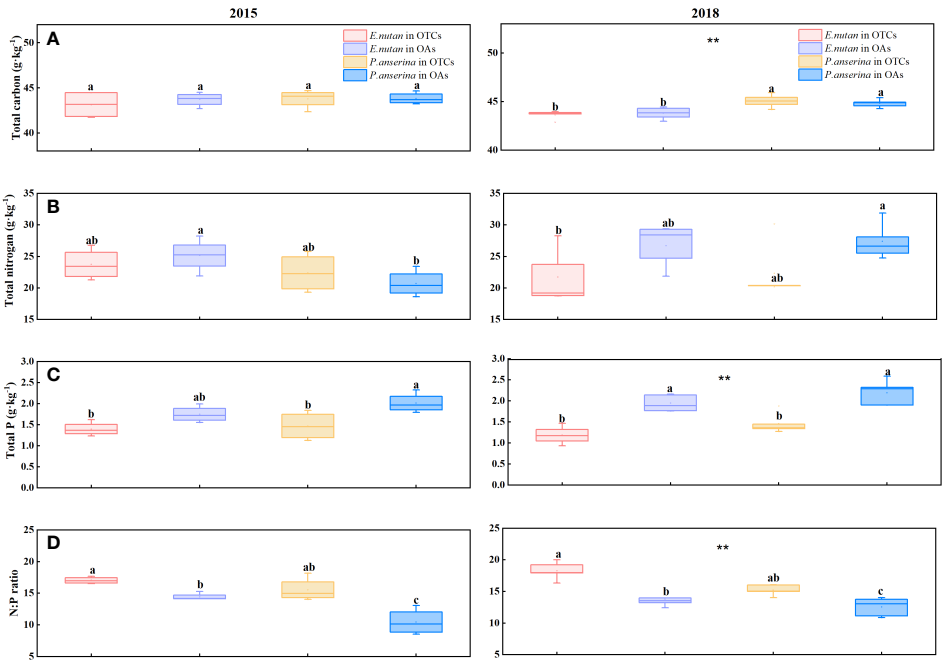

FIGURE 3
Effects of warming on the element content in *E. nutans* and *P. anserina* in different years. The values are presented as means ± SE, with different letters indicating significant differences among species in the same year under warming at $p< 0.05$. ** indicates significant differences between different years. **(A)** total carbon content, **(B)** total nitrogen content, **(C)** total phosphorus contents, **(D)** the N:P ratios. (The comparison of differences between species, treatments and years is shown in Supplementary Table S1).

TABLE 2 Changes in soil element content under simulated warming in 2015 and 2018.

	experiments	SOC (g kg $^{-1}$)	TC (g kg $^{-1}$)	TN (g kg $^{-1}$)	TP (g kg $^{-1}$)	AP (mg kg $^{-1}$)	AK (mg kg $^{-1}$)	NH_4^+-N (mg kg $^{-1}$)
2015	OTCs	28.17 ± 2.1	71.51 ± 1.1	2.74 ± 0.2	1.44 ± 0.1	4.45 ± 1.3	128.6 ± 10.6	170.5 ± 21.4
	OAs	30.26 ± 1.3	54.02 ± 1.4	3.09 ± 0.1	1.63 ± 0.1	6.21 ± 1.0	315.7 ± 17.2	249.1 ± 7.7
2018	OTCs	29.34 ± 1.0	67.77 ± 1.0	3.30 ± 0.1	1.31 ± 0.1	8.57 ± 0.8	170.0 ± 17.8	221.9 ± 12.4
	OAs	32.92 ± 2.4	63.22 ± 1.8	3.63 ± 0.3 a	2.04 ± 0.2	16.48 ± 2.7	218.9 ± 22.1	248.4 ± 16.9
significance	year	ns	ns	**	ns	**	ns	ns
	treats	ns	**	ns	ns	**	**	**
	year* treats	ns	**	ns	ns	ns	**	ns

Values are presented as means ± SE (n=6). ** indicates significant differences among different years and treatments at the level of $p< 0.05$, and ns indicates not significant. SOC, soil organic carbon; TC, total carbon; TN, total nitrogen; TP, total phosphorus; AP, soil available phosphorus; AK, soil available potassium. NH_4^+-N, soil ammonium nitrogen.

3.3 Main factors affect leaf photosynthetic capacity under warming

The data representing the interaction pathways between soil nutrients, atmospheric CO_2, leaf traits, and leaf photosynthetic capability in response to warming was adequately fit by structural equation models (SEM). It can be seen that soil nutrients have significant effects on leaf traits both in OTCs and OAs. The SEM analysis revealed that warming impacts leaf photosynthetic capability indirectly through soil nutrients, atmospheric CO_2, and leaf traits in both OAs and OTCs. Firstly, the temperature had a significant effect on atmospheric CO_2 and leaf traits in OTCs but not in OAs. Secondly, the photosynthetic capability of OTCs was more affected by temperature variations than that of OAs. Thirdly, the effects of temperature variation on leaf traits were greater in OTCs than in OAs. Furthermore, the correlation between leaf traits and photosynthetic capacity increased in OTCs, while the correlation between soil nutrients and photosynthetic capacity decreased (Figure 5). Finally, atmospheric CO_2 had a significant effect on leaf photosynthetic capacity in OAs but not in OTCs, indicating that the effect of atmospheric CO_2 on leaf photosynthetic capacity decreased with increasing temperature.

A PCA-Biplot was used to compare the variance in leaf traits among different species and treatments over a period of four years. The first and second PC axes explained 27.3% and 20.1%, respectively. For the two species, *E. nutans* showed a strong correlation with L_s, SLA, RWC, TN, TC, NP, *qN*, *Yield*, F_v/F_m and LDMC. *P. anserina* exhibited a strong correlation with P_n, G_s, T_r, LUE, SLV, TWC and TP (see the Supplementary Figure S2A). The warming treatment (OTCs) had a significant impact on the photosynthetic capability (photosynthesis and fluorescence) of species (see the Supplementary Figure S2B).

4 Discussion

4.1 Responses of leaf photosynthetic and LUE to climate warming

Alpine plants are largely restricted by low temperatures, and warming might directly reduce the impact of low temperatures on plant growth, even change the community structure and species composition of alpine meadows (Li et al., 2018; Zhou et al., 2021). Photosynthesis can reflect the physiological adaptability of plants under specific environmental conditions. Several studies suggest that alpine plants exhibit higher photosynthetic capacities and leaf nitrogen concentrations compared to the global average (Wright et al., 2004; He et al., 2006). The majority research has shown that

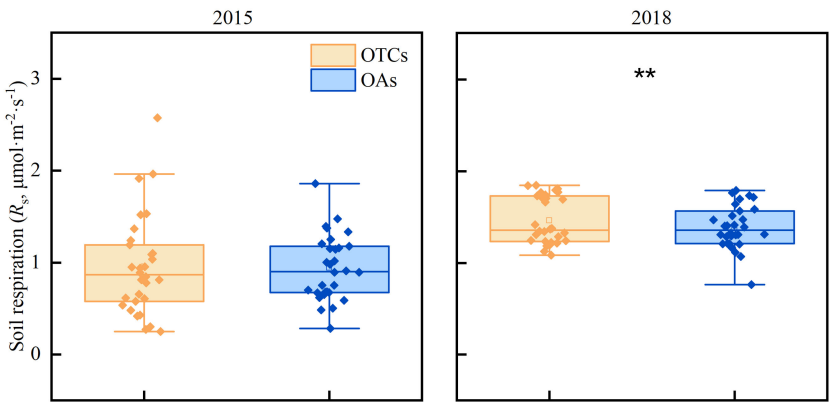

FIGURE 4
The effect of *in-situ* warming on soil respiration (R_s) in 2015 and 2018. ** indicates significant differences among different years at the level of $p< 0.05$.

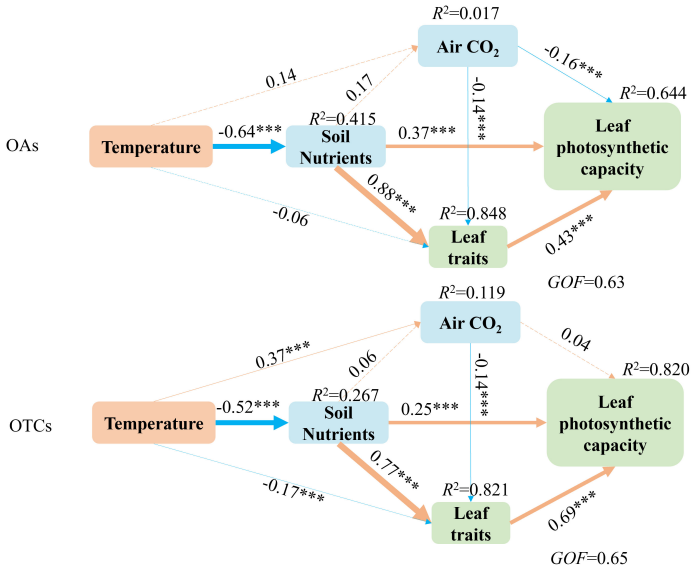

FIGURE 5
Structural equation models reveal direct and indirect influences of soil nutrients, atmospheric CO_2, leaf traits, and leaf photosynthetic capacity on warming. Single-arrowed pathways indicate the directional effect between variables. The values associated with pathways are the standardized path coefficients. The R^2-values are provided for soil nutrients, atmospheric CO_2, leaf traits, and leaf photosynthetic capacity to indicate the variance explained by the model (R^2). The width of the arrows indicates the strength of the relationships. Orange arrows indicate significant positive relationships, while blue arrows indicate significant negative relationships. The numbers on the line represent standardized path coefficients, and stars indicate significant correlations. ***p< 0.001.

warming has positive effects on plant photosynthesis. Fu et al. (2015) discovered that warming significantly increased in the P_n of the alpine plants on the Tibetan Plateau, which was related to the increase of stomatal conductance (g_s), chlorophyll (*Chl*) content, *yield*, and non-photochemical quenching of *Chl* fluorescence. Carroll et al. (2017) found that the photosynthesis of three dominant species (*Pinus contorta*, *P. ponderosa*, and *Populus tremuloides*) had different responses to warming. Climatic warming also affects leaf photosynthetic physiological parameters, such as *Chl* fluorescence, g_s, and intercellular CO_2 concentration (C_i), which are all temperature-dependent (Ruiz-Vera et al., 2013). In our research, higher g_s was linked to better photosynthetic carbon absorption capability. The g_s affects CO_2 diffusion from the atmosphere into the intercellular space of leaves, and high g_s promotes plant photosynthesis and C assimilation (Sugiura et al., 2020). Moreover, we observed a significant difference in the g_s of both species between the two durations of warming. Specifically, compared to the short-term warming, the two species exhibited a decrease in g_s during the medium-term warming, which can be attributed to a simultaneous decrease in P_n.

Photosynthesis provides a comprehensive depiction of a plant's physiological condition, which can be used to quantify growth differences between plants and the degree of environmental impact (Lin et al., 2017). The response of photosynthesis may differ between short-term and medium-term warming. Under short-term warming, the P_n of *E. nutans* decreased while that of *P. anserina* increased. However, the P_n of the two species had an opposite trend during medium-term warming. The P_n of *E. nutans* increased, while that of *P. anserina* decreased. Phenotypic plasticity is widely recognized as a primary mechanism by which plants adapt to variations in environmental factors, serving as an observed adaptation to short-term fluctuations in the environment (Gratani, 2014). The contrasting effects of short-term warming on P_n and T_r for *E. mutans* versus *P. anserina*, possibly attributed to phenotypic plasticity rather than adaptation. In the alpine meadow, *E. nutans* was the dominant species, while *P. anserina* was a common subordinate species. The height of a plant plays a crucial role in determining its ability to compete for light. Both of these two species have a distinct layered structure, and their photosynthetic capacity and LUE are significantly different. The competitive coexistence of different functional groups in alpine meadows is primarily attributed to their disparities in canopy photosynthetically active radiation, soil nutrient acquisition (Kleyer et al., 2019; Rao et al., 2023). Climate warming has resulted in a decline in soil nutrient and moisture, intensifying the competition between *E. nutans* and *P. anserina*. Consequently, this competition has led to changes in their leaf traits, ultimately impacting their photosynthetic capacity. In addition, climate change can directly influence plant photosynthesis through alterations in temperature and precipitation patterns. Ma et al. (2017) suggested that the two dominant species, *E. nutans* and *Stipa aliena*, were relatively insensitive to environmental changes, probably because of their greater ability to acquire nutrients and light. Warming increased the photoinhibition of *E. nutans* but decreased the photoinhibition of *P. anserina*, which is consistent with previous researches (Shi et al., 2010; Zhou et al., 2021).

The F_v/F_m value is a sensitive indicator of photoinhibition. In our study, the F_v/F_m value of the two species in the OTCs was higher than that of the OAs, indicating that the alpine plants were restricted by low temperatures, and warming improved their ability to resist stress

(Figure 2). Under medium-term warming, the F_v/F_m value of *P. anserina* was higher than that of *E. nutans*, indicating more effective carboxylation and quicker light-harvesting by the PSII antenna complexes. Changes in F_v/F_m value reflect up-or down-regulation of PSII, which is associated with changes in *q*P or *q*N in PSII (Wu et al., 2018). *q*N is an indicator of a plant's ability to reduce heat dissipation in its photosynthetic membranes, thereby minimizing chloroplast damage (Ware et al., 2015). *E. nutans* in the OTCs activated photoprotection and reduced photoinhibition mechanisms, resulting in a greater *q*N to dissipate excess heat and sustain C assimilation capacity.

Understanding the LUE of alpine plants is crucial for enhancing their productivity and mitigating the degradation of alpine meadows. Zhang et al. (2015) believed that the changes in plant height and coverage under warming directly affect their competition for light energy and LUE. Our study revealed that warming enhanced the LUE of both two species, with significant variations observed among different species and over different years of warming (Figure 1). In contrast to our findings, Zhou et al. (2016) suggest that simulated warming may reduce the LUE of alpine meadows due to the negative impact of warming-induced dry micro-environment on LUE, which masks the favorable effect of temperature rises. Overall, our results imply that both of the two species were impacted by climate change and that the short and medium-term impacts on various species varied. Warming improved the LUE of the two species, which was beneficial to the growth and productivity of alpine plants.

4.2 Response of leaf traits to climate warming

Leaf traits are important indicators of plant adaptation to environmental change because they are linked to the efficiency of plant resource acquisition and use (Li et al., 2018; Xu et al., 2018; Li et al., 2021). In addition, leaf traits account for the majority of the variation in ecosystem productivity (Sigdel et al., 2023). Numerous studies have demonstrated that leaf traits, such as leaf lifespan, leaf area, and leaf nutrient content, are highly sensitive to climate warming (Myers-Smith et al., 2019; Bjorkman et al., 2020). Warming directly affects leaf traits and indirectly affects plant photosynthesis and LUE through these traits. Our research indicate that the impact of warming on leaf photosynthetic capacity varies among the two species, which is related to their functional traits and soil nutrient availability (Figure 5). Under medium-term warming, both species' RWC and SLA increased. Additionally, the TWC and SLV of *E. nutans* increased and the LDMC of *P. anserina* also increased. Our findings support the hypothesis that phenotypic plasticity in certain plant traits can serve as a predictor for community performance under climate change.

SLA and leaf nitrogen content play a crucial role in carbon fixation (Díaz et al., 2016). According to Kattge et al. (2020), SLA exhibits sensitive to climate change and is closely associated with species-specific resource utilization. It plays a crucial role in influencing photosynthesis, light interception, and plant growth, while also serving as a predictor of competitiveness and environmental tolerance (Worthy et al., 2020). Plants with a larger leaf area are more efficient in capturing light and carbon. Our research showed that the SLA of the dominant species *E. nutans* is enhanced by warming, which implies higher resource acquisition in warmer climates. This finding is consistent with many other studies (Guittar et al., 2016; Liu et al., 2018). SLV is an important leaf functional trait, is influenced by factors such as leaf thickness, overall dimension, and dry matter content. It serves as an indicator of a plant's ability to adapt to extreme environments like cold and arid conditions (Su et al., 2018). Leaf volume is determined by the combination of photosynthetic area and thickness, representing the entirety of photosynthetic organs. This trait facilitates better comparison among different plant species. Su et al. (2018) proposed the concept of SLV and suggested that alpine plants with higher SLV would exhibit greater resistance to harsh environmental conditions. In our study, we observed a strong positive correlation between leaf SLV and leaf P_n during the medium-term warming (Figure 5). The higher the leaf P_n of plants, the greater the SLV; however, short-term warming exhibited an opposite trend. These results indicate that during the process of long-term adaptation to the environment, the photosynthetic capacity of plants and leaf traits are mutually adapted and coordinated.

Leaf nitrogen content is strongly correlated with photosynthetic capacity, as nitrogen is essential for the synthesis of Rubisco, which is the key enzyme in photosynthesis (Reich et al., 1994). We observed a positive correlation between leaf C and N content and LUE. Peng et al. (2020) suggested that warming slightly increased the coverage of legumes and the C: N ratio of all plants in the alpine meadow. Our investigation revealed that the C: N and N: P ratios of the two species' leaves increased under warming, which is consistent with Peng's findings. The alpine meadow subjected to experimental warming displayed higher leaf C: N and N: P ratios, indicating that plants were more efficient in utilizing nitrogen for growth. Plant communities exhibit both positive and negative interactions between different plant species (Callaway and Walker, 1997). Cui et al. (2023) confirmed that grasses exhibited a higher competitive ability compared to other functional groups, primarily attributed to their increased investment in roots and enhanced capacity for resource uptake.

4.3 Effects of environmental factors on light use efficiency of plants

The productivity of grasslands is influenced by the interactions between soil and climatic conditions (Shen et al., 2022). Our structural equation modeling revealed that warming indirectly impacts leaf photosynthetic capacity through factors such as soil nutrients, atmospheric CO_2, and leaf traits (Figure 5). Our previous studies have demonstrated that the optimal temperature range for alpine plants is between 20°C and 25°C (Zhou et al., 2017). During the vigorous growth period in 2015 and 2018, between 09:00 and 13:00 hours, we used an LI-6400 portable photosynthesis system to measure average air temperatures of approximately 28.5°C and 31.5°C. These temperatures exceeded the optimal range for alpine plants, resulting in a negative impact on leaf photosynthetic capacity.

Soil plays a crucial role in providing the majority of nutrients necessary for plant growth, and these nutrients are closely associated with how plant leaves utilize resources (Gao et al., 2019). The soil nutrients (N) have a significant impact on leaf N and plant photosynthesis (Yu et al., 2019), and a low soil phosphorus (P) may result in reduced leaf P content, thereby limiting overall plant function (Sun et al., 2019). Climate change modifies the physical and chemical properties of soil, thereby impacting the functioning of the alpine meadow ecosystem. Our findings indicate that short and medium-term experimental warming have similar impacts on soil nutrients. Warming reduced soil nutrient contents at depths of 0-30 cm (Table 2), indicating that warming stimulated soil nutrient cycling and organic matter decomposition, resulting in a decrease in soil C and N contents (Xu et al., 2022). However, some studies have shown inconsistent results regarding the responses of soil nutrients to climate warming. While some suggest that warming has no impact on soil C and N contents (Ning et al., 2019; Yang et al., 2022), others indicate an increase (White-Monsant et al., 2017). These contradictory results may be attributed to variations in temperature and duration of warming, as well as the diversity of grassland ecosystems. In our study, soil nutrient content did not change significantly under warming. This is because, in the case of relatively short-term warming experiments (< 5 years), it was challenging to significantly alter the vast soil carbon pool due to the substantial spatial heterogeneity in soil organic carbon among plots and the limited number of repeated warming experiments.

Several studies indicate a positive correlation between warming-induced changes in plant total biomass, above-ground biomass, and below-ground biomass with soil nutrient content. This subsequently impacts the LUE of plants (Song et al., 2019; Zhou et al., 2022). Shen et al. (2022) found that the change in soil pH and nutrient imbalance caused by N and P enrichment were the main factors impacting the photosynthetic characteristics of plant in the alpine steppe. In our study, the effects of soil nutrients on LUE were primarily mediated through their impact on leaf traits. The content of soil nitrogen significantly influences leaf N content and plant photosynthesis, while inadequate levels of soil P can lead to reduced leaf P content and limit leaf function (Gong and Gao, 2019; Sun et al., 2019).

Soil respiration (R_s) is expected to have positive feedback on global warming (Wang et al., 2021). Some studies suggest that short-term warming promotes soil respiration, but there is no consistent pattern under long-term warming and variations exist among ecosystems (Chen et al., 2016; Ganjurjav et al., 2018). According to García-Palacios et al. (2021), R_s is highly sensitive to temperature, and warming will stimulate R_s activation and accelerate its rate. Yu et al. (2019) found no significant effects of experimental warming on R_s. Our findings were similar to prior research that alpine meadow R_s increased in response to both short- and medium-term warming.

5 Conclusions

In this study, we conducted a 4-year in-situ field experiment to investigate the effects of warming on photosynthesis and LUE of alpine plants on the Tibetan Plateau. Our findings suggest that the two typical alpine species were affected by climate warming, and the effects of short and medium-term warming on different species exhibited significant species-specific variations. Warming improved the LUE of both species, which was beneficial to the growth and productivity of alpine plants. During the medium-term adaptation to the environment, the photosynthetic capacity of plants and leaf traits are mutually adapted and coordinated. Leaf traits, such as SLV, showed a significant positive correlation with leaf P_n. Additionally, warming primarily enhances leaf functional traits by altering soil nutrients and thus affects leaf photosynthetic capacity. Our findings will be useful in understanding the underlying mechanisms of alpine plant responses to global warming.

Data availability statement

The original contributions presented in the study are included in the article/Supplementary Material, further inquiries can be directed to the corresponding author/s.

Author contributions

ZZ: Writing – original draft, Writing – review & editing. PS: Supervision, Writing – review & editing. JY: Writing – review & editing, Visualization, Data curation. RS: Writing – review & editing, Investigation. XD: Writing – review & editing, Investigation.

Funding

The author(s) declare that financial support was received for the research, authorship, and/or publication of this article. This research was financially supported by the Strategic Priority Research Program of Chinese Academy of Sciences (XDA20050102), the Natural Science Foundation of Gansu Province (23JRRA608), and the National Natural Science Foundation of China (41701106, 41871043).

Conflict of interest

The authors declare that the research was conducted in the absence of any commercial or financial relationships that could be construed as a potential conflict of interest.

Publisher's note

All claims expressed in this article are solely those of the authors and do not necessarily represent those of their affiliated organizations, or those of the publisher, the editors and the reviewers. Any product

that may be evaluated in this article, or claim that may be made by its manufacturer, is not guaranteed or endorsed by the publisher.

Supplementary material

The Supplementary Material for this article can be found online at: https://www.frontiersin.org/articles/10.3389/fpls.2024.1353762/full#supplementary-material

SUPPLEMENTARY FIGURE 1
Air temperature at a height of 1.5 m (°C), soil temperature at 5 cm depth (°C), soil moisture at 5 cm depth (%), and daily precipitation (mm) during the growing season (from May to September) in open-top chambers (OTCs) and open areas (OAs) from 2015 to 2018.

SUPPLEMENTARY FIGURE 2
Principal Component Analysis (PCA) for the variance in leaf traits among different species and treatments. The horizontal axis represents the first principal component (PC1); the vertical axis represents the second principal component (PC2). E: *Elymus nutans*, P: *Potentilla anserina*, P_n: net photosynthetic rate, T_r: transpiration rate, g_s: stomatal conductance, LUE: light use efficiency, F_v/F_m: maximum photochemical efficiency of PSII, *yield*: effective photochemical efficiency, *q*P: photochemical quenching, *q*N: non-photochemical quenching (*q*N), TC: total carbon content, TN: total nitrogen content, TP: total phosphorus contents, NP: the N:P ratios. TWC: the total water content, RWC: relative water content, LDMC: leaf dry matter content, SLA: specific leaf area, SLV: specific leaf volume.

References

Allison, S. D., Romero-Olivares, A. L., Lu, Y., Taylor, J. W., and Treseder, K. K. (2018). Temperature sensitivities of extracellular enzyme V_{max} and K_m across thermal environments. *Global Change Biol.* 24, 2884–2897. doi: 10.1111/gcb.14045

Atkin, O., Bruhn, D., Hurry, V., and Tjoelker, M. (2005). The hot and the cold: unravelling the variable response of plant respiration to temperature. Evans review no. 2. *Funct. Plant Biol.* 32, 87–105. doi: 10.1071/FP03176

Bai, E., Li, S. L., Xu, W. H., Li, W., Dai, W. W., and Jiang, P. (2013). A meta-analysis of experimental warming effects on terrestrial nitrogen pools and dynamics. *New Phytol.* 199, 441–451. doi: 10.1111/nph.12252

Bjorkman, A. D., García Criado, M., Myers-Smith, I. H., Ravolainen, V., Jónsdöttir, I. S., Westergaard, K. B., et al. (2020). Status and trends in Arctic vegetation: evidence from experimental warming and long-term monitoring. *Ambio* 49, 678–692. doi: 10.1007/s13280-019-01161-6

Buzzard, V., Michaletz, S. T., Deng, Y., He, Z., Ning, D., Shen, L., et al. (2019). Continental scale structuring of forest and soil diversity via functional traits. *Nat. Ecol. Evol.* 3, 1298–1308. doi: 10.1038/s41559-019-0954-7

Callaway, R. M., and Walker, L. R. (1997). Competition and facilitation: A synthetic approach to interactions in plant communities. *Ecology* 78, 1958–1965. doi: 10.1890/0012-9658(1997)078[1958:CAFASA]2.0.CO;2

Carroll, C. J., Knapp, A. K., and Martin, P. H. (2017). Dominant tree species of the Colorado Rockies have divergent physiological and morphological responses to warming. *For. Ecol. Manage.* 402, 234–240. doi: 10.1016/j.foreco.2017.07.048

Chen, J., Luo, Y., Xia, J., Shi, Z., Jiang, L., Niu, S., et al. (2016). Differential responses of ecosystem respiration components to experimental warming in a meadow grassland on the Tibetan Plateau. *Agric. For. Meteorol.* 220, 21–29. doi: 10.1016/j.agrformet.2016.01.010

Cui, G., Pugnaire, F. I., Yang, L., Zhao, W., Ale, R., Shen, W., et al. (2023). Shrub mediated effects on soil nitrogen determines shrub-herbaceous interactions in drylands of the Tibetan Plateau. *Front. Plant Sci.* 14. doi: 10.3389/fpls.2023.1137365

Díaz, S., Kattge, J., Cornelissen, J. H. C., Wright, I. J., Lavorel, S., Dray, S., et al. (2016). The global spectrum of plant form and function. *Nature* 529, 167–171. doi: 10.1038/nature16489

Duan, M., Li, A., Wu, Y., Zhao, Z., Peng, C., DeLuca, T. H., et al. (2019). Differences of soil CO_2 flux in two contrasting subalpine ecosystems on the eastern edge of the Qinghai-Tibetan Plateau: A four-year study. *Atmos. Environ.* 198, 166–174. doi: 10.1016/j.atmosenv.2018.10.067

Feng, X. L., and Dietze, M. (2013). Scale dependence in the effects of leaf ecophysiological traits on photosynthesis: Bayesian parameterization of photosynthesis models. *New Phytol.* 200, 1132–1144. doi: 10.1111/nph.12454

Forkel, M., Carvalhais, N., Rödenbeck, C., Keeling, R., Heimann, M., Thonicke, K., et al. (2016). Enhanced seasonal CO_2 exchange caused by amplified plant productivity in northern ecosystems. *Science* 351, 696–699. doi: 10.1126/science.aac4971

Fu, Y. H., Gao, X. J., Zhu, Y. M., and Guo, D. (2021). Climate change projection over the Tibetan Plateau based on a set of RCM simulations. *Adv. Clim. Change Res.* 12, 313–321. doi: 10.1016/j.accre.2021.01.004

Fu, G., Shen, Z. X., Sun, W., Zhong, Z. M., Zhang, X. Z., and Zhou, Y. T. (2015). A meta-analysis of the effects of experimental warming on plant physiology and growth on the Tibetan Plateau. *J. Plant Growth. Regul.* 34, 57–65. doi: 10.1007/s00344-014-9442-0

Ganjurjav, H., Hu, G., Wan, Y., Li, Y., Danjiu, L., and Gao, Q. (2018). Different responses of ecosystem carbon exchange to warming in three types of alpine grassland on the central Qinghai–Tibetan Plateau. *Ecol. Evol.* 8, 1507–1520. doi: 10.1002/ece3.3741

Gao, J., Song, Z., and Liu, Y. (2019). Response mechanisms of leaf nutrients of endangered plant (*Acer catalpifolium*) to environmental factors varied at different growth stages. *Glob. Ecol. Conserv.* 17, e00521. doi: 10.1016/j.gecco.2019.e00521

García-Palacios, P., Crowther, T. W., Dacal, M., Hartley, I. P., Reinsch, S., Rinnan, R., et al. (2021). Evidence for large microbial-mediated losses of soil carbon under anthropogenic warming. *Nat. Rev. Earth Env.* 2, 507–517. doi: 10.1038/s43017-021-00178-4

Gong, H., and Gao, J. (2019). Soil and climatic drivers of plant SLA (specific leaf area). *Glob. Ecol. Conserv.* 20, e00696. doi: 10.1016/j.gecco.2019.e00696

Gratani, L. (2014). Plant phenotypic plasticity in response to environmental factors. *Adv. Bot.* 2014, 208747. doi: 10.1155/2014/208747

Guittar, J., Goldberg, D., Klanderud, K., Telford, R. J., and Vandvik, V. (2016). Can trait patterns along gradients predict plant community responses to climate change? *Ecology* 97, 2791–2801. doi: 10.1002/ecy.1500

He, J. S., Wang, Z. H., Wang, X. P., Schmid, B., Zuo, W. Y., Zhou, M., et al. (2006). A test of the generality of leaf trait relationships on the Tibetan Plateau. *New Phytol.* 170, 835–848. doi: 10.1111/j.1469-8137.2006.01704.x

Huang, W., Wang, W., Cao, M., Fu, G., Xia, J., Wang, Z., et al. (2021). Local climate and biodiversity affect the stability of China's grasslands in response to drought. *Sci. Total Environ.* 768, 145482. doi: 10.1016/j.scitotenv.2021.145482

Hughes, T. P., Kerry, J. T., Baird, A. H., Connolly, S. R., Dietzel, A., Eakin, C. M., et al. (2018). Global warming transforms coral reef assemblages. *Nature* 556, 492–496. doi: 10.1038/s41586-018-0041-2

Immerzeel, W. W., Lutz, A. F., Andrade, M., Bahl, A., Biemans, H., Bolch, T., et al. (2020). Importance and vulnerability of the world's water towers. *Nature* 577, 364–369. doi: 10.1038/s41586-019-1822-y

Jassey, V. E., and Signarbieux, C. (2019). Effects of climate warming on Sphagnum photosynthesis in peatlands depend on peat moisture and species-specific anatomical traits. *Glob. Change Biol.* 25, 3859–3870. doi: 10.1111/gcb.14788

Kattge, J., Bönisch, G., Díaz, S., Lavorel, S., Prentice, I. C., Leadley, P., et al. (2020). TRY plant trait database–enhanced coverage and open access. *Glob. Change Biol.* 26, 119–188. doi: 10.1111/gcb.14904

Kleyer, M., Trinogga, J., Cebrián-Piqueras, M. A., Trenkamp, A., Fløjgaard, C., Ejrnæs, R., et al. (2019). Trait correlation network analysis identifies biomass allocation traits and stem specific length as hub traits in herbaceous perennial plants. *J. Ecol.* 107, 829–842. doi: 10.1111/1365-2745.13066

Knapp, A. K., Chen, A., Griffin-Nolan, R. J., Baur, L. E., Carroll, C. J. W., Gray, J. E., et al. (2020). Resolving the Dust Bowl paradox of grassland responses to extreme drought. *Proc. Natl. Acad. Sci. U.S.A.* 117, 22249–22255. doi: 10.1073/pnas.1922030117

Lee, J. H., Kim, J. Y., Kim, J. I., Park, Y. J., and Park, C. M. (2020). Plant thermomorphogenic adaptation to global warming. *J. Plant Biol.* 63, 1–9. doi: 10.1007/s12374-020-09232-y

Li, C., Lai, C., Peng, F., Xue, X., You, Q., Liu, F., et al. (2021). Dominant plant functional group determine the response of the temporal stability of plant community biomass to 9-year warming on the Qinghai–Tibetan plateau. *Front. Plant Sci.* 1871. doi: 10.3389/fpls.2021.704138

Li, D., Li, X. X., Li, Z. S., Fu, Y., Zhang, J. T., Zhao, Y. J., et al. (2024). Drought limits vegetation carbon sequestration by affecting photosynthetic capacity of semi-arid ecosystems on the Loess Plateau. *Sci. Total. Environ.* 912, 168778. doi: 10.1016/j.scitotenv.2023.168778

Li, W., Wang, J. L., Zhang, X. J., Shi, S. L., and Cao, W. X. (2018). Effect of degradation and rebuilding of artificial grasslands on soil respiration and carbon and

nitrogen pools on an alpine meadow of the Qinghai-Tibetan Plateau. *Ecol. Eng.* 111, 134–142. doi: 10.1016/j.ecoleng.2017.10.013

Lin, J., Wang, Y., Sun, S., Mu, C., and Yan, X. (2017). Effects of arbuscular mycorrhizal fungi on the growth, photosynthesis and photosynthetic pigments of *Leymus chinensis* seedlings under salt-alkali stress and nitrogen deposition. *Sci. Total Environ.* 576, 234e241. doi: 10.1016/j.scitotenv.2016.10.091

Liu, G., Wang, L., Jiang, L., Pan, X., Huang, Z., Dong, M., et al. (2018). Specific leaf area predicts dryland litter decomposition via two mechanisms. *J. Ecol.* 106, 218–229. doi: 10.1111/1365-2745.12868

Ma, Z., Liu, H., Mi, Z., Zhang, Z., Wang, Y., Xu, W., et al. (2017). Climate warming reduces the temporal stability of plant community biomass production. *Nat. Commun.* 8, 15378. doi: 10.1038/ncomms15378

Masson-Delmotte, V., Zhai, P., Pirani, A., Connors, S., Péan, C., Berger, S., et al. (2021). Contribution of working group I to the sixth assessment report of the intergovernmental panel on climate change. *Climate Change: Phys. Sci. Basis*. doi: 10.1017/9781009157896

Medlyn, B. E. (1998). Physiological basis of the light use efficiency model. *Tree Physiol.* 18, 167–176. doi: 10.1093/treephys/18.3.167

Meng, F., Liu, D., Wang, Y., Wang, S., and Wang, T. (2023). Negative relationship between photosynthesis and late-stage canopy development and senescence over Tibetan Plateau. *Glob. Change Biol* 29, 3147–3158. doi: 10.1111/gcb.16668

Myers-Smith, I. H., Thomas, H. J. D., and Bjorkman, A. D. (2019). Plant traits inform predictions of tundra responses to global change. *New Phytol.* 221, 1742–1748. doi: 10.1111/nph.15592

Ning, Z., Li, Y., Yang, H., Zhang, Z., and Zhang, J. (2019). Stoichiometry and effects of carbon, nitrogen, and phosphorus in soil of desertified grasslands on community productivity and species diversity. *Acta Ecol. Sin.* 39(10), 3537–3546. doi: 10.5846/stxb201711242094

Peng, A., Klanderud, K., Wang, G., Zhang, L., Xiao, Y., and Yang, Y. (2020). Plant community responses to warming modified by soil moisture in the Tibetan Plateau. *Arct. Antarct. Alp. Res.* 52, 60–69. doi: 10.1080/15230430.2020.1712875

Perez-Harguindeguy, N., Diaz, S., Garnier, E., Lavorel, S., Poorter, H., Jaureguiberry, P., et al. (2013). New handbook for standardised measurement of plant functional traits worldwide. *Aust. Bot.* 61, 167–234. doi: 10.1071/BT12225

Rao, Q. Y., Chen, J. F., Chou, Q. C., Ren, W. J., Cao, T., Zhang, M., et al. (2023). Linking trait network parameters with plant growth across light gradients and seasons. *Funct. Ecol.* 37, 1732–1746. doi: 10.1111/1365-2435.14327

Reich, P. B., Walters, M. B., Ellsworth, D. S., and Uhl, C. (1994). Photosynthesis–nitrogen relations in Amazonian tree species. 1. Patterns among species and communities. *Oecologia* 97, 72–62. doi: 10.1007/BF00317909

Ruiz-Vera, U. M., Siebers, M., Gray, S. B., Drag, D. W., Rosenthal, D. M., Kimball, B. A., et al. (2013). Global warming can negate the expected CO_2 stimulation in photosynthesis and productivity for soybean grown in the Midwestern United States. *Plant Physiol.* 162, 410–423. doi: 10.1104/pp.112.211938

Shen, R. N., Zhang, Y. J., Zhu, J. T., Chen, N., Chen, Y., Zhao, G., et al. (2022). The interactive effects of nitrogen addition and increased precipitation on gross ecosystem productivity in an alpine meadow. *J. Plant Ecol.* 15, 168–179. doi: 10.1093/jpe/rtab081

Shi, F., Wu, Y., Wu, N., and Luo, P. (2010). Different growth and physiological responses to experimental warming of two dominant plant species *Elymus nutans* and *Potentilla anserina* in an alpine meadow of the eastern Tibetan Plateau. *Photosynthetica* 48, 437–445. doi: 10.1007/s11099-010-0058-8

Sigdel, S. R., Liang, E. Y., Rokaya, M. B., Rai, S., Dyola, N., Sun, J., et al. (2023). Functional traits of a plant species fingerprint ecosystem productivity along broad elevational gradients in the Himalayas. *Funct. Ecol.* 37, 383–394. doi: 10.1111/1365-2435.14226

Šímová, I., Rueda, M., and Hawkins, B. A. (2017). Stress from cold and drought as drivers of functional trait spectra in North American angiosperm tree assemblages. *Ecol. Evol.* 7, 7548–7559. doi: 10.1002/ece3.3297

Song, J., Wan, S., Piao, S., Knapp, A. K., Classen, A. T., Vicca, S., et al. (2019). A meta-analysis of 1,119 manipulative experiments on terrestrial carbon-cycling responses to global change. *Nat. Ecol. Evol.* 3, 1309–1320. doi: 10.1038/s41559-019-0958-3

Storkey, J., and Macdonald, A. J. (2022). The role of long-term experiments in validating trait-based approaches to achieving multifunctionality in grasslands. *Front. Agric. Sci. Eng.* 9, 187–196. doi: 10.15302/J-FASE-2021438

Su, P., Shi, R., Zhou, Z., and Xie, T. (2018). Characteristics and relationships of foliar element content and specific leaf volume of alpine plant functional groups. *Int. J. Agric. Biol.* 20, 1663–1671. doi: 10.17957/IJAB/15.0704

Sugiura, D., Terashima, I., and Evans, J. R. (2020). A decrease in mesophyll conductance by cell-wall thickening contributes to photosynthetic downregulation. *Plant Physiol.* 183, 1600–1611. doi: 10.1104/pp.20.00328

Sun, J., Liu, B., You, Y., Li, W., Liu, M., Shang, H., et al. (2019). Solar radiation regulates the leaf nitrogen and phosphorus stoichiometry across alpine meadows of the Tibetan Plateau. *Agric. For. Meteorol.* 271, 92–101. doi: 10.1016/j.agrformet.2019.02.041

Wang, Y., Song, C., Liu, H., Wang, S., Zeng, H., Luo, C., et al. (2021). Precipitation determines the magnitude and direction of interannual responses of soil respiration to experimental warming. *Plant Soil* 458, 75–91. doi: 10.1007/s11104-020-04438-y

Ware, M. A., Belgio, E., and Ruban, A. V. (2015). Photoprotective capacity of non-photochemical quenching in plants acclimated to different light intensities. *Photosynth. Res.* 126, 261–274. doi: 10.1007/s11120-015-0102-4

Wei, B., Zhang, D. Y., Wang, G. Q., Liu, Y., Li, Q. L., Zheng, Z. H., et al. (2023). Experimental warming altered plant functional traits and their coordination in a permafrost ecosystem. *New Phytol.* 240, 1802–1816. doi: 10.1111/nph.19115

White-Monsant, A., Clark, G., Chuen, M. N. K., and Tang, C. (2017). Experimental warming and antecedent fire alter leaf element composition and increase soil C: N ratio in sub-alpine open heathland. *Sci. Total Environ.* 595, 41–50. doi: 10.1016/j.scitotenv.2017.03.237

Worthy, S. J., Laughlin, D. C., Zambrano, J., Umaña, M. N., Zhang, C., Lin, L., et al. (2020). Alternative designs and tropical tree seedling growth performance landscapes. *Ecology* 101, e03007. doi: 10.1002/ecy.3007

Wright, I. J., Reich, P. B., Westoby, M., Ackerly, D. D., Baruch, Z., Bongers, F., et al. (2004). The worldwide leaf economics spectrum. *Nature* 428, 821–827. doi: 10.1038/nature02403

Wu, Y. J., Ren, C., Tian, Y., Zha, T. S., Liu, P., Bai, Y. J., et al. (2018). Photosynthetic gas-exchange and PSII photochemical acclimation to drought in a native and non-native xerophytic species (*Artemisia ordosica* and *Salix psammophila*). *Ecol. Indic.* 94, 130–138. doi: 10.1016/j.ecolind.2018.06.040

Wu, L., Ren, Y., Wan, J. Z., Wang, M., Wang, Z., Fu, F., et al. (2022). Effects of precipitation change and nitrogen and phosphorus additions on traits and abundance of *potentilla anserina* in an alpine meadow. *Atmosphere* 13, 1820. doi: 10.3390/atmos13111820

Xu, B., Wang, J., Wu, N., Wu, Y., and Shi, F. (2018). Seasonal and interannual dynamics of soil microbial biomass and available nitrogen in an alpine meadow in the eastern part of Qinghai–Tibet Plateau, China. *Biogeosciences* 15, 567–579. doi: 10.5194/bg-15-567-2018

Xu, M., Zhao, Z., Zhou, H., Ma, L., and Liu, X. (2022). Plant allometric growth enhanced by the change in soil stoichiometric characteristics with depth in an alpine meadow under climate warming. *Front. Plant Sci.* 13. doi: 10.3389/fpls.2022.860980

Yang, Y., Shi, G., Liu, Y., Ma, L., Zhang, Z., Jiang, S., et al. (2022). Experimental warming has not affected the changes in soil organic carbon during the growing season in an alpine meadow ecosystem on the Qinghai–Tibet plateau. *Front. Plant Sci.* 13. doi: 10.3389/fpls.2022.847680

Yao, H. Y., Li, X. Y., Zhang, C. C., Wang, P., Shi, F. Z., and Deng, Y. J. (2023). Tradeoff in the supply and demand for CO_2 dominates the divergence of net photosynthesis rates of functional plants in alpine ecosystems. *Ecohydrology* 16, e2487. doi: 10.1002/eco.2487

Yu, C. Q., Wang, J. W., Shen, Z. X., and Fu, G. (2019). Effects of experimental warming and increased precipitation on soil respiration in an alpine meadow in the Northern Tibetan Plateau. *Sci. Total. Environ.* 647, 1490–1497. doi: 10.1016/j.scitotenv.2018.08.111

Zhang, X. Z., Shen, Z. X., and Fu, G. (2015). A meta-analysis of the effects of experimental warming on soil carbon and nitrogen dynamics on the Tibetan Plateau. *Appl. Soil. Ecol.* 87, 32–38. doi: 10.1016/j.apsoil.2014.11.012

Zhang, Z., Sun, J., Liu, M., Shang, H., Wang, J., Wang, J., et al. (2022). Context-dependency in relationships between herbaceous plant leaf traits and abiotic factors. *Front. Plant Sci.* 13. doi: 10.3389/fpls.2022.757077

Zhou, Z. J., Su, P. X., Shi, R., and Xie, T. T. (2017). Light use efficiency of plants and the environmental impact factors in different alpine ecosystems. *Chin. J. Ecol.* 36, 1570. doi: 10.13292/j.1000-4890.201706.025

Zhou, Z. J., Su, P. X., Wu, X. K., Shi, R., and Ding, X. J. (2021). Leaf and community photosynthetic carbon assimilation of alpine plants under in-situ warming. *Front. Plant Sci.* 12. doi: 10.3389/fpls.2021.690077

Zhou, G., Terrer, C., Huang, A., Hungate, B. A., van Gestel, N., Zhou, X., et al. (2022). Nitrogen and water availability control plant carbon storage with warming. *Sci. Total. Environ.* 851, 158243. doi: 10.1016/j.scitotenv.2022.158243

Zhou, S., Zhang, Y., Caylor, K. K., Luo, Y., Xiao, X., Ciais, P., et al. (2016). Explaining inter-annual variability of gross primary productivity from plant phenology and physiology. *Agric. For. Meteorol.* 226, 246–256. doi: 10.1016/j.agrformet.2016.06.010

frontiers | Frontiers in Plant Science

TYPE Original Research
PUBLISHED 16 April 2024
DOI 10.3389/fpls.2024.1323445

OPEN ACCESS

EDITED BY
Virgil Alexandru Iordache,
University of Bucharest, Romania

REVIEWED BY
Xiao-Dong Yang,
Ningbo University, China
Zengyun Hu,
Chinese Academy of Sciences (CAS), China

*CORRESPONDENCE
Jianli Ding
dingjl@xju.edu.cn
Nigenare Amantai
ngnr94@stu.pku.edu.cn

RECEIVED 17 October 2023
ACCEPTED 26 March 2024
PUBLISHED 16 April 2024

CITATION
Ge X, Ding J, Amantai N, Xiong J and Wang J (2024) Responses of vegetation cover to hydro-climatic variations in Bosten Lake Watershed, NW China. *Front. Plant Sci.* 15:1323445. doi: 10.3389/fpls.2024.1323445

Responses of vegetation cover to hydro-climatic variations in Bosten Lake Watershed, NW China

Xiangyu Ge[1,2,3], Jianli Ding[1,2,3]*, Nigenare Amantai[4]*, Ju Xiong[1,2,3] and Jingzhe Wang[5,6]

[1]College of Geography and Remote Sensing Sciences, Xinjiang University, Urumqi, China, [2]Xinjiang Key Laboratory of Oasis Ecology, Xinjiang University, Urumqi, China, [3]Key Laboratory of Smart City and Environment Modelling of Higher Education Institute, Xinjiang University, Urumqi, China, [4]Institute of Ecology, College of Urban and Environmental Sciences, Key Laboratory for Earth Surface Processes of the Ministry of Education, Peking University, Beijing, China, [5]Institute of Applied Artificial Intelligence of the Guangdong-Hong Kong-Macao Greater Bay Area, Shenzhen Polytechnic University, Shenzhen, China, [6]School of Artificial Intelligence, Shenzhen Polytechnic University, Shenzhen, China

Amidst the backdrop of global climate change, it is imperative to comprehend the intricate connections among surface water, vegetation, and climatic shifts within watersheds, especially in fragile, arid ecosystems. However, these relationships across various timescales remain unclear. We employed the Ensemble Empirical Mode Decomposition (EEMD) method to analyze the multifaceted dynamics of surface water and vegetation in the Bosten Lake Watershed across multiple temporal scales. This analysis has shed light on how these elements interact with climate change, revealing significant insights. From March to October, approximately 14.9–16.8% of the areas with permanent water were susceptible to receding and drying up. Both the annual and monthly values of Bosten Lake's level and area exhibited a trend of initial decline followed by an increase, reaching their lowest point in 2013 (1,045.0 m and 906.6 km2, respectively). Approximately 7.7% of vegetated areas showed a significant increase in the Normalized Difference Vegetation Index (NDVI). NDVI volatility was observed in 23.4% of vegetated areas, primarily concentrated in the southern part of the study area and near Lake Bosten. Regarding the annual components (6 < T < 24 months), temperature, 3-month cumulative NDVI, and 3-month-leading precipitation exhibited the strongest correlation with changes in water level and surface area. For the interannual components (T≥ 24 months), NDVI, 3-month cumulative precipitation, and 3-month-leading temperature displayed the most robust correlation with alterations in water level and surface area. In both components, NDVI had a negative impact on Bosten Lake's water level and surface area, while temperature and precipitation exerted positive effects. Through comparative analysis, this study reveals the importance of temporal periodicity in developing adaptive strategies for achieving Sustainable Development Goals in dryland watersheds. This study introduces a robust methodology for dissecting trends within scale components of lake level and surface area and links these trends to climate variations and NDVI changes across different temporal scales. The inherent correlations uncovered in this research can serve as valuable guidance for future investigations into surface water dynamics in arid regions.

KEYWORDS

surface water, NDVI, spatiotemporal variations, time-lag effect, EEMD, Bosten Lake

1 Introduction

Climate change is causing widespread impacts on both the environment and human society. The latest IPCC Sixth Assessment Report (AR6) has underscored the alarming fact that global average surface temperatures from 2011 to 2020 were 1.1°C higher compared to 1850–1900 (Kikstra et al., 2022), with an unprecedented warming rate for at least two millennia (Hantemirov et al., 2022). The Nationally Determined Contributions (NDC) of 2021 warn that if greenhouse gas emissions persist, we could witness more than a 1.5°C increase in global temperatures by 2030 (Fu et al., 2022; Saisirirat et al., 2022). This escalation of global warming poses an escalating threat, especially for ecosystems in arid and semiarid regions, notably lakes and vegetation systems (Rustad, 2008; Wu et al., 2021; Hao and Li, 2022; Wang et al., 2022).

Lakes, being exceptionally sensitive to natural fluctuations, serve as invaluable indicators of global climate change and local environmental shifts (Adrian et al., 2009; Zhang et al., 2018b; Wang et al., 2019a). In arid and semi-arid regions, water plays a pivotal role in shaping ecosystems, directly influencing the development and evolution of aquatic ecosystems and their counterparts (Ndehedehe et al., 2018; Zhang et al., 2018a; Gao et al., 2023). Inland lakes, integral to regional water resources, significantly impact the eco-environmental well-being of oasis areas, particularly for vegetation ecosystems (Liu et al., 2018b; Xue et al., 2019; Zhang et al., 2022b). Vegetation, acting as a vital nexus between soil, atmosphere, and water, drives material circulation and energy exchange in various ecosystems (Sylvain and Wall, 2011; Wang et al., 2023). Vegetation is often used as an indicator of ecological conditions. Thus, exploring the dynamic fluctuations of lakes and vegetation cover in arid regions and understanding how they respond to hydroclimatic variations are imperative for regional ecological conservation and the pursuit of sustainable development goals (SDGs).

In arid regions, lake water resources (e.g., surface area, water level, and volume), vegetation (e.g., Normalized Difference Vegetation Index (NDVI), net primary productivity, and gross primary productivity), and hydroclimatic factors (e.g., temperature, precipitation, and runoff) have garnered global attention (Jiapaer et al., 2011; Voss et al., 2013; Chen et al., 2020; Kooch et al., 2022; Liu et al., 2023). The relationships between lake surface area and hydroclimatic factors and between NDVI and hydroclimatic factors have been extensively scrutinized across various spatial scales (Shen et al., 2017; Nourani et al., 2021; Ogou et al., 2022; Gbetkom et al., 2023). Previous studies have illustrated the strong correlations between lake surface area and variables like temperature and precipitation in arid regions. Additionally, researchers have delved into the mechanisms governing vegetation responses to changing environments (Zhao et al., 2020; Han et al., 2021). However, vegetation dynamics in arid regions are not solely influenced by regional climate; they are also closely tied to water conditions, especially pertaining to lake water resources (Yang et al., 2020; Tuersun et al., 2020; Hou and Rusuli, 2022). This underscores the potential for complex feedback loops linking vegetation, hydroclimatic factors, and lake surface area. Consequently, it is insufficient to study one-to-one relationships in isolation. In the northwestern inland region of China, the regional climatic pattern has shifted from warm-dry to warm-wet, particularly since the 21st century (Fahu et al., 2023). Consequently, both regional lake surface areas (and water levels) and NDVI have exhibited notable transformations, characterized by both definite patterns and occasional anomalies (Ge et al., 2022b). Bosten Lake, situated in China, is the biggest freshwater lake in arid regions (Wang et al., 2018). Yet, the interplay among lake surface area, NDVI, and hydroclimatic factors within the Bosen Lake watershed remains enigmatic. In the upper reaches of this watershed, the Bayanbulak Grassland is the source of many rivers, such as the Kaidu, Ili, and Manas rivers, serving as a crucial ecological barrier in arid Xinjiang (Ye et al., 2017; Yao et al., 2018; Cheng et al., 2023). Meanwhile, the Kongque River in the lower reaches is not only the primary contributor of water to the Tarim River but also a significant contributor to the Lop Nur lake, playing a pivotal role in maintaining the ecological equilibrium of the entire Tarim watershed (Chen et al., 2006; Yang et al., 2020; Zhang et al., 2021). Although regional annual hydrological and meteorological factors, lake area, and vegetation cover in the Bosen Lake watershed have been studied to some extent, these studies have primarily focused on the late 20th century. Few attempts have been made to analyze monthly changes in these indicators and their relationships, particularly over the past two decades (Ge et al., 2022a). Given the backdrop of global warming, scrutinizing the intricate relationships among these elements can provide valuable insights into how lake surface area, vegetation, and hydroclimatic factors respond to evolving environments.

While some studies have explored the connection between climate change and water levels, area, and vegetation cover in the Bosten Lake watershed (Maimaiti et al., 2016; Yao et al., 2018; Wufu et al., 2020; Yanfei et al., 2021; Tang et al., 2022). The most have quantified the relative impacts of climate and vegetation variables on a single time scale, often making linear assumptions. This narrow focus overlooks the multi-timescale nature of these interactions, leading to underestimated impacts (Liu et al., 2018a). Consequently, a multi-timescale approach is essential for assessing the relative influence of climate change on vegetation and surface water changes. The ensemble empirical mode decomposition (EEMD) is particularly adept at handling non-stationary signals (Wu and Huang, 2009), This method is particularly effective in handling nonstationary signals. The residue captures the nonlinear trend of the data, including trend reversals, in addition to monotonic trends (Ji et al., 2014; Pan et al., 2018). Compared to wavelet analysis, EEMD is less affected by the length of the time series and is more adaptable to inherent data characteristics. It also reduces mode mixing and improves noise handling. EEMD is a reliable tool for extracting underlying physical information from nonlinear and nonstationary time series (Pan et al., 2018). Thus, EEMD stands as a suitable technique for uncovering the relationships between multi-time scale climate, surface water, and vegetation, and has been widely used (Wen et al., 2017; Liu et al., 2018a, 2021).

Given the challenges that have arisen in the Bosten Lake watershed over the past two decades, characterizing the regional

lake surface area, vegetation, and hydroclimatic factors is paramount. In this study, we employed the EEMD method to extract vegetation dynamics, surface water variations, and climate changes at multiple timescales. We then explored the relationships between these variables across various timescales, enriching our scientific understanding of conservation and restoration efforts for fragile ecosystems dependent on vegetation and water resources. Our objectives are: (1) To identify significant changes in the trends of vegetation, water levels, and area within the Bosten Lake in the past 2 decades. (2) To analyze the trends in the water level, area, NDVI, and climate change at different timescales. (3) To uncover the intricate relationships between these variables at different timescales.

2 Materials and methods

2.1 Study area

The Bosten Lake watershed is situated in the northeastern part of Xinjiang (82°80′–88°63′E, 40°73′–43°57′N), covering approximately 68,687 km^2 (Tuersun et al., 2020) (Figure 1). The watershed has a complex topography consisting of watersheds, mountains, and canyons. It spans an altitude range of 853–4,812 m (Tuersun et al., 2020). Precipitation in this region is mostly concentrated in May-September, with an average annual precipitation of 188.1 mm (Tuersun et al., 2020). Bosten Lake, the largest inland freshwater lake in the watershed, serves both as the tail lake of the Kaidu River and the source of Peacock Lake (Yao et al., 2018). Consequently, fluctuations in water resources directly impact the local ecosystemon development and evolution.

2.2 Data acquisition and processing

The main steps followed in this study are shown in Figure 2.

We sourced the Global Surface Water (GSW) dataset (30 m), provided by the Joint Research Centre (Pekel et al., 2016). This dataset offers maps displaying surface water location and temporal distribution from 1984 to 2021, along with statistics on surface water extent and changes. With an error rates of 1% for misclassification and 5% for omission. Researchers have consistently recognized it as a reliable reference since its 2016 release (Gorelick et al., 2017). We processed this dataset to extract monthly water frequency with a resolution of 1 km, all within GEE platform. Additionally, we employed the Hydroweb project (https://hydroweb.theia-land.fr/) as a database for water-level time series for lakes, reservoirs, and rivers (Crétaux et al., 2011). We collected the monthly water level and area data of the Bosten Lake Watershed from 2002 to 2020.

The Normalized Difference Vegetation Index (NDVI), derived from remote sensing, gauges vegetation's capacity to absorb solar radiation and reflects its coverage and growth to a certain extent. Consequently, NDVI is a key metric for monitoring ecological and

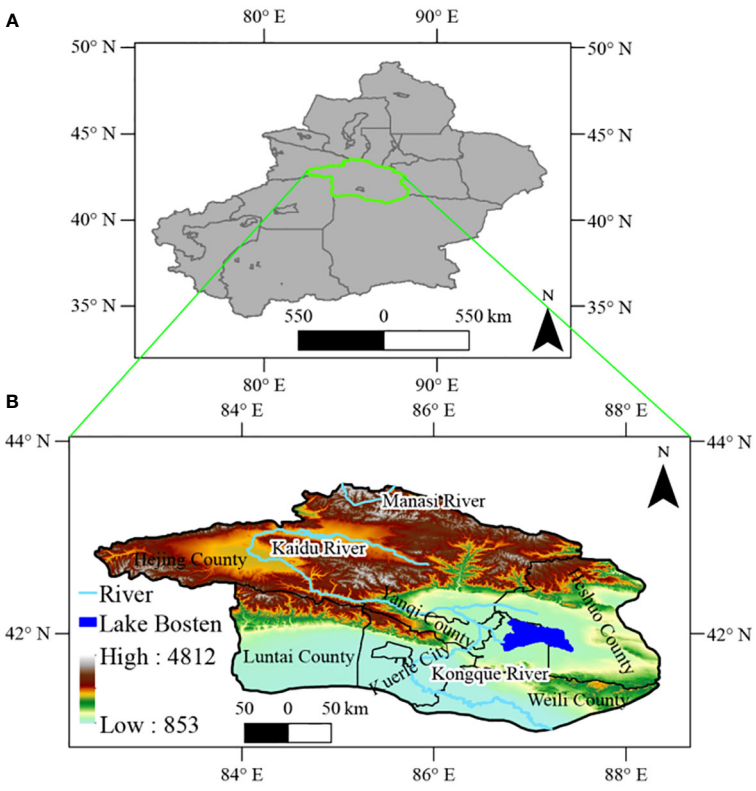

FIGURE 1
Geographic location **(A)** and DEM map **(B)** of the Bosten Lake Watershed.

FIGURE 2
Primary analysis process and framework for this study.

environmental changes on regional and global scales. Monthly NDVI data in the last two decades were obtained from the National Earth System Science Data Center of China (http://www.geodata.cn). This dataset was generated through monthly synthesis, mosaics, and clipping of the MOD13A2 V6 product (Didan, 2015). NDVI values between 0 and 0.1 represent non-vegetated areas (Liu et al., 2018b), so we masked areas with NDVI values below 0.1, considering pixels with NDVI ≥ 0.1 during the growing season (March–October) as stable vegetation areas.

Monthly precipitation and temperature data from 1901 to 2021 (~1 km), were obtained from the National Tibetan Plateau Scientific Data Center (https://data.tpdc.ac.cn/) (Ding and Peng, 2020).

2.3 Statistical analyses

In this study, Change point analysis (CPA) was used to estimate the area and hydrology of Lake Bosten via the R package 'changepoint' (Killick and Eckley, 2014). We used coefficients of variation to quantify the spatial variability of interannual changes in vegetation (Jiang et al., 2015). heil-Sen median trend analysis and the Mann-Kendall test can be used to analyze pixel-level trends in climatic elements (Fensholt et al., 2012; Deng et al., 2020). We used partial correlation analysis to decouple the interactions between lake level (area), NDVI, precipitation, and temperature. To further explore the relationship between the monthly response of lake level (area) and other variables (NDVI, precipitation, and temperature) (Wang et al., 2013). To further explore response relationships between lake water level (area) and other variables (NDVI, precipitation, and temperature) on a monthly scale, we conducted partial correlation analysis with time-lag (-accumulation), building upon the approach of (Gessner et al., 2013; Amantai et al., 2024).

2.4 Ensemble empirical mode decomposition

Natural phenomena time-series data, such as NDVI, climate variables, and hydrological variables, are typically nonlinear and non-stationary (Verma and Dutta, 2013; Wen et al., 2017). Interannual variability is often affected by noise, fluctuations, or mutations, leading to an insufficient understanding of the interannual variability problem (Verbesselt et al., 2010). To analyze the complex interannual changes in climate factors,

vegetation changes and hydrological processes, we decomposed these time series using EEMD.

Time series data (t) were decomposed into an intrinsic mode function (IMF) components and a residual using the EEMD method. Each IMF component has a respective mean period T, calculated by counting the number of extrema divided by twice the length of the data (t) (Hawinkel et al., 2015). Following the framework suggested by Hawinkel, the n IMFs and residuals were classified into noise IMFs, annual IMFs, and interannual IMFs based on their mean periods T (as shown in Figure 2). Referring to Wen et al. (Wen et al., 2017), in this study, IMFs with T < 6 months were grouped as noise IMFs, those with T between 6 and 24 months were grouped as annual IMFs (seasonal change components), and the remaining IMFs and the residuals were grouped as interannual IMFs, representing overall trend components. The sums of the grouped IMFs were presented as the noise component (Cnoise), annual component (Cannual), and interannual component (Cinterannual) (Supplementary Figures S1–S5).

3 Results

3.1 Surface water spatiotemporal distribution pattern

First, we utilized the GSW data to analyze the monthly water frequency and spatial distribution of each pixel point in Bosten Lake from 2001 to 2020 (excluding data from November to February). The monthly frequency remained constant at 100%, indicating a consistent presence of permanent surface water. However, there were fluctuations. From March to April, the permanent water area increased to approximately 1443.76 km^2, subsequently declining to its lowest of 1396.40 km^2 in August, followed by a rebound to 1407.08 km^2 from September to October. During this period (March to October), approximately lake's surface area experienced a risk of receding and drying (Figure 3).

Next, we examined the monthly and annual average change trends of the area and water level of Bosten Lake (Figure 4). The monthly average water level exhibited an upward trend from January to April, stabilizing around 1046.5 m and fluctuating within 0.2 m from April to October, while it decreased from October to December. The lake area peaked at around 966.6 km^2 from January to April. From April to December, the area varied within a 5 km^2 range. However, the yearly averages indicated a continuous decline in both water level and area, reaching their lowest points in 2013 (1045.0 m and 906.6 km^2, respectively) and subsequently increasing to 1047.61 m and 1017.8 km^2, respectively, in 2020.

We applied CPA to explore shifts in the area and water level time series of Bosten Lake using Hydroweb project data (Figure 5). Two change points were identified, occurring in June 2006 and January 2016. This analysis revealed three stages of change from 2002 to 2020: a rapid reduction stage (January 2002 to June 2006) with change rates of −0.0607 m/month, and −1.6726 km^2/month, respectively and an R square as high as 0.91 and 0.87, respectively; a stable period (June 2006 to January 2016) with R squares of only 0.02 and 0.03; a gradual increase stage (January 2016 to December 2020) with increasing rates of 0.0046 m/month and 0.1423 km^2/month and R squares of 0.2 and 0.18, respectively.

3.2 Regional NDVI change characteristics

We analyzed spatio-temporal variations of NDVI (Figures 6A–D) in the Bosten Lake Watershed across seasons (i.e., areas with NDVI ≥ 0.1). NDVI increased from spring to winter and then decreased, with mean values of 0.18, 0.34, 0.20, and 0.14, respectively. The average NDVI of the growing season (March to October) (Figure 6E) ranged from 0.1 to 0.63 and was 0.27. High NDVI values were mainly concentrated in the upper reaches of the Kaidu River, west of Bosten Lake, and west of the Kongque River from spring to autumn. Conversely, NDVI values decreased in most areas during the winter, except for certain mountainous regions.

The average coefficient of variation of the NDVI in the past 20 years was 0.17 (Figure 7). Lower levels of volatility were predominantly found in the northwestern mountains and upper reaches of the Kaidu River. Conversely, in the plain areas adjacent to the mountain base, specifically in the southern study area and southeast of the Bosten Lake, medium and high levels of volatility were observed. Approximately 66.4% of vegetated areas had medium to high volatility, with 23.4% displaying high volatility (Table 1), suggesting significant fluctuations in vegetation coverage within the Bosten Lake watershed.

Stable vegetated areas (NDVI ≥ 0.1 during the growing season) exhibited an increase in NDVI from 2001 to 2020 (Figure 8), with an average Theil-Sen median slope of 2 (10^{-3}·yr^{-1}), ranging from −0.018 to 0.026. NDVI improved (i.e., with a Theil-Sen median slope >= 0.0005), remained stable (i.e., with a Theil-Sen median |slope| <= 0.0005), and degraded (i.e., with a Theil-Sen median slope < −0.0005) in 7.7%, 83.3%, and 9.0% of the vegetated areas, respectively. The area with significantly improved NDVI was mainly located west of the Konque River and near Lake Boston, correlating with regions of high volatility.

3.3 Spatio-temporal dynamics of precipitation and temperature

Temperature slightly decreased in this study over the last 2 decades (Figure 9A), with an average Theil-Sen median slope of −0.002 (°C/yr), ranging from −0.072 to 0.084. Conversely, precipitation increased (Figure 9B), with an average Theil-Sen median slope of 0.87 (mm/yr), ranging from −2.26 to 5.35. Temperature and precipitation increased in 34.1% and 88.9% of the study areas, respectively, while they remained stable in 4.3% and 0.1% of the study areas, respectively. However, the temperature decreased in 61.6% of the areas compared to 11.0% for precipitation. Temperature changes were spatially diverse, with some northern areas experiencing increases due to higher terrain, while the lower southern research area and upper reaches of the Kaidu River saw decreases. The changes in precipitation were more uniform in spatial distribution except in the northern and

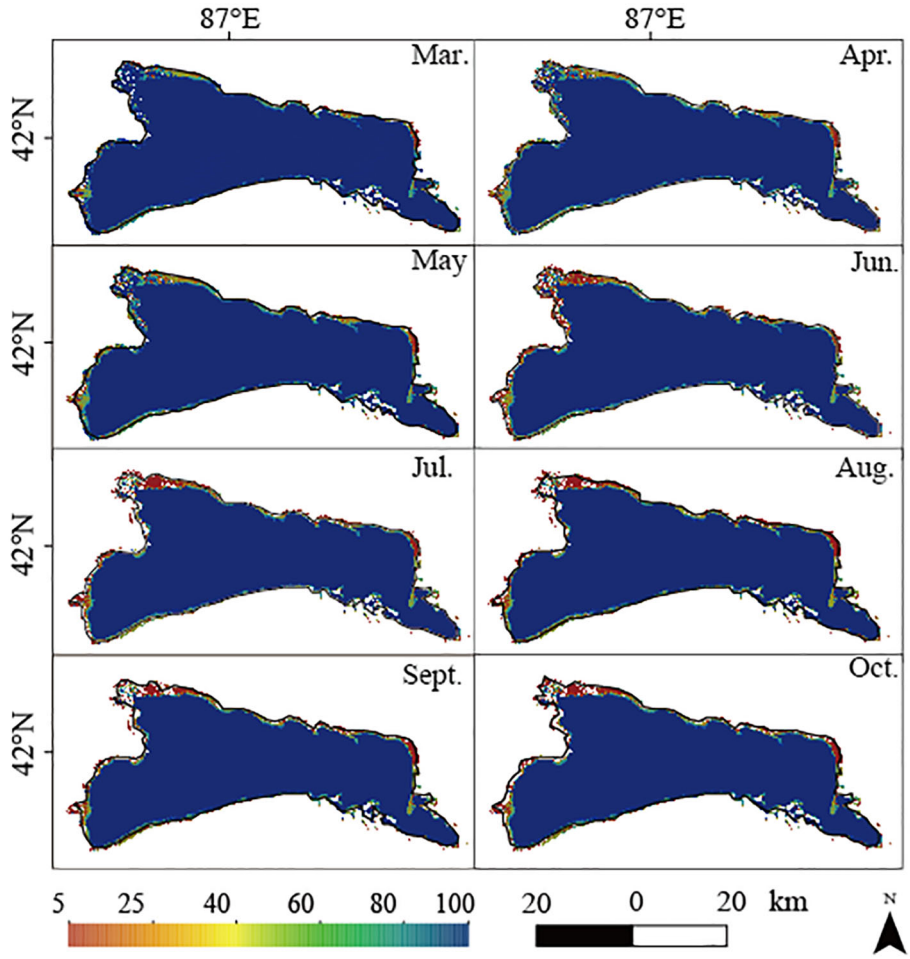

FIGURE 3
The spatio-temporal variation characteristics of the monthly water frequency.

southeastern parts of the study area where there was an increasing trend in precipitation.

3.4 Correlations among water level, area, NDVI, and climatic factors in different components

3.4.1 Variation trends of water level, area, NDVI and climate factors in different components

We calculated correlation coefficients among raw values of water level, area, NDVI, and climate variables. Precipitation and temperature showed strong correlations with NDVI (correlation coefficients of 0.82 and 0.90, respectively), but the correlations between water level, area, and other factors did not reach significance (Supplementary Table S2).

As water level and area did not exhibit straightforward stationary patterns, we employed the EEMD method to differentiate between their annual and interannual components (Supplementary Figures S1–S5). By comparing these components across the five parameters, we could validate their changes throughout the observation period (Figure 10). Within this plot, each curve's values are normalized on the sum of amplitudes, combining annual components and averaged seasonal components. Our analysis revealed consistent trends in water level and area throughout the year, reaching their peak in May. In contrast, the variations in NDVI and precipitation displayed synchronization, albeit with a lag compared to the water level and area, peaking in July. Temperature's seasonal components fell in between water level (area) and NDVI (precipitation) in terms of timing, occurring earlier than precipitation and NDVI, but without the same magnitude of change range as water level (area). Temperature, however, also peaked in July. Over the years, water level and area exhibited a consistent trend of initial decline followed by increase, hitting their lowest point in 2013. Temperature and precipitation showed fluctuating downward and upward trends, respectively, with peaks in 2007, 2009, and 2016, and a trough in 2011 and 2018, while NDVI exhibited an upward trend post-2011.

3.4.2 Inner relationship of water level, area, NDVI, and climate factors in different components

To perform a comprehensive joint analysis of climate, vegetation, and hydrology, we conducted partial correlation, time-lag and time-

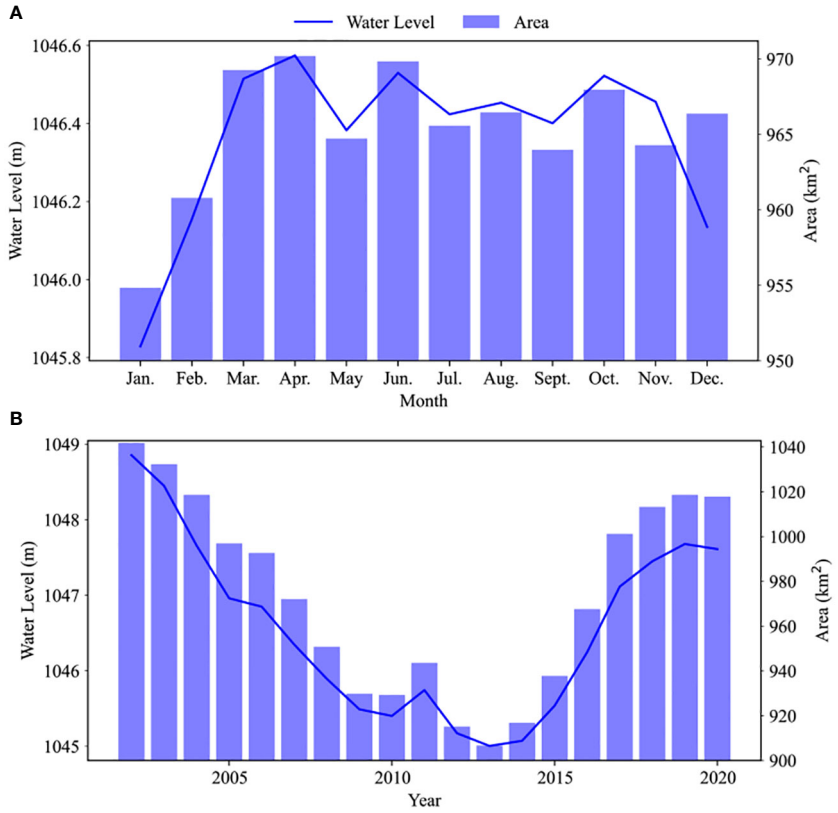

FIGURE 4
The monthly **(A)** and annual **(B)** average change trends of the area and water level in Bosten Lake.

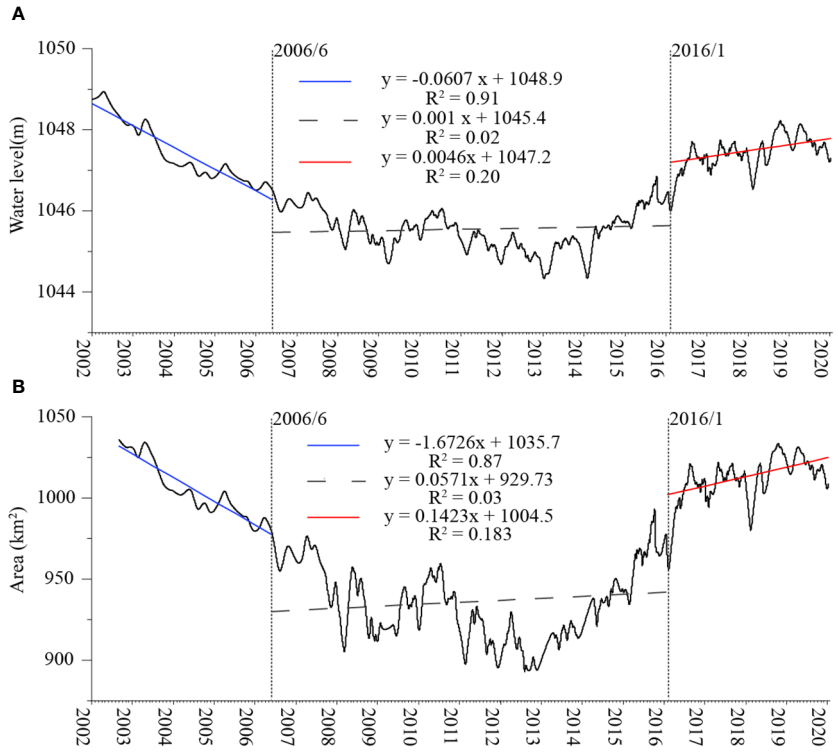

FIGURE 5
Results of change point analysis of water level **(A)** and area **(B)**.

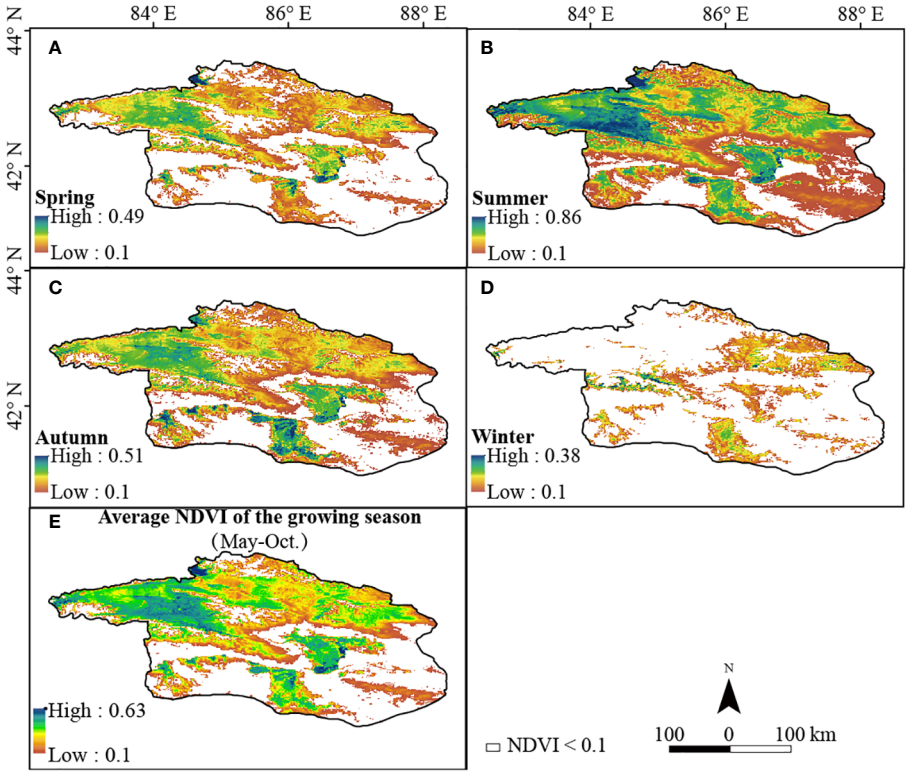

FIGURE 6
The spatio-temporal variation characteristics of the NDVI in four seasons **(A–D)**. **(E)** is average NDVI of the growing season (May-Oct.).

accumulation analyses of water level (area), NDVI, precipitation, and temperature for the two components. These analyses revealed differences in time-lag and time-accumulated effects between the components when compared with the raw data. In both components, the partial correlation between water level (area) and NDVI, precipitation, and temperature surpassed the significance threshold of 0.05, resulting in significantly improved correlation coefficients.

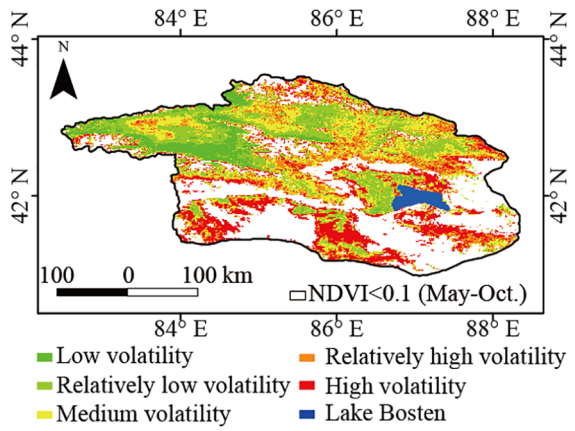

FIGURE 7
Spatial distribution of the coefficient of variation of the inter-annul NDVI in the Bosten Lake Watershed from 2001 to 2020.

For the annual components, the strongest correlation was observed between temperature and water level (area), reaching up to 0.352 (0.440), indicating a positive relationship. Precipitation followed, exhibiting a correlation coefficient of 0.278 (0.234), while NDVI displayed a negative correlation with water level, with a coefficient of −0.158 (−0.284). In contrast, for the interannual components, the correlation coefficients were generally lower than those in the seasonal components. The values between temperature, precipitation, NDVI, and water level (area) were 0.218 (0.210), 0.147 (0.193), and −0.155 (−0.142), respectively. The time-lag and time-accumulated effects differed as well. In the case of seasonal components, temperature and water level (area) changed in sync, with a 3-month lag between precipitation and water level and a 3-month accumulation effect between NDVI and water level.

TABLE 1 Coefficient of variation of NDVI in the Bosten Lake Watershed.

CVNDVI	Volatility degree	Area percentage (%)
≥0.20	High-volatility	23.4%
0.15 ≤ CVNDVI < 0.20	Relative-high volatility	16.9%
0.10 ≤ CVNDVI < 0.15	Medium volatility	26.1%
0.05 ≤ CVNDVI < 0.10	Relatively low volatility	25.1%
<0.05	Low volatility	8.5%

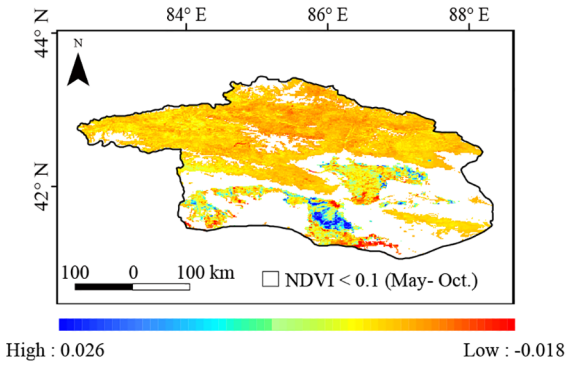

FIGURE 8
Spatial distribution of the Theil-Sen slopes for NDVI in the Bosten Lake Watershed from 2001 to 2020.

Conversely, for the annual component, there was a 3-month lag between temperature and water level (area), while precipitation and water level exhibited a 3-month accumulation effect. Notably, NDVI and water level changed simultaneously.

4 Discussion

4.1 Possible response mechanisms

The energy balance and dynamic processes of the hydrological cycle are at the heart of the complex relationships between vegetation, climate and hydrological parameters. Climate change is an important controlling factor. Naturally, precipitation significantly influences regional water bodies and levels. In arid and semi-arid regions like the Bosten Lake area, lake hydrological conditions are particularly sensitive to inflow runoff. To better understand how water area and level in the study area respond to these influences, we conducted analyses using regional hydrometeorological datasets.

Between 1960 and 2019, the regional average inflow runoff reached 3.97×10^9 m^3 (Figure 11). In terms of the variation trend, the overall inflow increased at a rate of 1.90×10^8 m^3/10a ($p < 0.05$), but there were also evident phased changes. Overall, the runoff changes in the Kaidu, Huangshuigou, and Qingshui rivers were consistent with the total inflow runoff, with relatively large interannual changes in the Kaidu River. In comparison, the Huangshuigou and Qingshuihe rivers experienced stable changes

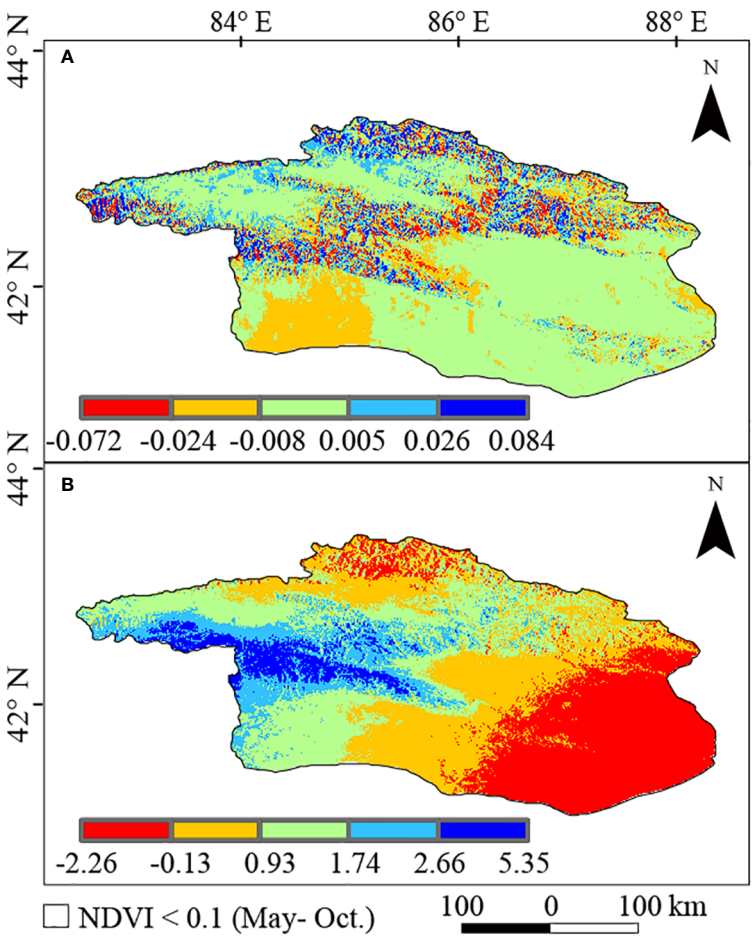

FIGURE 9
Spatial distribution of the Theil-Sen slopes for temperature **(A)**, precipitation **(B)** in the Bosten Lake Watershed from 2001 to 2020.

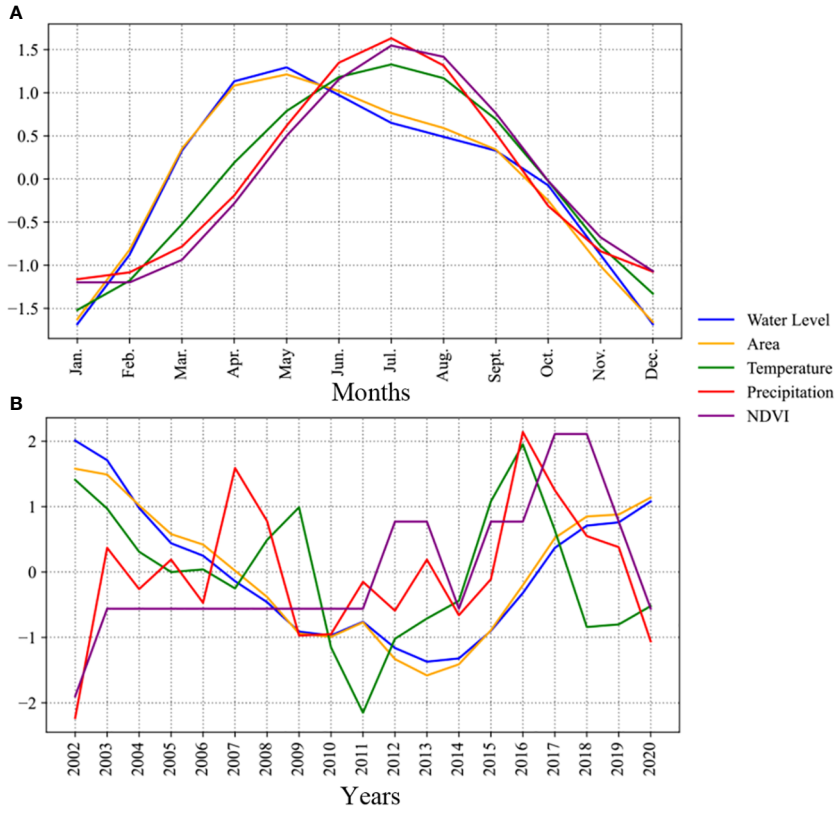

FIGURE 10
Seasonality **(A)** and trends **(B)** of water level, area, temperature, precipitation and NDVI in the Bosten Lake Watershed.

before the 21st century, and there have been significant interannual fluctuations since then.

The average runoff distribution for each month of the Kaidu and Huangshuigou Rivers shows a single-peak pattern. The Kaidu River's dry season lasts from November to March, accounting for approximately 20% of the year, with the highest runoff occurring from June to August each year, making up approximately 45% of the annual total. The flow occurs in July of each year. Huangshuigou's dry season lasts even longer, from October to April, accounting for approximately 27% of the annual runoff, while the wet season is

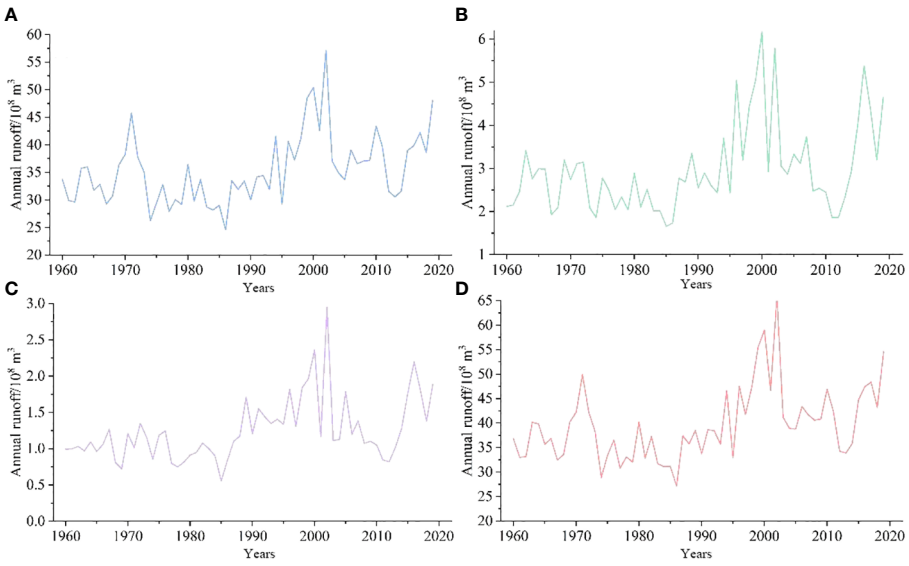

FIGURE 11
Annual runoff in Bosten Lake Watershed. **(A)** Kaidu River, **(B)** Huangshuigou River, **(C)** Qingshuihe River, and **(D)** Total runoff.

mainly from June to August, representing approximately 57% of the annual runoff. As shown in Figure 12, the changes in Huangshuigou from October to April of each year are not evident. Beginning in May, the average monthly runoff increased significantly. The runoff distribution is more concentrated from May to September. The runoff from the Qingshuihe River was similar to that from the Huangshuigou River.

Previous research has emphasized that Bosten Lake relies primarily on surface runoff, with the Kaidu River contributing a significant portion (84.7%) compared to precipitation (5.2%) (Yanfei et al., 2021). This suggests that, in this context, inflow, especially from the Kaidu River, has a more substantial impact on the lake's water level and area, aligning with the correlation between Kaidu River runoff and lake water level and area changes. Notably, fluctuations in runoff from various hydrological stations from 2005 to 2015 did not exhibit an overall trend, coinciding with the relatively stable water level and area of Bosten Lake in 2006 and 2016 (Figure 5). Moreover, the stability of the lake water level and area from April to October corresponds to the dry period from November to March for the Kaidu River (Figure 12).

The variation in the Kaidu River's runoff is a complex process influenced by multiple factors. In this watershed, runoff replenishment primarily results from mountain precipitation (61.5%) and snowmelt (38.5%) (Yao et al., 2018). Interestingly, despite precipitation constituting the majority of this influence, the correlation between precipitation and Bosten Lake's water level and area is not significant.

This phenomenon can be attributed to the distribution of precipitation and snowmelt over the runoff year. Snow accumulation in the Kaidu River watershed begins in November and persists until March (Zhao et al., 2021). With rising temperatures in April and May, snowmelt becomes the primary source of river replenishment (Zhao et al., 2021). During this period, spring snowmelt-induced floods are common, and even on April 24, 2011, they exceeded summer floods (Zhao et al., 2021). Studies have shown that from April to July, snowmelt contributes to over 55% of the annual runoff (Chen et al., 2015). Conversely, precipitation in the Kaidu River watershed over the past 60 years has exhibited a highly uneven trend, primarily concentrated in the summer (Yao et al., 2018). For example, in locations like Huangshuigou, most of the annual precipitation occurs during the summer, with seasonal precipitation contributing up to 90% of the annual total. Monthly variations in annual precipitation can be extreme, reaching up to 135 times (Yao et al., 2018).

Considering these factors, the temporal distribution of precipitation and snowmelt during a wet year, along with their regulatory impacts on aquatic systems, could potentially mask the straightforward correlation between precipitation levels and the fluctuations in both water level and surface area of Bosten Lake. Although precipitation significantly influences overall runoff, in the specific context of Bosten Lake, the relationship between precipitation and lake water level and area might be influenced by intricate factors, rendering it statistically insignificant.

4.2 Interference of anthropogenic activities

Human economic activities have profoundly impacted the ecological security and sustainable development of the Bosten Lake watershed over the past decade. Increased human activities, particularly those related to agricultural irrigation, industrial water usage, and domestic water consumption, have influenced the inflow volume of the Bosten Lake (Yao et al., 2018). The expansion of agricultural and irrigation areas, coupled with rapid socioeconomic growth, has led to a rapid increase in water intake and consumption for irrigation, resulting in reduced the inflow volume of the Bosten Lake and subsequent declines in water levels (Yao et al., 2018). The

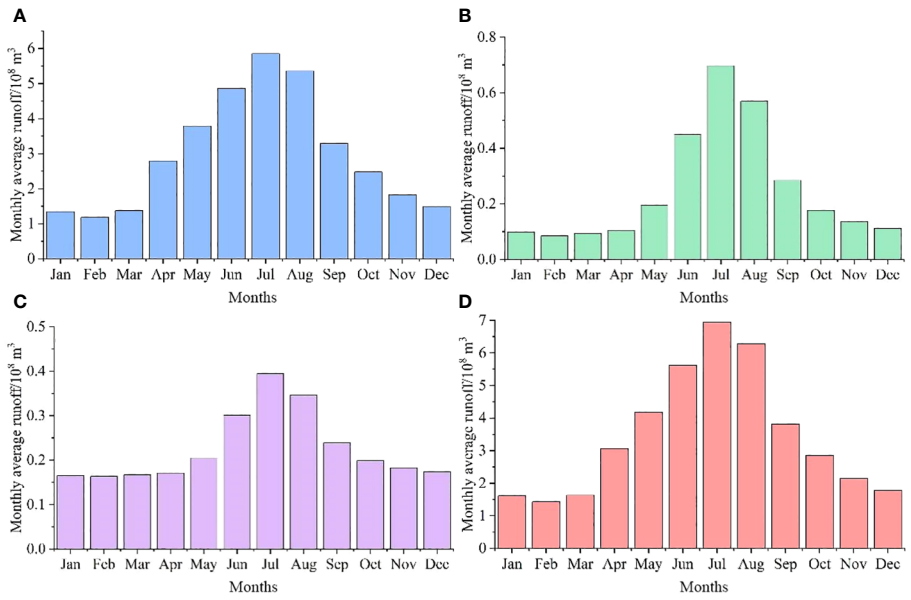

FIGURE 12
Monthly runoff in Bosten Lake Watershed. **(A)** Kaidu River, **(B)** Huangshuigou River, **(C)** Qingshuihe River, and **(D)** Total runoff.

influence of human activities on the lake's inflow has grown progressively, especially in the 21st century, with their impact intensity reaching 80.80% (Junqiang et al., 2021).

Additionally, ecological water transfer projects have affected the Bosten Lake watershed since 2000. While these projects have had positive effects on groundwater recovery and vegetation restoration downstream of the Tarim River (Yao et al., 2018), reduced water inflow from the Kaidu River and increased economic water usage have led to continued declines in Bosten Lake's water level, leading to severe water scarcity in the downstream Kuche River area and environmental degradation (Junqiang et al., 2021). Fortunately, from 2016 to 2019, ecological water transfer from Bosten Lake to the downstream Kuche River reached a cumulative volume of 1.7×10^9 m^3, halting the degradation of the downstream watershed (Junqiang et al., 2021). This is confirmed by the changes in flow observed at the Tashidian hydrological station in the Kuche River (Figure 13).

In conclusion, human activities have significantly impacted the water resources and ecological environment of the Bosten Lake watershed. Factors such as agricultural irrigation, ecological water transfer, and economic development have variously altered the lake's hydrological cycle, exacerbated by uncertainties in water resources due to global warming. The future trajectory of Bosten Lake will depend on achieving a balance between human needs and ecological preservation within the framework of sustainable development. While some success has been achieved in ecological restoration, the negative effects of human activities and climate change on wetland water bodies and vegetation must be acknowledged for effective management and control measures. Planned hydrological engineering to regulate seasonal hydrological processes and improve the efficiency of water use may be the key to coping with water resource problems in the future. Addressing the varying influencing factors in different periods and regions is crucial for achieving sustainable development and ecological security in the Bosten Lake wetlands.

4.3 Relationship among water level, area, climate, and NDVI variations at multiple time scales

Previous studies examining the correlation between Bosten Lake's water level and area and climate change have yielded inconsistent conclusions. Dai et al. suggested that annual average evaporation, temperature, and precipitation are closely linked to dynamic changes in the lake's area (Dai et al., 2020), while Peng et al. found that the interannual variation in the lake area showed no significant correlation with precipitation, evaporation, and accumulated temperature, but exhibited higher correlations with intra-seasonal variations in these meteorological factors (Yanfei et al., 2021). Overall, NDVI in the Bosten Lake watershed was negatively correlated with temperature on an interannual scale, while it was positively correlated with precipitation. On a monthly scale, NDVI exhibited strong positive correlations with both precipitation and temperature. However, limited research exists on the relationship among lake area, water level, and NDVI changes. Our study indicates that, although NDVI maintains a robust positive correlation with precipitation (correlation coefficient of 0.82) and temperature (correlation coefficient of 0.79) on a monthly scale, the correlations between monthly lake water level, area, temperature, precipitation, and NDVI did not reach significance (Supplementary Table S2). Nevertheless, through EEMD decomposition, we revealed that the relationship among lake water level, area, climate, and NDVI changed over different time scales, achieving significance ($p < 0.05$), influenced by the cumulative effects of varying hydrothermal conditions.

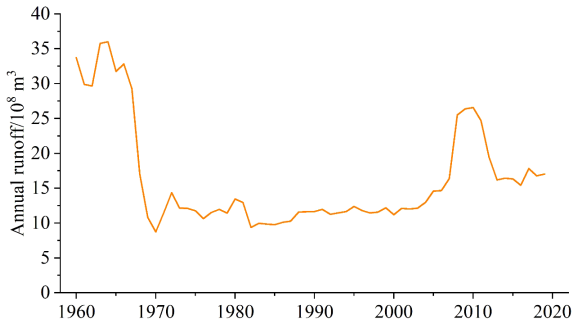

FIGURE 13
Runoff of Tashidian hydrological station.

At the annual scale ($6 < T < 24$ months), the strongest positive correlation was observed among the lake water level, area, and temperature, exhibiting simultaneous changes (Supplementary Table S3). This correlation is likely due to rising temperatures leading to increased glacial meltwater and subsequently augmenting the inflow volume of the lake. Following temperature, precipitation had a significant influence, positively correlating with lake water level and area but with a 3-month lag. This pattern corresponds with research on other lakes in arid regions, such as Lake Chad, where the lake's response to changes in watershed rainfall was delayed by 112 days (Gbetkom et al., 2023). The delay in lake water level and area changes compared to precipitation can be attributed to the arid soil's high infiltration rates, which initially absorb increased precipitation and become saturated. As precipitation continues, reduced infiltration rates cause more runoff, gradually diminishing soil moisture input and causing the lag in lake changes (Wang et al., 2019b).

Furthermore, there was a negative correlation between lake water level, area, and the 3-month cumulative NDVI, potentially due to vegetation intercepting surface runoff, thereby reducing the volume of water entering the lake (Huang et al., 2023).

At the interannual scale ($T > 24$ months), which represents the overall trend, the correlations among lake water level, area, temperature, precipitation, and NDVI were weaker than those at the annual scale, and the lagged cumulative effects varied (Supplementary Table S3). As the temporal scale increased, the effects of temperature and NDVI on lake water levels accelerated gradually, whereas the influence of precipitation slowed down. Over longer timescales, gradual temperature changes and shifts in vegetation cover can have cumulative effects on lake water levels. For instance, increasing temperatures may enhance evaporation rates, contributing to a more pronounced effect on water levels over time (Woolway et al., 2020; Zhai and Tao, 2021). Similarly, changes

in vegetation cover can affect runoff patterns and water retention, resulting in gradual and amplified effects on lake water levels (Zhai and Tao, 2021). Precipitation, particularly in arid and semiarid regions, can exhibit high annual variability. Over longer time scales, the influence of individual precipitation events might average out, leading to a reduced impact on lake water levels compared to other factors like temperature and vegetation changes. Research has indicated that since the mid-1980s, under the influence of global climate change, extreme precipitation events in the arid northwestern region of China have shown trends of increased intensity, duration, and frequency (Hu et al., 2021). The Tianshan region in Xinjiang stands out for its frequent extreme hydrological events, marked by the highest annual extreme precipitation occurrences, particularly concentrated in the central Tianshan mountain area with notable intensity (Yao et al., 2018). This increase in both the frequency and intensity of extreme precipitation events has led to increased annual precipitation, significantly affecting the interannual variability of the Kaidu River's runoff. Additionally, the arid nature of the region's soil could lead to high initial infiltration rates (Wang et al., 2019b), causing increased precipitation to be absorbed and not immediately reflected in the lake water levels. Therefore, these varying characteristics might result in longer-lasting influences of temperature and NDVI on lake water levels over extended time scales, whereas the effects of precipitation may be more pronounced in the short term but exhibit greater fluctuations over time.

4.4 Temporal variability in vegetation response to climate and its possible reasons

We also calculated the spatial pattern of the time-lag and time-accumulation months of climatic factors affecting NDVI on a monthly scale in the Bosten Lake watershed from 2001 to 2020 (Figure 14). The main combinations of time-lag and time-accumulation months for precipitation were TL-0-TA-1 (0-month lag and 1-month accumulation), TL-2-TA-0, and TL-0-TA-2, accounting for 28.4%, 22.9%, and 14.5%, respectively (Figure 14). The primary combinations for temperature were TL-1-TA-0 (1-month lag and 0-month accumulation), TL-0-TA-1, and TL-3-TA-0, accounting for 25.0%, 20.4%, and 13.6%, respectively (Figure 14). Generally, the time-lag effects of precipitation and temperature were significant in the western and northern parts of the study area, whereas the time-accumulation effects were significant around Bosten Lake. However, in the southern part of the study area, the time-accumulation effect of precipitation and the time-lag effect of temperature played a role simultaneously.

The climatic and topographical conditions in the northwestern part of the watershed likely resulted in a complex interplay among precipitation, temperature, and vegetation growth. Glacial meltwater serves as a crucial water source for vegetation growth in this region (Yao et al., 2018). Rising temperatures lead to increased glacier melting, higher runoff, enhanced vegetation coverage, and ecological benefits (Li et al., 2015). The intricate interactions of precipitation with soil cycling and plant transport gradually supply the needed water through soil infiltration and root absorption (Bodner et al., 2015). Due to the delayed effects of this process, the response of vegetation growth to precipitation and temperature may exhibit a lag. In contrast, in the southern region, with lower elevation and relatively sparse vegetation, precipitation can be swiftly absorbed by the soil or discharged through surface runoff. However, the cumulative impact of precipitation may accumulate over time, augmenting soil moisture content and stimulating vegetation growth. Conversely, temperature variations might lag in impacting vegetation growth, with limited vegetation cover leading to a more direct influence of temperature on soil and water heat exchange processes (Bodner et al., 2015).

This study explored the multi-timescale relationships between hydrology, vegetation dynamics and climate change in the Bosten Lake basin. It provided a scientific understanding of water resource management (lake chief scheme) in the basin to help policy formulation. With better observational data (high spatial and temporal resolution), the methodology of this study can be applied to better understand long-term trends and patterns. The interactions between climatic factors, hydrology, vegetation and human activities are complex, and the long-term impacts of climate change on ecosystems remain uncertain. Therefore, future research will require the development of predictive models and scenario simulations combining hydrological, ecological and socio-economic data.

4.5 Watersheds and SDGs in dryland: a comparative analysis

This study examined the relationship between lakes, vegetation, and climate change in dryland watersheds, which was relevant to the advancement of the SDGs. Climatic factors are the dominant factors of lake and NDVI changes in dryland watersheds (Woolway et al., 2020). By comparison, most studies indicated that temperature exerted a more significant impact on vegetation (Tan et al., 2018; Zhang et al., 2020; Rousta et al., 2023). However, in both the Aral Sea study and this study, it was found that the impact of precipitation on vegetation was more significant (Duan et al., 2022). The amount of precipitation determines the amount of surface water available (Berdimbetov et al., 2021). Vegetation interception plays a moderating role in watersheds of drylands (Zhang et al., 2022a). Ecological restoration therefore focuses on restoring vegetation and enhancing its resistance. Compared to previous studies, this study explored the lag effect of climate on NDVI in watershed landscapes, which aided in the development of ecological policies for arid ecosystems (Dai et al., 2020). In addition, the studies found that warmer temperatures and increased evapotranspiration were the primary drivers of lake shrinkage in drylands (Kiage and Douglas, 2020; Tuersun et al., 2020). It is noteworthy that the periodicity between them is more vital among climate, NDVI, and lake changes. Human activities can have positive effects after recognizing ecological and hydrological processes. Anthropogenic water resource management has been effective in mitigating the decline in ecosystem functioning within the watershed caused by climate change (Bryan et al., 2018). We recommend researchers should clarify not only the interrelationships between climate, vegetation, and lakes but also time-lag and time-

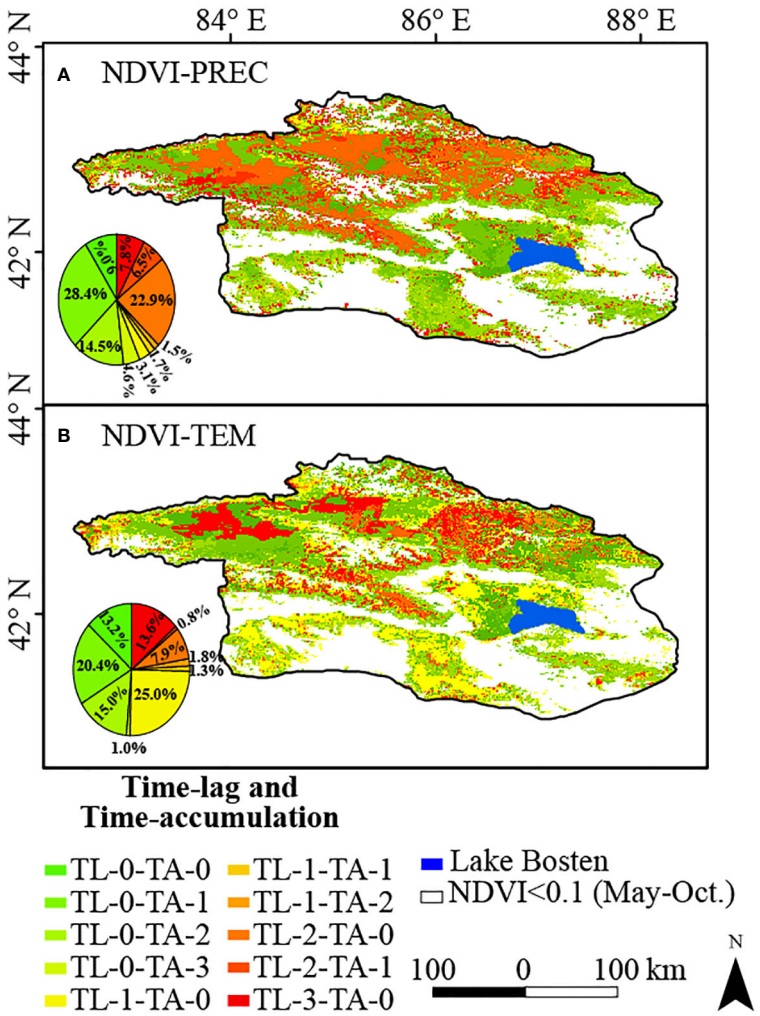

FIGURE 14
The effects of **(A)** precipitation, **(B)** temperature time-lag and time-accumulation to NDVI in the Bosten Lake Watershed from 2001 to 2020.

accumulation. These findings can help in developing more resilient ecosystem management strategies by considering ecological and hydrological processes to advance the SDGs for dryland ecosystems.

5 Conclusion

Bosten Lake, China's largest inland freshwater lake, has undergone significant transformations in recent years. This study employed the EEMD method to analyze the multi-time scale relationship among surface water, vegetation dynamics, and climate change in the Bosten Lake watershed. The water level and area of Bosten Lake have experienced three distinct phases: rapid decline (January 2001–June 2006), stability (June 2006-January 2016), and gradual increase (January 2016-December 2020). Vegetation within the watershed exhibited notable fluctuations, with 7.7% of the vegetation demonstrating a greening trend. Human activities have influenced the original time series, resulting in limited correlation at the monthly scale. Significantly, EEMD uncovered the underlying trends and correlations in the data. The correlations at the intra-annual scale surpassed those at the interannual scale. With an increasing time scale, the cumulative lag effect becomes more pronounced, accelerating the influence of temperature and NDVI values on lake water levels, while diminishing the impact of precipitation. The outcomes of this study enhance our understanding of the complex relationships among surface water, vegetation dynamics, and climate change across multiple timescales.

Data availability statement

Publicly available datasets were analyzed in this study. This data can be found here: https://hydroweb.theia-land.fr/, http://www.geodata.cn.

Author contributions

XG: Formal analysis, Funding acquisition, Resources, Writing – original draft, Writing – review & editing. JD: Data curation, Project

administration, Supervision, Validation, Writing – review & editing. NA: Data curation, Investigation, Methodology, Software, Writing – review & editing. JX: Formal analysis, Visualization, Writing – review & editing. JW: Investigation, Resources, Supervision, Writing – original draft.

Funding

The author(s) declare financial support was received for the research, authorship, and/or publication of this article. This work was jointly supported by the Tianchi Talent Introduction Programme (Young Doctor), the Project of 2024 Philosophy and Social Science Internal Cultivation (24FPY001), the Universities Basic Research Operating Expenses Scientific Research Projects of Xinjiang (XJEDU2023P019), Basic Research Program of Shenzhen (20220811173316001), Specific Innovation Program of the department of Education of Guangdong Province (2023KTSCX315), Shenzhen Polytechnic Research Fund (6023310031K, 6023271008K), Open Research Fund Program of MNR Key Laboratory for Geo-Environmental Monitoring of Great Bay Area (GEMLab-2023014).

Conflict of interest

The authors declare that the research was conducted in the absence of any commercial or financial relationships that could be construed as a potential conflict of interest.

Publisher's note

Supplementary material

The Supplementary Material for this article can be found online at: https://www.frontiersin.org/articles/10.3389/fpls.2024.1323445/full#supplementary-material

SUPPLEMENTARY TABLE 1
Time-Lag and time-accumulation correlation analysis combination.

SUPPLEMENTARY TABLE 2
Correlation coefficient statistics of raw data.

SUPPLEMENTARY TABLE 3
Results of partial correlation and time-lag (-accumulation) analysis.

SUPPLEMENTARY FIGURE 1
Applying EEMD to extract seasonal, annual, and interannual components of Areal time series in the Bosten Lake Watershed. "T" means the average period of each IMF.

SUPPLEMENTARY FIGURE 2
Applying EEMD to extract Cseasonal, Cannual, and Cinterannual components of Water level.

SUPPLEMENTARY FIGURE 3
Applying EEMD to extract Cseasonal, Cannual, and Cinterannual components of NDVI.

SUPPLEMENTARY FIGURE 4
Applying EEMD to extract Cseasonal, Cannual, and Cinterannual components of precipitation.

SUPPLEMENTARY FIGURE 5
Applying EEMD to extract Cseasonal, Cannual, and Cinterannual components of temperature.

References

Adrian, R., O'Reilly, C. M., Zagarese, H., Baines, S. B., Hessen, D. O., Keller, W., et al. (2009). Lakes as sentinels of climate change. *Limnol Oceanogr.* 54, 2283–2297. doi: 10.4319/lo.2009.54.6_part_2.2283

Amantai, N., Meng, Y., Wang, J., Ge, X., and Tang, Z. (2024). Climate overtakes vegetation greening in regulating spatiotemporal patterns of soil moisture in arid Central Asia in recent 35 years. *GIScience Remote Sens.* 61, 2286744. doi: 10.1080/15481603.2023.2286744

Berdimbetov, T., Ilyas, S., Ma, Z., Bilal, M., and Nietullaeva, S. (2021). Climatic change and human activities link to vegetation dynamics in the aral sea basin using NDVI. *Earth Syst. Environ.* 5, 303–318. doi: 10.1007/s41748-021-00224-7

Bodner, G., Nakhforoosh, A., and Kaul, H.-P. (2015). Management of crop water under drought: a review. *Agron. Sustain. Dev.* 35, 401–442. doi: 10.1007/s13593-015-0283-4

Bryan, B. A., Gao, L., Ye, Y., Sun, X., Connor, J. D., Crossman, N. D., et al. (2018). China's response to a national land-system sustainability emergency. *Nature* 559, 193–204. doi: 10.1038/s41586-018-0280-2

Chen, F., Huang, X., Zhang, J., Holmes, J., and Chen, J. (2006). Humid little ice age in arid central Asia documented by Bosten Lake, Xinjiang, China. *Sci. China Ser. D: Earth Sci.* 49, 1280–1290. doi: 10.1007/s11430-006-2027-4

Chen, H., Liu, H., Chen, X., and Qiao, Y. (2020). Analysis on impacts of hydro-climatic changes and human activities on available water changes in Central Asia 737, 139779. doi: 10.1016/j.scitotenv.2020.139779

Chen, Y., Li, Z., Fan, Y., Wang, H., and Deng, H. (2015). Progress and prospects of climate change impacts on hydrology in the arid region of northwest China. *Environ. Res.* 139, 11–19. doi: 10.1016/j.envres.2014.12.029

Cheng, C., Zhang, F., Li, X., Tan, M. L., Kumar, P., Johnson, B. A., et al. (2023). Variations in water storage of Bosten Lake, China, over the last two decades based on multi-source satellite data. *J Hydrol Reg Stud.* 49, 101496. doi: 10.1016/j.ejrh.2023.101496

Crétaux, J.-F., Arsen, A., Calmant, S., Kouraev, A., Vuglinski, V., Bergé-Nguyen, M., et al. (2011). SOLS: A lake database to monitor in the Near Real Time water level and storage variations from remote sensing data. *Adv Space Res.* 47, 1497–1507. doi: 10.1016/j.asr.2011.01.004

Dai, X., Yang, X., Wang, M., Gao, Y., Liu, S., and Zhang, J. (2020). The dynamic change of bosten lake area in response to climate in the past 30 years. *Water* 12, 4. doi: 10.3390/w12010004

Deng, Y., Wang, S., Bai, X., Luo, G., Wu, L., Chen, F., et al. (2020). Vegetation greening intensified soil drying in some semi-arid and arid areas of the world. *Agric For Meteorol.* 292, 108103. doi: 10.1016/j.agrformet.2020.108103

Didan, K. University of Arizona, Alfredo Huete and University of Technology Sydney and MODAPS SIPS - NASA (2015). *MOD13A2 MODIS/Terra Vegetation Indices 16-Day L3 Global 1km SIN Grid.* NASA LP DAAC. doi: 10.5067/MODIS/MOD13A2.006

Ding, Y., and Peng, S. (2020). Spatiotemporal trends and attribution of drought across China from 1901–2100. *Sustainability* 12, 477. doi: 10.3390/su12020477

Duan, Z., Wang, X., Shakhimardan, S., Sun, L., Liu, W., and Luo, Y. (2022). Impacts of lake water change on vegetation development in the retreat area of the Aral Sea. *J. Hydrology* 613, 128416. doi: 10.1016/j.jhydrol.2022.128416

Fahu, C., Tingting, X., Yujie, Y., Shengqian, C., Feng, C., Wei, H., et al. (2023). Discussion of the "warming and wetting" trend and its future variation in the drylands

of Northwest China under global warming. *Sci. China Earth Sci.* 66, 1241–1257. doi: 10.1007/s11430-022-1098-x

Fensholt, R., Langanke, T., Rasmussen, K., Reenberg, A., Prince, S. D., Tucker, C., et al. (2012). Greenness in semi-arid areas across the globe 1981–2007—an Earth Observing Satellite based analysis of trends and drivers. *Remote Sens Environ.* 121, 144–158. doi: 10.1016/j.rse.2012.01.017

Fu, B., Li, J., Gasser, T., Ciais, P., Piao, S., Tao, S., et al. (2022). Climate warming mitigation from nationally determined contributions. *Adv Atmos Sci.* 39, 1217–1228. doi: 10.1007/s00376-022-1396-8

Gao, H., Liu, X., Wei, L., Li, X., and Li, J. (2023). Dynamic simulation of the water-energy-food nexus (WEFN) based on a new nexus in arid zone: A case study in Ningxia, China. *Sci Total Environ.* 898, 165593. doi: 10.1016/j.scitotenv.2023.165593

Gbetkom, P. G., Crétaux, J.-F., Tchilibou, M., Carret, A., Delhoume, M. , Bergé-Nguyen, M., et al. (2023). Lake Chad vegetation cover and surface water variations in response to rainfall fluctuations under recent climate conditions, (2000– 2020). Sci Total Environ. 857, 159302. doi: 10.1016/j.scitotenv.2022.159302

Ge, X., Ding, J., Teng, D., Wang, J., Huo, T., Jin, X., et al. (2022a). Updated soil salinity with fine spatial resolution and high accuracy: The synergy of Sentinel-2 MSI, environmental covariates and hybrid machine learning approaches. *Catena* 212, 106054. doi: 10.1016/j.catena.2022.106054

Ge, X., Ding, J., Teng, D., Xie, B., Zhang, X., Wang, J., et al. (2022b). Exploring the capability of Gaofen-5 hyperspectral data for assessing soil salinity risks. *Int J Appl Earth Obs Geoinf.* 112, 102969. doi: 10.1016/j.jag.2022.102969

Gessner, U., Naeimi, V., Klein, I., Kuenzer, C., Klein, D., Dech, S. J. G., et al. (2013). The relationship between precipitation anomalies and satellite-derived vegetation activity in Central Asia. *Glob Planet Change.* 110, 74–87. doi: 10.1016/j.gloplacha.2012.09.007

Gorelick, N., Hancher, M., Dixon, M., Ilyushchenko, S., Thau, D., and Moore, R. (2017). Google Earth Engine: Planetary-scale geospatial analysis for everyone. *Remote Sens. Environ.* 202, 18–27. doi: 10.1016/j.rse.2017.06.031

Han, Z., Huang, Q., Huang, S., Leng, G., Bai, Q., Liang, H., et al. (2021). Spatial-temporal dynamics of agricultural drought in the Loess Plateau under a changing environment: Characteristics and potential influencing factors. *Agricultural Water Management* 244, 106540. doi: 10.1016/j.agwat.2020.106540

Hantemirov, R. M., Corona, C., Guillet, S., Shiyatov, S. G., Stoffel, M., Osborn, T. J., et al. (2022). Current Siberian heating is unprecedented during the past seven millennia. *Nat Commun.* 13, 4968. doi: 10.1038/s41467-022-32629-x

Hao, S., and Li, F. (2022). Water sources for typical desert vegetation in the Ebinur Lake basin. *J. Geographical Sci.* 32, 1103–1118. doi: 10.1007/s11442-022-1987-4

Hawinkel, P., Swinnen, E., Lhermitte, S., Verbist, B., Van Orshoven, J., and Muys, B. (2015). A time series processing tool to extract climate-driven interannual vegetation dynamics using Ensemble Empirical Mode Decomposition (EEMD). *Remote Sens. Environ.* 169, 375–389. doi: 10.1016/j.rse.2015.08.024

Hou, J., and Rusuli, Y. (2022). Assessment of soil salinization risk by remote sensing-based ecological index (RSEI) in the bosten lake watershed, Xinjiang in northwest China. *Sustainability* 14 (12), 7118. doi: 10.3390/su14127118

Hu, W., Yao, J., He, Q., and Chen, J. (2021). Changes in precipitation amounts and extremes across Xinjiang (northwest China) and their connection to climate indices. *PeerJ* 9. doi: 10.7717/peerj.10792

Huang, Y., Yao, B., Li, Y., Zhang, H., and Wang, S. (2023). Deciphering Hulun lake level dynamics and periodical response to climate change during 1961–2020. *J. Hydrology: Regional Stud.* 46, 101352. doi: 10.1016/j.ejrh.2023.101352

Ji, F., Wu, Z., Huang, J., and Chassignet, E. P. (2014). Evolution of land surface air temperature trend. *Nat Clim Chang.* 4, 462–466. doi: 10.1038/nclimate2223

Jiang, W., Yuan, L., Wang, W., Cao, R., Zhang, Y., and Shen, W. (2015). Spatio-temporal analysis of vegetation variation in the Yellow River Basin. *Ecological Indicators* 51, 117–126. doi: 10.1016/j.ecolind.2014.07.031

Jiapaer, G., Chen, X., Bao, A. J. A., and Meteorology, F. (2011). A comparison of methods for estimating fractional vegetation cover in arid regions. *Agric For Meteorol.* 151, 1698–1710. doi: 10.1016/j.agrformet.2011.07.004

Kiage, L. M., and Douglas, P. (2020). Linkages between land cover change, lake shrinkage, and sublacustrine influence determined from remote sensing of select Rift Valley Lakes in Kenya. *Sci. Total Environ.* 709, 136022. doi: 10.1016/j.scitotenv.2019.136022

Kikstra, J. S., Nicholls, Z. R., Smith, C. J., Lewis, J., Lamboll, R. D., Byers, E., et al. (2022). The IPCC Sixth Assessment Report WGIII climate assessment of mitigation pathways: from emissions to global temperatures. *Geosci. Model Dev.* 15, 9075–9109. doi: 10.5194/gmd-15-9075-2022

Killick, R., and Eckley, I. (2014). changepoint: An R package for changepoint analysis. *J Stat Softw.* 58, 1–19. doi: 10.18637/jss.v058.i03

Kooch, Y., Amani, M., and Abedi, M. (2022). Vegetation degradation threatens soil health in a mountainous semi-arid region. *Sci Total Environ.* 830, 154827. doi: 10.1016/j.scitotenv.2022.154827

Li, Z., Chen, Y., Li, W., Deng, H., and Fang, G. (2015). Potential impacts of climate change on vegetation dynamics in Central Asia. *J Geophys Res.: Atmospheres* 120, 12345–12356. doi: 10.1002/2015JD023618

Liu, H., Jia, J., Lin, Z., Wang, Z., and Gong, H. (2021). Relationship between net primary production and climate change in different vegetation zones based on EEMD detrending – A case study of Northwest China. *Ecol. Indic.* 122, 107276. doi: 10.1016/j.ecolind.2020.107276

Liu, L., Peng, J., Li, G., Guan, J., Han, W., Ju, X., et al. (2023). Effects of drought and climate factors on vegetation dynamics in Central Asia from 1982 to 2020. *J Environ Manage.* 328, 116997. doi: 10.1016/j.jenvman.2022.116997

Liu, H., Zhang, M., Lin, Z., and Xu, X. (2018a). Spatial heterogeneity of the relationship between vegetation dynamics and climate change and their driving forces at multiple time scales in Southwest China. *Agric. For. Meteorology* 256-257, 10–21. doi: 10.1016/j.agrformet.2018.02.015

Liu, L., Zhang, Y., Wu, S., Li, S., and Qin, D. (2018b). Water memory effects and their impacts on global vegetation productivity and resilience. *Sci Rep.* 8, 2962. doi: 10.1038/s41598-018-21339-4

Maimaiti, A., Wang, L. M., Yan, F., Zhang, J., and Ma, Y. X. (2016). "Quantitative analysis of land use and land cover changes from the multi-temporal remote sensing data in the Bosten Lake Basin, Chinese Tian Shan," in *3rd International Symposium on Earth Observation for Arid and Semi-Arid Environments (ISEO)* (Acad Sci Republ Tajikistan, Dushanbe, TAJIKISTAN).

Ndehedehe, C. E., Agutu, N. O., and Okwuashi, O. (2018). Is terrestrial water storage a useful indicator in assessing the impacts of climate variability on crop yield in semi-arid ecosystems? *Ecological Indicators* 88, 51–62. doi: 10.1016/j.ecolind.2018.01.026

Nourani, V., Tootoonchi, R., and Andaryani, S. (2021). Investigation of climate, land cover and lake level pattern changes and interactions using remotely sensed data and wavelet analysis. *Ecological Informatics* 64, 101330. doi: 10.1016/j.ecoinf.2021.101330

Ogou, F. K., Igbawua, T. J. T., and Climatology, A. (2022). Investigation of changes in vegetation cover associated with changes in its hydro-climatic drivers in recent decades over North Sub-Saharan Africa. *Theor Appl Climatol.* 149, 1135–1152. doi: 10.1007/s00704-022-04088-3

Pan, N., Feng, X., Fu, B., Wang, S., Ji, F., and Pan, S. (2018). Increasing global vegetation browning hidden in overall vegetation greening: Insights from time-varying trends. *Remote Sens Environ.* 214, 59–72. doi: 10.1016/j.rse.2018.05.018

Pekel, J.-F., Cottam, A., Gorelick, N., and Belward, A. S. (2016). High-resolution mapping of global surface water and its long-term changes. *Nature* 540, 418–422. doi: 10.1038/nature20584

Rousta, I., Sharif, M., Heidari, S., Kiani, A., Olafsson, H., Krzyszczak, J., et al. (2023). Climatic variables impact on inland lakes water levels and area fluctuations in an arid/semi-arid region of Iran, Iraq, and Turkey based on the remote sensing data. *Earth Sci. Inf.* 16, 1611–1635. doi: 10.1007/s12145-023-00995-9

Rustad, L. E. (2008). The response of terrestrial ecosystems to global climate change: towards an integrated approach. *Sci Total Environ.* 404, 222–235. doi: 10.1016/j.scitotenv.2008.04.050

Saisirirat, P., Rushman, J. F., Silva, K., and Chollacoop, N. (2022). Contribution of road transport to the attainment of Ghana's nationally determined contribution (NDC) through biofuel Integration. *Energies* 15, 880. doi: 10.3390/en15030880

Shen, Q., Gao, G., Lü, Y., Wang, S., Jiang, X., and Fu, B. (2017). River flow is critical for vegetation dynamics: lessons from multi-scale analysis in a hyper-arid endorheic basin. *Sci Total Environ.* 603, 290–298. doi: 10.1016/j.scitotenv.2017.06.087

Sylvain, Z. A., and Wall, D. H. (2011). Linking soil biodiversity and vegetation: implications for a changing planet. *Am J Bot.* 98, 517–527. doi: 10.3732/ajb.1000305

Tan, C., Guo, B., Kuang, H., Yang, H., and Ma, M. (2018). Lake area changes and their influence on factors in arid and semi-arid regions along the silk road. *Remote Sens.* 10 (4), 595. doi: 10.3390/rs10040595

Tang, X., Xie, G., Deng, J., Shao, K., Hu, Y., He, J., et al. (2022). Effects of climate change and anthropogenic activities on lake environmental dynamics: A case study in Lake Bosten Catchment, NW China. *J. Environ. Manage.* 319, 115764. doi: 10.1016/j.jenvman.2022.115764

Tuersun, A., Rusuli, Y., Maimaiti, A., Maitudi, M., and Alimu, K. (2020). Spatiotemporal characteristics of evapotranspiration and driving factors in the bosten lake watershed, China. *CLEAN – Soil Air Water* 48, 1900246. doi: 10.1002/clen.201900246

Verbesselt, J., Hyndman, R., Newnham, G., and Culvenor, D. (2010). Detecting trend and seasonal changes in satellite image time series. *Remote Sens Environ.* 114 (1), 106–115. doi: 10.1016/j.rse.2009.08.014

Verma, R., and Dutta, S. (2013). Vegetation dynamics from denoised NDVI using empirical mode decomposition. *Journal of the Indian Society of Remote Sensing* 41, 555–566. doi: 10.1007/s12524-012-0246-z

Voss, K. A., Famiglietti, J. S., Lo, M., De Linage, C., Rodell, M., and Swenson, S. C. (2013). Groundwater depletion in the Middle East from GRACE with implications for transboundary water management in the Tigrismentary.o.R.S.that Iran region. *Water Resour Res.* 49, 904–914. doi: 10.1002/wrcr.20078

Wang, J., Ding, J., Li, G., Liang, J., Yu, D., Aishan, T., et al. (2019a). Dynamic detection of water surface area of Ebinur Lake using multi-source satellite data (Landsat and Sentinel-1A) and its responses to changing environment. *CATENA* 177, 189–201. doi: 10.1016/j.catena.2019.02.020

Wang, Y., Shen, Y., Chen, Y., and Guo, Y. (2013). Vegetation dynamics and their response to hydroclimatic factors in the Tarim River Basin, China. *Ecohydrology* 6, 927–936. doi: 10.1002/eco.1255

Wang, Y., Yang, J., Chen, Y., Fang, G., Duan, W., Li, Y., et al. (2019b). Quantifying the effects of climate and vegetation on soil moisture in an arid area, China. *Water* 11, 767. doi: 10.3390/w11040767

Wang, J., Zhang, F., Jim, C.-Y., Chan, N. W., Johnson, V. C., Liu, C., et al. (2022). Spatio-temporal variations and drivers of ecological carrying capacity in a typical mountain-oasis-desert area, Xinjiang, China. *Ecological Engineering* 180, 106672. doi: 10.1016/j.ecoleng.2022.106672

Wang, J., Zhen, J., Hu, W., Chen, S., Lizaga, I., Zeraatpisheh, M., et al. (2023). Remote sensing of soil degradation: Progress and perspective. *International Soil and Water Conservation Research* 11 (3), 429–454. doi: 10.1016/j.iswcr.2023.03.002

Wang, Y., Zhou, X., and Engel, B. (2018). Water environment carrying capacity in Bosten Lake basin. *J Clean Prod.* 199, 574–583. doi: 10.1016/j.jclepro.2018.07.202

Wen, Z., Wu, S., Chen, J., and Lü, M. (2017). NDVI indicated long-term interannual changes in vegetation activities and their responses to climatic and anthropogenic factors in the Three Gorges Reservoir Region, China. *Sci. Total Environ.* 574, 947–959. doi: 10.1016/j.scitotenv.2016.09.049

Woolway, R. I., Kraemer, B. M., Lenters, J. D., Merchant, C. J., O'Reilly, C. M., and Sharma, S. (2020). Global lake responses to climate change. *Nat. Rev. Earth Environ.* 1, 388–403. doi: 10.1038/s43017-020-0067-5

Wu, G. L., Cheng, Z., Alatalo, J. M., Zhao, J., and Liu, Y. (2021). Climate warming consistently reduces grassland ecosystem productivity. *Earth's Future* 9, e2020EF001837. doi: 10.1029/2020EF001837

Wu, Z., and Huang, N. (2009). Ensemble empirical mode decomposition: a noise-assisted data analysis method. *Adv Adapt Data Anal.* 1, 1–41. doi: 10.1142/S1793536909000047

Wufu, A., Wang, H., Chen, Y., Rusuli, Y., Ma, L., Yang, S., et al. (2020). Lake water volume fluctuations in response to climate change in Xinjiang, China from 2002 to 2018. *PeerJ* 8, e9683. doi: 10.7717/peerj.9683

Xue, J., Gui, D., Lei, J., Sun, H., Zeng, F., Mao, D., et al. (2019). Oasification: An unable evasive process in fighting against desertification for the sustainable development of arid and semiarid regions of China. *Catena* 179, 197–209. doi: 10.1016/j.catena.2019.03.029

Yanfei, P., Zhongqin, L., Xiaojun, Y., Jianxin, M., Weixiao, H., and Panpan, W. (2021). Area change and cause analysis of bosten lake based on multi-source remote sensing data and GEE platform. *J. Geo-information Sci.* 23, 1131–1153. doi: 10.18307/2023.0122

Yang, H., Xu, J., Chen, Y., Li, D., Zuo, J., Zhu, N., et al. (2020). Has the Bosten Lake Basin been dry or wet during the climate transition in Northwest China in the past 30 years? *Theor Appl Climatol.* 141, 627–644. doi: 10.1007/s00704-020-03209-0

Yao, J., Chen, Y., Zhao, Y., and Yu, X. (2018). Hydroclimatic changes of Lake Bosten in Northwest China during the last decades. *Sci. Rep.* 8 (1), 9118. doi: 10.1038/s41598-018-27466-2

Ye, Z., Li, W., Chen, Y., Qiu, J., and Aji, D. (2017). Investigation of the safety threshold of eco-environmental water demands for the Bosten Lake wetlands, western China. *Quaternary International* 440, 130–136. doi: 10.1016/j.quaint.2016.12.030

Zhai, R., and Tao, F. (2021). Climate change in China affects runoff and terrestrial ecosystem water retention more than changes in leaf area index and land use/cover over the period 1982–2015. *J Geophys Res Biogeosci.* 126. doi: 10.1029/2020JG005902

Zhang, Z., Chang, J., Xu, C.-Y., Zhou, Y., Wu, Y., Chen, X., et al. (2018b). The response of lake area and vegetation cover variations to climate change over the Qinghai-Tibetan Plateau during the past 30 years. *Sci Total Environ.* 635, 443–451. doi: 10.1016/j.scitotenv.2018.04.113

Zhang, J., Ding, J., Wu, P., Tan, J., Huang, S., Teng, D., et al. (2020). Assessing arid inland lake watershed area and vegetation response to multiple temporal scales of drought across the ebinur lake watershed. *Sci. Rep.* 10, 1354. doi: 10.1038/s41598-020-57898-8

Zhang, H., Jin, G., and Yu, Y. (2018a). Review of river basin water resource management in China. *Water* 10, 425. doi: 10.3390/w10040425

Zhang, Q., Lv, X., Yu, X., Ni, Y., Ma, L., and Liu, Z. (2022a). Species and spatial differences in vegetation rainfall interception capacity: A synthesis and meta-analysis in China. *CATENA* 213, 106223. doi: 10.1016/j.catena.2022.106223

Zhang, Q., Sun, C., Chen, Y., Chen, W., Xiang, Y., Li, J., et al. (2022b). Recent oasis dynamics and ecological security in the Tarim River Basin, Central Asia. *Sustainability* 14, 3372. doi: 10.3390/su14063372

Zhang, Z., Xu, E., and Zhang, H. (2021). Complex network and redundancy analysis of spatial–temporal dynamic changes and driving forces behind changes in oases within the Tarim Basin in northwestern China. *CATENA* 201, 105216. doi: 10.1016/j.catena.2021.105216

Zhao, J., Huang, S., Huang, Q., Wang, H., Leng, G., and Fang, W. (2020). Time-lagged response of vegetation dynamics to climatic and teleconnection factors. *Catena* 189, 104474. doi: 10.1016/j.catena.2020.104474

Zhao, B., Sun, H., Yan, D., Wei, G., Tuo, Y., and Zhang, W. (2021). Quantifying changes and drivers of runoff in the Kaidu River Basin associated with plausible climate scenarios. *J. Hydrology: Regional Stud.* 38, 100968.

frontiers | Frontiers in Plant Science

TYPE Original Research
PUBLISHED 06 September 2024
DOI 10.3389/fpls.2024.1440993

OPEN ACCESS

EDITED BY
Samuel Kuria Kiboi,
University of Nairobi, Kenya

REVIEWED BY
Feng Chen,
Yunnan University, China
Ronghua Li,
South China Agricultural University, China

*CORRESPONDENCE
Xiaojuan Xu
kattyxiaoj@163.com
Kun Zhang
zhangkun@nies.org
Jie Qiu
qiujie@nies.org

RECEIVED 30 May 2024
ACCEPTED 12 August 2024
PUBLISHED 06 September 2024

CITATION
Xu X, Jiao F, Liu J, Ma J, Lin D, Gong H, Yang Y, Lin N, Wu Q, Zhu Y, Qiu J, Zhang K and Zou C (2024) Stability of gross primary productivity and its sensitivity to climate variability in China.
Front. Plant Sci. 15:1440993.
doi: 10.3389/fpls.2024.1440993

Stability of gross primary productivity and its sensitivity to climate variability in China

Xiaojuan Xu[1*], Fusheng Jiao[2], Jing Liu[1], Jie Ma[1], Dayi Lin[1], Haibo Gong[3], Yue Yang[1], Naifeng Lin[1], Qian Wu[1], Yingying Zhu[1], Jie Qiu[1*], Kun Zhang[1*] and Changxin Zou[1]

[1]Ecological Protection and Restoration Center, Nanjing Institute of Environmental Sciences, MEE, Nanjing, China, [2]School of Geography, Nanjing Normal University, Nanjing, China, [3]College of Urban, and Environmental Sciences, Peking University, Beijing, China

Identifying the stability and sensitivity of land ecosystems to climate change is vital for exploring nature-based solutions. However, the underlying mechanisms governing ecosystem stability and sensitivity, especially in regions with overlapping ecological projects, remain unclear. based on Mann-Kendall, stability analysis method, and multiple regression method, this study quantified the stability and sensitivity of gross primary productivity (GPP) to climate variables [temperature, vapor pressure deficit (VPD), soil moisture, and radiation] in China from 1982 to 2019. Our findings revealed the following: (1) GPP demonstrated an increased trend with lower stability in Eastern regions, whereas a decreasing trend with higher stability was observed in Western and Southwest China. Notably, the stability of GPP was highest (74.58%) in areas with five overlapping ecological projects: Grain to Green, Natural Forest Resource Protection Project, Three-River Ecological Conservation and Restoration Project, Return Grazing to Grassland Project, and Three-North Shelter Forestation Project. (2) In regions with minimal or no overlapping ecological projects, temperature and radiation jointly dominated GPP variations. In contrast, water-related factors (VPD and soil moisture) significantly affected GPP in areas with multiple overlapping ecological projects. (3) In the southwestern and northeastern regions, GPP exhibited the highest sensitivity to climate change, whereas, in the eastern coastal areas and Tibet, GPP showed low sensitivity to climate change. In the Loess Plateau, where five ecological projects overlap extensively, carbon sinks primarily demonstrate a monotonic increasing trend, high stability, and low sensitivity to climate change. This study aimed to assess the stability of the land ecosystems and delineate their sensitivity to climate changes, thereby laying the groundwork for understanding ecosystem resilience.

KEYWORDS

gross primary productivity, sensitivity, stability, climate change, ecological engineering

1 Introduction

Understanding the stability and sensitivity of terrestrial ecosystems is crucial for accurate predictions of ecosystem dynamics and for informing policies to mitigate climate change (Seddon et al., 2016; Pennekamp et al., 2018; Wang et al., 2022). Ecosystem stability plays a key role in regulating the terrestrial carbon cycle and atmospheric carbon dioxide levels (Messori et al., 2019). With the increasing frequency of extreme weather events due to climate change, inter-annual fluctuations in vegetation growth are rising, indicating a decline in ecosystem stability (Holden et al., 2014; Hu et al., 2023; Zhang et al., 2024b). Sensitivity is defined as the extent to which an ecosystem responds to disturbance and the duration, and it remains in its original state varies across ecosystems (Hu et al., 2021; Li et al., 2022). Differences in ecosystem sensitivity to climate change can disrupt ecological interactions, threatening ecosystem functioning (Walker et al., 2004; Carlson et al., 2012; Thackeray et al., 2016; Nikinmaa et al., 2020; Chen et al., 2022). Studying both stability and sensitivity together provides a comprehensive understanding of ecosystem dynamics, offering robust scientific support for conservation strategies and climate change mitigation efforts (Piao et al., 2020). Ecosystems with lower stability exhibit heightened responses to disturbance and greater sensitivity to environmental perturbations (Hu et al., 2021). Therefore, identifying regions of ecosystem instability and high ecological sensitivity is essential for pinpointing areas vulnerable to ecological change (Thackeray et al., 2016).

Ecosystem gross primary productivity (GPP), which represents the cumulative photosynthetic carbon sequestration by all leaves measured at the ecosystem scale, denotes the comprehensive uptake of CO_2 within the ecosystem (Anav et al., 2015; Cheng et al., 2017). GPP is a vital indicator of the terrestrial carbon cycle, marking the beginning of carbon sequestration in ecosystems and providing a robust measure of terrestrial carbon uptake (Anav et al., 2015; Xu et al., 2022). The stability and sensitivity of GPP introduce significant uncertainty regarding the resilience and resistance of ecosystems (Liu et al., 2023a). Under minimal or undisturbed conditions, GPP exhibited high stability with negligible fluctuations (Lin et al., 2023). Conversely, when external disturbances exceed GPP's threshold tolerance, it becomes destabilized and more sensitive to the external environment, making it highly susceptible to climate change (Chen et al., 2017). Therefore, it is imperative to understand the stability of GPP and its sensitivity to environmental variables.

Studies have demonstrated the significant role of climate variables as key regulators of ecosystem processes, making them pivotal external drivers (Qiao and Xia, 2024; Wang et al., 2024). Consequently, the stability and sensitivity of GPP to climate change are essential components of terrestrial ecosystem dynamics (Anav et al., 2015; Chen et al., 2017; Gao et al., 2018; Piao et al., 2019; Xu et al., 2019). Prior research has identified temperature, radiation, soil moisture, and vapor pressure deficit (VPD) as the primary drivers of GPP variations (Nord-Larsen et al., 2019; Anderegg et al., 2020; Hu et al., 2023; Zhang et al., 2024a). Elevated temperatures significantly stimulated GPP until reaching an optimal threshold (He et al., 2022b; Kan et al., 2023). Increased solar radiation was the principal contributor to the observed rise in GPP (Cui et al., 2021). Warming enhances leaf photosynthesis under high soil moisture conditions, whereas drought impedes it (Dong et al., 2022; Guo et al., 2023). In regions with limited water availability, air drying inhibits GPP increase, leading to reduced vegetation growth. Furthermore, heat-induced elevation in VPD has been linked to accelerated vegetation mortality at the forest-grassland interface (Konings et al., 2017; He et al., 2022a). In semi-arid and arid regions, vegetation responsiveness to soil moisture has significantly increased over time (Shen et al., 2021; Li et al., 2022). However, prior research has primarily focused on elucidating the driving mechanisms behind GPP trends, with limited clarity on GPP sensitivity to climate variables (Hooper et al., 2017; Li et al., 2018).

China has undertaken several major projects to safeguard and rehabilitate ecosystems, including the Three North Shelterbelt Forestation Project, the Grain to Green Project, the Natural Forest Resource Protection Project, the Beijing-Tianjin Sandstorms Source Control Project, the Yangtze River Shelterbelt Forestation Project, the Pearl River Shelterbelt Forestation Project, the Return Grazing to Grassland Project, the Three-River Ecological Conservation and Restoration Project, and the Desertification Control in the Karst region of Southwest China (Niu et al., 2022; Chang et al., 2023). Currently, 17.42% of the vegetated land is affected by one ecological project, and 78.87% of the area is affected by the overlapping effects of multiple ecological projects (Shao et al., 2023). Existing studies primarily focused on the carbon cycle in a single project, neglecting the overlapping effects (Niu et al., 2023; Shao et al., 2023). There is an urgent need to elucidate the stability, driving mechanisms, and sensitivity of GPP in both singular and overlapping ecological project areas (Shao et al., 2023). This endeavor is crucial not merely for evaluating carbon sequestration potential and sink enhancement within major ecological ventures but also for achieving the "carbon neutrality" goal.

This study aimed to enhance our understanding of the sensitivity of GPP to climate variables in overlapping ecological engineering regions, focusing on two primary aspects: the stability of GPP and its sensitivity to climate change. To achieve these, we first analyzed the trend change and stability change of GPP from 1982 to 2019 in overlapping ecological engineering areas. Second, we explored the driving mechanisms of the GPP in overlapping ecological engineering areas. Finally, we revealed the sensitivity of GPP to climate change in overlapping ecological engineering areas. This research enhances comprehension of ecosystem sensitivity to climate change and contributes to an improved understanding of ecosystem stability.

2 Materials and methods

2.1 Study area

Since the late 1970s, China implemented a series of ecological projects, including the Three North Shelterbelt Forestation Project, the Grain to Green Project, the Natural Forest Resource Protection Project, the Beijing-Tianjin Sandstorms Source Control Project, the Yangtze River Shelterbelt Forestation Project, the Pearl River

Shelterbelt Forestation Project, Return Grazing to Grassland Project, the Three-River Ecological Conversation and Restoration Project, and the Desertification Control in Karst region of Southwest China (Figure 1), with a total area of ecological engineering zones of about 9.3×10^6 km^2 (Shao et al., 2023). The boundaries of the nine engineering zones were downloaded from the National Ecological Science Data Center (http://www.nesdc.org.cn/).

Based on the spatial convergence of nine major ecological project implementation scopes (Figure 2), nearly 96.29% of China's land area lies within ecological project implementation zones, which may be a single ecological works implementation area or multiple ecological works overlapping implementation areas. Conversely, only 3.71% of the territory lacks ecological project implementation, primarily concentrated along the southern coast. One ecological engineering project implementation zones cover approximately 17.42% of China's territory, predominantly distributed along the eastern coast and encompassing the Return Grazing Lands to Grasslands initiative in Tibet. Overlapping implementation areas of ecological engineering projects span approximately 78.87% of the national land area. Notably, the largest overlapping areas involve three ecological projects, encompassing approximately 33.99% of China's land area, predominantly situated in central regions such as the Grain to Green Project, the Yangtze River Shelterbelt Project, and the Desertification Control in Karst Regions of Southwest China. Additionally, the most extensive overlaps involve five ecological projects, constituting around 3.87% of China's land area, concentrated in the Three River Region and Yellow River Basin.

2.2 Data sources

We collected the GPP from the Breathing Earth System Simulator version 2.0 (BESS v2.0) in the period of 1982–2019 at a spatial resolution of 0.05° (https://www.environment.snu.ac.kr/bessv2). BESS is a coupled remote-sensed and process-based model. This model was developed to qualify global land-atmosphere flux exchange by integrating key physical and biochemical processes (Jiang and Ryu, 2016; Li et al., 2023). This GPP product was consistent with flux observations and showed a better performance than other remote-sensed GPP products (Chang et al., 2024). First, a two-leaf, two-stream canopy radiative transfer model was used to calculate absorbed photosynthetically active radiation and near-infrared radiation in sunlit and shaded canopies. Then, the relative proportions of C3 and C4 plants were determined by a plant functional type–dependent look-up table method. An optimality-based model was used to quantify the maximum canopy carboxylation rate of C3 and C4 plants at a standardized temperature (25°C). Next, a revised Farquhar model was adopted to compute GPP for sunlit and shaded C3 and C4 plant canopies separately in an iterative manner. Finally, the sum of the

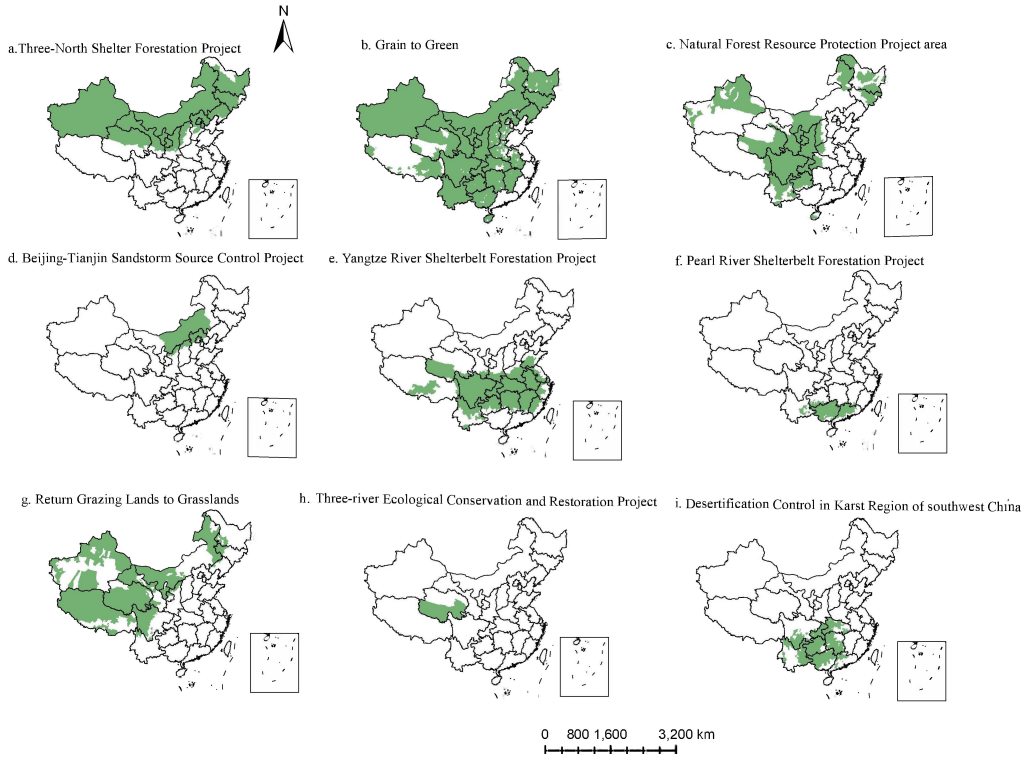

FIGURE 1
The spatial distribution of the nine ecological engineering. **(A)** Three-North Shelter Forestation Project; **(B)** Grain to Green; **(C)** Natural Forest Resource Project area; **(D)** Beijing-Tianjin Sandstorm Source Control Project; **(E)** Yangtze-River Shelterbelt Forestation Project; **(F)** Pearl River Shelterbelt Project. **(G)** Return Grazing Land to Grasslands; **(H)** Three-river Ecological Conservation and Restoration Project; **(I)** Desertification Control in Karst Region of southwest China.

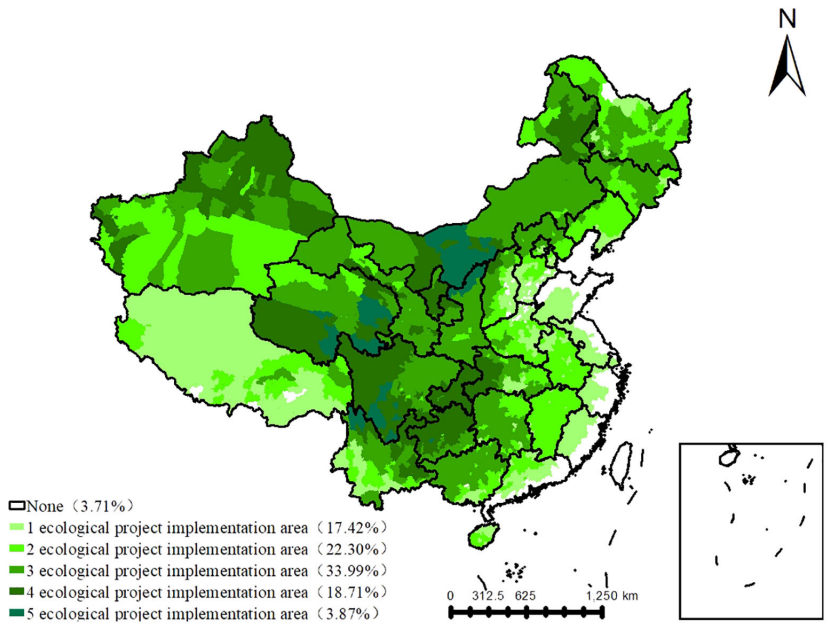

FIGURE 2
The spatial distribution of the overlapped ecological engineering.

relative GPP fixed by C3 and C4 plants was computed to determine the carbon flux quantity in each land grid cell.

The climatic datasets utilized in this study, named TerraClimate, comprised essential variables including air temperature (TEM), soil moisture (SM), VPD, and downward shortwave radiation (RAD). These datasets were procured from the Climatology Lab (Abatzoglou et al., 2018). Acquired from three distinct sources—WorldClim, Climate Research Unit (CRU), and Japanese 55-year Reanalysis (JRA-55), the climatic datasets underwent refinement using the Multivariate Adaptive Constructed Analogs technique to enhance spatial resolution through downscaled monthly time series. This approach has demonstrated superiority over direct daily interpolated bias correction methods, particularly in regions characterized by intricate topography (Jiao et al., 2024). Offering monthly climate insights and climatic water balance dynamics for terrestrial surfaces worldwide, the climatic datasets span from 1958 to 2020. Notably, the data are accessible at a spatial resolution of 1/24°, approximately equivalent to 4 km.

2.3 Methods

The Mann–Kendall test is a non-parametric statistical method used to detect monotonic trends in time series data. This method does not require the data to adhere to a specific distribution nor does it assume a linear relationship (Mann, 1945). It has significant advantages in identifying trends in time series data, particularly when dealing with complex, nonlinear data (Liu et al., 2016). Consequently, this study employs the Mann–Kendall method to analyze trends in GPP.

For the GPP time series, the statistic S_k is defined as follows (Chen et al., 2012):

$$S_k = \sum_{i=1}^{k} r_i, (k = 2, 3, \cdots, n) \tag{1}$$

with

$$r_i = \begin{cases} 1, x_j - x_i > 0 \\ 0, x_j - x_i \le 0 \end{cases}, (j = 1, 2, \cdots, i) \tag{2}$$

In Equation 2 x_i and x_j are the ith data value in time series.

The GPP trends can be identified by utilizing the standard normal test statistic (UF_k), which can be calculated as follows:

$$UF_k = \frac{[S_k - E(S_k)]}{[Var(S_k)]^{1/2}}, (k = 2, 3, 4, \cdots n) \tag{3}$$

where $UF_1 = 0$. $E(S_k)$ and $Var(S_k)$ are the mean and variance of S_k, which can be calculated as follows:

$$E(S_k) = n(n-1)/4 \tag{4}$$

$$Var(S_k) = n(n-1)(2n+5)/72 \tag{5}$$

Positive (negative) values of UF_k indicate GPP exhibits increasing (decreasing) trends. A typical significance level of α = 0.05 was used in the test with $UF_{1-\alpha/2}$=1.96. If $|UF_k|$>1.96, then GPP passed the significant test. The Mann–Kendall test was done in MATLAB R2019.

The stability of GPP was evaluated by calculating the coefficient of variation (Zhang et al., 2019). All factors were de-trended before stability analysis (Lin et al., 2023).

$$GPP_{detrend,year} = GPP_{year} - GPP_{trend,year} + GPP_{mean} \quad (6)$$

$$GPP_{trend,year} = a \times year + b \quad (7)$$

where GPP_{year} is the raw annual GPP data; $GPP_{trend,year}$ is the GPP trend with each year, and its coefficients are calculated by the linear method. We denote the size of the variable by GPP_{mean}, which is averaged from GPP_{year}. The de-trended variable for each year is denoted by $GPP_{detrend,year}$. The stability of GPP was then calculated from the de-trended data:

$$GPP_{stability} = \frac{\sqrt{\frac{\sum(GPP_{detrend,year} - GPP_{mean})^2}{N}}}{GPP_{mean}} \quad (8)$$

The larger $GPP_{stability}$, the more volatile GPP and less stable it is. In addition, based on natural interval methods, we also classified the GPP stability into five levels (stability, relatively stable, moderate stability, relatively unstable, and unstable). The natural interval method relies on inherent data groups.

To assess the impacts of four climate variables (TEM, VPD, SM, and RAD) on the GPP variations, we employed a multiple linear regression model to compute the linear associations between de-trended GPP and de-trended climatic time series (Equation 9):

$$GPP = a \times S_{TEM} + b \times S_{VPD} + c \times S_{SM} + d \times S_{RAD} \quad (9)$$

where GPP indicated the standardized anomalies of GPP; S_{TEM}, S_{VPD}, S_{SM}, and S_{RAD} represented the standardized anomalies of temperature, VPD, soil moisture, and radiation; a, b, c, and d were the corresponding standardized regression coefficients of the four climatic factors

The magnitude of each standardized regression coefficient indicated the relative significance of the driving forces. In this study, the largest regression coefficients were the main driving factor on the GPP. The climate weights for each driver were reshaped to a range of 0 to 1 (using the minimum and maximum value of any of the climate coefficient values) to further calculate the ecological sensitivity index.

We constructed a flowchart (Figure 3) to illustrate the stability and sensitivity analysis. The sensitivity index of GPP in this study was a proxy of the sum of the response magnitude of vegetation to climate changes. To evaluate the sensitivity index of GPP, all variables were de-trended by subtracting the trend from the original data. The variance of GPP and its driving factors was then computed from 1982 to 2019. The residuals obtained from the linear approach were utilized to establish the mean-variance connection for both GPP and climate variables at each pixel. The residuals were normalized to a scale of 0 to 100 for each variable. Sensitivity metrics were calculated as the logarithm base $\log_{10}$-transformed ratios of GPP variability and each of the climate variables. Each ratio was then multiplied by the climate weight,

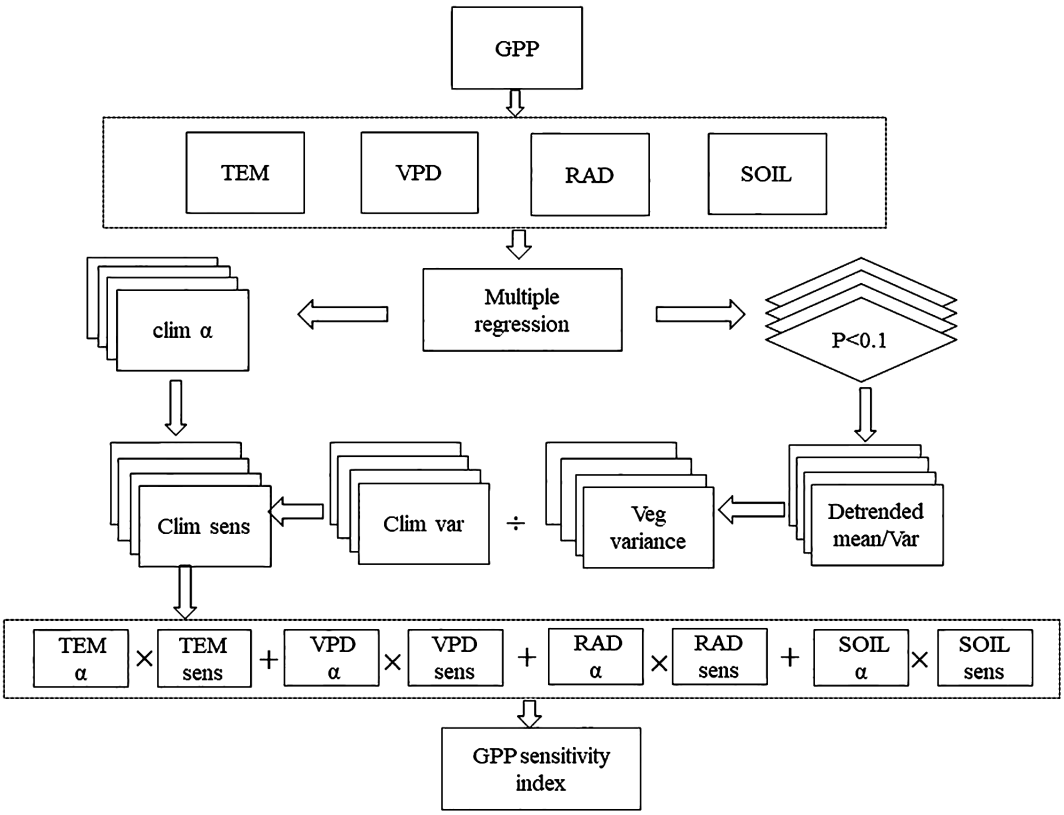

FIGURE 3
The flowchart for calculating the stability and sensitivity index of GPP.

indicating the significance of the climate variable in influencing the variability of the GPP (Seddon et al., 2016). Finally, the sensitivity index of GPP was qualified by the sum of the weighted ratio of air temperature, soil moisture, VPD, and radiation (Figure 3). Data analyses were conducted using MATLAB R2019b and ArcGIS 10.7.

3 Results

3.1 The trend and stability of GPP

As shown in Figure 4A, GPP had a significant trend from 1982 to 2019, with an increased rate of 3.3892 gC m^{-2} $year^{-1}$. Before 2000, GPP exhibited relatively smooth inter-annual fluctuations; however, after 2000, GPP showed significant increasing trends with sharp inter-annual fluctuations (Figure 4B). A total of 65.74% of the GPP in China experienced increasing trends from 1982 to 2019, especially in the pastoral ecological zones in the northeast of China, the Loess Plateau, the Qinling, and the southeast coastal areas (Figure 4C). The region was consistent with the key ecological restoration projects, such as the Grain to Green projects and the Natural Forest Protection project. However, in the arid and semi-arid regions of the northwest, the southwest, and the low reaches of the Yangtze River, the GPP had decreased trends. Figure 4D highlighted that the instability of GPP was primarily concentrated in the North China Plain, the Southeast Coast, and the Southwest Karst region, whereas GPP demonstrated greater stability in the Qinghai-Tibetan Plateau and arid and semi-arid regions.

In the ecological engineering areas (Figure 5 and Table 1), GPP with greatest percentage of increasing trends in the region with the highest number of overlapping ecological projects, reaching 81.97%. These areas were mainly located in the overlapping implementation of five ecological projects, such as the Grain to Green, the Natural Forest Resource Protection Project, the Three-River Ecological Conservation and Restoration Project, and the Three-North Shelter Forestation Project. The percentage of increasing trends in GPP was relatively higher in the Southeast Coastal Region, which showed a 72.36% increase in GPP. The favorable hydrothermal conditions along the eastern coast were conducive to vegetation carbon sequestration and sink enhancement. In addition, relatively high percentage increases in GPP were observed in regions with the implementation of a single ecological project, particularly in the eastern part of the Grain to Green area and the western part of the Return Grazing to Grassland area. Conversely, areas where two or three ecological programs overlapped experienced lower rates of increase in GPP. This can be attributed to the relatively poor

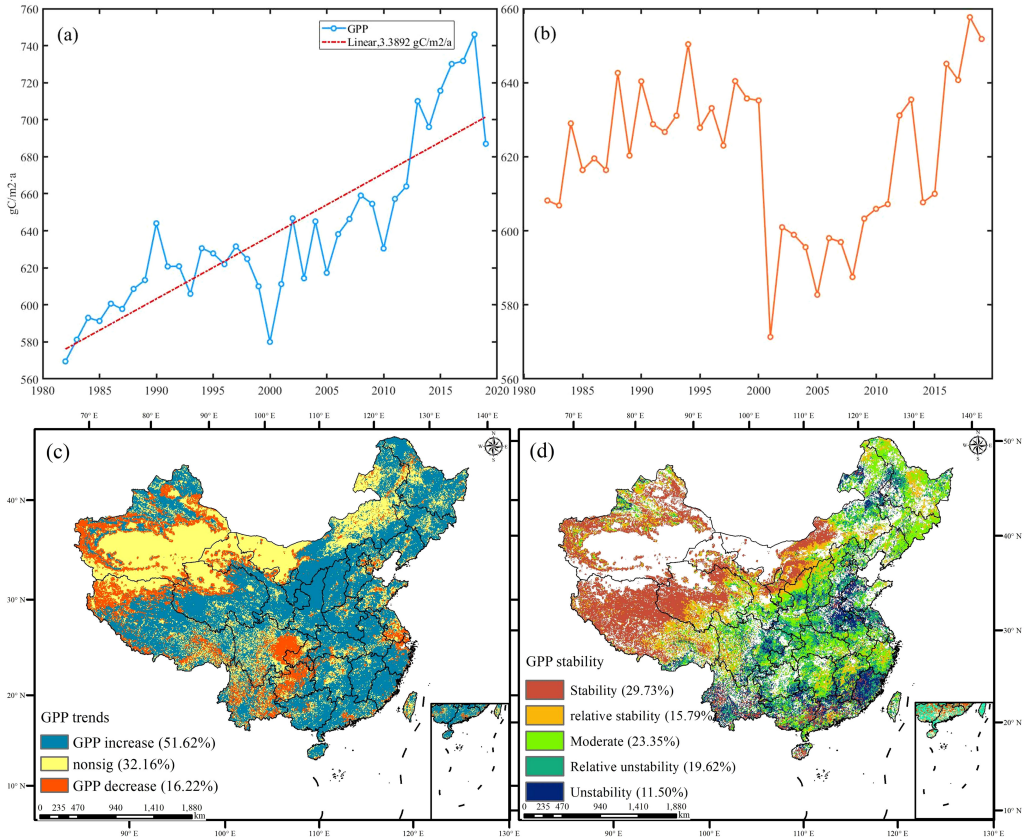

FIGURE 4
The trend and stability of GPP from 1982 to 2019 in China [**(A)** the linear trend of GPP, **(B)** the inter-annual fluctuation of GPP, **(C)** the spatial distribution of GPP, and **(D)** the stability of GPP].

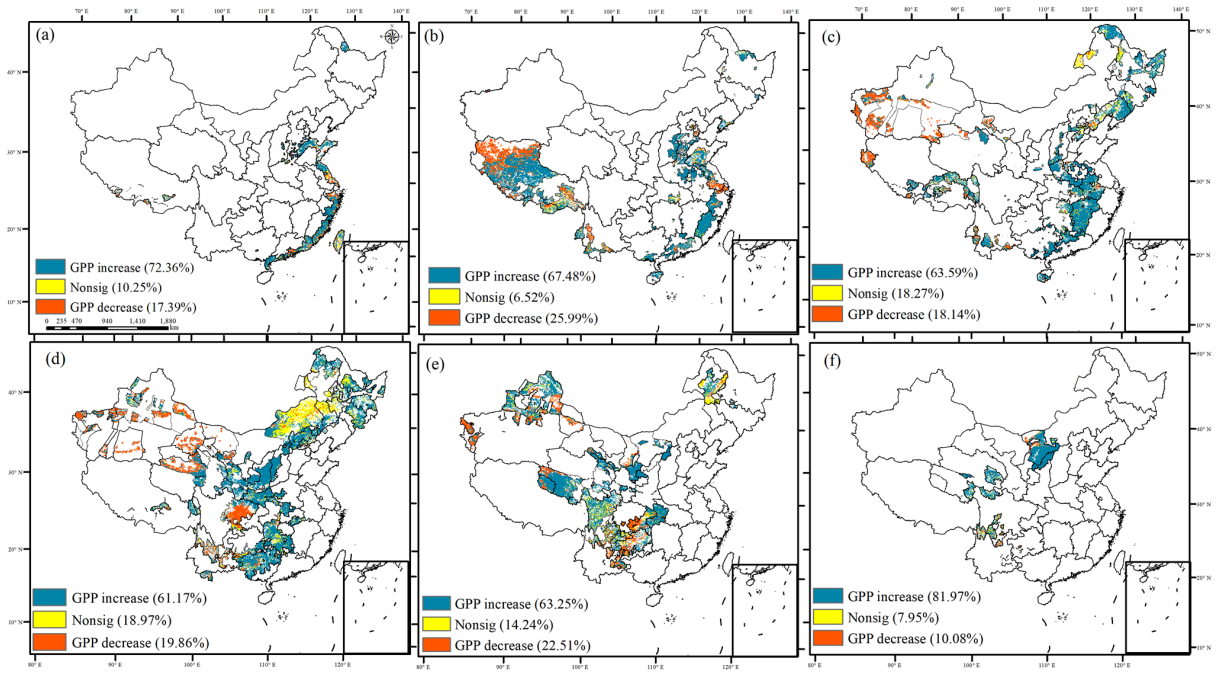

FIGURE 5
The trend of GPP from 1982 to 2019 in ecological engineering areas [**(A)** zero ecological project areas, **(B)** one ecological project area, **(C)** two ecological project areas, **(D)** three ecological project areas, **(E)** four ecological project areas, and **(F)** five ecological project areas].

hydrothermal conditions in the northwestern region, resulting in GPP dominated by insignificant changes and exhibiting a lower rate of increase compared to the eastern region.

In the ecological engineering areas, the highest percentage of stability in GPP was in the implementation areas of five overlapping ecological engineering regions, accounting for 74.58% (Figure 6; Table 2). These areas were mainly located in the areas of overlapping ecological projects such as Grain to Green, Natural Forest Resource Protection Project, Three-River Ecological Conservation and Restoration Project, and Three-North Shelter Forestation Project. The second high percentage of stability in GPP was mainly concentrated in the Tibetan with Return Grazing Lands to Grasslands. However, in no ecological project, as well as two or three overlapping ecological projects, the percentage of instability in GPP was relatively low.

3.2 The dominant role of four climate variables in GPP variations

The dominant climatic factors influencing GPP are illustrated in Figure 7. Temperature was the primary factor affecting 42.51% of the area, followed by VPD at 24.34%, solar radiation at 22.35%, and soil moisture at 10.81%. Temperature-dominated GPP variations were mainly observed in the Tibetan Plateau and Yellow River Basin, which also exhibited a median stable increase in GPP. VPD-dominated GPP variations were found in the Southwest Karst region, Inner Mongolia, and Heilongjiang, showing a median and non-significant decrease. Soil moisture was the dominant factor in northwestern and southwestern China, leading to a decrease in GPP with a strong stability. Radiation-dominated areas were concentrated in southern China and the northernmost regions, where GPP increases were relatively unstable. Although temperature and radiation promoted GPP variations, temperature contributed significantly to GPP stability.

In regions with overlapping ecological engineering projects, temperature emerged as the primary driver of GPP (Figure 8; Table 3). Temperature and solar radiation were the main drivers in areas without ecological engineering projects or with fewer overlapping projects, such as Tibet and the Eastern China Coast. VPD and soil moisture contributed to GPP variations in regions with higher overlapping ecological engineering implementations. Specifically, VPD had a higher relative contribution to GPP in the Northeast, Northwest, and Southwest regions, where three or four overlapping

TABLE 1 The trend of GPP from 1981 to 2019 in ecological project areas.

Overlapping ecological projects	Increasing trends	Non-sig	Decreasing trends
0 ecological project	72.36%	10.25%	17.39%
1 ecological project	67.48%	6.52%	25.99%
2 ecological projects	63.59%	18.27%	18.14%
3 ecological projects	61.17%	18.97%	19.86%
4 ecological projects	63.25%	14.24%	22.51%
5 ecological projects	81.97%	7.95%	10.08%

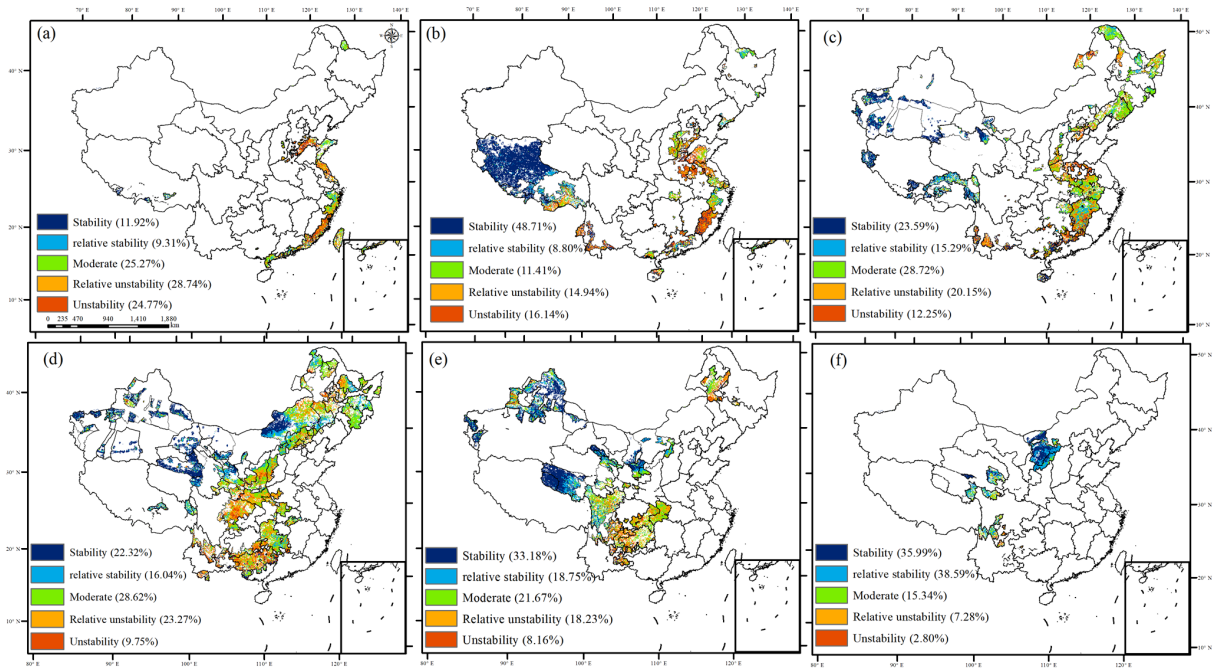

FIGURE 6
The stability of GPP from 1981 to 2019 in ecological project areas [**(A)** zero ecological project areas, **(B)** one ecological project area, **(C)** two ecological project areas, **(D)** three ecological project areas, **(E)** four ecological project areas, and **(F)** five ecological project areas].

ecological projects were prevalent, whereas soil moisture played a more prominent role in regions with five overlapping projects.

3.3 The sensitivity of GPP to climate change

The sensitivity of GPP to climate change was examined using four climate factors [temperature (TEM), vapor pressure deficit (VPD), solar radiation (RAD), and soil moisture (SOIL)] (Figure 9). The spatial distribution of the GPP sensitivity index (GSI) corresponded closely with GPP trends and stability. GPP exhibiting a significant increase or stability showed lower sensitivity to climate change, whereas GPP with a decreasing trend or instability exhibited a high sensitivity to climate change. More than 39.27% of China exhibited a high or relatively high GSI, primarily concentrated in the east coast, arid northwest region, Inner Mongolia, and the Southwest Karst region, where no or few ecological projects had been implemented. Conversely, the low and relatively low GSI accounted for 25.76%, mainly observed in the Yangtze River belt, northeastern China, and the Tibetan Plateau, where four or five ecological projects have been implemented (Figure 10 and Table 4). These findings suggest that the spatial distribution of decreasing trends or instability in GPP aligns with highly sensitive areas of GPP.

4 Discussion

4.1 Stability of GPP in the overlapping ecological engineering areas

Previous studies have predominantly focused on the GPP dynamics, often overlooking the stability and the impact of overlapping ecological projects on GPP (Seddon et al., 2016; Liu et al., 2023b). Our study revealed that 65.74% of GPP was

TABLE 2 The stability of GPP from 1981 to 2019 in ecological project areas.

Overlapping ecological projects	Stability	Relative stability	Moderate	Relative instability	Instability
0 ecological project	11.92%	9.31%	25.27%	28.74%	24.77%
1 ecological project	48.71%	8.80%	11.41%	14.94%	16.14%
2 ecological projects	23.59%	15.29%	28.72%	20.15%	12.25%
3 ecological projects	22.32%	16.04%	28.62%	23.27%	9.75%
4 ecological projects	33.18%	18.75%	21.67%	18.23%	8.16%
5 ecological projects	35.99%	38.59%	15.34%	7.28%	2.80%

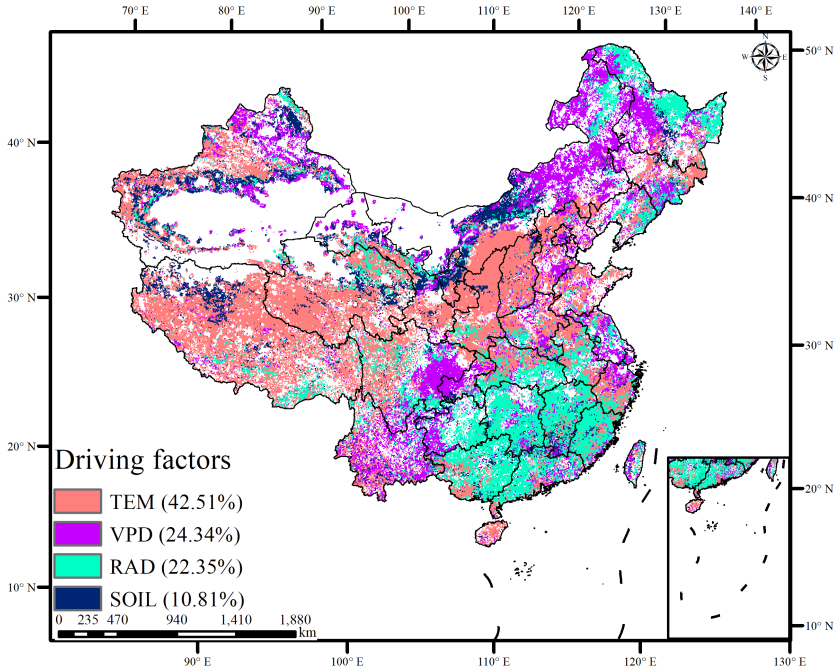

FIGURE 7
The dominant role of four climate variables to GPP variations (TEM, temperature; VPD, vapor pressure deficit; RAD, radiation; SOIL, soil moisture).

increasing, primarily in the eastern coastal areas and overlapping implementation of five ecological projects, such as the Grain to Green, the Natural Forest Resource Protection Project, the Three-River Ecological Conservation and Restoration Project, and the Three-North Shelter Forestation Project. Conversely, 20.90% of GPP showed a downward trend, mainly in two specific regions: areas with overlapping implementation of the Three-North Protective Forest Project and the Grain to Green Project, and

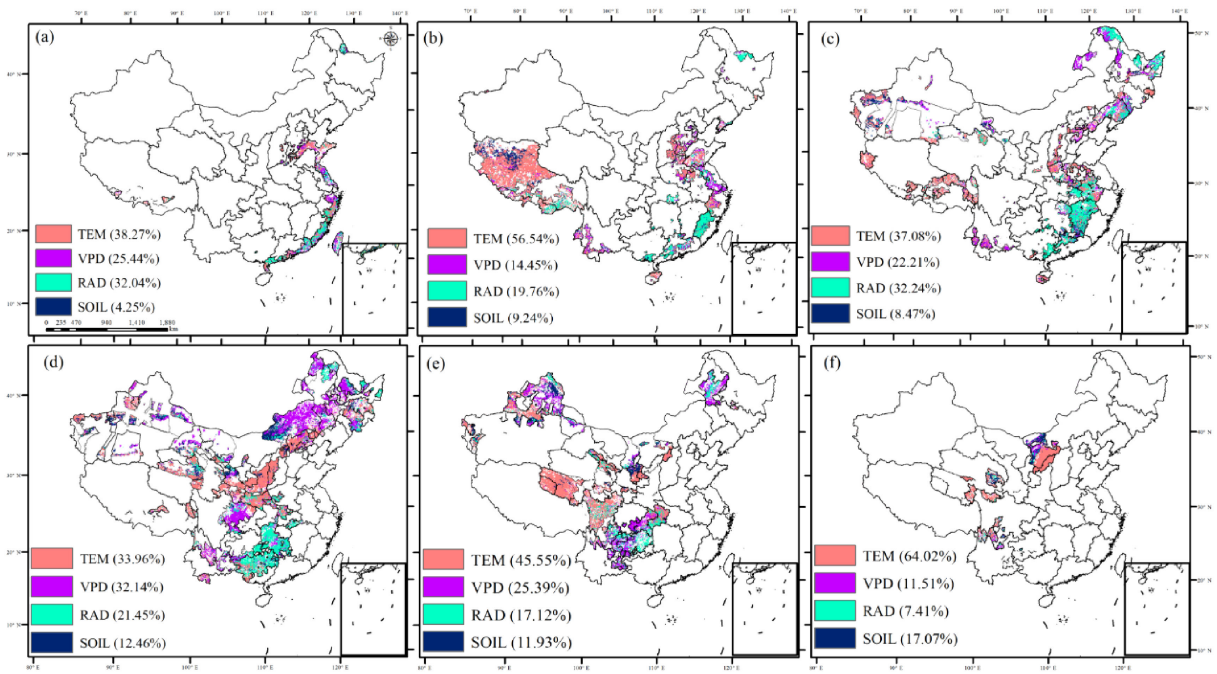

FIGURE 8
The dominant role of four climate variables to GPP variations in ecological project areas [TEM, temperature; VPD, vapor pressure deficit; RAD, solar radiation; SOIL, soil moisture; **(A)** zero ecological project areas, **(B)** one ecological project area, **(C)** two ecological project areas, **(D)** three ecological project areas, **(E)** four ecological project areas, and **(F)** five ecological project areas].

TABLE 3 The dominant role of four climate variables to GPP variations in ecological project areas.

Overlapping ecological projects	TEM	VPD	RAD	SOIL
0 ecological project	38.27%	25.44%	32.04%	4.25%
1 ecological project	56.54%	14.45%	19.76%	9.24%
2 ecological projects	37.08%	22.21%	32.24%	8.47%
3 ecological projects	33.96%	32.14%	21.45%	12.46%
4 ecological projects	45.55%	25.39%	17.12%	11.93%
5 ecological projects	64.02%	11.51%	7.41%	17.07%

TEM, temperature; VPD, vapor pressure deficit; RAD, solar radiation; SOIL, soil moisture.

regions where the Yangtze River Protective Forest Project and the rocky desertification management of the southwestern Karst region overlap. The former areas showed a strong stability, whereas the latter had relatively lower stability. Northwestern China's arid climate, characterized by water scarcity and high evapotranspiration, is unfavorable for carbon storage (Zhang et al., 2021; Xu et al., 2023). Previous research highlighted that restoration effects have promoted ecosystem recovery in the karst area in southwest China (Yue et al., 2022). However, our findings suggested that the GPP exhibited decreasing but unstable trends in regions where the Yangtze River Protective Forest Project overlaps with the rocky desertification management of the southwestern Karst region. This suggests heightened susceptibility to environmental perturbations. The Southwest Karst region's troughs and valleys are prone to water leakage and droughts, whereas its depressions and basins experience waterlogging, both of which hinder vegetation growth and reduce carbon sequestration (Wang et al., 2021; Zhu et al., 2023b).

4.2 Driving mechanism of GPP in the overlapping ecological engineering areas

The relative response of GPP to environmental perturbations and its driving factors is crucial for ecosystem resilience (Chen et al., 2017; Gao et al., 2018; Piao et al., 2019). Understanding the underlying processes within ecosystems is essential for exploring the sustainability and sensitivity of future carbon cycles and for providing a foundation for nature-based solutions (Zhang et al., 2019; Piao et al., 2022). Previous studies have shown that climate change has direct and significant effects on GPP (Wang et al., 2023; Zhu et al., 2023a). In regions with no or few overlapping ecological projects, temperature and radiation were the primary drivers of GPP changes. However, in regions affected by multiple overlapping ecological projects, water-related factors (VPD and soil moisture) were the primary drivers of GPP changes. This is primarily because the eastern region, with its favorable thermal and hydrological conditions, exhibits high vegetation cover and strong carbon sink capacity, contributing to carbon sink increases even in the absence or minimal presence of ecological projects (Lian et al., 2020). Conversely, in the northwest and southwest of China, harsh climatic conditions and limited moisture are the main factors restricting carbon sink growth; thus, the influence of precipitation-related factors is more pronounced (Liu et al., 2022, 2023a). Therefore, human intervention is necessary to prevent GPP decline and promote its increase in these regions.

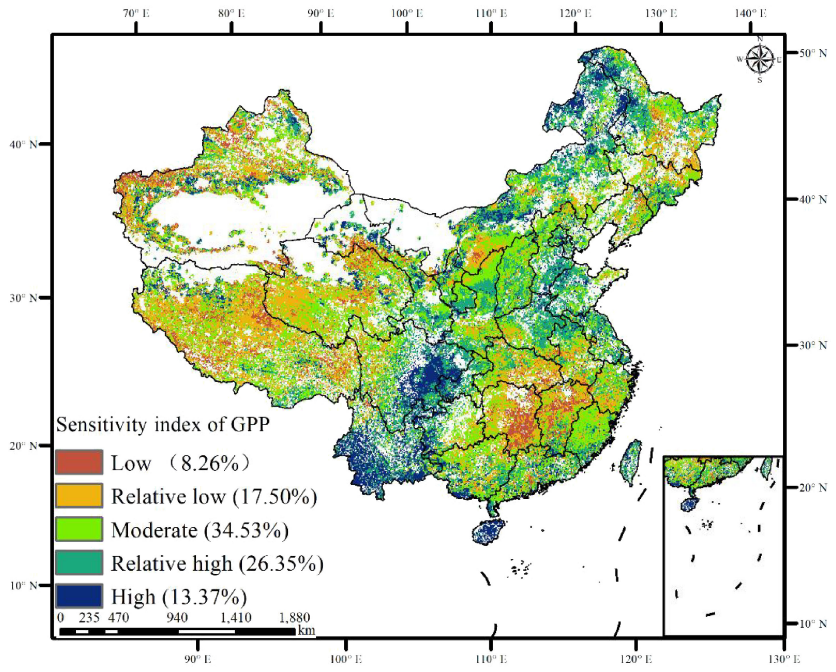

FIGURE 9
Sensitivity index of GPP in China.

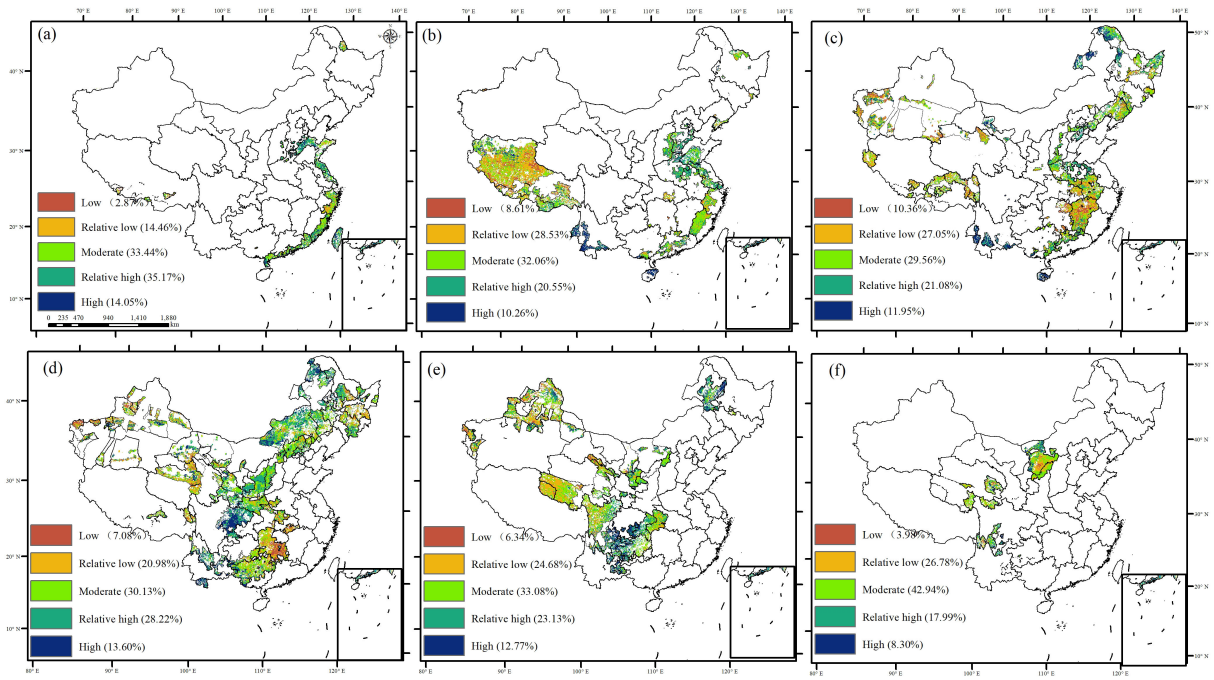

FIGURE 10
Sensitivity index of GPP in ecological project areas [**(A)** zero ecological project areas, **(B)** one ecological project area, **(C)** two ecological project areas, **(D)** three ecological project areas, **(E)** four ecological project areas, and **(F)** five ecological project areas].

4.3 The sensitivity of GPP to climate change in overlapping ecological engineering

GPP in areas with overlapping ecological projects was highly sensitive to human activities, particularly in ecological restoration priority areas such as the Loess Plateau and the Yangtze River economic belt. On the Loess Plateau, the implementation of various management measures and ecological construction projects, including slope management, integrated watershed management, ecological restoration programs, and the Grain for Green Program (GGP), has significantly increased forest and grassland vegetation coverage. Since the GGP's inception, vegetation coverage on the Loess Plateau has risen from 31.6% in 1999 to 67% in 2020, marking a historic transformation from degradation to significant greening (Bai et al., 2019; Chen et al., 2021b). Post-2000, the rate of growth of greenness in the Loess Plateau has outpaced the national average (Kou et al., 2021). This restoration has substantially increased carbon sequestration, transforming the Loess Plateau from a carbon source to a carbon sink, especially in hilly and gully areas where farmland has been returned to forests and grasslands (Zheng et al., 2019). Conversely, the Yangtze River Economic Belt, characterized by dense populations, industrial activities, and high socio-economic development, exhibits a continuous decline in GPP due to extensive construction and arable land use (Jiang et al., 2022).

The decreased and unstable GPP in the China karst and northwest desertification region was highly sensitive to climate change, driven mainly by increased vapor pressure deficit (VPD) and decreased soil moisture. Ecological engineering has been shown to increase vegetation growth and carbon stock in the karst region of southwest China (Tong et al., 2018, 2020). However, this region is still challenged by the distribution of soil and water resources and rapid hydrological changes, resulting in slow soil formation rates, poor water-holding capacity, and low ecological recoverability (Jiao et al., 2024). Low soil water availability and high atmospheric saturation air pressure differences are the main drivers of vegetation greening stress

TABLE 4 Sensitivity index of GPP in ecological project areas.

Overlapping ecological projects	Low	Relatively low	Moderate	Relatively high	High
0 ecological project	2.87%	14.46%	33.44%	35.17%	14.05%
1 ecological project	8.61%	28.53%	32.06%	20.55%	10.26%
2 ecological projects	10.36%	27.05%	29.56%	21.08%	11.95%
3 ecological projects	7.08%	20.98%	30.13%	28.22%	13.60%
4 ecological projects	6.34%	24.68%	33.08%	23.13%	12.77%
5 ecological projects	3.98%	26.78%	42.94%	17.99%	8.30%

in the karst region (Song et al., 2022). Drought stress due to water scarcity limits the recovery and stability of karst ecosystems, making GPP highly sensitive to climate change (Konings et al., 2017). Additionally, terracing and deforestation on slopes greater than 25° have further damaged the already fragile ecosystems in these areas (Wang et al., 2019, 2021). Vegetation requires significant amounts of energy and nutrients, with soil moisture being crucial, particularly in semi-arid areas (Li et al., 2022). Global climate change is decreasing soil moisture in many regions due to increasing the demand for water evaporation by warming (Carminati and Javaux, 2020). Furthermore, increased vegetation due to climate warming has exacerbated soil drying in arid regions (Deng et al., 2020; Liu et al., 2023c). The decertified area, situated in a climate-sensitive zone with a fragile ecological environment, showed that GPP was highly responsive to soil moisture, with decreased soil moisture being the primary cause of reduced GPP (Song et al., 2022). Soil moisture is essential for the normal growth of vegetation and the sustainable development of agriculture, forestry, and grassland industries in the Loess Plateau region (Li et al., 2022). In semi-arid and arid areas, the relationship between vegetation and soil moisture is more pronounced, and insufficient soil moisture restricts plant growth on the Loess Plateau and in the dry northwest region.

4.4 Implications and limitations

This study primarily relies on the reliability of data. While GPP has been accurately estimated in previous studies, recent remote sensing-based global terrestrial carbon, water, and energy budgets remain uncertain (Chen et al., 2021a). Previous integrated flux models have advanced the monitoring of the terrestrial carbon cycle, but they only partially incorporated coupled land-atmosphere fluxes (Yan et al., 2019). Consequently, gaining a comprehensive understanding of the terrestrial carbon cycle alongside other processes remains challenging. These uncoupled scenarios may overlook critical dynamics of fundamental terrestrial biophysical processes, and using different forcing data for individual flux models can lead to internal inconsistencies between carbon and other flux estimates, resulting in significant biases in global annual flux budgets (Zhou et al., 2016). Furthermore, individual flux products can introduce significant biases in estimating ecosystem functional properties (Chang et al., 2024). Therefore, this study utilized an improved satellite-based model of coupled processes, the BESS v2.0. This new version integrated a newly developed ecosystem respiration module and an optimal maximum rate of carboxylation (V_{cmax}) based model, extending the temporal coverage of the flux dataset from 1982 to 2019. BESS v2.0 products better match flux site observations than other products, ensuring that BESS v2.0 is a reliable and independent set of products from other global satellites and contributing to research related to global carbon, water, and energy budgets in a coupled and comprehensive manner. Notably, carbon flux estimates by BESS in the tropics showed significant differences compared to other models (Zhou et al., 2016). This divergence can be attributed to several factors. First, the reliability of remote-sensed GPP products is compromised by poor-quality forcing data in the tropics due to prolonged cloud contamination. Second, carbon fluxes may not closely follow vegetation indices due to oversaturation but are more sensitive to meteorological factors. Third, the less prominent variation obtained by satellite-derived key forcing data and insufficient spatial coverage of flux site observations in tropical forests likely contributed to the comparatively low performance in some data-driven models (Jiang and Ryu, 2016). Additionally, the significant bias over croplands may be partly due to the lack of distinction between C3 and C4 crops in some machine-learning GPP products (Jiang and Ryu, 2016). We also noted that other proxies, such as solar-induced fluorescence (SIF), may perform well as suggested. However, the available data from SIF start only from 2000, limiting our understanding of long-term GPP dynamics (Jiang and Ryu, 2016). Future research should consider combining SIF with vegetation indices to extend the SIF-GPP relationship back to the start of the remote sensing era in the 1980s.

Investigating the impact of climatic variations on interannual variability of land carbon flux remains crucial (Piao et al., 2020). However, quantifying the influence of other variables such as land cover changes (urbanization) and vegetation growth stages on GPP trends proves challenging due to their complexity (Seddon et al., 2016). This study focused exclusively on climate change effects; therefore, we did not present results on land cover changes or vegetation growth stages directly driving GPP variations. Nevertheless, these stages may modulate vegetation responses to climatic shifts. Notably, recent observations suggest a weakening relationship between GPP and temperature (Piao et al., 2014). Hence, future research should adopt novel methodologies to comprehensively assess GPP changes. While our investigation primarily addressed annual-scale climatic controls, ongoing discussions persist regarding seasonal variability. Environmental impacts during spring, summer, and autumn may differ significantly. Thus, future studies could explore how GPP responds to climate fluctuations across diverse temporal scales.

Despite some inevitable limitations, we point out that our results can help future researchers better understand the stability of GPP and its driving mechanisms, providing scientific support for ecological protection projects.

5 Conclusions

This study investigated the stability and sensitivity of GPP to climate variability in China in the last four decades and then explored the driving mechanisms of GPP variations. The meaningful findings are as follows: GPP generally showed an increased trend, with less stability in Eastern regions, whereas a decreased trend with higher stability was observed in Western and Southwest China. Notably, GPP stability was highest (74.58%) in areas with five overlapping ecological projects: Grain to Green, Natural Forest Resource Protection, Three-River Ecological Conservation and Restoration, Return Grazing to Grassland, and Three-North Shelter Forestation. In regions with minimal or no overlapping ecological projects, temperature and radiation mainly influenced GPP variations. In contrast, water-related factors (VPD and soil moisture) significantly affected GPP in areas with multiple overlapping ecological projects. Particularly in areas impacted by the simultaneous implementation of the five projects, GPP showed an increasing trend (81.97%) and lower sensitivity (3.98%) to climate change.

Data availability statement

The original contributions presented in the study are included in the article/Supplementary Material. Further inquiries can be directed to the corresponding author.

Author contributions

XX: Conceptualization, Data curation, Formal analysis, Funding acquisition, Investigation, Project administration, Resources, Software, Validation, Visualization, Writing – original draft, Writing – review & editing. FJ: Investigation, Methodology, Project administration, Validation, Writing – original draft, Writing – review & editing. HG: Investigation, Project administration, Supervision, Writing – original draft, Writing – review & editing. JL: Funding acquisition, Project administration, Resources, Software, Supervision, Validation, Visualization, Writing – original draft. JM: Writing – review & editing, Data curation, Validation, Visualization, Software. KZ: Methodology, Project administration, Resources, Writing – original draft. DL: Writing – review & editing, Formal analysis, Validation, Visualization. YY: Project administration, Software, Supervision, Writing – original draft. NL: Formal analysis, Writing – original draft. QW: Investigation, Software, Writing – original draft. YZ: Data curation, Methodology, Writing – original draft. JQ: Methodology, Project administration, Supervision, Writing – original draft. CZ: Project administration, Validation, Visualization, Writing – original draft.

Funding

The author(s) declare financial support was received for the research, authorship, and/or publication of this article. This work was supported by the National Natural Science Foundation of Jiangsu Province (BK20220205, SBK2024042983), the National Key R&D Program of China (2021YFB3901104), the Special Fund of the Jiangsu for Carbon Peak and Carbon Neutralization Science and Technology Innovation (BK20220021), the National Natural Science Foundation of China (42101103), and the Special Fund of the Chinese Central Government for Basic Scientific Research Operations in the commonweal Research Institute (GYZX210405, GYZX240304).

Conflict of interest

The authors declare that the research was conducted in the absence of any commercial or financial relationships that could be construed as a potential conflict of interest.

Publisher's note

All claims expressed in this article are solely those of the authors and do not necessarily represent those of their affiliated organizations, or those of the publisher, the editors and the reviewers. Any product that may be evaluated in this article, or claim that may be made by its manufacturer, is not guaranteed or endorsed by the publisher.

Supplementary material

The Supplementary Material for this article can be found online at: https://www.frontiersin.org/articles/10.3389/fpls.2024.1440993/full#supplementary-material

SUPPLEMENTARY FIGURE S1
The trend of driving factors on GPP from 1982 to 2019 in China [**(A)** Temperature; **(B)** VPD; **(C)** radiation; **(D)** soil moisture].

References

Abatzoglou, J. T., Dobrowski, S. Z., Parks, S. A., and Hegewisch, K. C. (2018). TerraClimate, a high-resolution global dataset of monthly climate and climatic water balance from 1958-2015. *Sci Data.* 5, 170191.

Anav, A., Friedlingstein, P., Beer, C., Ciais, P., Harper, A., Jones, C., et al. (2015). Spatiotemporal patterns of terrestrial gross primary production: A review. *Rev. Geophys.* 53, 785–818. doi: 10.1002/2015rg000483

Anderegg, W. R. L., Trugman, A. T., Badgley, G., Anderson, C. M., Bartuska, A., Ciais, P., et al. (2020). Climate-driven risks to the climate mitigation potential of forests. *Science* 368, 1–9. doi: 10.1126/science.aaz7005

Bai, M., Mo, X., Liu, S., and Hu, S. (2019). Contributions of climate change and vegetation greening to evapotranspiration trend in a typical hilly-gully basin on the Loess Plateau, China. *Sci. Total Environ.* 657, 325–339. doi: 10.1016/j.scitotenv.2018.11.360

Carlson, J. L., Haffenden, R. A., Bassett, G. W., Buehring, W. A., Collins, M. J. III, Folga, S. M., et al. (2012). doi: 10.2172/1044521

Carminati, A., and Javaux, M. (2020). Soil rather than xylem vulnerability controls stomatal response to drought. *Trends Plant Sci.* 25, 868–880. doi: 10.1016/j.tplants.2020.04.003

Chang, J., Yue, Y., Tong, X., Brandt, M., Zhang, C., Zhang, X., et al. (2023). Rural outmigration generates a carbon sink in South China karst. *Prog. Phys. Geogr.: Earth Environ.* 47, 03091333231154177. doi: 10.1177/03091333231154177

Chang, X., Feng, Q., Ning, T., Xi, H., and Yin, Z. (2024). Modelling and attributing growing season GPP change by improving Budyko's limitation framework in the inland river basin of Northwestern China. *Agric. For. Meteorol.* 355, 1–12. doi: 10.1016/j.agrformet.2024.110139

Chen, Z., Chen, Y., and Li, W. (2012). Response of runoff to change of atmospheric 0° C level height in summer in arid region of Northwest China. *Sci. China Earth Sci.* 55, 1533–1544. doi: 10.1007/s11430-012-4472-6

Chen, Y., Feng, X., Tian, H., Wu, X., Gao, Z., Feng, Y., et al. (2021b). Accelerated increase in vegetation carbon sequestration in China after 2010: A turning point resulting from climate and human interaction. *Glob Chang. Biol.* 27, 5848–5864. doi: 10.1111/gcb.15854

Chen, Y., Kelly, R., Genet, H., Lara, M. J., Chipman, M. L., McGuire, A. D., et al. (2022). Resilience and sensitivity of ecosystem carbon stocks to fire-regime change in Alaskan tundra. *Sci. Total Environ.* 806, 151482. doi: 10.1016/j.scitotenv.2021.151482

Chen, M., Rafique, R., Asrar, G. R., Bond-Lamberty, B., Ciais, P., Zhao, F., et al. (2017). Regional contribution to variability and trends of global gross primary productivity. *Environ. Res. Lett.* 12, 233–240. doi: 10.1088/1748-9326/aa8978

Chen, S., Zhang, Y., Wu, Q., Liu, S., Song, C., Xiao, J., et al. (2021a). Vegetation structural change and CO2 fertilization more than offset gross primary production decline caused by reduced solar radiation in China. *Agric. For. Meteorol.* 296, 1–12. doi: 10.1016/j.agrformet.2020.108207

Cheng, L., Zhang, L., Wang, Y. P., Canadell, J. G., Chiew, F. H. S., Beringer, J., et al. (2017). Recent increases in terrestrial carbon uptake at little cost to the water cycle. *Nat. Commun.* 8, 110. doi: 10.1038/s41467-017-00114-5

Cui, J., Yang, H., Huntingford, C., Kooperman, G. J., Lian, X., He, M., et al. (2021). Vegetation response to rising CO2 amplifies contrasts in water resources between global wet and dry land areas. *Geophys. Res. Lett.* 48, 1–12. doi: 10.1029/2021gl094293

Deng, Y., Wang, S., Bai, X., Luo, G., Wu, L., Chen, F., et al. (2020). Vegetation greening intensified soil drying in some semi-arid and arid areas of the world. *Agr. For. Meteorol.* 585, 292–293. doi: 10.1016/j.agrformet.2020.108103

Dong, J., Li, L., Li, Y., and Yu, Q. (2022). Inter-comparisons of mean, trend and interannual variability of global terrestrial gross primary production retrieved from remote sensing approach. *Sci. Total Environ.* 822, 153343. doi: 10.1016/j.scitotenv.2022.153343

Gao, J., Jiao, K., and Wu, S. (2018). Quantitative assessment of ecosystem vulnerability to climate change: methodology and application in China. *Environ. Res. Lett.* 13, 1–12. doi: 10.1088/1748-9326/aadd2e

Guo, W., Huang, S., Huang, Q., Leng, G., Mu, Z., Han, Z., et al. (2023). Drought trigger thresholds for different levels of vegetation loss in China and their dynamics. *Agr. For. Meteorol.* 331. doi: 10.1016/j.agrformet.2023.109349

He, B., Chen, C., Lin, S., Yuan, W., Chen, H. W., Chen, D., et al. (2022a). Worldwide impacts of atmospheric vapor pressure deficit on the interannual variability of terrestrial carbon sinks. *Natl. Sci. Rev.* 9, nwab150. doi: 10.1093/nsr/nwab150

He, M., Lian, X., Cui, J., Xu, H., and Piao, S. (2022b). Vegetation physiological response to increasing atmospheric CO2 slows the decreases in the seasonal amplitude of temperature. *Geophys. Res. Lett.* 49, 1–8. doi: 10.1029/2022gl097829

Holden, E., Linnerud, K., and Banister, D. (2014). Sustainable development: Our Common Future revisited. *Global Environ. Change* 26, 130–139. doi: 10.1016/j.gloenvcha.2014.04.006

Hooper, T., Beaumont, N., Griffiths, C., Langmead, O., and Somerfield, P. J. (2017). Assessing the sensitivity of ecosystem services to changing pressures. *Ecosys. Serv.* 24, 160–169. doi: 10.1016/j.ecoser.2017.02.016

Hu, M., Chen, Y., Chen, F., Zhao, X., Yue, W., Cao, H., et al. (2023). Climate change increases the instability of the water supply for hydropower stations on the Tibetan Plateau. *Environ. Res. Lett.* 18, 114040. doi: 10.1088/1748-9326/ad0311

Hu, X., Ma, C., Huang, P., and Guo, X. (2021). Ecological vulnerability assessment based on AHP-PSR method and analysis of its single parameter sensitivity and spatial autocorrelation for ecological protection – A case of Weifang City, China. *Ecol. Indic.* 125, 1–16. doi: 10.1016/j.ecolind.2021.107464

Jiang, Y., Guan, D., He, X., Yin, B., Zhou, L., Sun, L., et al. (2022). Quantification of the coupling relationship between ecological compensation and ecosystem services in the Yangtze River Economic Belt, China. *Land Use Policy* 114, 1434–1445. doi: 10.1016/j.landusepol.2022.105995

Jiang, C., and Ryu, Y. (2016). Multi-scale evaluation of global gross primary productivity and evapotranspiration products derived from Breathing Earth System Simulator (BESS). *Remote Sens. Environ.* 186, 528–547. doi: 10.1016/j.rse.2016.08.030

Jiao, F., Xu, X., Zhang, M., Gong, H., Sheng, H., Wang, K., et al. (2024). Bedrock regulated climatic controls on the interannual variation of land sink in South-West China karst through soil water availability. *Catena* 237, 1–12. doi: 10.1016/j.catena.2024.107819

Kan, F., Lian, X., Cui, J., Chen, A., Mao, J., He, M., et al. (2023). Discrepant trends in global land-surface and air temperatures controlled by vegetation biophysical feedbacks. *Environ. Res. Lett.* 18, 1–7. doi: 10.1088/1748-9326/ad0680

Konings, A. G., Williams, A. P., and Gentine, P. (2017). Sensitivity of grassland productivity to aridity controlled by stomatal and xylem regulation. *Nat. Geosci.* 10, 284–288. doi: 10.1038/ngeo2903

Kou, P., Xu, Q., Jin, Z., Yunus, A. P., Luo, X., and Liu, M. (2021). Complex anthropogenic interaction on vegetation greening in the Chinese Loess Plateau. *Sci. Total Environ.* 778, 146065. doi: 10.1016/j.scitotenv.2021.146065

Li, W., Migliavacca, M., Forkel, M., Denissen, J. M. C., Reichstein, M., Yang, H., et al. (2022). Widespread increasing vegetation sensitivity to soil moisture. *Nat. Commun.* 13, 3959. doi: 10.1038/s41467-022-31667-9

Li, B., Ryu, Y., Jiang, C., Dechant, B., Liu, J., Yan, Y., et al. (2023). BESSv2.0: A satellite-based and coupled-process model for quantifying long-term global land–atmosphere fluxes. *Remote Sens. Environ.* 295, 1–13. doi: 10.1016/j.rse.2023.113696

Li, D., Wu, S., Liu, L., Zhang, Y., and Li, S. (2018). Vulnerability of the global terrestrial ecosystems to climate change. *Glob Chang. Biol.* 24, 4095–4106. doi: 10.1111/gcb.14327

Lian, J., Chen, H., Wang, F., Nie, Y., and Wang, K. (2020). Separating the relative contributions of climate change and ecological restoration to runoff change in a mesoscale karst basin. *Catena* 194, 1–12. doi: 10.1016/j.catena.2020.104705

Lin, S., Hu, Z., Wang, Y., Chen, X., He, B., Song, Z., et al. (2023). Underestimated interannual variability of terrestrial vegetation production by terrestrial ecosystem models. *Global Biogeochem. Cy* 37, 1–12. doi: 10.1029/2023gb007696

Liu, Z., Chen, Z., Yu, G., Zhang, W., Zhang, T., and Han, L. (2023c). The role of climate, vegetation, and soil factors on carbon fluxes in Chinese drylands. *Front. Plant Sci.* 14. doi: 10.3389/fpls.2023.1060066

Liu, P., Chi, Y., Chen, J., and Zhou, L. (2023b). Global climate regulates dimensions of terrestrial ecosystem stability. *Ecosphere* 14, 1–12. doi: 10.1002/ecs2.4577

Liu, H., Wang, Z., Wang, Z., Zeng, Y., Xue, P., and Zhang, M. (2023a). Stability of the ecosystem gross primary productivity increasing in Chinese forestry ecological engineering area. *Agric. Ecosyst. Environ.* 356, 1–11. doi: 10.1016/j.agee.2023.108636

Liu, H., Xu, X., Lin, Z., Zhang, M., Ying, M., Huang, C., et al. (2016). Climatic and human impacts on quasi-periodic and abrupt changes of sedimentation rate at multiple time scales in Lake Taihu, China. *J. Hydrol.* 543, 739–748. doi: 10.1016/j.jhydrol.2016.10.046

Liu, C., Zhang, X., Wang, T., Chen, G., Zhu, K., Wang, Q., et al. (2022). Detection of vegetation coverage changes in the Yellow River Basin from 2003 to 2020. *Ecol. Indic.* 138, 1–15. doi: 10.1016/j.ecolind.2022.108818

Mann, H. B. (1945). Nonparametric test against trend. *Econometrica* 13, 245–259. doi: 10.2307/1907187

Messori, G., Ruiz-Pérez, G., Manzoni, S., and Vico, G. (2019). Climate drivers of the terrestrial carbon cycle variability in Europe. *Environ. Res. Lett.* 14, 1–15. doi: 10.1088/1748-9326/ab1ac0

Nikinmaa, L., Lindner, M., Cantarello, E., Jump, A. S., Seidl, R., Winkel, G., et al. (2020). Reviewing the use of resilience concepts in forest sciences. *Curr. For Rep.* 6, 61–80. doi: 10.1007/s40725-020-00110-x

Niu, L., Shao, Q., Ning, J., and Huang, H. (2022). Ecological changes and the tradeoff and synergy of ecosystem services in western China. *J. Geographical Sci.* 32, 1059–1075. doi: 10.1007/s11442-022-1985-6

Niu, L., Shao, Q., Ning, J., Liu, S., Zhang, X., and Zhang, T. (2023). The assessment of ecological restoration effects on Beijing-Tianjin Sandstorm Source Control Project area during 2000–2019. *Ecol. Eng.* 186, 1–12. doi: 10.1016/j.ecoleng.2022.106831

Nord-Larsen, T., Vesterdal, L., Bentsen, N. S., and Larsen, J. B. (2019). Ecosystem carbon stocks and their temporal resilience in a semi-natural beech-dominated forest. *For. Ecol. Manag.* 447, 67–76. doi: 10.1016/j.foreco.2019.05.038

Pennekamp, F., Pontarp, M., Tabi, A., Altermatt, F., Alther, R., Choffat, Y., et al. (2018). Biodiversity increases and decreases ecosystem stability. *Nature* 563, 109–112. doi: 10.1038/s41586-018-0627-8

Piao, S., He, Y., Wang, X., and Chen, F. (2022). Estimation of China's terrestrial ecosystem carbon sink: Methods, progress and prospects. *Sci. China Earth Sci.* 65, 641–651. doi: 10.1007/s11430-021-9892-6

Piao, S., Nan, H., Huntingford, C., Ciais, P., Friedlingstein, P., Sitch, S., et al. (2014). Evidence for a weakening relationship between interannual temperature variability and northern vegetation activity. *Nat. Commun.* 5, 5018. doi: 10.1038/ncomms6018

Piao, S., Wang, X., Park, T., Chen, C., Lian, X., He, Y., et al. (2019). Characteristics, drivers and feedbacks of global greening. *Nat. Rev. Earth Environ.* 1, 14–27. doi: 10.1038/s43017-019-0001-x

Piao, S., Wang, X., Wang, K., Li, X., Bastos, A., Canadell, J. G., et al. (2020). Interannual variation of terrestrial carbon cycle: Issues and perspectives. *Glob Chang. Biol.* 26, 300–318. doi: 10.1111/gcb.14884

Qiao, L., and Xia, H. (2024). The impact of drought time scales and characteristics on gross primary productivity in China from 2001 to 2020. *Geo-spatial Inf. Sci.* 651, 1–19. doi: 10.1080/10095020.2024.2315279

Seddon, A. W., Macias-Fauria, M., Long, P. R., Benz, D., and Willis, K. J. (2016). Sensitivity of global terrestrial ecosystems to climate variability. *Nature* 531, 229–232. doi: 10.1038/nature16986

Shao, Q., Liu, S., Ning, J., Liu, G., Yang, F., Zhang, X., et al. (2023). Remote sensing assessment of the ecological benefits provided by national key ecological projects in China during 2000–2019. *J. Geographical Sci.* 33, 1587–1613. doi: 10.1007/s11442-023-2144-4

Shen, Z., Zhang, Q., Piao, S., Peñuelas, J., Stenseth, N. C., Chen, D., et al. (2021). Mining can exacerbate global degradation of dryland. *Geophys. Res. Lett.* 48, 1–10. doi: 10.1029/2021gl094490

Song, W., Feng, Y., and Wang, Z. (2022). Ecological restoration programs dominate vegetation greening in China. *Sci. Total Environ.* 848, 157729. doi: 10.1016/j.scitotenv.2022.157729

Thackeray, S. J., Henrys, P. A., Hemming, D., Bell, J. R., Botham, M. S., Burthe, S., et al. (2016). Phenological sensitivity to climate across taxa and trophic levels. *Nature* 535, 241–245. doi: 10.1038/nature18608

Tong, X., Brandt, M., Yue, Y., Ciais, P., Rudbeck Jepsen, M., Penuelas, J., et al. (2020). Forest management in southern China generates short term extensive carbon sequestration. *Nat. Commun.* 11, 129. doi: 10.1038/s41467-019-13798-8

Tong, X., Brandt, M., Yue, Y., Horion, S., Wang, K., Keersmaecker, W. D., et al. (2018). Increased vegetation growth and carbon stock in China karst via ecological engineering. *Nat. Sustainabil.* 1, 44–50. doi: 10.1038/s41893-017-0004-x

Walker, B., Holling, C. S., Carpenter, S. R., and Kinzig, A. P. (2004). Resilience, adaptability and transformability in social-ecological systems. *Ecol. Soc.* 9. doi: 10.5751/es-00650-090205

Wang, M., Ding, Z., Wu, C., Song, L., Ma, M., Yu, P., et al. (2021). Divergent responses of ecosystem water-use efficiency to extreme seasonal droughts in Southwest China. *Sci. Total Environ.* 760, 143427. doi: 10.1016/j.scitotenv.2020.143427

Wang, K., Piao, S., He, Y., Liu, Y., and He, H. (2022). Spatial variations and mechanisms for the stability of terrestrial carbon sink in China. *Sci. China Earth Sci.* 66, 227–236. doi: 10.1007/s11430-021-1003-5

Wang, Y., Xue, K., Hu, R., Ding, B., Zeng, H., Li, R., et al. (2023). Vegetation structural shift tells environmental changes on the Tibetan Plateau over 40 years. *Sci. Bull. (Beijing)* 68, 1928–1937. doi: 10.1016/j.scib.2023.07.035

Wang, K., Zhang, C., Chen, H., Yue, Y., Zhang, W., Zhang, M., et al. (2019). Karst landscapes of China: patterns, ecosystem processes and services. *Landscape Ecol.* 34, 2743–2763. doi: 10.1007/s10980-019-00912-w

Wang, T., Zhang, Y., Yue, C., Wang, Y., Wang, X., Lyu, G., et al. (2024). Progress and challenges in remotely sensed terrestrial carbon fluxes. *Geo-spatial Inf. Sci.*, 1–21. doi: 10.1080/10095020.2024.2336599

Xu, X., Jiao, F., Liu, H., Gong, H., Zou, C., Lin, N., et al. (2022). Persistence of increasing vegetation gross primary production under the interactions of climate change and land use changes in Northwest China. *Sci. Total Environ.* 834, 155086. doi: 10.1016/j.scitotenv.2022.155086

Xu, X., Liu, J., Jiao, F., Zhang, K., Ye, X., Gong, H., et al. (2023). Ecological engineering induced carbon sinks shifting from decreasing to increasing during 1981-2019 in China. *Sci. Total Environ.* 864, 161037. doi: 10.1016/j.scitotenv.2022.161037

Xu, H., Zhao, C., and Wang, X. (2019). Spatiotemporal differentiation of the terrestrial gross primary production response to climate constraints in a dryland mountain ecosystem of northwestern China. *Agr. For. Meteorol.*, 276–277. doi: 10.1016/j.agrformet.2019.107628

Yan, H., Wang, S. Q., Wang, J. B., Cao, Y., Xu, L. L., Wu, M. X., et al. (2019). Multi-model analysis of climate impacts on plant photosynthesis in China during 2000–2015. *Int. J. Climatol.* 39, 5539–5555. doi: 10.1002/joc.6170

Yue, Y., Qi, X., Wang, K., Liao, C., Tong, X., Brandt, M., et al. (2022). Large scale rocky desertification reversal in South China karst. *Prog. Phys. Geogr.: Earth Environ.* 46, 661–675. doi: 10.1177/03091333221083111

Zhang, H., Li, L., Zhao, X., Chen, F., Wei, J., Feng, Z., et al. (2024a). Changes in vegetation NDVI and its response to climate change and human activities in the ferGhana basin from 1982 to 2015. *Remote Sens.* 16, 1–9. doi: 10.3390/rs16071296

Zhang, L., Ren, X., Wang, J., He, H., Wang, S., Wang, M., et al. (2019). Interannual variability of terrestrial net ecosystem productivity over China: regional contributions and climate attribution. *Environ. Res. Lett.* 14, 1–9. doi: 10.1088/1748-9326/aaec95

Zhang, X., Wang, Y. P., Rayner, P. J., Ciais, P., Huang, K., Luo, Y., et al. (2021). A small climate-amplifying effect of climate-carbon cycle feedback. *Nat. Commun.* 12, 2952. doi: 10.1038/s41467-021-22392-w

Zhang, Y., Wang, H., Shao, X., Liu, H., Zhu, H., Wang, L., et al. (2024b). High-resolution reconstruction of April–September precipitation and major extreme drougts in China over the past ~530 years. *Sci. Bull.* 1–19. doi: 10.1016/j.scib.2024.06.034

Zheng, K., Wei, J. Z., Pei, J. Y., Cheng, H., Zhang, X. L., Huang, F. Q., et al. (2019). Impacts of climate change and human activities on grassland vegetation variation in the Chinese Loess Plateau. *Sci. Total Environ.* 660, 236–244. doi: 10.1016/j.scitotenv.2019.01.022

Zhou, S., Zhang, Y., Caylor, K. K., Luo, Y., Xiao, X., Ciais, P., et al. (2016). Explaining inter-annual variability of gross primary productivity from plant phenology and physiology. *Agric. For. Meteorol.* 226-227, 246–256. doi: 10.1016/j.agrformet.2016.06.010

Zhu, Q., Chen, H., Peng, C., Liu, J., Piao, S., He, J. S., et al. (2023a). An early warning signal for grassland degradation on the Qinghai-Tibetan Plateau. *Nat. Commun.* 14, 6406. doi: 10.1038/s41467-023-42099-4

Zhu, X., Liu, H., He, W., Wu, L., and Liu, F. (2023b). Regolith water storage patterns determine vegetation productivity in global karst regions. *Geoderma* 430, 1–7. doi: 10.1016/j.geoderma.2022.116292

frontiers | Frontiers in Plant Science

TYPE Original Research
PUBLISHED 26 November 2024
DOI 10.3389/fpls.2024.1482077

OPEN ACCESS

EDITED BY
Samuel Kuria Kiboi,
University of Nairobi, Kenya

REVIEWED BY
Jiangzhou Xia,
Tianjin Normal University, China
Hanxi Wang,
Harbin Normal University, China

*CORRESPONDENCE
Jie Qiu
qiujie@nies.org
Changxin Zou
zouchangxin@nies.org
Kun Zhang
zhangkun@nies.org

RECEIVED 17 August 2024
ACCEPTED 31 October 2024
PUBLISHED 26 November 2024

CITATION
Xu X, Jiao F, Lin D, Qiu J, Zou C and Zhang K (2024) Assessment of the potential for carbon sink enhancement in the overlapping ecological project areas of China. *Front. Plant Sci.* 15:1482077. doi: 10.3389/fpls.2024.1482077

Assessment of the potential for carbon sink enhancement in the overlapping ecological project areas of China

Xiaojuan Xu[1], Fusheng Jiao[2], Dayi Lin[1], Jie Qiu[1*], Changxin Zou[1*] and Kun Zhang[1*]

[1]Nanjing Institute of Environmental Sciences, Ministry of Ecology and Environmental of the People's Republic of China, Nanjing, China, [2]School of Geography, Nanjing Normal University, Nanjing, China

Ecological engineering can significantly improve ecosystem carbon sequestration. However, few studies have projected the carbon sink trends in regions where ecological engineering projects overlap and have not considered the different climate change conditions and land use scenarios. Using the ensemble empirical mode decomposition method and machine learning algorithms (enhanced boosted regression trees), the aims of this study to elucidate the stability of carbon sinks and their driving mechanisms in areas where ecological projects overlap and to predict the potential enhancement in carbon sinks under varying climate and human activity scenarios. The findings revealed that: (1) The carbon sinks clearly and steadily increased in regions where five ecological projects were implemented from 1982 to 2019. In contrast, the carbon sinks did not significantly increase in regions with two or three ecological projects. (2) As the number of ecological projects increased, the impact of human activities on the carbon sinks gradually decreased. In eastern China, rapid economic development and significant interference from human activities hindered the growth of carbon sinks. In contrast, in western China, the warming and humidification trend of the climate, large-scale afforestation, and other ecological projects have significantly improved carbon sinks. (3) The regions with five overlapping ecological projects exhibited the greatest enhancement and stability of carbon sinks under different scenarios. Compared with the SSP585 scenario, under the SSP126 scenario, the carbon sinks increased, and their stability was greater. Achieving carbon neutrality requires major ecological projects to account for the limitations imposed by climatic conditions. Instead of isolated projects or the implementation of single restoration measures, a comprehensive approach that uses the synergistic effects of combined ecological strategies is recommended.

KEYWORDS

carbon sinks, prediction, climate change, stability, ecological projects

1 Introduction

Ecological engineering is critical for enhancing terrestrial carbon sinks, which are essential for mitigating climate change through the absorption of carbon dioxide (CO_2) and its sequestration in terrestrial ecosystems (Zhang et al., 2022; Niu et al., 2023; Li et al., 2024; Xia et al., 2024). Since the 1980s, China has initiated several significant ecological projects, including the Three North Shelterbelt Forestation Project, the Grain to Green Project, the Natural Forest Resource Protection Project, and the Desertification Control in the Karst Region of Southwest China Project (Yang et al., 2022; Tong et al., 2023). Currently, 17.42% of China is influenced by a single ecological engineering project, while 78.87% is affected by multiple ecological engineering projects (Shao et al., 2023). However, previous studies have mainly focused on the trends and driving mechanisms of carbon sinks under individual ecological engineering projects, and little attention has been paid to the combined effects of multiple overlapping projects. Furthermore, the prospects for carbon sequestration and the enhancement of carbon sinks within overlaying ecological engineering project areas remain ambiguous. In addition, it remains unclear whether overlapping ecological projects can contribute more to the increase in carbon sinks than single ecological projects, and whether the carbon peaking and carbon neutrality targets can be realized in the near future (Zhao et al., 2021). Thus, it is necessary to assess the stability and driving mechanisms of carbon sinks, and to predict their potential enhancement under different scenarios in overlapping ecological engineering project areas (Yue et al., 2020).

Ecosystem stability is crucial for regulating the terrestrial carbon cycle and atmospheric CO_2 levels (Messori et al., 2019; Arani et al., 2021). Understanding the stability of terrestrial ecosystems can improve the accuracy of predictions of ecosystem changes and provide information for developing climate change mitigation policies (Seddon et al., 2016; Pennekamp et al., 2018; Wang et al., 2022b). The main function of carbon sinks is to absorb CO_2, thereby reducing greenhouse gas concentrations in the atmosphere. Stabilized increasing carbon sinks can effectively store CO_2 over a long period, mitigating the increase in global temperatures (Piao et al., 2020; Wang et al., 2022a). An unstable trend of carbon sinks may lead to the release of CO_2, further exacerbating climate change and leading to ecosystem imbalance (Liu et al., 2023a; Wang et al., 2024). However, due to the increasing frequency of extreme weather events driven by climate change, interannual fluctuations in carbon sinks are increasing, indicating a decline in ecosystem stability (Holden et al., 2014; Hu et al., 2021).

Understanding the driving mechanisms of the stability of carbon sinks is crucial for the effective implementation of carbon neutrality policies (Liu et al., 2023b; Zhang et al., 2023b). Previous research has shown that temperature, precipitation, and radiation can directly influence vegetation photosynthesis and the carbon sequestration capacity (Wang et al., 2022b; Jin et al., 2023). A low soil moisture content and high atmospheric vapor pressure deficit (VPD) are the main driving factors of water stress and contribute to the reduction of carbon sinks (Li et al., 2022). In recent years, engineered water shortages have occurred frequently, exacerbating drought stress and thus limiting the stability of carbon sinks. Studies have shown that economic development and rural population reduction have promoted vegetation restoration and increased carbon sequestration (Chang et al., 2023). Additionally, China has implemented to several ecological engineering projects to enhance carbon sequestration, such as rocky desertification control, the Grain for Green Project, and the Natural Forest Protection Project (Tong et al., 2023). However, previous studies have rarely considered the combined impacts of climate change, human disturbances, and ecological restoration projects (Zhu and Lo, 2022; Chang et al., 2023). These factors, whether individually or interactively, affect the stability of carbon sink. Studies have indeed explored the relative importance of drivers of carbon sink trends (Wang et al., 2023; Jiao et al., 2024). However, the driving mechanisms for the stability of carbon sinks, particularly, in overlapping ecological engineering areas, remain unclear (Thackeray et al., 2016; Li et al., 2022).

Predicting the stability of carbon sinks is crucial for enhancing ecosystem carbon sequestration capacity and identifying areas at risk of carbon sequestration degradation (Yazdandoost et al., 2021; Xu et al., 2023a). Previous studies have shown that if the atmospheric CO_2 concentration peaks at around 2060 and remains stable (carbon neutrality scenario), the global terrestrial carbon sink will gradually decrease starting around 2060, with an estimated reduction of 50% by 2100 (Zhang and Hanaoka, 2021; Zhang et al., 2023a). The rate of China's terrestrial carbon sink is increasing, and it is expected to approach zero by 2100 (carbon neutrality scenario). Current studies have primarily predicted fluctuations in the carbon sequestration rates, but often few long-term predictions of carbon sink trends and stability have been conducted (Cai et al., 2022; Xu et al., 2022a). The prediction of carbon sink trends and stability can reveal whether China's carbon sinks can maintain carbon neutrality, and lays the foundation for the development of theoretical frameworks to support carbon emission mitigation strategies and climate change adaptation plans (Zheng et al., 2020; Yazdandoost et al., 2021). These projections form the foundation for developing theoretical frameworks that support carbon emission mitigation strategies and formulate climate change adaptation plans (Zhang and Hanaoka, 2021). China's key ecological engineering zones have extensive distributions, covering various geographic landscapes and climate systems (Shao et al., 2023). In ecologically fragile and economically underdeveloped areas, there is clear opposition between ecological preservation and resource utilization (Wang et al., 2024). This dichotomy introduces a layer of uncertainty into the prediction of carbon sink stability. Furthermore, there remains a pressing need for comprehensive assessments that address the risks associated with carbon sink degradation. This opposition introduces a layer of uncertainty in the prediction of carbon sink stability. Therefore, it is necessary to predict the stability of China's carbon sinks for 2060 and 2100 under different climate and land use change (LUC) scenarios.

Based on the ensemble empirical mode decomposition (EEMD) method and machine algorithm (enhanced boosted regression tree

(BRT)), in this study, we explored to explore the nonlinear trends and stability of carbon sinks from 1982 to 2019 in overlapped ecological engineering project areas in China. In addition, the trend and stability of carbon sinks for 2060 and 2100 were predicted under different climate change and human activity scenarios. More specifically, we (i) assessed the stability of carbon sinks in China from 1982 to 2019; (ii) investigated the driving mechanisms for the stability of carbon sinks; and (iii) predicted the future trends and stability under different shared socioeconomic pathway scenarios (SSP126 and SSP585).

2 Material and methods

2.1 Study area

China has launched nine key national engineering projects (Figure 1). These projects cover an extensive ecological engineering zone, with a total area of approximately 9.3 million km^2. According to the spatial distributions of the implementation scope of the nine ecological engineering projects (Figures 1A–I), 96.29% of the regions are ecological engineering implementation areas. Only 3.71% of the regions remain unaffected by any ecological project, and project are primarily concentrated along the southern coast of China. The areas of overlapping ecological projects account for 78.87% of the national land area. Notably, three overlapping projects, namely, the Grain to Green Project, the Yangtze River Shelterbelt Project, and the Desertification Control in the Karst Region of Southwest China Project, cover the largest area encompassing 33.99% of China's land and are mainly located in central China. The largest area of overlapping projects includes five ecological projects, covering 3.87% of China's land area, primarily in the Three-River region of Qinghai, central and western Inner Mongolia, northern Shaanxi, southwestern Sichuan, and northern Yunnan.

2.2 Data source

Net Ecosystem Productivity (NEP) is a key indicator in discerning whether an ecosystem functions as a carbon sink or source. When NEP surpasses zero, it denotes that the fixed carbon outweighs the carbon consumed by heterotrophic respiration, thereby designating the ecosystem as a carbon sink. Conversely, when NEP falls below zero, it signifies that the fixed carbon is less than the carbon consumed by heterotrophic respiration, categorizing the ecosystem as a carbon source (Piao et al., 2022a). Thus, NEP greater than zero is adopted as the criterion for identifying a carbon sink. The dataset was sourced from the Resource and Environment Data Platform with a spatial resolution of 0.072°from 1981 to 2019 (http://www.nesdc.org.cn/). The NEP data were obtained from the mechanistic ecological boreal ecosystem productivity simulator (BEPS) driven by remote sensing vegetation parameter (leaf area index, aggregation index, and surface coverage) data, meteorological data, soil texture data, and atmospheric CO_2 concentration data (Chen et al., 2019).

The climate change data, including air temperature (TEM), precipitation (PRE), soil moisture (SOIL), VPD, and downward shortwave radiation (RAD) data, were provided by the Climatology Lab (Abatzoglou et al., 2018). This climatic product has multiple data sources, including WorldClim, the Climate Research Unit, and the Japanese 55-year Reanalysis dataset. To enhance the spatial resolution, the multivariate adaptive constructed analogs method

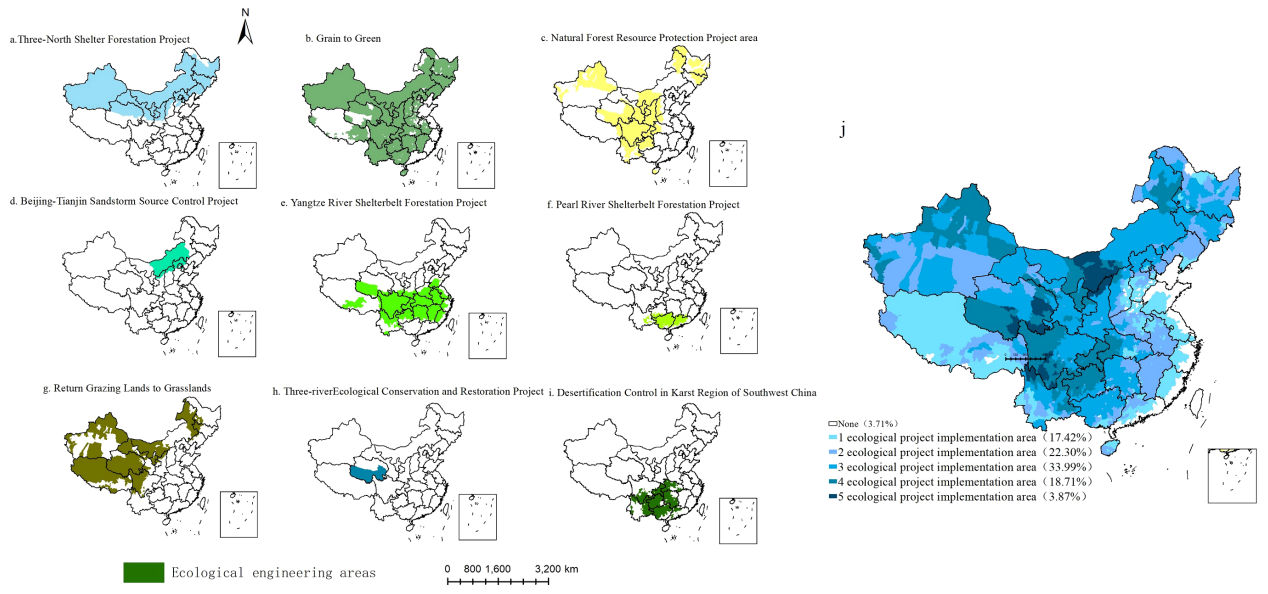

FIGURE 1
The spatial distribution of the single and overlapping ecological engineering projects. (**A**. the Three North Shelterbelt Forestation Project, **B**. the Grain to Green Project, **C**. the Natural Forest Resource Protection Project, **D**. the Beijing-Tianjin Sandstorms Source Control Project, **E**. the Yangtze River Shelterbelt Forestation Project, **F**. the Pearl River Shelterbelt Forestation Project, **G**. Return Grazing to Grassland Project, **H**. the Three-river Ecological Conversation and Restoration Project, **I**. the Desertification Control in Karst region of Southwest China).

was used to downscale the monthly time series. This method has been proven to be superior to direct daily interpolated bias correction, particularly in regions with complex topography (Jiao et al., 2024). The climatic datasets provide monthly climate and climatic water balance information for terrestrial surfaces worldwide, covering the period from 1958 to 2020. The data have a spatial resolution of 1/24 of a degree, approximately equivalent to 4 km.

The human activities considered in this study included the LUC, population density (POP), gross domestic product (GDP), and anthropogenic emissions of CO_2 and N_2O. The land use data, obtained from the Resource and Environment Data Platform (http://www.resdc.cn/), were for 1980, 1990, 1995, 2000, 2005, 2010, 2015, and 2020 and had a spatial resolution of 30 m (Liu et al., 2018). The land use types were divided into five types: farmland, forest, grassland, urban and rural land, and other land. The LUC data were derived using the transfer matrix method. The GDP and population density data, obtained from the Resource and Environment Data Cloud Platform (http://www.resdc.cn/), were for 1995, 2000, 2005, 2010, 2015, and 2020 and had a spatial resolution of 30m. The anthropogenic CO_2 and N_2O emission data were obtained from the Global Atmospheric Research Emissions Database, covered the period from 1981 to 2019, and had a spatial resolution of 0.1°.

The future climate variables under different scenarios (SSP126 and SSP585) from 2020 to 2100 were provided by Phase 6 of the Coupled Model Intercomparison Project (CMIP6) (https://esgf-node.llnl.gov/search/cmip6/) (Zhang et al., 2023a). The future population and economy data under different scenarios (SSP126 and SSP585) were provided by Chen et al. (2020) with a resolution of 0.1° grid and encompasses a timespan from 2020 to 2100 (Chen et al., 2020) (https://www.nature.com/articles/s41597-020-0421-y).

All of the data were resampled to 0.072°, consistent with the carbon sink data.

2.3 Trend of carbon sinks

The EEMD method is an advanced data analysis technique that decomposes complex signals into a finite number of intrinsic mode functions (IMFs) and residual components (Figures 2, 3) (Wu et al., 2007). It improves the Empirical Mode Decomposition (EMD) method by addressing limitations such as mode mixing and boundary effects (Pan et al., 2018). EEMD efficiently handles non-smooth and nonlinear signals, making it ideal for analyzing time-series data across various domains (Ji et al., 2014). Its adaptability and robustness have led to its widespread application in signal processing, trend extraction, and feature analysis (Xu et al., 2022b). Furthermore, by identifying and quantifying intrinsic periodicities and trends within ecosystems, EEMD facilitates the assessment of the ecosystem's responsiveness to external perturbations, thereby elucidating the ecosystem's stability.

The EEMD method involves adding multiple realizations of white noise, known as ensemble members, to the original signal to suppress noise and improve the decomposition accuracy. Each ensemble member undergoes individual processing via EMD, resulting in multiple IMFs. The final IMFs and residual components are derived by averaging the IMFs of all of the ensemble members (Ji et al., 2014). In this study, EEMD was used

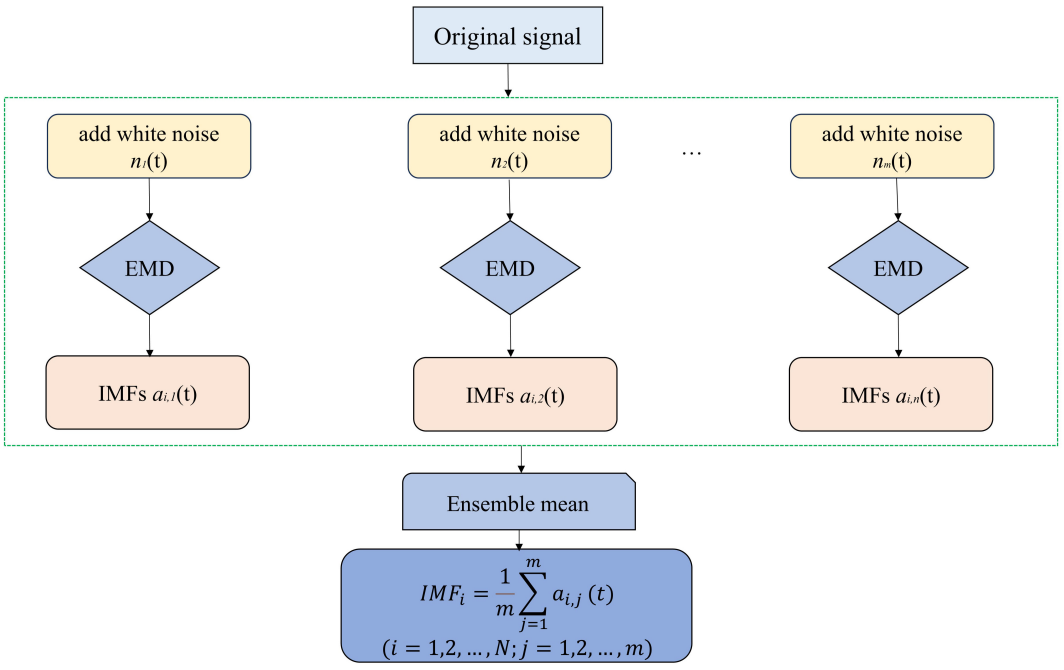

FIGURE 2
EEMD decomposition of long-time series process.

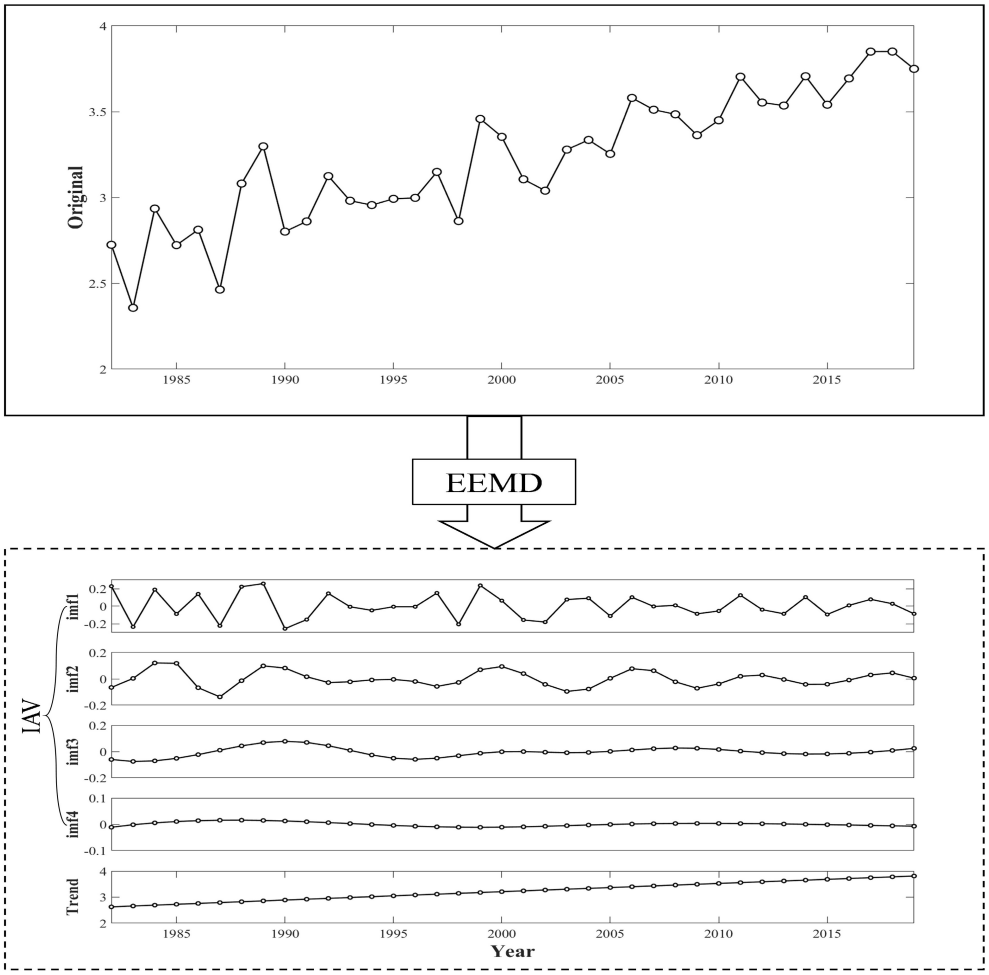

FIGURE 3
EEMD decomposition of inter-annual fluctuations (IVA) and trend terms (Trend) for carbon sinks.

to extract the residual components of carbon sinks and to calculate the rates of change of these components. This analysis identified one significant trend and four types of trends of carbon sinks: increasing, decreasing, decreasing to increasing (positive reversals), and increasing to decreasing (negative reversals) (Figure 4).

2.4 Stability of carbon sinks

The stability of NEP was assessed by calculating the coefficient of variation (CV) of the detrended data (Zhang et al., 2019; Piao et al., 2020). The EEMD method was used to remove the trends from the NEP data, ensuring that the analysis focused on the inherent variability of the NEP data rather than the long-term trends (Lin et al., 2023).

$$NEP_{\det rend,year} = NEP_{year} - NEP_{trend,year} + \mathrm{NEP}_{mean}$$

$$NEP_{trend,year} = a \times year + b$$

NEP_{year} is the raw annual NEP data. $NEP_{trend,year}$ is the NEP trend for each year, and the coefficients are calculated using a linear method. The mean NEP_{mean} is averaged from NEP_{year}. The detrended variable for each year is denoted as $NEP_{\det rend,year}$. NEP_{CV} is calculated using these detrended data:

$$NEP_{CV} = \frac{\sqrt{\frac{\sum (NEP_{\det rend,year} - NEP_{mean})^2}{N}}}{NEP_{mean}}$$

The larger NEP_{CV} is, the more volatile and less stable the NEP trend is. In this study, NEP_{CV} was classified into five levels: stable, relatively stable, moderately stable, relatively unstable, and unstable. The natural interval method, which relies on inherent data groupings, was used to conduct this classification. This method clusters similar values together while maximizing the differences between classes, ensuring that the elements are categorized based on significant discrepancies in the data values.

2.5 Enhanced boosted regression tree

The enhanced boosted regression tree (BRT) method has a robust framework for analyzing complex ecological data and making reliable predictions (Elith et al., 2008). This method's flexibility in handling nonlinear relationships and its ability to

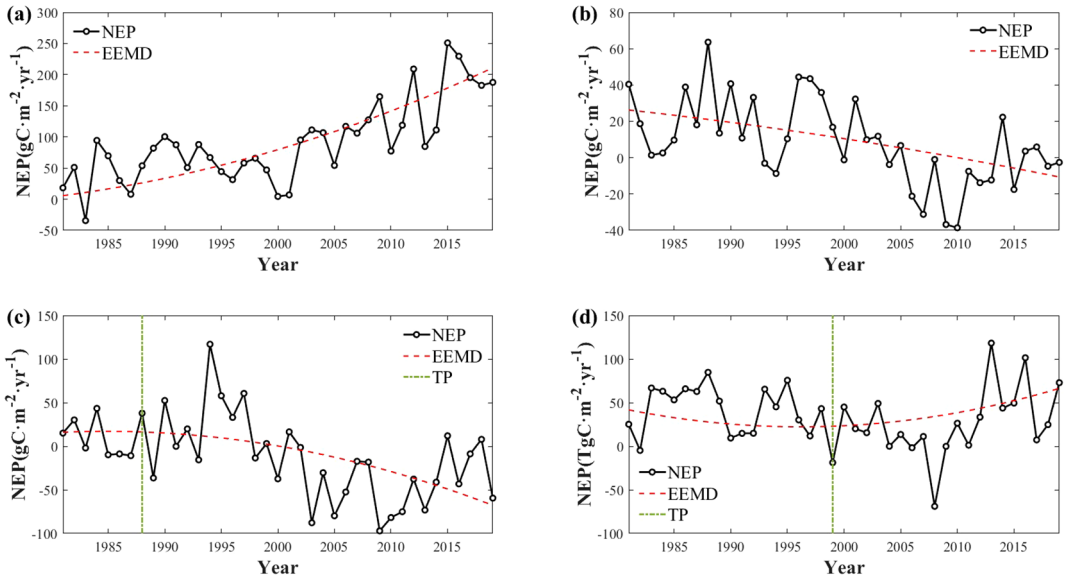

FIGURE 4
Four significant non-linear trends in EEMD-decomposed carbon sinks [**(A)** monotonically increasing; **(B)** monotonically decreasing; **(C)** negative shifts; **(D)** positive shifts, with the TPs are turning points].

incorporate interactions among predictors make it an indispensable tool in ecological and environmental research (Czarniecka-Wiera et al., 2020). It constructs multiple regression trees through iterative random sampling and self-learning, evaluates the influence of the independent variables on the dependent variable, and uses the remaining data for cross-validation. This approach is not constrained by the temporal sequence of data, thereby increasing its robustness. The BRT method is proficient in identifying key variables, nonlinear relationships, and the interactions between and relative importance of factors influencing the stability of carbon sinks. In this study, the relative importance of human activities (anthropogenic emissions of CO_2 and N_2O, LUCs, economic development, and population density) and climate change (temperature, precipitation, soil moisture, atmospheric VPD, and solar radiation) on the stability of carbon sinks was extracted using the BRT method.

In this study, a subsample of 75% was selected from the carbon sinks as a training sample, and the rest were used as validation samples. A 10-fold cross-validation method was executed for the BRT model. Meanwhile, 10 iterations were run on the BRT model to reduce model uncertainty and all results were averaged. To measure the model accuracy, the AUC was used to validate the fitting accuracy between the carbon sink stability and the driver. Model accuracy can be judged as excellent if AUC ≥ 0.9, good if 0.8< AUC< 0.9, accurate if 0.7< AUC< 0.8, and poor if 0.6< AUC< 0.7. As shown in Supplementary Table S1, the average AUC value of 0.88 > 0.8 indicates good fitting accuracy for carbon sink stability.

In addition, the BRT model enabled the simulation and prediction of the trend and stability of carbon sinks across various scenarios, offering insights into their sustainability. The iterative boosting approach improves the predictive performance by combining multiple weak models to form a strong predictive model (Elith et al., 2008). Drawing upon data for two shared socioeconomic pathways (SSP126 and SSP585) provided by the CMIP6, in this study, we used the BRT model to forecast the long-term trends and stability of carbon sinks within the ecological engineering zones for 2060 and 2100 under different climate and human activity scenarios. We used this model to classify the significant increases and positive shifts in the trends of carbon sinks as the carbon sink increases and decreases and the negative shifts as the carbon sink decreases. Furthermore, it was used to identify future ecological restoration areas and key protection zones, as well as to investigate nature-based carbon sequestration management models.

3 Results

3.1 Trend of carbon sinks in overlapping ecological project areas

China's carbon sinks exhibited a steadily increasing trend, with a growth rate of 0.9888 gC m^{-2} yr^{-1} (Figure 5A). Moreover, using the EEMD method, it was found that the carbon sinks exhibited a nonlinear increasing trend. Before 1995, the carbon sink fluctuations increased. After 1995, the carbon sinks experienced rapid growth. This suggests an accelerating trend of carbon sink enhancement. The interannual fluctuations in the carbon sinks ranged from −16.81 to 17.68 gC m^{-2} $year^{-1}$. Smaller fluctuations occurred before 2000, and larger fluctuations occurred after 2000. Consequently, it is imperative to elucidate the changes in the stability of the carbon sinks.

On a spatial scale, the significant trends in the carbon sinks covered 41.68% of China (Figure 5B). The increasing trends and positive reversals of the carbon sinks constituted 16.77% and 20.55%, respectively, while the decreasing trends and negative

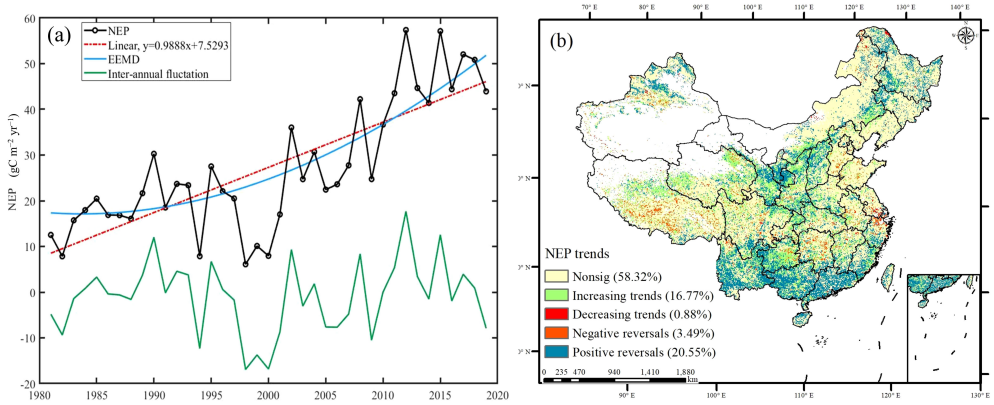

FIGURE 5
The nonlinear trends of carbon sinks in China. (**A**: the linear nonlinear trends of carbon sinks, **B**: the spatial distribution of nonlinear trends in carbon sinks).

reversals accounted for only 0.88% and 3.49%, respectively (Figure 5). The areas exhibiting increasing trends of carbon sinks primarily occurred in the northern part of the Tibetan Plateau and the southwestern region. The positive reversals predominantly occurred in the southwest region, southeast coast, Loess Plateau, and northeastern region. The increasing trends and positive trends of carbon sinks were mainly concentrated in areas where the Grain to Green, Returning Pasture to Grassland Project, and Rocky Desertification Control projects overlapped. Conversely, the decreasing trends and negative reversals primarily occurred in the Tibetan Plateau, Yangtze River Basin, and northern plain areas (Figure 5B).

In the ecological engineering areas, the proportion of increasing trends of carbon sinks increased as the number of overlapping ecological projects increased (Figure 6). The carbon sinks increased in 29.55% of the regions where five ecological engineering projects overlapped, such as the Grain to Green, Natural Forest Resource Protection Projects, Return Grazing Lands to Grasslands, and Desertification Control in the Karst Region of Southwest China projects. Conversely, as the number of ecological engineering

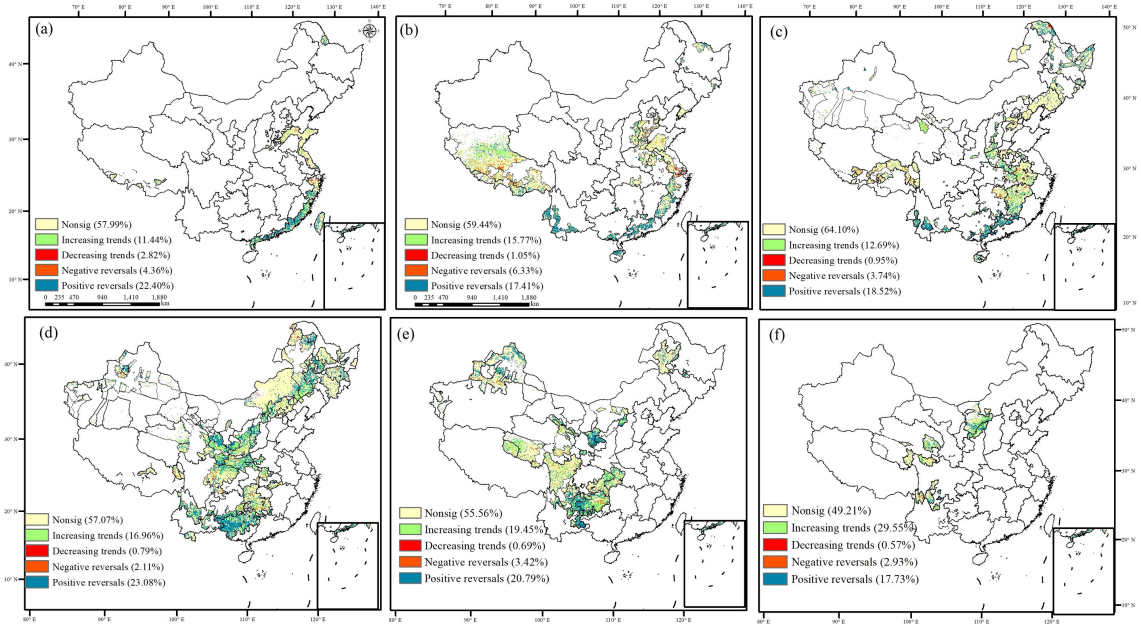

FIGURE 6
The trend of NEP from 1981 to 2019 in ecological project areas [**(A)** 0 ecological project areas; **(B)** 1 ecological project area; **(C)** 2 ecological project areas; **(D)** 3 ecological project areas; **(E)** 4 ecological project areas; **(F)** 5 ecological project areas].

projects increased, the proportion of decreasing trends and negative reversals of the carbon sinks decreased. Notably, the proportion of positive reversals of the carbon sinks did not consistently increase as the number of overlapping ecological engineering projects increased. It peaked in areas where three ecological engineering initiatives were implemented. These areas, primarily located in Southwest China, the Yellow River Basin, and the Northeast China Plain, overlapped with projects such as the Grain to Green, Natural Forest Resource Protection Project, Three-North Shelter Forestation Projects, and Desertification Control in the Karst Region of Southwest China Project areas.

3.2 Stability of carbon sinks in overlapping ecological project areas

The spatial distribution of the stability of carbon sinks across China exhibited notable variations (Figure 7). Regions such as the South Karst area, Southeast Hill area, North China Plain, and Northeast China Plain exhibited larger interannual fluctuations in the carbon sinks, indicating instability. Moreover, these areas exhibited increasing trends or positive reversals alongside significant carbon sinks. The carbon sinks were stable in northern Xinjiang and the southern part of the Tibetan Plateau. However, despite this stability, these regions experienced insignificant changes or negative reversals of the carbon sinks. Thus, the stability of the carbon sinks did not consistently correspond with their increasing trends.

In the ecological engineering areas, the highest percentage of stable carbon sinks were located in regions where five overlapping ecological engineering initiatives were implemented, and the stability of carbon sinks reached 35.66% (Figure 8). These areas were primarily located within the overlapping engineering regions, such as the Grain to Green Project, Natural Forest Resource Protection Project, Three-River Ecological Conservation and Restoration Project, and Three-North Shelter Forestation Project areas. The second-highest percentage of stable carbon sinks were primarily concentrated in regions with a single ecological implementation area, namely, the Return Grazing Lands to Grasslands Project area in Tibet. The regions with a high percentage of unstable carbon sinks were mainly located in areas with the overlapping implementation of two or three ecological projects, such as the northeastern and southeastern parts of China. This suggests that the implementation of five overlapping ecological projects contributed to the increase in the stability of carbon sinks.

3.3 Relative importance of driving factors of the stability of carbon sinks

Based on the BRT model, climate change and human activities made comparable contributions to the stability of carbon sinks,

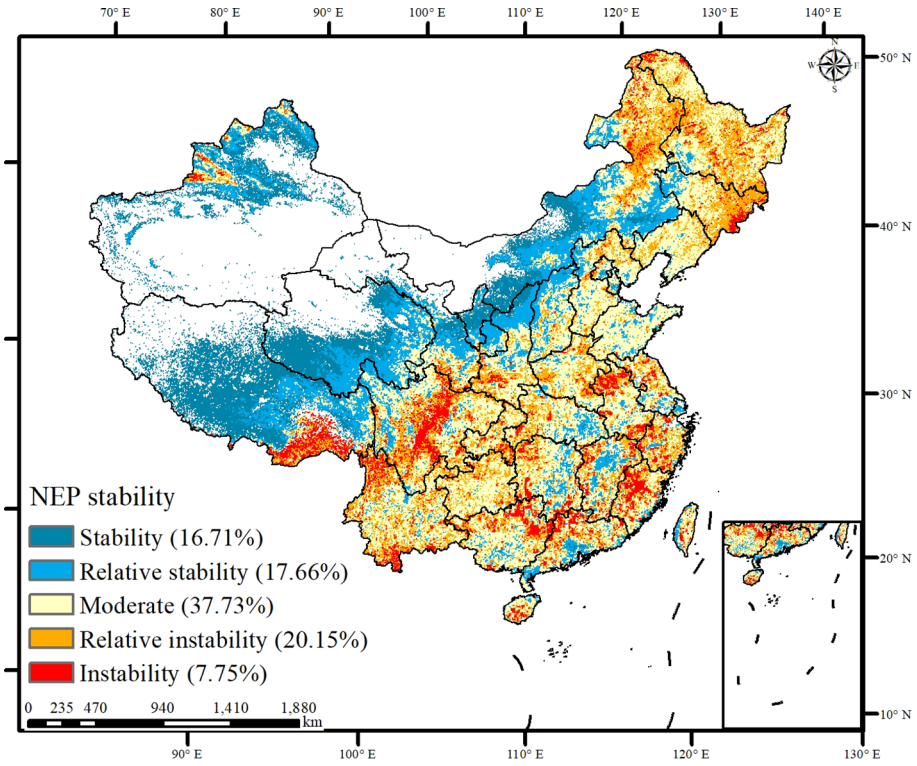

FIGURE 7
The stability of carbon sinks in China.

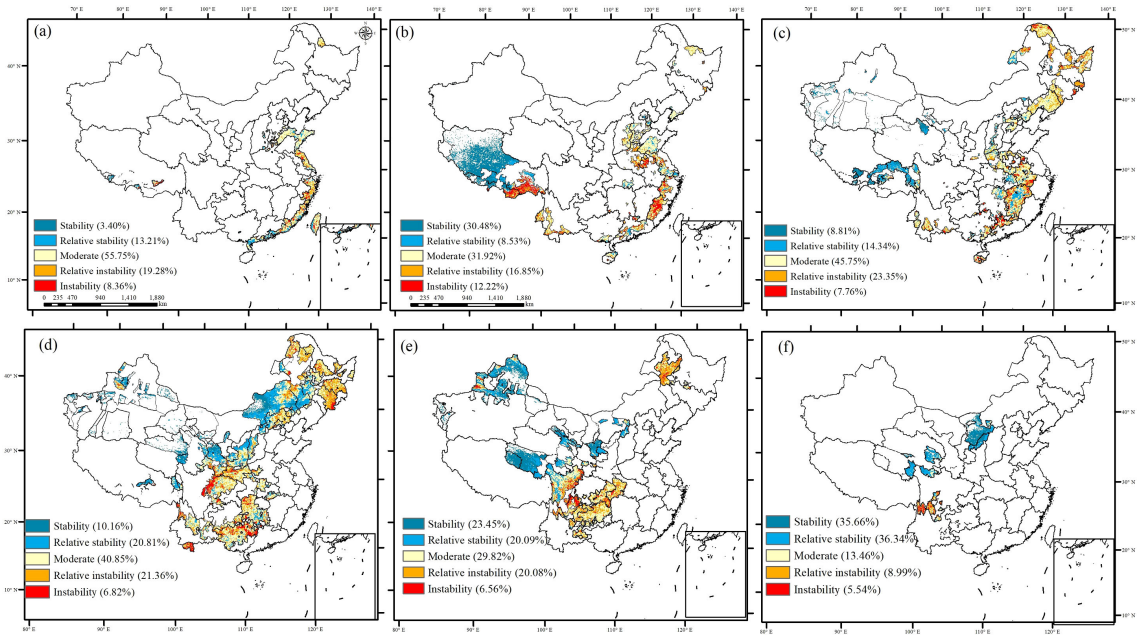

FIGURE 8
The stability of NEP from 1981 to 2019 in ecological project areas [**(A)** 0 ecological project areas; **(B)** 1 ecological project area; **(C)** 2 ecological project areas; **(D)** 3 ecological project areas; **(E)** 4 ecological project areas; **(F)** 5 ecological project areas].

accounting for 50.28% and 49.72%, respectively (Figure 9). The soil moisture, solar radiation, and air temperature were relatively important climatic factors, accounting for 15.95%, 10.83%, and 10.13%, respectively, whereas the VPD and precipitation had less significant effects. The anthropogenic CO_2 emissions and LUC were significant anthropogenic factors, contributing 20.84% and 16.62%, respectively, whereas the GDP, anthropogenic N_2O emissions, and population density (POP) were less important. This suggests that the soil moisture content and CO_2 emissions primarily drove the increase in carbon sinks.

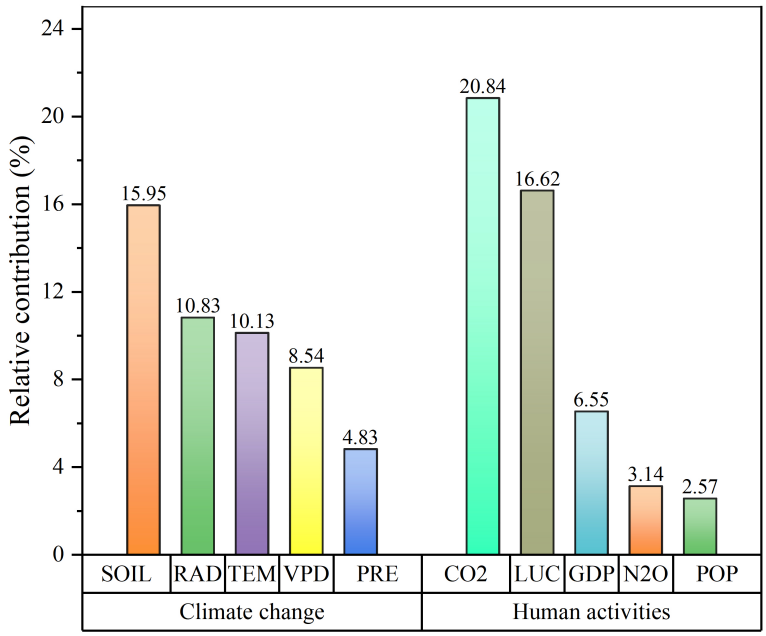

FIGURE 9
The relative importance of driving factors on the carbon sinks in China (VPD, vapor pressure deficit; TEM, air temperature; PRE, precipitation; SOIL, soil moisture; LUC, land use change; POP, population density; GDP, gross domestic product).

Human activities had a minimal impact on the carbon sinks in the eastern region where either no ecological engineering projects or only a single project was implemented (Figure 10). In the regions with one ecological engineering project, human activities contributed 63.90% to the importance of the carbon sinks, and the CO_2 emissions were the primary contributor. With increasing number of overlapping ecological projects, the climate factors contributed more to the carbon sinks. In areas such as the Yellow River Basin and the Three Rivers region, where five ecological projects were implemented, climate change contributed 72.96% to the carbon sinks, and precipitation was the most significant factor, contributing 36.59%. Conversely, in the three or four ecological projects overlapped, the soil moisture content made a relatively high contribution, accounting for 17.33% and 24.56%, respectively.

3.4 Prediction of carbon sinks in overlapping ecological project areas

Under SSP126, the degradation of carbon sinks decreases from 5.69% to 4.49% between 2060 and 2100, and the most significant reductions occur in Tibet, the Yangtze River belt, and the Pearl River region (Figure 11). Conversely, the enhancement of carbon sinks undergoes relatively minor changes, accounting for 34.96% and 33.32% in 2060 and 2100, respectively, and these changes are primarily concentrated in the Yellow River belt and Southwest China. The stability of carbon sinks changes by 23.85% and 24.86% in 2060 and 2100, respectively, and these changes predominantly occur in northwest China and Tibet. Conversely, the instability of carbon sinks changes by 4.93% and 6.43% in 2060 and 2100, respectively, and these changes primarily occur across northeast and southwest China. Under SSP126, rapid technological advancements, the promotion of sustainable economic growth by economic globalization, the development of low-carbon energy technologies, alongside reduced energy intensity and increased environmental awareness, and the widespread adoption of renewable energy sources collectively contribute to reducing the degradation of carbon sinks. As a result, the carbon sinks shift toward greater stability.

Under SSP585, the degradation of carbon sinks increases from 4.86% to 7.24% between 2060 and 2100 and is primarily driven by significant shifts in previously stable regions (Figure 12). The most notable changes occur in Tibet and the Beijing-Tianjin-Hebei area. The carbon sinks exhibit a significantly higher rate of decline by 2100 under SSP585 than the trends of carbon sinks from 1982 to 2019, particularly in the Tibetan Plateau region where the carbon

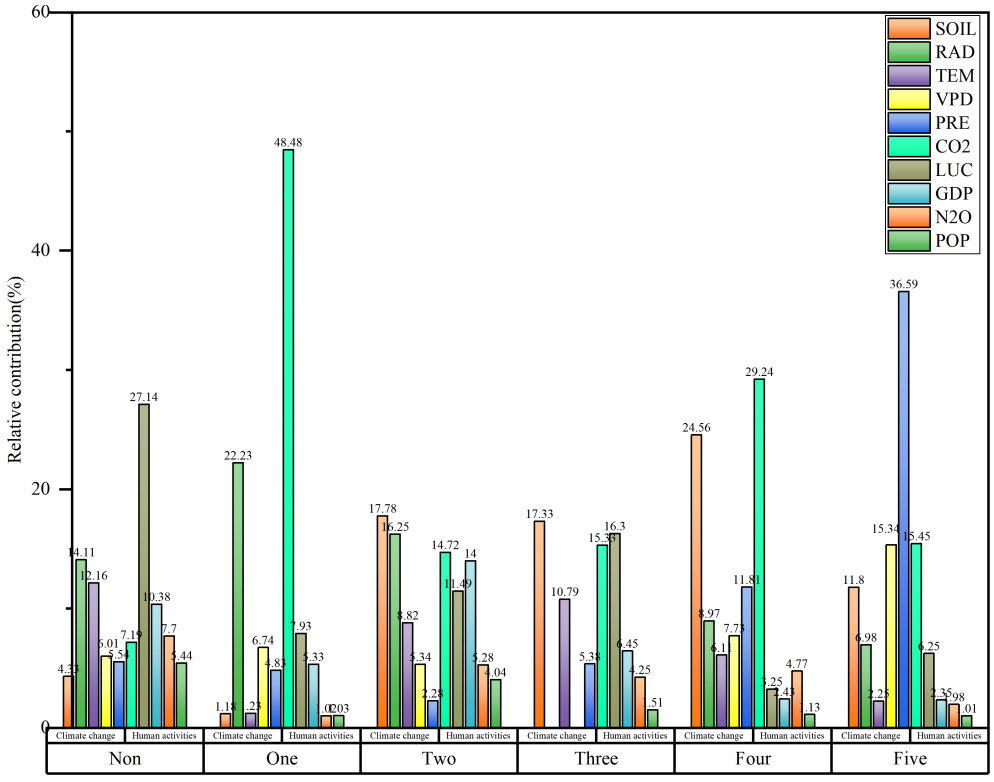

FIGURE 10
The relative importance of driving factors on the carbon sinks in ecological project areas (Orange color: human activity factors; Green color: climate change factors; Non: 0 ecological project areas; One: 1 ecological project area; Two: 2 ecological project areas; Three: 3 ecological project areas; Four: 4 ecological project areas; (VPD, vapor pressure deficit; TEM, air temperature; PRE, precipitation; SOIL, soil moisture; LUC, land use change; POP, population density; GDP, gross domestic product).

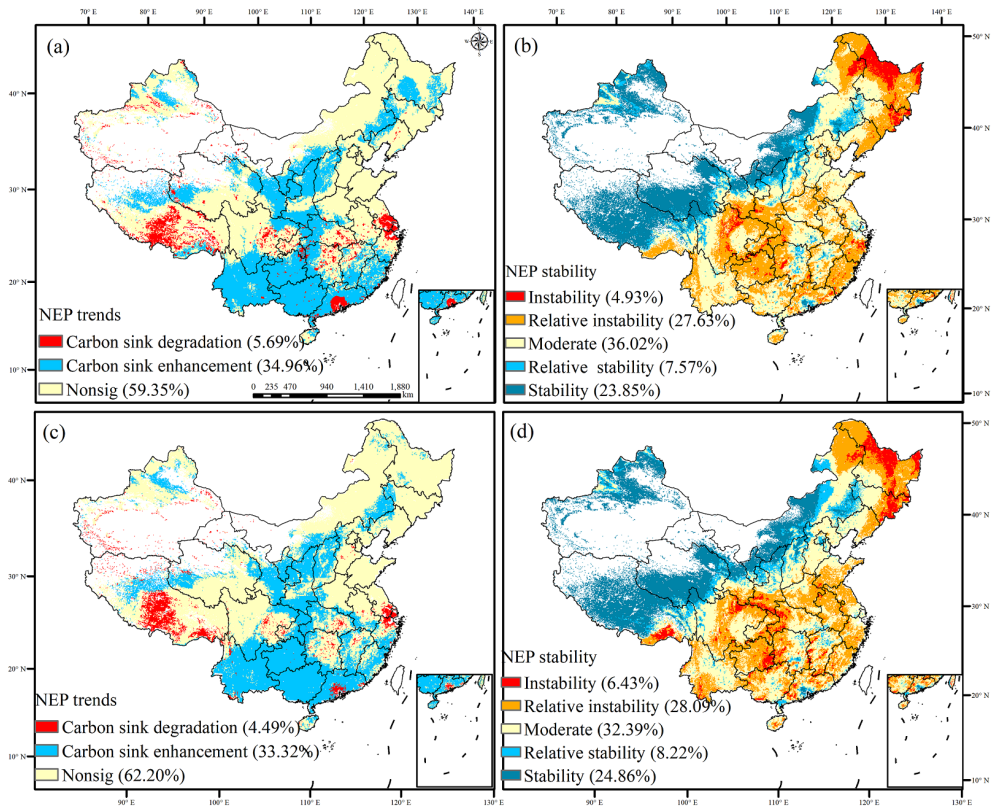

FIGURE 11
Trend and stability of carbon sink under the SSP126 scenario in 2060 and 2100 [**(A, B)** the trend and stability of carbon sink in 2060; **(C, D)** the trend and stability of carbon sink in 2100].

sinks experience considerable degradation. Conversely, the percentage of carbon sink change remains relatively stable, and these changes primarily occur in the Loess Plateau and southwestern China. The stability of carbon sinks between 2060 and 2100 exhibits minimal variations, and the stable carbon sinks in northwest China experience insignificant changes. The regions with unstable carbon sinks are primarily located in southwest China, which are characterized by an increasing trend of carbon sinks but face heightened degradation risks. SSP585 includes a high reliance on conventional energy sources. As a result, the carbon sinks persist in a degraded state and exhibit increased instability.

The areas with no, one, or two ecological engineering projects exhibit a higher proportion of carbon sink degradation (Figure 13). Conversely, in the regions influenced by four or five overlapping ecological engineering projects, the proportion of carbon sink enhancement increases with increasing number of projects. Under SSP126, by 2100, the Loess Plateau and Three-River region, affected by five overlapping ecological engineering projects, exhibit a carbon sink enhancement proportion of 41.80%, and the proportion of degraded carbon sinks is only 0.61%. The proportion of carbon sink stability increases with increasing number of overlapping ecological projects, aligning closely with the observed trend. By 2060, under SSP126, the areas with five overlapping ecological projects exhibit a stability proportion of 62.06%, and the instability is only 0.25%. The proportion of areas with decreasing trends of carbon sinks is higher under SSP585 than under SSP126.

4 Discussion

4.1 Trend and stability of carbon sinks in overlapping ecological engineering projects

Previous studies have used various methodologies, such as Empirical Mode Decomposition (EMD), Ensemble Empirical Mode Decomposition (EEMD), and wavelet analysis, to investigate the intricate dynamics of carbon sinks (Seddon et al., 2016; Liu et al., 2023c). Nevertheless, the complex interplay between climate change and anthropogenic activities results in significant interannual variability and instability of carbon sinks (Wang et al., 2023). This variability often manifests as spatial differences between the observed trends and the underlying stability of carbon sinks (Liu et al., 2023b). In addition, it is not clear whether overlapping ecological projects can contribute more to the increase in carbon sinks than single ecological projects (Cai et al., 2020). In this study, we addressed this research gap by conducting an in-depth examination of carbon sink stability. Our findings revealed that the regions in the east, characterized by either the absence of ecological projects or minimal overlap of projects tended to exhibit relatively weaker carbon sink stability. In contrast, areas such as the Loess Plateau and the Three-River source region, characterized by multiple overlapping ecological projects, had enhanced carbon sink stability. This observed variability

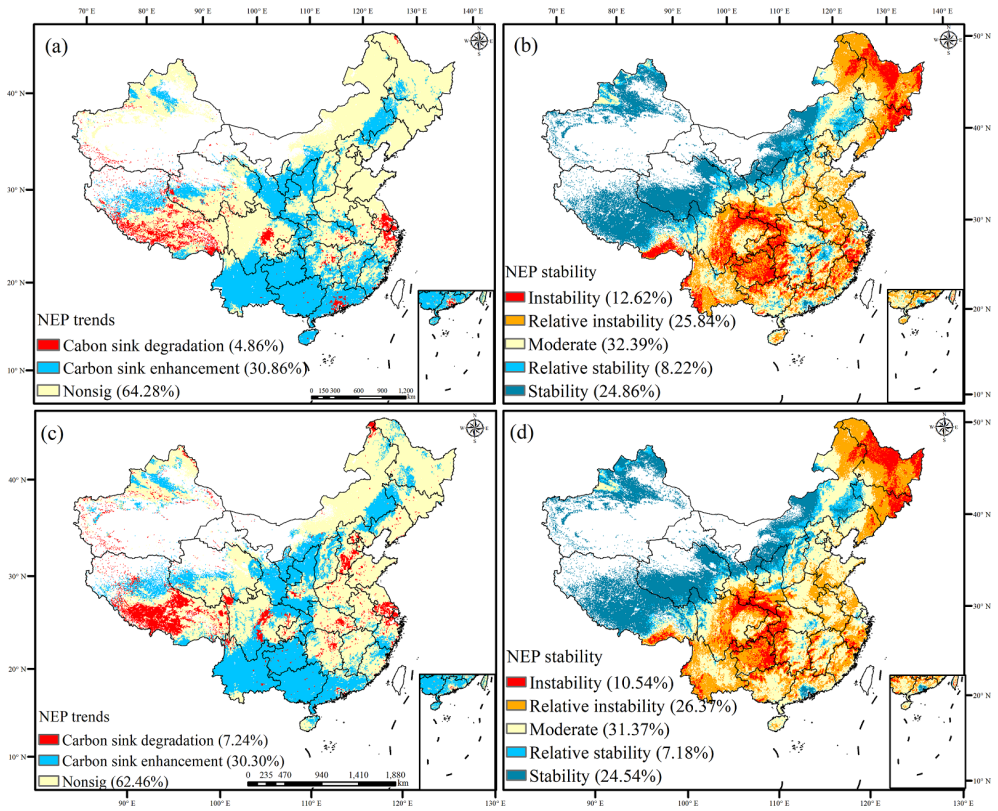

FIGURE 12
Trend and stability of carbon sink under the SSP585 scenario in 2060 and 2100 [**(A, B)** the trend and stability of carbon sink in 2060; **(C, D)** the trend and stability of carbon sink in 2100].

underscores the critical importance of strengthening ecosystem carbon sink functions and customizing carbon neutrality strategies to suit specific regional conditions (Wang et al., 2022b). In areas with stable carbon sinks, maintaining existing ecological measures is essential for increasing the capacity and stability of carbon sinks. Conversely, in areas with less stable terrestrial carbon sinks, measures that must be taken include reducing anthropogenic disturbances, expanding ecological measures, and implementing diversified restoration strategies, all of which are aimed at enhancing the stability of carbon sinks and ensuring their long-term sustainability (Wang et al., 2023).

4.2 Driving mechanism of carbon sinks

Enhancing carbon sinks in terrestrial ecosystems requires a thorough understanding of the responses of carbon sink stability to climatic variations and human activities (Wang et al., 2022a, 2022). On the national scale, the impacts of human activities and climate change on the stability of carbon sinks are almost equal. Among the various anthropogenic factors, the CO_2 emissions and LUC are especially critical in determining carbon sink stability. Regarding the climate factors, the soil moisture content and solar radiation are key determinants of carbon sink stability. Human activities have a substantial impact in regions such as the North China Plain, the Northeast China Plain, and the eastern coastal areas where the stability of carbon sinks is relatively low. The impacts of LUCs and anthropogenic CO_2 emissions are particularly noteworthy in areas along the eastern coast and on the North China Plain and Northeast China Plain where ecological interventions are minimal (Zheng et al., 2019). The eastern region, characterized by intensive human disturbances, has undergone rapid economic development, which has been frequently accompanied by increased energy consumption and accelerated industrialization, resulting in substantial carbon emissions (Wang et al., 2022a). Industrial processes, transportation, and energy production significantly contribute to CO_2 emissions, a potent greenhouse gas (Wu et al., 2021). Concurrently, rapid urbanization and land development activities lead to widespread deforestation, wetland degradation, and conversion of land to urban or agricultural land, reducing carbon stocks in ecosystems and diminishing the overall carbon sink capacity (Zhu et al., 2021).

The greater the number of overlapping ecological projects is, the more significant contribution of climate change to the stability of carbon sinks is, particularly in areas where five ecological projects overlap, in which the relative importance of the climate reaches 72.96%. In regions where five ecological engineering projects overlap, the ecological environments frequently exhibit increased fragility and greater susceptibility to the impacts of climate change. This increased sensitivity implies that variations in climatic conditions may result in more substantial and widespread consequences for the ecosystem, including alterations of the vegetation pattern, loss of biodiversity, and modification of the

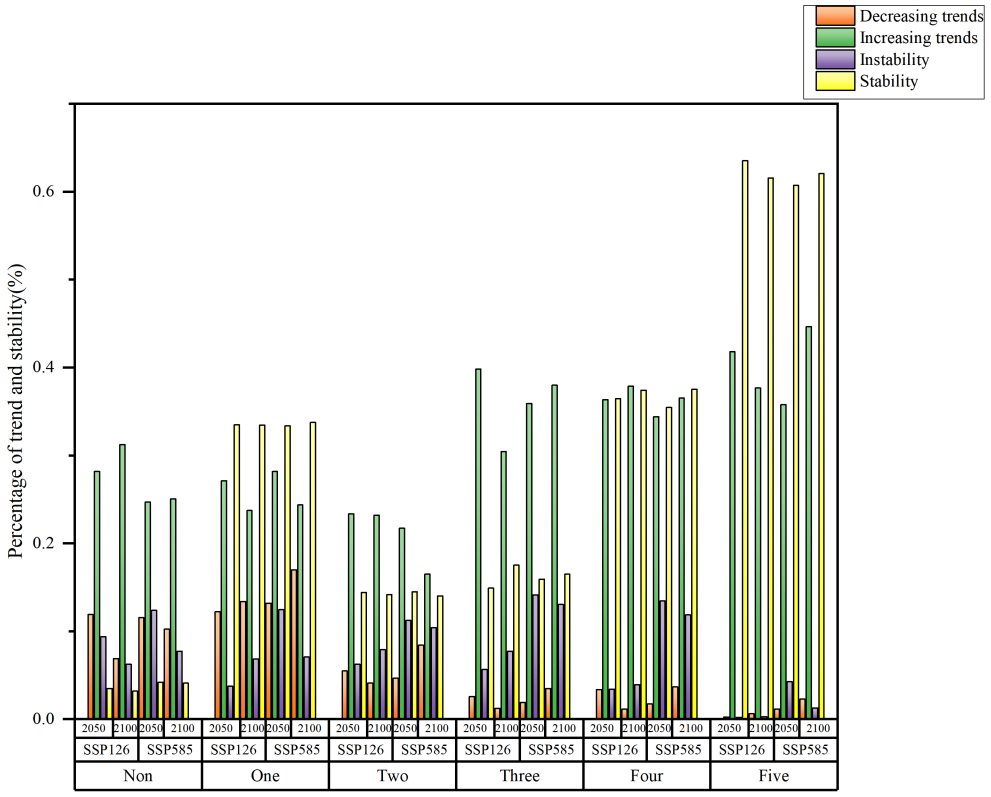

FIGURE 13
Trend and stability of carbon sink under the SSP126 and SSP245 scenarios in 2060 and 2100 in different ecological projects.

hydrological cycle (Fan et al., 2015). Given the inherent fragility of these ecological environments, the implementation of ecological engineering initiatives in such areas requires heightened consideration of climatic factors. Two primary rationales underscore the increased impact of climate change on carbon sequestration: 1) Climate fluctuations have the potential to cause substantial transformation within ecosystems, thereby affecting the stability and efficiency of carbon sequestration. For example, rising temperatures may trigger vegetation changes and may prolong the growing season, thereby affecting plant growth and the carbon absorption capacity (Wang et al., 2022a). 2) Regions characterized by ecological vulnerability are generally more susceptible to the adverse effects of extreme climate events, such as droughts and floods, which can result in abrupt and severe repercussions for carbon sequestration (Wang et al., 2021). Consequently, when implementing ecological engineering initiatives in these areas, particular emphasis must be placed on climatic factors, and measures should be adopted to mitigate the impacts of climate change on carbon sequestration (Ma et al., 2019).

In the northwest and southwest regions of China, where three or four ecological projects overlap, the contribution of soil moisture to carbon sink stability is relatively high, accounting for 17.33% and 24.56%, respectively. In the southwestern karst region, characterized by uneven distributions of water and soil resources and hydrological fluctuations, the rate of soil formation is slow, the water retention capacity is low, and the potential for ecological restoration is low (Wang et al., 2019). Previous studies have found that insufficient soil moisture and a high atmospheric VPD are the primary factors hindering vegetation greening in karst areas, which is consistent with the result with our study (Yue et al., 2022). Drought-induced stress resulting from water scarcity has the potential to impede the recovery and sustained growth of karst ecosystems, making ground vegetation productivity highly sensitive to climate change-driven variations in vapor pressure deficit (Qiao and Xia, 2024). Furthermore, human activities, such as terracing and deforestation, exacerbate the vulnerability of already fragile karst ecosystems, particularly in areas with slopes of greater than 25° (Chen et al., 2023). Ensuring adequate soil moisture, which is crucial for supporting vegetation growth, is imperative, particularly in semi-arid regions. Global climate change is exacerbating the decline in soil moisture across numerous regions, primarily due to reduced precipitation and increased evaporation of soil caused by increased temperatures (Yue et al., 2020).

The northwest region of China, where one or two ecological projects overlap, plays a significant role in global climate change and is characterized by complex ecological systems. Previous research has highlighted the significant relationship between carbon sinks and soil moisture dynamics and has identified the decline in soil moisture as a primary driver of carbon sink reduction (Song et al., 2022; Du et al., 2024). Soil moisture plays a crucial role in supporting optimal vegetation growth in semi-arid and arid environments (Zhou et al., 2018). Consequently, insufficient soil moisture restricts sustained plant growth in the arid regions of northwest China, increasing the vulnerability of carbon sinks to climatic variations (Qiao and Xia, 2024). The prevailing climate in

this region is predominantly a temperate continental climate, and moisture availability significantly influences vegetation dynamics in this region. Decreasing precipitation levels contribute to increases in temperatures and radiation exposure, thereby intensifying drought conditions (Piao et al., 2020).

Therefore, in response to factors affecting the stability of carbon sinks, appropriate measures should be implemented (Chen and Yu, 2019). In ecological engineering zones that are highly sensitive to climate dynamics, enhancing meteorological disaster warning systems, establishing emergency response mechanisms, and implementing disaster prevention measures effectively are imperative for strengthening the resilience of ecosystems and societies against catastrophic events (Piao et al., 2022b). For instance, it is essential to improve the management of water conservancy irrigation and drainage projects in conjunction with advanced weather forecasting to mitigate the effects of sudden precipitation fluctuations on soil moisture levels and reduce the occurrence of extreme climate events (Chen and Yu, 2019). In regions heavily affected by human activities, comprehensive soil and water conservation initiatives and ecological restoration projects should be implemented, with strict adherence to ecological protection boundaries and the preservation of biodiversity (Wang et al., 2024). Furthermore, strengthening the establishment of nature reserves is crucial for mitigating forest mortality caused by extreme climate events, thereby improving carbon sink stability.

4.3 Sustainability of carbon sinks in overlapping ecological engineering project areas

Carbon sink forecasting is crucial for the development of effective climate policies by governments and international organizations (Xu et al., 2022a). By understanding the trends and stability of carbon sinks, targeted emission reduction measures and carbon trading policies can be developed to more effectively address climate change (Zhang and Hanaoka, 2021). Current research has predominantly focused on short-term fluctuations in carbon sequestration rates, and long-term forecasts that consider various climate and land use scenarios are lacking (Xu et al., 2022a). Long-term predictions can quantify interannual variations and reveal trends, thereby providing a theoretical basis for the development of systematic carbon reduction strategies and providing technical support for climate change mitigation efforts (Piao et al., 2020; Wu et al., 2024). In this study, we projected future trends of carbon sinks in China under SSP126 and SSP585 scenarios. our research results indicated that by 2100, under SSP126 scenario, carbon sinks in southern China and the Yellow River Basin will expect to exhibit a stable increasing trend. This suggests that ecosystems in these regions will gradually recover, with continuous improvement in the carbon absorption capacity. Conversely, the carbon sinks in Tibet are projected to exhibit a stable degradation, indicating persistent deterioration of ecosystem health and a gradual decrease in the carbon capacity of carbon. Additionally, the Yangtze River Basin is expected to experience an unstable decreasing carbon sink trend, likely due to environmental changes and human activities that cause fluctuations in the carbon absorption capacity (Xu et al., 2023b).

Under SSP585 scenario, the proportions of degraded and unstable carbon sinks will significantly increase, particularly in Tibet and economically developed urban areas such as the Yangtze River Delta and the Beijing-Tianjin-Hebei region. The carbon sinks in these areas will not only severely degraded but will also become extremely unstable, indicating that, under this high-emission scenario, ecosystems face greater stress and challenges (Nooni et al., 2021). As major economic centers of China, the Yangtze River Delta and the Beijing-Tianjin-Hebei region have dense populations and frequent industrial activities, which lead to high carbon emissions. Under this high-emission scenario, these factors will further exacerbate the degradation and instability of carbon sinks. In regions characterized by the presence of only one or two overlapping ecological projects, such as southwestern and northeastern China, the stability of carbon sink will exhibit conspicuous inadequacy. This deficiency primarily arises from the slow economic development and a pronounced reliance on conventional energy sources. These factors impede efforts to stabilize carbon sinks, particularly within the constraints of limited ecological interventions (Yue et al., 2022). In contrast, locations such as the Loess Plateau and the Three-River region, where multiple ecological initiatives are concurrently being implemented, will derive substantial advantages from the synergistic interplay among these initiatives, thus significantly bolstering both the stability and efficacy of carbon sinks (Niu et al., 2022). Consequently, these regions manifest elevated proportions of both stable and enhanced carbon sinks under SSP126 and SSP585.

Therefore, the implementation of significant ecological engineering projects should thoroughly account for the limiting factors imposed by climatic conditions, thereby avoiding the applications of singular ecological projects or isolated restoration measures (Niu et al., 2022). Moreover, it is crucial to fully harness the synergistic potential inherent in a comprehensive array of ecological engineering interventions (Shao et al., 2023). This approach strengthens the ecosystem's capacity to withstand endure external disruptions, including natural disasters and climate fluctuations, thereby enhancing the ecosystem' resilience and stability (Wang et al., 2024). Accelerating the trajectory of ecosystem recovery and expediting the attainment of ecological equilibrium can be facilitated through complementary actions.

5 Conclusions

Using the ensemble empirical mode decomposition method and machine learning algorithms (enhanced boosted regression trees), the aims of this study to elucidate the stability of carbon sinks and their driving mechanisms in areas where ecological projects overlap and to predict the potential enhancement in carbon sinks under varying climate and human activity scenarios. The findings revealed that: (1) The carbon sinks clearly and steadily increased in regions where five ecological projects were implemented from 1982 to 2019. In contrast, the carbon sinks did not significantly increase in regions with two or three ecological projects. (2) As the number of ecological projects increased, the impact of human activities on the carbon sinks gradually decreased. In eastern China, rapid

economic development and significant interference from human activities hindered the growth of carbon sinks. In contrast, in western China, the warming and humidification trend of the climate, large-scale afforestation, and other ecological projects have significantly improved carbon sinks. (3) The regions with five overlapping ecological projects exhibited the greatest enhancement and stability of carbon sinks under different scenarios. Compared with the SSP585 scenario, under the SSP126 scenario, the carbon sinks increased, and their stability was greater.

Data availability statement

The original contributions presented in the study are included in the article/Supplementary Material. Further inquiries can be directed to the corresponding authors.

Author contributions

XX: Writing – original draft, Visualization, Validation, Funding acquisition, Formal analysis, Conceptualization. FJ: Writing – original draft, Visualization, Project administration, Methodology, Conceptualization. DL: Writing – original draft, Project administration, Methodology, Data curation. JQ: Writing – original draft, Project administration, Formal analysis, Conceptualization. CZ: Writing – original draft, Investigation, Formal analysis, Conceptualization. KZ: Writing – original draft, Project administration, Methodology, Data curation.

Funding

The author(s) declare financial support was received for the research, authorship, and/or publication of this article. This work was supported by the National Natural Science Foundation of Jiangsu Province (BK20240277, BK20220205), the National Key R&D Program of China (2021YFB3901104), the Special Fund of the Jiangsu for Carbon Peak and Carbon Neutralization Science and Technology Innovation (BK20220021), the National Natural Science Foundation of China (42101103), the Science and Technology Fundamental Resources Investigation Program of China (2023FY100101), and the Special Fund of the Chinese Central Government for Basic Scientific Research Operations in the commonweal Research Institute (GYZX210405, GYZX240304).

Conflict of interest

The authors declare that the research was conducted in the absence of any commercial or financial relationships that could be construed as a potential conflict of interest.

Publisher's note

Supplementary material

The Supplementary Material for this article can be found online at: https://www.frontiersin.org/articles/10.3389/fpls.2024.1482077/full#supplementary-material

References

Abatzoglou, J. T., Dobrowski, S. Z., Parks, S. A., and Hegewisch, K. C. (2018). TerraClimate, a high-resolution global dataset of monthly climate and climatic water balance from 1958-2015. *Sci Data.* 5, 170191. doi: 10.1038/sdata.2017.191

Arani, B. M. S., Carpenter, S. R., Lahti, L., van Nes, E. H., and Scheffer, M. (2021). Exit time as a measure of ecological resilience. *Science* 372, 1–9. doi: 10.1126/science.aay4895

Cai, D., Ge, Q., Wang, X., Liu, B., Goudie, A. S., and Hu, S. (2020). Contributions of ecological programs to vegetation restoration in arid and semiarid China. *Environ. Res. Lett.* 15, 1–11. doi: 10.1088/1748-9326/abbde9

Cai, W., He, N., Li, M., Xu, L., Wang, L., Zhu, J., et al. (2022). Carbon sequestration of Chinese forests from 2010 to 2060: spatiotemporal dynamics and its regulatory strategies. *Sci. Bull. (Beijing).* 67, 836–843. doi: 10.1016/j.scib.2021.12.012

Chang, J., Yue, Y., Tong, X., Brandt, M., Zhang, C., Zhang, X., et al. (2023). Rural outmigration generates a carbon sink in South China karst. *Prog. Phys. Geography: Earth Environ.* 47 (5), 03091333231154177. doi: 10.1177/03091333231154177

Chen, Y., Guo, F., Wang, J., Cai, W., Wang, C., and Wang, K. (2020). Provincial and gridded population projection for China under shared socioeconomic pathways from 2010 to 2100. *Sci. Data.* 7, 83. doi: 10.1038/s41597-020-0421-y

Chen, J. M., Ju, W., Ciais, P., Viovy, N., Liu, R., Liu, Y., et al. (2019). Vegetation structural change since 1981 significantly enhanced the terrestrial carbon sink. *Nat. Commun.* 10, 4259. doi: 10.1038/s41467-019-12257-8

Chen, L., Tan, L., Zhao, M., Sinha, A., Wang, T., and Gao, Y. (2023). Karst carbon sink processes and effects: A review. *Quaternary Int.* 652, 63–73. doi: 10.1016/j.quaint.2023.02.009

Chen, Z., and Yu, G. (2019). Spatial variations and controls of carbon use efficiency in China's terrestrial ecosystems. *Sci. Rep.* 9, 19516. doi: 10.1038/s41598-019-56115-5

Czarniecka-Wiera, M., Szymura, T. H., and Kacki, Z. (2020). Understanding the importance of spatial scale in the patterns of grassland invasions. *Sci. Total Environ.* 727, 138669. doi: 10.1016/j.scitotenv.2020.138669

Du, C., Bai, X., Li, Y., Tan, Q., Zhao, C., Luo, G., et al. (2024). Storage, form, and influencing factors of karst inorganic carbon in a carbonate area in China. *Sci. China Earth Sci.* 67, 725–739. doi: 10.1007/s11430-023-1249-9

Elith, J., Leathwick, J. R., and Hastie, T. (2008). A working guide to boosted regression trees. *J. Anim. Ecology.* 77, 802–813. doi: 10.1111/j.1365-2656.2008.01390.x

Fan, X. G., Ma, Z. G., Yang, Q., Han, Y. H., and Mahmood, R. (2015). Land use/land cover changes and regional climate over the Loess Plateau during 2001-2009. Part II: interrelationship from observations. *CLIMATIC CHANGE.* 129, 441–455. doi: 10.1007/s10584-014-1068-5

Holden, E., Linnerud, K., and Banister, D. (2014). Sustainable development: Our Common Future revisited. *Global Environ. Change.* 26, 130–139. doi: 10.1016/j.gloenvcha.2014.04.006

Hu, X., Ma, C., Huang, P., and Guo, X. (2021). Ecological vulnerability assessment based on AHP-PSR method and analysis of its single parameter sensitivity and spatial autocorrelation for ecological protection – A case of Weifang City, China. *Ecol. Indic.* 125, 1–16. doi: 10.1016/j.ecolind.2021.107464

Ji, F., Wu, Z., Huang, J., and Chassignet, E. P. (2014). Evolution of land surface air temperature trend. *Nat. Climate Change.* 4, 462–466. doi: 10.1038/nclimate2223

Jiao, F., Xu, X., Zhang, M., Gong, H., Sheng, H., Wang, K., et al. (2024). Bedrock regulated climatic controls on the interannual variation of land sink in South-West China karst through soil water availability. *Catena.* 237, 1–12. doi: 10.1016/j.catena.2024.107819

Jin, Z., You, Q., Zuo, Z., Li, M., Sun, G., Pepin, N., et al. (2023). Increased sensitivity of greening to afforestation in China over the recent 20 years. *Agric. For. Meteorology* 339, 1–14. doi: 10.1016/j.agrformet.2023.109561

Li, S., Liu, Y., Wei, G., Bi, M., and He, B.-J. (2024). Carbon surplus or carbon deficit under land use transformation in China? *Land Use Policy* 143, 1–14. doi: 10.1016/j.landusepol.2024.107218

Li, W., Migliavacca, M., Forkel, M., Denissen, J. M. C., Reichstein, M., Yang, H., et al. (2022). Widespread increasing vegetation sensitivity to soil moisture. *Nat. Commun.* 13, 3959. doi: 10.1038/s41467-022-31667-9

Lin, S., Hu, Z., Wang, Y., Chen, X., He, B., Song, Z., et al. (2023). Underestimated interannual variability of terrestrial vegetation production by terrestrial ecosystem models. *Global Biogeochemical Cycles* 37, 1–15. doi: 10.1029/2023gb007696

Liu, P., Chi, Y., Chen, J., and Zhou, L. (2023c). Global climate regulates dimensions of terrestrial ecosystem stability. *Ecosphere* 14, 1–12. doi: 10.1002/ecs2.4577

Liu, J., Ning, J., Kuang, W., Xu, X., Zhang, S., Yan, Z., et al. (2018). Spatio-temporal patterns and characteristics of land-use change in China during 2010-2015. *Acta Geographica Sinica.* 73, 789–802. doi: 10.11821/dlxb201805001

Liu, H., Wang, Z., Wang, Z., Zeng, Y., Xue, P., and Zhang, M. (2023a). Stability of the ecosystem gross primary productivity increasing in Chinese forestry ecological engineering area. *Agriculture Ecosyst. Environ.* 356, 1–11. doi: 10.1016/j.agee.2023.108636

Ma, Z. H., Yan, N. N., Wu, B. F., Stein, A., Zhu, W. W., and Zeng, H. W. (2019). Variation in actual evapotranspiration following changes in climate and vegetation cover during an ecological restoration perio (2000-2015) in the Loess Plateau, China. *Sci. Total Environment.* 689, 534–545. doi: 10.1016/j.scitotenv.2019.06.155

Messori, G., Ruiz-Pérez, G., Manzoni, S., and Vico, G. (2019). Climate drivers of the terrestrial carbon cycle variability in Europe. *Environ. Res. Lett.* 14, 1–20. doi: 10.1088/1748-9326/ab1ac0

Niu, L., Shao, Q., Ning, J., and Huang, H. (2022). Ecological changes and the tradeoff and synergy of ecosystem services in western China. *J. Geographical Sci.* 32, 1059–1075. doi: 10.1007/s11442-022-1985-6

Niu, S., Song, L., Wang, J., Luo, Y., and Yu, G. (2023). Dynamic carbon-nitrogen coupling under global change. *Sci. China Life Sci.* 186 (2023), 1–12. doi: 10.1007/s11427-022-2245-y

Nooni, I. K., Hagan, D. F. T., Wang, G., Ullah, W., Lu, J., Li, S., et al. (2021). Future changes in simulated evapotranspiration across continental africa based on CMIP6 CNRM-CM6. *Int. J. Environ. Res. Public Health* 18, 1–17. doi: 10.3390/ijerph18136760

Pan, N., Feng, X., Fu, B., Wang, S., Ji, F., and Pan, S. (2018). Increasing global vegetation browning hidden in overall vegetation greening: Insights from time-varying trends. *Remote Sens. Environment.* 214, 59–72. doi: 10.1016/j.rse.2018.05.018

Pennekamp, F., Pontarp, M., Tabi, A., Altermatt, F., Alther, R., Choffat, Y., et al. (2018). Biodiversity increases and decreases ecosystem stability. *Nature.* 563, 109–112. doi: 10.1038/s41586-018-0627-8

Piao, S., He, Y., Wang, X., and Chen, F. (2022a). Estimation of China's terrestrial ecosystem carbon sink: Methods, progress and prospects. *Sci. China Earth Sci.* 65, 641–651. doi: 10.1007/s11430-021-9892-6

Piao, S., Wang, X., Wang, K., Li, X., Bastos, A., Canadell, J. G., et al. (2020). Interannual variation of terrestrial carbon cycle: Issues and perspectives. *Glob Chang Biol.* 26, 300–318. doi: 10.1111/gcb.14884

Piao, S., Yue, C., Ding, J., and Guo, Z. (2022b). Perspectives on the role of terrestrial ecosystems in the 'carbon neutrality' strategy. *Sci. China Earth Sci.* 65, 1178–1186. doi: 10.1007/s11430-022-9926-6

Qiao, L., and Xia, H. (2024). The impact of drought time scales and characteristics on gross primary productivity in China from 2001 to 2020. *Geo-spatial Inf. Sci.*, 1–19. doi: 10.1080/10095020.2024.2315279

Seddon, A. W., Macias-Fauria, M., Long, P. R., Benz, D., and Willis, K. J. (2016). Sensitivity of global terrestrial ecosystems to climate variability. *Nature.* 531, 229–232. doi: 10.1038/nature16986

Shao, Q., Liu, S., Ning, J., Liu, G., Yang, F., Zhang, X., et al. (2023). Remote sensing assessment of the ecological benefits provided by national key ecological projects in China during 2000–2019. *J. Geographical Sci.* 33, 1587–1613. doi: 10.1007/s11442-023-2144-4

Song, Y., Jiao, W., Wang, J., and Wang, L. (2022). Increased global vegetation productivity despite rising atmospheric dryness over the last two decades. *Earth's Future* 10. doi: 10.1029/2021EF002634

Thackeray, S. J., Henrys, P. A., Hemming, D., Bell, J. R., Botham, M. S., Burthe, S., et al. (2016). Phenological sensitivity to climate across taxa and trophic levels. *Nature.* 535, 241–245. doi: 10.1038/nature18608

Tong, X., Brandt, M., Yue, Y., Zhang, X., Fensholt, R., Ciais, P., et al. (2023). Reforestation policies around 2000 in southern China led to forest densification and expansion in the 2010s. *Commun. Earth Environ.* 4, 1–18. doi: 10.1038/s43247-023-00923-1

Wang, K., Bastos, A., Ciais, P., Wang, X., Rodenbeck, C., Gentine, P., et al. (2022a). Regional and seasonal partitioning of water and temperature controls on global land carbon uptake variability. *Nat. Commun.* 13, 3469. doi: 10.1038/s41467-022-31175-w

Wang, M., Ding, Z., Wu, C., Song, L., Ma, M., Yu, P., et al. (2021). Divergent responses of ecosystem water-use efficiency to extreme seasonal droughts in Southwest China. *Sci. Total Environ.* 760, 143427. doi: 10.1016/j.scitotenv.2020.143427

Wang, Z., Fu, B., Wu, X., Li, Y., Feng, Y., Wang, S., et al. (2023). Vegetation resilience does not increase consistently with greening in China's Loess Plateau. *Commun. Earth Environ.* 4, 1–14. doi: 10.1038/s43247-023-01000-3

Wang, K., Piao, S., He, Y., Liu, Y., and He, H. (2022b). Spatial variations and mechanisms for the stability of terrestrial carbon sink in China. *Sci. China Earth Sci.* 66, 227–236. doi: 10.1007/s11430-021-1003-5

Wang, K., Yue, Y., Brandt, M., and Tong, X. (2019). Karst ecosystem observation and assessment at local and regional scales. *InterCarto. InterGIS.* 25, 43–47. doi: 10.35595/2414-9179-2019-2-25-43-47

Wang, T., Zhang, Y., Yue, C., Wang, Y., Wang, X., Lyu, G., et al. (2024). Progress and challenges in remotely sensed terrestrial carbon fluxes. *Geo-spatial Inf. Sci.*, 1–21. doi: 10.1080/10095020.2024.2336599

Wu, Z., Huang, N. E., Long, S. R., and Peng, C. K. (2007). On the trend, detrending, and variability of nonlinear and nonstationary time series. *Proc. Natl. Acad. Sci. U S A.* 104, 14889–14894. doi: 10.1073/pnas.0701020104

Wu, X., Shen, C., Shi, L., Wan, Y., Ding, J., and Wen, Q. (2024). Spatio-temporal evolution characteristics and simulation prediction of carbon storage: A case study in Sanjiangyuan Area, China. *Ecol. Inf.* 80, 1–14. doi: 10.1016/j.ecoinf.2024.102485

Wu, F., Yang, X., Shen, Z., Bian, D., and Babuna, P. (2021). Exploring sustainability and decoupling effects of natural capital utilization in China: Evidence from a provincial three-dimensional ecological footprint. *J. Cleaner Production* 295, 1–17. doi: 10.1016/j.jclepro.2021.126486

Xia, X., Ren, P., Wang, X., Liu, D., Chen, X., Dan, L., et al. (2024). The carbon budget of China: 1980-2021. *Sci. Bull. (Beijing).* 69, 114–124. doi: 10.1016/j.scib.2023.11.016

Xu, X., Jiao, F., Liu, H., Gong, H., Zou, C., Lin, N., et al. (2022a). Persistence of increasing vegetation gross primary production under the interactions of climate change and land use changes in Northwest China. *Sci. Total Environ.* 834, 155086. doi: 10.1016/j.scitotenv.2022.155086

Xu, X., Liu, J., Jiao, F., Zhang, K., Yang, Y., Qiu, J., et al. (2023b). Spatial variations and mechanisms for the stability of water use efficiency in China. *Front. Plant Sci.* 14. doi: 10.3389/fpls.2023.1254395

Xu, X., Liu, J., Jiao, F., Zhang, K., Ye, X., Gong, H., et al. (2022b). Ecological engineering induced carbon sinks shifting from decreasing to increasing during 1981-2019 in China. *Sci. Total Environ.* 864, 161037. doi: 10.1016/j.scitotenv.2022.161037

Xu, H., Yue, C., Zhang, Y., Liu, D., and Piao, S. (2023a). Forestation at the right time with the right species can generate persistent carbon benefits in China. *Proc. Natl. Acad. Sci. U S A.* 120, e2304988120. doi: 10.1073/pnas.2304988120

Yang, Y., Shi, Y., Sun, W., Chang, J., Zhu, J., Chen, L., et al. (2022). Terrestrial carbon sinks in China and around the world and their contribution to carbon neutrality. *Sci. China Life Sci.* 65, 861–895. doi: 10.1007/s11427-021-2045-5

Yazdandoost, F., Moradian, S., Izadi, A., and Aghakouchak, A. (2021). Evaluation of CMIP6 precipitation simulations across different climatic zones: Uncertainty and model intercomparison. *Atmospheric Res.* 250, 1–20. doi: 10.1016/j.atmosres.2020.105369

Yue, Y., Liao, C., Tong, X., Wu, Z., Fensholt, R., Prishchepov, A., et al. (2020). Large scale reforestation of farmlands on sloping hills in South China karst. *Landscape Ecology.* 35, 1445–1458. doi: 10.1007/s10980-020-01026-4

Yue, Y., Qi, X., Wang, K., Liao, C., Tong, X., Brandt, M., et al. (2022). Large scale rocky desertification reversal in South China karst. *Prog. Phys. Geography: Earth Environment.* 46, 661–675. doi: 10.1177/03091333221083111

Zhang, T., Cheng, C., and Wu, X. (2023a). Mapping the spatial heterogeneity of global land use and land cover from 2020 to 2100 at a 1 km resolution. *Sci. Data.* 10, 748. doi: 10.1038/s41597-023-02637-7

Zhang, R., and Hanaoka, T. (2021). Deployment of electric vehicles in China to meet the carbon neutral target by 2060: Provincial disparities in energy systems, CO2 emissions, and cost effectiveness. *Resources Conserv. Recycling* 170, 1–10. doi: 10.1016/j.resconrec.2021.105622

Zhang, L., Ren, X., Wang, J., He, H., Wang, S., Wang, M., et al. (2019). Interannual variability of terrestrial net ecosystem productivity over China: regional contributions and climate attribution. *Environ. Res. Lett.* 14, 1–9. doi: 10.1088/1748-9326/aaec95

Zhang, W., Schurgers, G., Penuelas, J., Fensholt, R., Yang, H., Tang, J., et al. (2023b). Recent decrease of the impact of tropical temperature on the carbon cycle linked to increased precipitation. *Nat. Commun.* 14, 965. doi: 10.1038/s41467-023-36727-2

Zhang, T., Xu, X., Jiang, H., Qiao, S., Guan, M., Huang, Y., et al. (2022). Widespread decline in winds promoted the growth of vegetation. *Sci. Total Environ.* 825, 153682. doi: 10.1016/j.scitotenv.2022.153682

Zhao, T., Xia, C., Suo, X., and Cao, S. (2021). Cost-benefit evaluation of Chinese ecological restoration programs. *Acta Ecologica Sinica*. 41, 4757–4764. doi: 10.5846/stxb202011223000

Zheng, Y., Shen, R., Wang, Y., Li, X., Liu, S., Liang, S., et al. (2020). Improved estimate of global gross primary production for reproducing its long-term variation 1982–2017. *Earth System Sci. Data*. 12, 2725–2746. doi: 10.5194/essd-12-2725-2020

Zheng, K., Wei, J. Z., Pei, J. Y., Cheng, H., Zhang, X. L., Huang, F. Q., et al. (2019). Impacts of climate change and human activities on grassland vegetation variation in the Chinese Loess Plateau. *Sci. Total Environment*. 660, 236–244. doi: 10.1016/j.scitotenv.2019.01.022

Zhou, W., Yang, H., Zhou, L., Chen, Y., Huang, L., and Ju, W. (2018). Dynamics of grassland carbon sequestration and its coupling relation with hydrothermal factor of Inner Mongolia. *Ecol. Indicators*. 95, 1–11. doi: 10.1016/j.ecolind.2018.07.008

Zhu, L., and Lo, K. (2022). Eco-socialism and the political ecology of forest conservation in the Greater Khingan Range, China. *POLITICAL Geogr*. 93, 45–59. doi: 10.1016/j.polgeo.2021.102533

Zhu, A. X., Wang, Z., Liu, Z.-M., Jiang, Y.-C., Qin, J.-Y., Wang, P.-Y., et al. (2021). Land development and utilization for carbon neutralization. *J. Natural Resour*. 36, 45–59. doi: 10.31497/zrzyxb.20211201

frontiers | Frontiers in Plant Science

TYPE Original Research
PUBLISHED 19 February 2025
DOI 10.3389/fpls.2025.1438343

OPEN ACCESS

EDITED BY
Samuel Kuria Kiboi,
University of Nairobi, Kenya

REVIEWED BY
Ting Hua,
Norwegian University of Science and Technology, Norway
Nitu Wu,
Inner Mongolia Agricultural University, China

*CORRESPONDENCE
Yingjie Wu
mkswuyj@163.com

RECEIVED 25 May 2024
ACCEPTED 14 January 2025
PUBLISHED 19 February 2025

CITATION
Sinan W, Wu Y, Wang W, Guo J and Li M (2025) Loss rate of net primary productivity under drought stress on the Yinshanbeilu of Inner Mongolia, China.
Front. Plant Sci. 16:1438343.
doi: 10.3389/fpls.2025.1438343

Loss rate of net primary productivity under drought stress on the Yinshanbeilu of Inner Mongolia, China

Wang Sinan[1,2], Yingjie Wu[1,2]*, Wenjun Wang[1,2], Jianyin Guo[1,2] and Mingyang Li[3]

[1]Institute of Water Resources of Pastoral Area, Ministry of Water Resources, Hohhot, China, [2]Yinshanbeilu Grassland Eco-Hydrology National Observation and Research Station, China Institute of Water Resources and Hydropower Research, Beijing, China, [3]Shandong Provincial Key Laboratory of Water Resources and Environment, Water Resources Research Institute of Shandong Province, Jinan, China

Introduction: The increasing intensity and frequency of droughts seriously threaten the structure and function of terrestrial ecosystems. In order to ensure the normal play of ecosystem service function under future stress, the temporal and spatial characteristics of ecosystem productivity response to drought need to be explored.

Methods: The net primary production (NPP) of vegetation in the Yinshanbeilu was calculated using the Carnegie-Ames-Stanford Approach (CASA) model, and subsequent study concentrated on the NPP's geographical and temporal variable characteristics. By the calculation of the standard precipitation evapotranspiration index (SPEI), the study also sought to examine the relationship between drought and NPP at various time scales. Researchers also built drought loss rate curves based on various fertility stages using the vulnerability curve construction method.

Results and discussion: Findings revealed that the SPEI had varying degrees of efficacy in capturing drought conditions at various time frames. Nonetheless, the SPEI's spatial distribution, which shows a wet distribution in the east and an arid distribution in the west, exhibited identical characteristics for all scales and may be used to indicate drought. Significant interannual variation was seen in the NPP of the study area's vegetation, which fluctuated in an upward direction from 2000 to 2020. 75.89%, 77.23%, 81.35%, and 83.56% of the area were found to have a positive correlation between the SPEI and vegetation NPP at various time scales, with 42.53%, 48.15%, 90.72%, and 92.75% of the area passing the significance test ($p < 0.05$), in that order. Their results showed that as the SPEI time scale was increased, the link between vegetation NPP and SPEI became stronger. The loss rate of vegetation NPP fluctuated and grew regularly with the expansion of drought degree, varying between 20-50%, according to drought loss rate curves created for each fertility period.

KEYWORDS

net primary productivity, drought, response, loss rate, CASA model

1 Introduction

It is widely acknowledged that drought is a serious natural disaster with huge global economic repercussions. In fact, drought-related economic losses account for a substantial portion of all natural disaster losses (Liu et al., 2020a). Additionally, the persistence of drought can lead to a range of cascading effects, including reduced soil water resources for vegetation growth, inhibited photosynthesis, and the induction of natural disasters such as dust storms and fires. These consequences may drastically reduce ecosystems' capacity to serve as carbon sinks, which may eventually lower vegetation productivity (Nejadrekabi et al., 2022; Tian et al., 2019; Wang et al., 2022a). As a result, understanding the impacts of drought on vegetation presence is crucial for enhancing ecosystem stability (Ding et al., 2022; Geng et al., 2022; Shi et al., 2022; Soleimani-Motlagh et al., 2022). Furthermore, given the potential for increases in the intensity, frequency, and duration of drought, it is essential to explore strategies aimed at mitigating these negative effects and preserving the functional structure of terrestrial ecosystems.

Numerous researchers have made use of drought indices in order to accurately measure complex instances of drought. These indices, which include the Palmer Drought Index (PDSI), the Standardized Precipitation Index (SPI), and the Standardized Precipitation Evapotranspiration Index (SPEI), are designed to more accurately reflect the spatial and temporal characteristics of drought (Laimighofer and Laaha, 2022; Ramirez et al., 2022; Wahla et al., 2022; Xu et al., 2022). Several scientific investigations have indicated that vegetation responses to drought stress involve the closure or reduction in size of vegetation stomata, impacting CO_2 uptake, and subsequently, vegetation photosynthesis (Gang et al., 2022; Wei et al., 2022a), These effects are particularly pronounced in areas characterized by arid and semi-arid weather, which feature more vulnerable terrestrial ecosystems (Geng et al., 2023). Specifically, a widespread drought incident markedly diminishes the net primary productivity of plant communities (Li et al., 2020a). Furthermore, it has been observed that vegetation NPP and SPEI are predominantly positively correlated, particularly in the 20-50°N latitude range, where vegetation is more sensitive to drought stress (Liu et al., 2021b). As droughts become more frequent and persistent, the loss in vegetation NPP amplifies significantly (Sun et al., 2016). The reaction of NPP to drought displays geographical variability and is subject to multiple uncertainties during analysis (Khatri-Chhetri et al., 2021). One illustration of this is the research of Kljun et al. (2007) on poplar forests in southern Canada, which revealed that severe drought events of extended duration and high intensity suppressed both vegetation respiration and photosynthesis to a similar degree, ultimately resulting in little alteration of vegetation NPP. However, under mild or moderate drought conditions, ecosystem photosynthesis remained largely unaffected while respiration was considerably reduced, and this led to the observed increase in vegetation NPP. Consequently, it is clear that while current studies tend to concur that drought-induced water stress typically reduces vegetation NPP via stomatal closure, there is considerable variability in the response to drought across different regions, biomes, and land use types, as well as in relation to ambient climate conditions, which can all influence vegetation response (Tong et al., 2023; Yuan et al., 2022; Zhao et al., 2019a). Currently, the majority of studies are concentrated on the decrease in NPP during drought episodes. However, an essential aspect regarding quantifying the susceptibility of vegetation NPP to drought has yet to be examined. Additionally, additional exploration into the temporal response of NPP to drought is necessary.

There is a fragile ecological zone in China that is arid and semi-arid, and the Yinshanbeilu region of Inner Mongolia is located within this zone. As a consequence of this, the amount of moisture that is accessible plays a significant part in determining the degree to which vegetation is able to prosper in this area (Wang et al., 2022b). A number of ecological problems, including ecological and vegetation degradation, as well as water shortages, have surfaced as a direct result of the exacerbation of climate change brought on by human activities in the region. The main objectives of this paper were to (1) reveal the spatial and temporal evolution of multi-scale drought in grasslands and to identify the years of drought occurrence; (2) estimation of NPP by CASA model to reveal the spatial and temporal variation pattern of regional NPP; and (3) construct a drought disaster loss rate curve for vegetation during the agricultural production period and quantitatively evaluate the effects of different drought levels on vegetation productivity. This offered a plausible method for promptly assessing the loss due to drought in vegetation. This research is an innovative attempt in the field of assessing the effects of drought on vegetation, and it offers important new theoretical insights.

2 Materials and methods

2.1 Study area

Yinshanbeilu is a transitional agricultural and pastoral area situated between the Yinshan Mountains and the Mongolian Plateau (Figure 1). The coordinates are 107°17′~116°53′E and 40°43′~43°23′N, respectively. Twelve banners and counties make up the administrative jurisdiction, which covers a massive 97,250.5 km^2. temperatures averaging 1.3–3.9°C, evaporation rates averaging 1,748–2,300 mm, precipitation averaging 200–400 mm, and frost-free periods typically ranging from 102–121 days. Soil wind erosion, desertification, soil erosion, land degradation, and other ecological and environmental problems are becoming increasingly serious as a result of land use changes and human activities, severely limiting the growth of local economies and societies (Li et al., 2023).

2.2 Data sources

2.2.1 Remote sensing data

NDVI data using MOD13A2 (https://search.earthdata.nasa.gov/search), the time series of 2000-2020, the 16 days of synthetic products, and a spatial resolution of 1 km. MCD12Q1 yearly synthetic products from 2000 to 2020 were used to collect vegetation type data. Time series from 2000 to 2020 utilizing NPP data with MOD17A3HGF yearly synthetic products. The data at a

resolution of 1 km were resampled after pre-processing, including reprojection, Mosaic, and clipping, for input into the CASA model and data comparison.

2.2.2 Meteorological data

The National Weather Service's website (http://data.cma.cn) was utilized to download the meteorological data for this article, which included yearly precipitation and the percentage of average annual bright sunlight for the years 2000 to 2020. AUSPLIN interpolation software was used to analyze the data. After interpolation, the spatial resolution is 1 km when combined with the digital elevation model in the study area.

2.3 Methods

2.3.1 NPP

In the CASA model, which is one of the several major light energy utilization models currently absorbed, vegetation net primary productivity was determined by variables absorbed by vegetation in photosynthetic active radiation (APAR) and in light energy conversion (ε). The NPP calculation model adopted in this study is an improved CASA model (Xue et al., 2022). Its calculation formula is as follows:

$$NPP(x,t) = APAR(x,t) \times \varepsilon(x,t) \quad (1)$$

In this equation, APAR (x, t) represents solar Photoactive radiation received by pixel x in month t, and in this case, ε (x, t) represents actual light energy utilization of pixel x in month t.

2.3.2 SPEI

By factoring in the effects of precipitation and temperature on water balance, SPEI is used to evaluate and predict drought conditions at different time intervals. In this study, the monthly difference between evapotranspiration and precipitation is calculated after the potential evapotranspiration has been established using the Thornthwaite method. SPEI-1, SPEI-3, SPEI-6, and SPEI-12 are calculated for monthly, 3-month, 6-month, and 12-month intervals, respectively, after the difference series has been normalized using the 3-parameter log-logistic probability distribution. Methods for determining SPEI are described in detail in the cited works (Stagge et al., 2015; Wang et al., 2015).

The current research aims to investigate the effects of droughts on plant life. So, we're looking at the drought condition that typically occurs during plant growth (April–September). Given that the drought condition is represented by the September SPEI-6 value for six months spanning the period from April to September, thus encompassing the entire growing season, the September SPEI-6 value has been used to formulate the drought loss rate curve.

2.3.3 Correlation analysis

Analysis of correlation is a method that can be used to determine whether or not there is a connection between two or more factor variables. This can be done by comparing the levels of similarity between the factors. The Pearson correlation coefficient method has been selected to analyze the internal relationship between the two variables (Li et al., 2021). The formula used in this calculation is articulated below.

$$R = \frac{\sum_{i=0}^{n}(x_i - \overline{x})(y - \overline{y})}{\sqrt{\sum_{i=0}^{n}(x_i - \overline{x})^2}\sqrt{\sum_{i=0}^{n}(y - \overline{y})^2}} \quad (2)$$

In this equation, x_i said the first years of NPP values, $\overline{x}$ Represents the mean value of NPP over the years, $\overline{y}$ Represents the mean SPEI over the years.

2.3.4 Construction of drought loss rate curve

Based on CASA model, the regional NPP was estimated. As a representation of drought vulnerability, the drought loss rate curve based on CASA model was constructed. The details are as follows:

(1) Identification of drought. The SPEI index of vegetation growth season was used to judge the drought degree from April to September, and the SPEI values of all stations were no drought (SPEI≥0) or no more than 3 stations were no more than light drought (-1≤SPEI <0) month is drought free month. The identification results are shown in Table 1.

(2) According to the SPEI values identified at each station, the SPEI index raster map year by year, and the spatial resolution was consistent with the regional NPP raster map, both being 1km×1km. At the same time, GIS spatial analysis technology was used to extract the pixel value of SPEI index into the grid where the vegetation was located,

TABLE 1 Monthly drought in the growing season at the Yinshanbeilu from 2000 to 2020.

Month	Normal year	Dry year
4	2000,2001,2002,2003,2005,2007,2010,2011,2012,2013,2015,2017,2019,2020	2004,2006,2008,2009,2014,2016,2018
5	2000,2002,2003,2005,2006,2007,2010,2011,2012,2014,2015,2016,2017,2019,2020	2001,2004,2008,2009,2013,2018
6	2000,2002,2003,2004,2006,2008,2010,2012,2013,2014,2015,2016,2017,2019	2001,2005,2007,2009,2011,2018,2020
7	2001,2002,2003,2004,2006,2008,2012,2013,2014,2015,2016,2019	2000,2005,2007,2009,2010,2011,2017,2018,2020
8	2000,2002,2003,2004,2008,2012,2015,2016,2018,2019,2020	2001,2005,2006,2007,2009,2010,2011,2013,2014,2017
9	2002,2003,2004,2008,2010,2012,2013,2014,2015,2016,2018,2019,2020	2000,2001,2005,2006,2007,2009,2011,2017

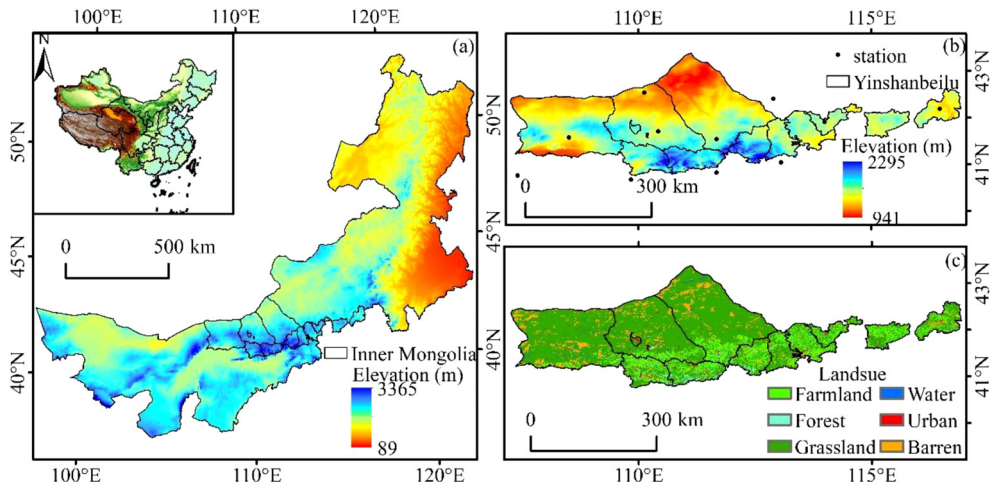

FIGURE 1
Location of the study area. **(A)** location relative to Inner Mongolia, **(B)** Elevation, meteorological stations, and **(C)** land cover.

and it was used to represent the drought risk value of the vegetation on a grid basis.

(3) Obtaining monthly NPP data for the study area for the 2000-2000, and the raster map of the regional vegetation growth season from April to September was selected from it, which was also extracted into the grid where the vegetation was located, and used as the grid value of vegetation drought vulnerability year by year, month by month.

(4) Calculate the drought loss rate, that is, the NPP loss rate of vegetation caused by drought. The NPP values of vegetation corresponding to normal months are considered as normal values, and the average values of vegetation NPP in all normal years are taken as the normal values of vegetation NPP in that month without drought. Therefore, the pixel-by-pixel drought loss rate can be calculated as follows:

$$NPP_{LDR} = \frac{NPP_{NO} - NPP_{DR}}{NPP_{NO}} \times 100\,\% \quad (3)$$

Where, NPP_{LDR} represents the NPP loss rate of drought-induced vegetation; NPP_{NO} represents the vegetation NPP in normal months; NPP_{DR} indicates the value of the NPP produced by plants during the month of drought.

It is acceptable that the loss rate of ecosystem is between 10%-20% (van Minnen et al., 2002). In this study, 20% NPP loss rate of vegetation is represented as the threshold line of drought loss. When the NPP loss rate of vegetation exceeds 20%, drought loss event begins to occur.

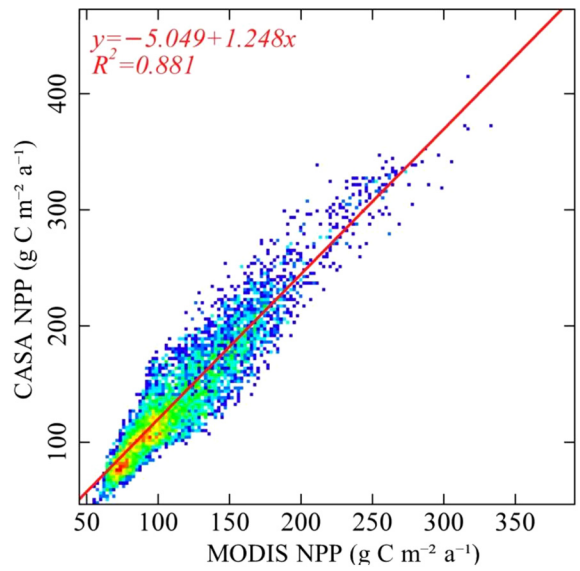

FIGURE 2
Accuracy verification of simulation results.

3 Results

3.1 Model accuracy verification

This study aimed to compare the estimated results obtained from the CASA model with the MOD17A3 data products spanning the period from 2000 to 2020, The two results are in good agreement(R^2 = 0.881), thereby making it a suitable candidate for further analysis (Figure 2).

3.2 Spatial and temporal trends of SPEI

Observations presented in Figure 3 demonstrate that the SPEI displays varying degrees of accuracy in detecting drought conditions at the northern base of Yinshanbeilu depending on the time scale under consideration. Despite this, SPEI exhibits similar spatial distribution trends for drought at different scales, characterized by an east-west distribution pattern, depicting wet conditions in the east and dry conditions in the west.

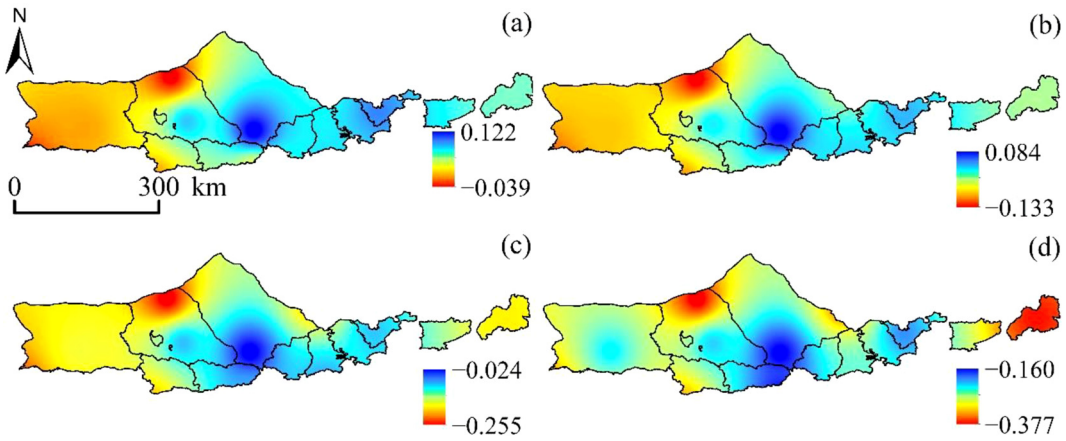

FIGURE 3
SPEI spatial distribution. **(A)** SPEI-1, **(B)** SPEI-3, **(C)** SPEI-6, and **(D)** SPEI-12.

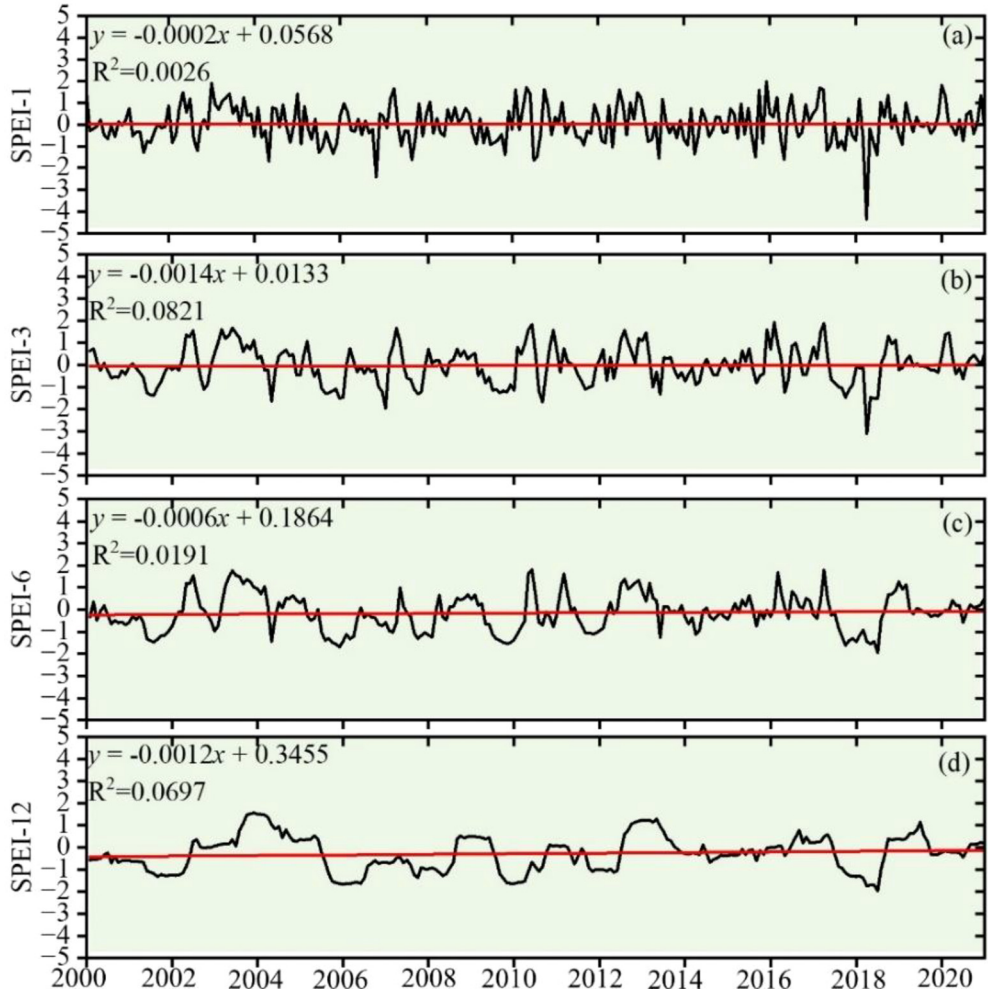

FIGURE 4
SPEI time variation trend. **(A)** SPEI-1, **(B)** SPEI-3, **(C)** SPEI-6, and **(D)** SPEI-12.

As can be seen in Figure 4, the sensitivity of the fluctuation of SPEI values at multiple scales from 2000 to 2020 is obviously different, showing a trend that is slightly decreasing at different time scales. This change can be seen across the board. The occurrence of drought is unpredictable and happens on a regular basis, and the multi-scale SPEI indexes in 2005, 2009, 2010, and 2019 show a clear turnaround, demonstrating a "down-rising-declining-rising trend." The frequent occurrence of droughts followed by floods in each month is reflected by the fact that SPEI-1 experiences significant swings along the value of 0. This demonstrates the seasonal change pattern of dryness and wetness in the study area. The variability of the SPEI-12 is manageable, which enables it to comprehend the overarching pattern of drought progression.

Figure 5 reveals that the variation trend of SPEI-1 is gradually increasing from west to east, with clear evidence of horizontal zonality rule. This can be seen to be the case with a value of -0.006~0.019/a. The area demonstrates a moderately weak downward trend, with the downward trend accounting for 84.25% of the total area and the upward trend accounting for 15.75% of the total area, respectively. Furthermore, only 5.44% of the area passes the significance test at the 0.05 level. They are found most frequently in the area of the study that is located to the east. Only 4.63% of the area met the criteria for significance when the test was performed at the level of 0.05, and the variation trend of SPEI-3 was -0.005~0.021/a. The SPEI-6 displayed a trend of -0.003~0.026/a, and the significance test found that only 4.12% of the area met the criteria for passing at the level of 0.05. The significance level of the significance test was set at 0.05, and the variation trend of SPEI-12 was -0.007~0.049/a. Only 1.71% of the area passed the significance test. In conclusion, between the years 2000 and 2020, the SPEI index in the western area exhibited a negative tendency across several time intervals, which suggested that the region tended to be dry. This pattern was consistent across all time scales. On the other hand, the SPEI index in the majority of the eastern area showed an upward trend, which suggested that these places exhibited a tendency towards being wetter. This was the case despite the fact that the western region continued to show a downward trend.

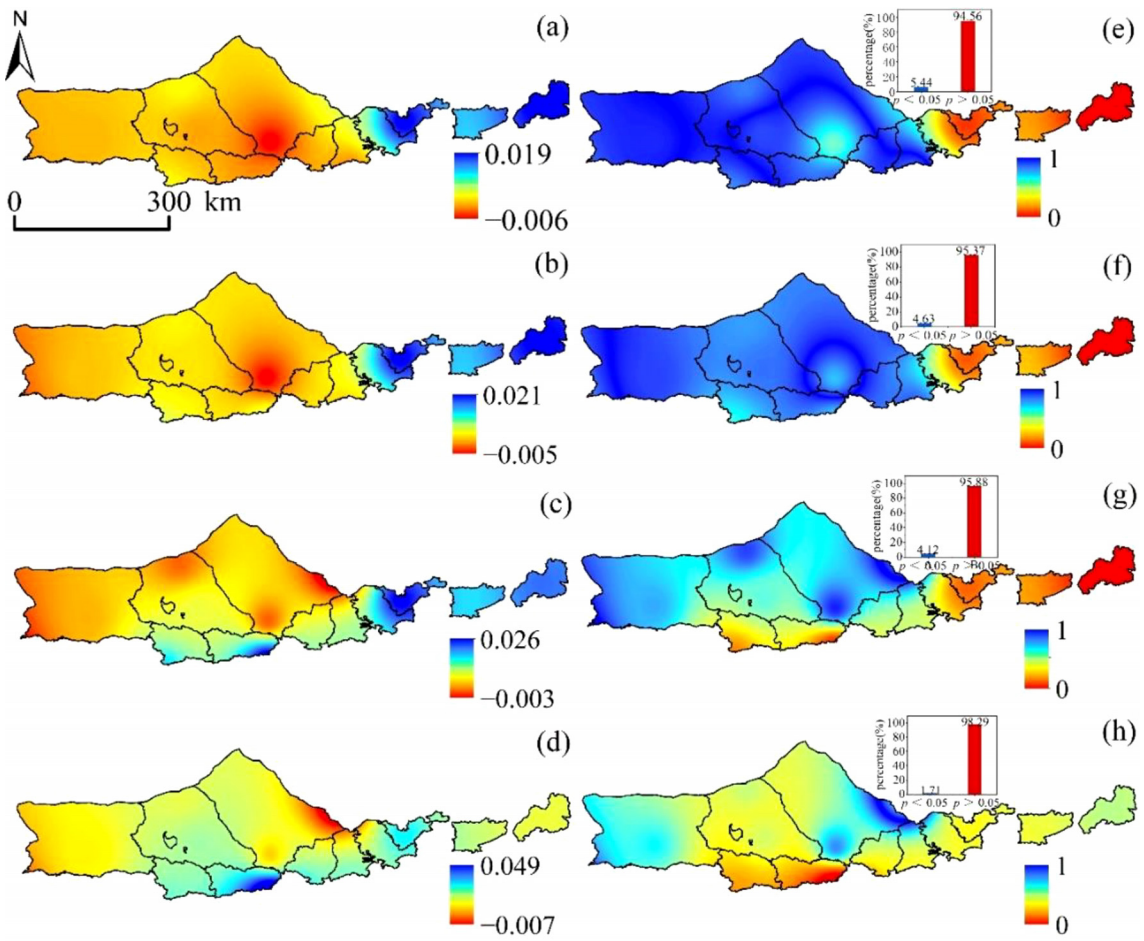

FIGURE 5
SPEI spatial variation trend:**(A)** SPEI-1, **(B)** SPEI-3, **(C)** SPEI-6, and **(D)** SPEI-12. SPEI significant change trend:**(E)** SPEI-1, **(F)** SPEI-3, **(G)** SPEI-6, and **(H)** SPEI-12.

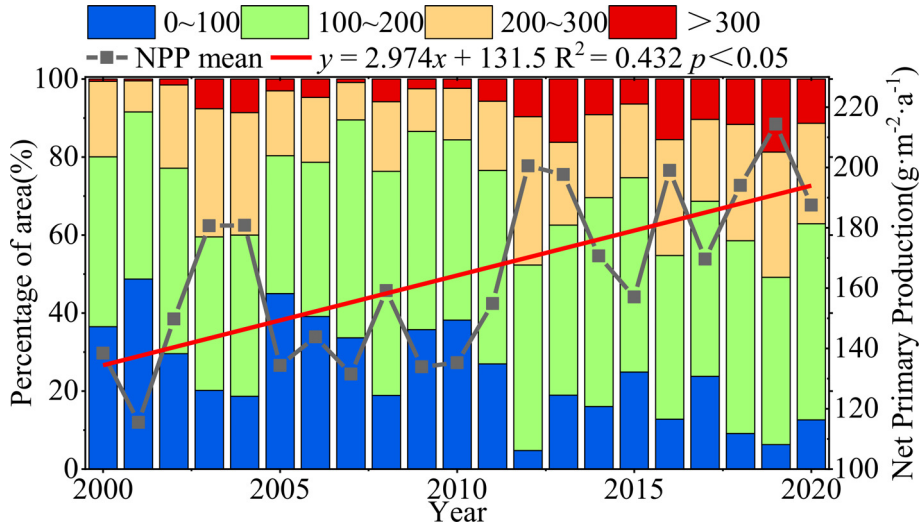

FIGURE 6
Interannual variation in vegetation NPP and variation in area occupied by NPP mean grading.

3.3 Spatial and temporal trends of NPP

From 2000 to 2020, the mean NPP of vegetation at the northern foot of Yinshan showed great inter-annual variation, and showed a trend of fluctuation and increase, with an increase rate of 2.974g·m^{-2}·a^{-1}. The area percentage of NPP in the northern foothill of Yinshan was divided into four grades: 0~100 g·m^{-2}·a^{-1},100~200 g·m^{-2}·a^{-1},200~300 g·m^{-2}·a^{-1},>300 g·m^{-2}·a^{-1}. The results showed that the area proportion of vegetation NPP in the range of 0 ~ 100 g·m^{-2}·a^{-1} was 45.01% in 2005, and the area proportion in this area tended to decrease during the whole study period. The NPP of vegetation ranges from 100 to 200 g·m^{-2}·a^{-1}, and the maximum area proportion is 35.29% ~ 57.39%. The mean NPP of vegetation in the area larger than 300 g·m^{-2}·a^{-1} fluctuated between 0.46% and 16.22%, and showed a slow rising trend (Figure 6).

The slope of the vegetation NPP fitted in the Yinshanbeilu from 2000 to 2020 varied from -5.135 to 14.811 g·m^{-2}·a^{-1} (Figure 7), and the proportion of the region with a rising trend was 99.49%, spread in most parts of the research area. In Huade and Shangdu counties, as well as in the southwestern section of Siziwangqi, the majority of the land that showed no significant increase in the amount of vegetation NPP was located in the regions that were dominated by arable land. This accounted for 22.03% of the total land area (p> 0.05). The significance test (p> 0.05) was passed by the regions that accounted for 23.75% of the total area, while the highly significant test ((p <0.01) was passed by the regions that accounted for 54.22% of the total area. The Hurst index of vegetation NPP in the Yinshanbeilu ranged from 0.066 to 0.626, with a mean value of 0.396, and the proportion of the image elements with a Hurst index less than 0.5 was 62.36%. This suggests that the inverse persistence

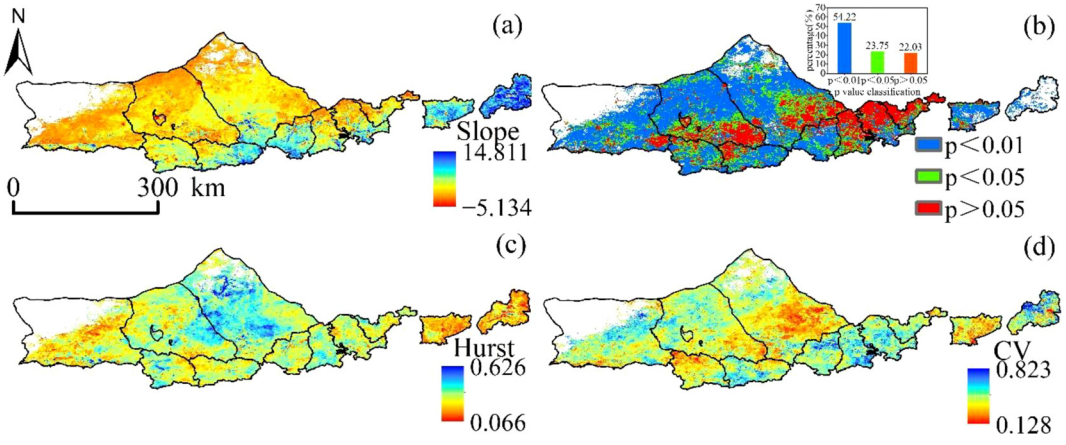

FIGURE 7
Yinshanbeilu change distribution features **(A)** spatial trend distribution, **(B)** significance distribution, **(C)** Hurst distribution, and **(D)** coefficient of variation distribution during 2000-2020.

of vegetation NPP change in the Yinshanbeilu is greater than the positive persistence in the future, which implies that the tendency of vegetation NPP shift will be reverted at some point in the future. The yearly mean value of the NPP produced by vegetation in the northern half of the Yinshanbeilu is predicted to have a low coefficient of variation from the years 2000 to 2020, and the percentage of the regional image elements with the coefficient of variation below 0.25 is 89.89%, which indicates that the mean value of the vegetation NPP time series in the northern part of the Yinshanbeilu is relatively stable. This was determined by comparing the percentage of the regional image elements with the coefficient of variation below 0.25. The coefficients of variation ranging from 0.250 to 0.823 are most often seen in regions that have experienced significant shifts in land use and regions that have been significantly impacted by human activities.

3.4 The correlation between SPEI and NPP

SPEI (SPEI -1, SPEI -3, SPEI -6, and SPEI -12) and vegetation NPP had correlation values of -0.221 to 0.822, -0.299 to 0.851, -0.186 to 0.947, and -0.291 to 0.926, respectively, over a variety of time periods (Figure 8). The average coefficients of correlation were 0.408, 0.427, 0.602, and 0.623. The overall geographical distribution is "low in the southwest and high in the northeast." The percentages of SPEI positively linked with NPP at each time scale were 75.89%, 77.23%, 81.35%, and 83.56%, with 42.53%, 48.15%, 90.72%, and 92.75%, respectively, passing the significance test ($p<0.05$). vegetation NPP and SPEI that strengthened with decreasing SPEI time scale, indicating that Yinshanbeilu's NPP responded relatively well to drought changes on an annual scale but poorly to those on a medium- and short-term basis, especially to a short-term surface water anomaly and a seasonal scale.

3.5 Loss rate of NPP under drought stress

As can be seen from Figure 9, The variation range of NPP loss rate caused by drought was 2.351~46.238%, 13.621~49.596%, 0.849~39.873%, 4.023~49.921% and 0.397-47.685 in different growth periods of vegetation in the vegetation growing season (each month was taken as a growth period of vegetation in this study) %, 0.558~49.886%, and the average loss rates were 23.64%, 28.53%, 29.18%, 32.86%, and 32.95%, respectively. Generally, the spatial distribution pattern is "low in the west and high in the east".

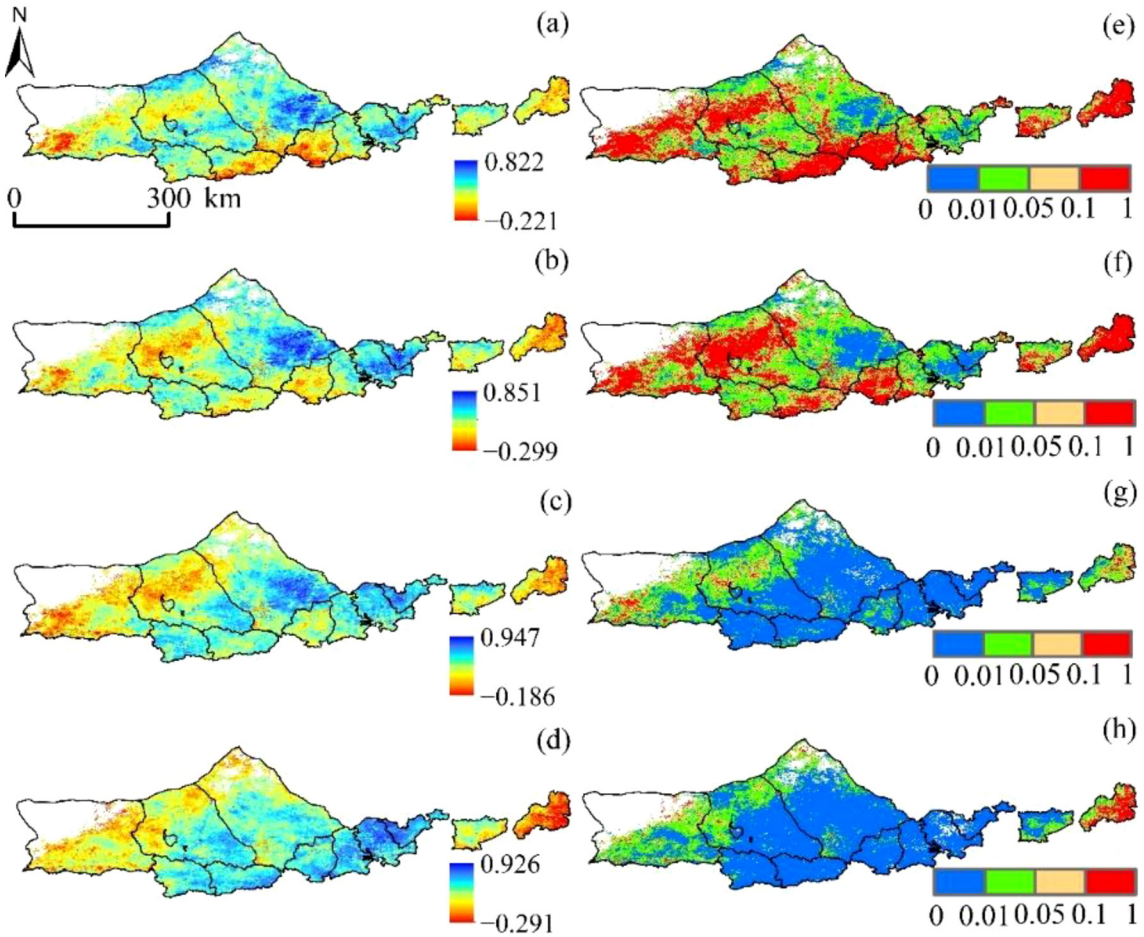

FIGURE 8
Correlation between SPEI and vegetation NPP at different time scales:**(A)** SPEI-1, **(B)** SPEI-3, **(C)** SPEI-6, and **(D)** SPEI-12. The significance of SPEI and vegetation NPP at different time scales: **(E)** SPEI-1, **(F)** SPEI-3, **(G)** SPEI-6, and **(H)** SPEI -12.

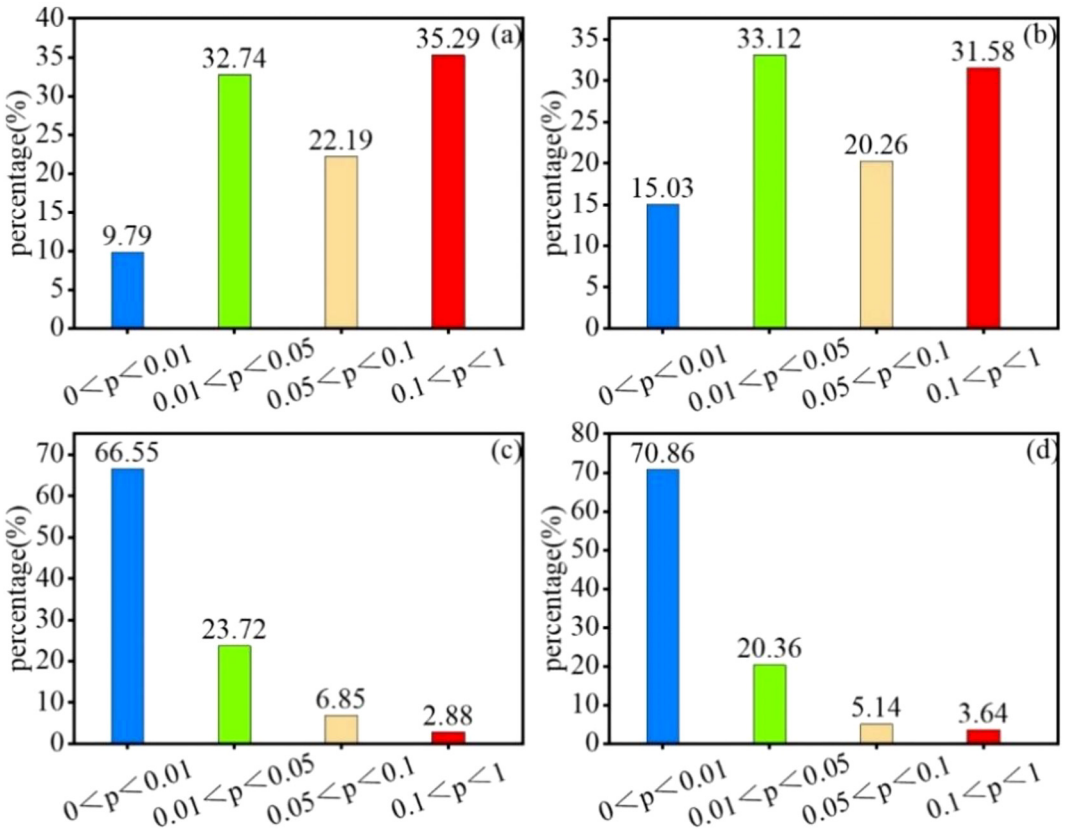

FIGURE 9
Percentage significance of SPEI vs. NPP at different time scales. **(A)** SPEI-1, **(B)** SPEI-3, **(C)** SPEI-6, and **(D)** SPEI-12.

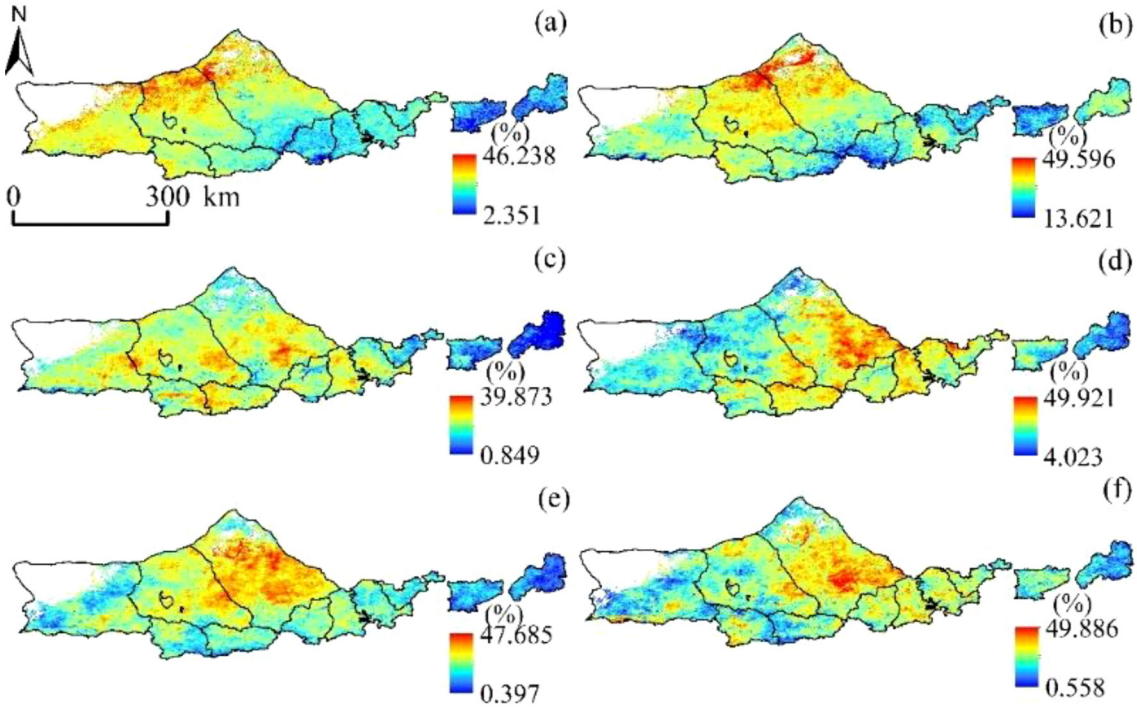

FIGURE 10
NPP loss rate of vegetation due to drought occurrence. **(A)** April, **(B)** May, **(C)** June, **(D)** July **(E)** August, and **(F)** September.

In this study, positive pixels with SPEI index were excluded and NPP losses of vegetation were only considered when the SPEI index represented drought (Figure 10). Then, NPP loss rates caused by different drought degrees were fitted to obtain monthly drought loss rate curves of regional vegetation growth seasons. The results passed the 0.05 significance test. The R^2 values of each growth period were 0.81, 0.81, 0.82, 0.89, 0.84 and 0.85, respectively, indicating that the curve fitting accuracy of drought loss rate was high, which could be used for drought loss analysis.

On the whole, vegetation NPP is more sensitive to the occurrence and development of drought. With the increase of drought degree, the loss rate of vegetation NPP in each growth period also fluctuates and increases gradually, and the fluctuation range of the loss rate is 20-50% (Figure 11). In the drought loss rate curve in April, there were two obvious peaks at SPEI of -1.25 and -1.75. In April, the grassland is in the greening period. When the drought degree is light drought, the NPP loss rate of vegetation fluctuates between 20-35%, and the fluctuation is relatively gentle. When the drought degree changed from light drought to severe drought, the NPP loss rate increased rapidly and fluctuated between 35 and 45%. When the degree of drought is extreme drought, the NPP loss rate of vegetation changes slowly and stabilizes between 45-50%, which may be due to the fact that the soil has a certain moisture in the early stage, so that the NPP of vegetation can still maintain at about 50% even if the extreme drought disaster occurs. From May to August, with the worsening of drought, the loss rate showed an increasing trend. Among them, the NPP loss rate fluctuated between 20-50% in May. When the drought degree reached extreme drought, the loss stabilized at 45% and fluctuated with the severity of drought again. In July, due to the low drought degree in July from 2000 to 2020, the maximum drought level only reached the severe drought level, and the NPP loss of vegetation showed an exponential rising trend. However, despite the low drought degree, the NPP loss of vegetation fluctuated between 20-40%, indicating that the drought occurred in July had a greater impact on grassland NPP. This month is the most critical month for the accumulation of forage production. From June to August, when the degree of drought reached severe drought or extreme drought, the increase rate of NPP loss rate was slow and fluctuated between 40-50%. For September, the NPP loss rate of vegetation also showed an increasing trend. When the drought degree reached between moderate drought and severe drought, the NPP loss rate fluctuated between 40-45%. However, when the drought degree reached severe drought, the NPP loss rate showed an accelerating trend, which may be related to the fact that grassland harvesting and storage had begun in some areas in September. In conclusion, NPP of vegetation is sensitive to drought. Even under light drought conditions, NPP of grassland will lose 10-20%, especially in July.

4 Discussion

4.1 Characteristics of vegetation NPP and drought

In this study, it was found that NPP of vegetation at the Yinshanbeilu increased significantly at a rate of 2.974 $g{\cdot}m^{-2}{\cdot}a^{-1}$ from 2000 to 2020 ($p < 0.05$), which is basically consistent with the results of (Liu et al., 2020b). However, there are still uncertainties about the main driving factors of this change. Zhao et al. (2019b) the accumulation of organic matter in vegetation was jointly influenced by increased precipitation and temperature, with precipitation having a stronger impact than temperature.

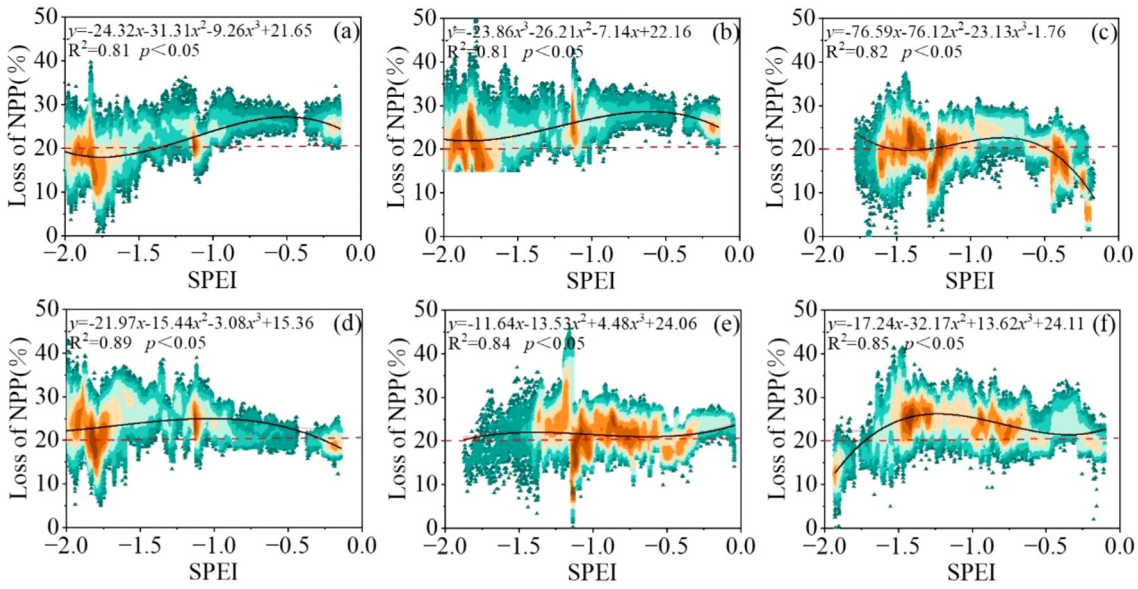

FIGURE 11
Drought loss rate curve of different months. **(A)** April, **(B)** May, **(C)** June, **(D)** July **(E)** August, and **(F)** September. (Note:The red dotted line represents the threshold for drought damage).

Liu et al. (2021a) pointed out the surface temperature has a considerable effect on the development of plants, although the degree to which this influence is exerted changes with height. Human activities have a bigger influence on the growth of vegetation in low-altitude locations than temperature does; nevertheless, warming has a more dramatic effect on boosting the productivity of vegetation in high-altitude places. The majority of the study area is made up of agricultural land, low-cover grassland, and desert. The area suffers from an unreliable water supply, low precipitation, high evaporation, low soil water content, and severe drought, all of which inhibit the accumulation and fixation of carbon in the region's plant life (Zhang et al., 2020). Concurrently, human activities demonstrate a dualistic influence on the environment. Furthermore, the presence of radiation, atmospheric concentration of CO_2, crop yield, and their compounded consequences can also generate a discernible impact on the escalation of vegetation productivity (Guo et al., 2021; Pei et al., 2020; Yang et al., 2020).

In this research, the SPEI index was calculated by using the temperature and precipitation data collected from a total of 12 sites. It was discovered that the consequences of climate change led to a less severe drought in the eastern areas, while the circumstances of drought became worse in the western regions. This was the outcome of a drop in the severity of drought in the eastern regions. The western portions of the research area were mostly home to the regions that were experiencing the most severe levels of drought. The steady ascent in amounts of precipitation was the key contributor to this development, and it was accountable for it. Concurrently, a decrease in wind speed and an increase in the sunlight duration greatly contributed to the reduction in potential evapotranspiration, which is consistent with the results of the research that used the SPEI index (Pei et al., 2020; Wei et al., 2022b). This indicates that SPEI can accurately reflect drought conditions in the study area.

4.2 Effects of drought on vegetation NPP

Atmospheric drought caused by insufficient precipitation will affect soil, vegetation, runoff and groundwater to varying degrees, and then cause agricultural drought and ecosystem drought (Lai et al., 2018). Drought-induced water deficit and osmotic stress can significantly impede plant growth and development, reduce crop yields, and may even result in plant mortality under severe cases (Doughty et al., 2015). Numerous researchers from the United States have investigated the effect that drought has on vegetation response at regional scales. The findings of these studies, which were conducted in areas such as the Loess Plateau, Inner Mongolia, Northeast China, and Northwest China, validate the substantial ramifications that drought has on the productivity of vegetation (Feng et al., 2016; Guo et al., 2021; Yan et al., 2021; Zhou et al., 2015). Within the scope of this specific research, an investigation into the degree to which the levels of NPP and SPEI at Yinshanbeilu changed throughout the course of a variety of time periods was carried out and analyzed. The findings showed that there is a positive link between the values of NPP and SPEI, which suggests that a water shortage may have a major influence on the development of vegetation. In addition, when looking at the regions that were subjected to the significance test, it was discovered that the correlation between drought and NPP increased with the accumulation of drought over a more extended time scale. This finding highlights the greater impact that long-term drought has on the NPP of vegetation in Yinshanbeilu. These results are consistent with those of other research that shown the impact of drought accumulation on NDVI in geographical areas that are characterized as being generally dry (Li et al., 2020b). Varied levels of water availability may either facilitate or impede the progress of plant growth and maturation, thereby influencing the ongoing phase of the plant's life cycle. In essence, the current state of a plant's life cycle is contingent upon the preceding stage (Lei et al., 2015). Moreover, it is important to note that rising temperatures and extreme weather events, including drought, have a direct impact on the evapotranspiration of both soil water and vegetation canopy water. This results in heightened levels of transpiration and surface dryness, ultimately causing erosive damage by strong solar radiation and wind, along with extreme precipitation. Such erosive effects lead to decreased grip of vegetation roots, further compounding the increase of evapotranspiration in deep soil (Yan et al., 2022).

Yinshanbeilu finds itself situated in areas defined as arid and semi-arid, facing the persistent challenges of wind and water erosion throughout the year. Drought conditions may impede vegetation growth, reduce biomass, and elevate vegetation mortality rates, ultimately exacerbating soil desertification. Some areas have surprisingly yielded a negative correlation between drought and NPP. This discovery is suggested to arise from the plant species in these arid and semi-arid areas, who have adapted to their harsh environment with notable drought tolerance, therefore exhibiting exceptional growth patterns even under drought stress. Additionally, such vegetation can lower their water stress by way of reduced stomatal conductance, which enhances water use efficiency, and augments vegetation growth as a result (Fathi-Taperasht et al., 2022; Qin et al., 2022).

4.3 Uncertainties and limitations

In the current investigation, we will be computing the standard precipitation evapotranspiration index by making use of data that has been interpolated from several meteorological stations. After that, we evaluate the geographical as well as the temporal patterns of drought, keeping in mind that there is a possibility that there will be more ambiguity in the findings of the study. It is possible to construct a more complex regional drought monitoring model through the combination of data from remote sensing and observations from ground-based meteorological stations as the accuracy of meteorological satellite data continues to increase in tandem with the extension of relevant data series over a longer period of time (Wu et al., 2022; Xing et al., 2023). This is something that can be done by integrating the data.

The application of the CASA model served as a means to simulate vegetation NPP in the Yinshanbeilu and compare it with

the MODIS NPP data for validation. However, the validation and analysis of field measurement data in specific geographical areas require further attention. Conducting field monitoring and data collection will be prioritized in the future to enhance the demonstrable effectiveness of the CASA model in monitoring the NPP of vegetation in the Yinshanbeilu.

Current research investigating the determinants of vegetation NPP has predominantly concentrated on drought-related factors, with limited attention being paid to the effects of human activities. Such activities may significantly impact the distribution and decomposition of NPP, thereby having direct implications on an ecosystem's material and energy cycles (Zhang et al., 2022). According to the findings of previous studies, human activities have two fundamental impacts on the NPP of plants. To begin, human activities may cause shifts in the kinds of land use, which may ultimately result in a decrease in the NPP of plants. Second, the intentional conservation efforts that have been performed by humans are the key contributors to the rise in the NPP of plants. Grassland ecosystems, in compared to other types of vegetation communities, are more sensitive to the effect that human activities have on the NPP of vegetation and are hence more fragile. As a result, the next step in study will concentrate on determining how changes in NPP occur in vegetation as a result of the effect of human activities.

5 Conclusions

The present study aimed to develop drought loss rate curves through the assessment of net primary productivity losses caused by varying intensities of drought. This approach can serve as a valuable tool for offering guidance on the sustainable development of terrestrial ecosystems in Yinshanbeilu, as well as mitigation measures for tackling drought-related disasters.

(1) During 2000-2020, the western multi-timescale SPEI indices all show a decreasing trend, indicating that the region tends to be arid, while most of the eastern regions show an increasing trend in multi-timescale SPEI indices, indicating that these regions show a trend of becoming wetter.

(2) The mean vegetation NPP values from 2000 to 2020 showed a large interannual variation and a fluctuating upward trend with a growth rate of 2.974 $g{\cdot}m^{-2}{\cdot}a^{-1}$.

(3) The proportion of places having a positive correlation between SPEI and vegetation NPP at various time scales was 75.89%, 77.23%, 81.35%, and 83.56%, respectively. This demonstrates that the connection between vegetation NPP and SPEI grew when the SPEI time scale was raised.

(4) Vegetation NPP is more sensitive to drought response, and even light drought conditions can lead to 10-20% loss of grassland NPP, especially in July when vegetation NPP is more sensitive to drought response.

Data availability statement

The raw data supporting the conclusions of this article will be made available by the authors, without undue reservation.

Author contributions

WS: Writing – original draft. YW: Writing – review & editing, Methodology. WW: Methodology, Writing – review & editing. JG: Formal analysis, Writing – review & editing. ML: Software, Writing – review & editing.

Funding

The author(s) declare financial support was received for the research, authorship, and/or publication of this article. This study was patronized by Inner Mongolia Autonomous Region Scientific Research Infrastructure and Platform (2023KYPT0002); IWHR Research&Development Support Program (MK110145B0012024; Central Guidance for Local Science and Technology Development Fund Projects (2024ZY0002).

Conflict of interest

The authors declare that the research was conducted in the absence of any commercial or financial relationships that could be construed as a potential conflict of interest.

Publisher's note

References

Ding, Y., He, X., Zhou, Z., Hu, J., Cai, H., Wang, X., et al. (2022). Response of vegetation to drought and yield monitoring based on NDVI and SIF. *CATENA* 219, 106328. doi: 10.1016/j.catena.2022.106328

Doughty, C. E., Metcalfe, D. B., Girardin, C. A. J., Amézquita, F. F., Cabrera, D. G., Huasco, W. H., et al. (2015). Drought impact on forest carbon dynamics and fluxes in Amazonia. *Nature* 519, 78–82. doi: 10.1038/nature14213

Fathi-Taperasht, A., Shafizadeh-Moghadam, H., and Kouchakzadeh, M. (2022). MODIS-based evaluation of agricultural drought, water use efficiency and post-drought in Iran; considering the influence of heterogeneous climatic regions. *J. Cleaner Production* 374, 133836. doi: 10.1016/j.jclepro.2022.133836

Feng, X., Fu, B., Piao, S., Wang, S., Ciais, P., Zeng, Z., et al. (2016). Revegetation in China's Loess Plateau is approaching sustainable water resource limits. *Nat. Climate Change* 6, 1019–1022. doi: 10.1038/nclimate3092

Gang, C., Wang, Z., You, Y., Liu, Y., Xu, R., Bian, Z., et al. (2022). Divergent responses of terrestrial carbon use efficiency to climate variation from 2000 to 2018. *Global Planetary Change* 208, 103709. doi: 10.1016/j.gloplacha.2021.103709

Geng, G., Yang, R., Chen, Q., Deng, T., Yue, M., Zhang, B., et al. (2023). Tracking the influence of drought events on winter wheat using long-term gross primary production and yield in the Wei River Basin, China. *Agric. Water Manage.* 275, 108019. doi: 10.1016/j.agwat.2022.108019

Geng, G., Yang, R., and Liu, L. (2022). Downscaled solar-induced chlorophyll fluorescence has great potential for monitoring the response of vegetation to drought in the Yellow River Basin, China: Insights from an extreme event. *Ecol. Indic.* 138, 108801. doi: 10.1016/j.ecolind.2022.108801

Guo, D., Song, X., Hu, R., Cai, S., Zhu, X., and Hao, Y. (2021). Grassland type-dependent spatiotemporal characteristics of productivity in Inner Mongolia and its response to climate factors. *Sci. Total Environ.* 775, 145644. doi: 10.1016/j.scitotenv.2021.145644

Khatri-Chhetri, P., Hendryx, S. M., Hartfield, K. A., Crimmins, M. A., van Leeuwen, W. J. D., and Kane, V. R. (2021). Assessing vegetation response to multi-scalar drought across the mojave, sonoran, chihuahuan deserts and apache highlands in the southwest United States. *Remote Sens.* 13 (6), 1103. doi: 10.3390/rs13061103

Kljun, N., Black, T. A., Griffis, T. J., Barr, A. G., Gaumont-Guay, D., Morgenstern, K., et al. (2007). Response of net ecosystem productivity of three boreal forest stands to drought. *Ecosystems* 10, 1039–1055. doi: 10.1007/s10021-007-9088-x

Lai, C., Li, J., Wang, Z., Wu, X., Zeng, Z., Chen, X., et al. (2018). Drought-induced reduction in net primary productivity across mainland China from 1982 to 2015. *Remote Sens.* 10, 1433. doi: 10.3390/rs10091433

Laimighofer, J., and Laaha, G. (2022). How standard are standardized drought indices? Uncertainty components for the SPI & SPEI case. *J. Hydrology* 613, 128385. doi: 10.1016/j.jhydrol.2022.128385

Lei, T., Wu, J., Li, X., Geng, G., Shao, C., Zhou, H., et al. (2015). A new framework for evaluating the impacts of drought on net primary productivity of grassland. *Sci. Total Environ.* 536, 161–172. doi: 10.1016/j.scitotenv.2015.06.138

Li, H., Wang, J., Liu, H., Miao, H., and Liu, J. (2023). Responses of vegetation yield to precipitation and reference evapotranspiration in a desert steppe in Inner Mongolia, China. *J. Arid Land* 15 (4), 477–490. doi: 10.1007/s40333-023-0051-2

Li, J., Wang, Z., and Lai, C. (2020a). Severe drought events inducing large decrease of net primary productivity in mainland China during 1982–2015. *Sci. Total Environ.* 703, 135541. doi: 10.1016/j.scitotenv.2019.135541

Li, J., Zhou, K., and Chen, F. (2020b). Drought severity classification based on threshold level method and drought effects on NPP. *Theor. Appl. Climatology* 142, 675–686. doi: 10.1007/s00704-020-03348-4

Li, M., Yu, H., Meng, B., Sun, Y., Zhang, J., Zhang, H., et al. (2021). Drought reduces the effectiveness of ecological projects: Perspectives from the inter-annual variability of vegetation index. *Ecol. Indic.* 130, 108158. doi: 10.1016/j.ecolind.2021.108158

Liu, H., Zhang, A., Liu, C., Zhao, Y., Zhao, A., and Wang, D. (2021a). Analysis of the time-lag effects of climate factors on grassland productivity in inner Mongolia. *Global Ecol. Conserv.* 30, e01751. doi: 10.1016/j.gecco.2021.e01751

Liu, Y.-y., Zhang, Z.-y., Tong, L.-j., Wang, Q., Zhou, W., Wang, Z.-q., et al. (2020b). Spatiotemporal dynamics of China's grassland NPP and its driving factors. *Chin. J. Ecol.* 39, 349. doi: 10.13292/j.1000-4890.202002.005

Liu, Q., Zhang, S., Zhang, H., Bai, Y., and Zhang, J. (2020a). Monitoring drought using composite drought indices based on remote sensing. *Sci. total Environ.* 711, 134585. doi: 10.1016/j.scitotenv.2019.134585

Liu, Y., Zhou, R., Wen, Z., Khalifa, M., Zheng, C., Ren, H., et al. (2021b). Assessing the impacts of drought on net primary productivity of global land biomes in different climate zones. *Ecol. Indic.* 130, 108146. doi: 10.1016/j.ecolind.2021.108146

Nejadrekabi, M., Eslamian, S., and Zareian, M. J. (2022). Spatial statistics techniques for SPEI and NDVI drought indices: A case study of Khuzestan Province. *Int. J. Environ. Sci. Technol.* 19, 6573–6594. doi: 10.1007/s13762-021-03852-8

Pei, Z., Fang, S., Wang, L., and Yang, W. (2020). Comparative analysis of drought indicated by the SPI and SPEI at various timescales in inner Mongolia, China. *Water* 12 (7), 1925. doi: 10.3390/w12071925

Qin, G., Meng, Z., and Fu, Y. (2022). Drought and water-use efficiency are dominant environmental factors affecting greenness in the Yellow River Basin, China. *Sci. Total Environ.* 834, 155479. doi: 10.1016/j.scitotenv.2022.155479

Ramirez, S. G., Hales, R. C., Williams, G. P., and Jones, N. L. (2022). Extending SC-PDSI-PM with neural network regression using GLDAS data and Permutation Feature Importance. *Environ. Model. Software* 157, 105475. doi: 10.1016/j.envsoft.2022.105475

Shi, M., Yuan, Z., Shi, X., Li, M., Chen, F., and Li, Y. (2022). Drought assessment of terrestrial ecosystems in the Yangtze River Basin, China. *J. Cleaner Production* 362, 132234. doi: 10.1016/j.jclepro.2022.132234

Soleimani-Motlagh, M., Soleimani-Sardo, M., and Mossivand, A. M. (2022). The efficiency of the Standardized Evapotranspiration Deficit Index (SEDI) in assessing the impact of drought on vegetation cover. *Environ. Monit. Assess.* 194, 299. doi: 10.1007/s10661-022-09972-z

Stagge, J. H., Tallaksen, L. M., Gudmundsson, L., Van Loon, A. F., and Stahl, K. (2015). Candidate distributions for climatological drought indices (SPI and SPEI). *Int. J. Climatology* 35, 4027–4040. doi: 10.1002/joc.2015.35.issue-13

Sun, B., Zhao, H., and Wang, X. (2016). Effects of drought on net primary productivity: Roles of temperature, drought intensity, and duration. *Chin. Geographical Sci.* 26, 270–282. doi: 10.1007/s11769-016-0804-3

Tian, F., Wu, J., Liu, L., Leng, S., Yang, J., Zhao, W., et al. (2019). Exceptional Drought across Southeastern Australia Caused by Extreme Lack of Precipitation and Its Impacts on NDVI and SIF in 2018 Exceptional Drought across Southeastern Australia Caused by Extreme Lack of Precipitation and Its Impacts on NDVI and SIF in 2018. *Remote Sens.* 12 (1), 54. doi: 10.3390/rs12010054

Tong, S., Bao, G., Bao, Y., and Huang, X. (2023). Monitoring of long-term vegetation dynamics and responses to droughts of various timescales in Inner Mongolia. *Ecosphere* 14, e4415. doi: 10.1002/ecs2.v14.2

van Minnen, J. G., Onigkeit, J., and Alcamo, J. (2002). Critical climate change as an approach to assess climate change impacts in Europe: development and application. *Environ. Sci. Policy* 5, 335–347. doi: 10.1016/S1462-9011(02)00044-8

Wahla, S. S., Kazmi, J. H., Sharifi, A., Shirazi, S. A., Tariq, A., and Joyell Smith, H. (2022). Assessing spatio-temporal mapping and monitoring of climatic variability using SPEI and RF machine learning models. *Geocarto Int.* 37 (27), 14963–14982. doi: 10.1080/10106049.2022.2093411

Wang, S., Li, R., Wu, Y., and Zhao, S. (2022a). Effects of multi-temporal scale drought on vegetation dynamics in Inner Mongolia from 1982 to 2015, China. *Ecol. Indic.* 136, 108666. doi: 10.1016/j.ecolind.2022.108666

Wang, S., Li, R., Wu, Y., and Zhao, S. (2022b). Vegetation dynamics and their response to hydrothermal conditions in Inner Mongolia, China. *Global Ecol. Conserv.* 34, e02034. doi: 10.1016/j.gecco.2022.e02034

Wang, W., Zhu, Y., Xu, R., and Liu, J. (2015). Drought severity change in China during 1961–2012 indicated by SPI and SPEI. *Natural Hazards* 75, 2437–2451. doi: 10.1007/s11069-014-1436-5

Wei, X., He, W., Zhou, Y., Ju, W., Xiao, J., Li, X., et al. (2022a). Global assessment of lagged and cumulative effects of drought on grassland gross primary production. *Ecol. Indic.* 136, 108646. doi: 10.1016/j.ecolind.2022.108646

Wei, Y., Zhu, L., Chen, Y., Cao, X., and Yu, H. (2022b). Spatiotemporal variations in drought and vegetation response in inner Mongolia from 1982 to 2019. *Remote Sens.* 14 (15), 3803. doi: 10.3390/rs14153803

Wu, X., Zhang, R., Bento, V. A., Leng, S., Qi, J., Zeng, J., et al. (2022). The effect of drought on vegetation gross primary productivity under different vegetation types across China from 2001 to 2020. *Remote Sens.* 14, 4658. doi: 10.3390/rs14184658

Xing, X., Wu, M., Scholze, M., Kaminski, T., Vossbeck, M., Lu, Z., et al. (2023). Soil moisture assimilation improves terrestrial biosphere model GPP responses to sub-annual drought at continental scale. *Remote Sens.* 15, 676. doi: 10.3390/rs15030676

Xu, D., Zhang, Q., Ding, Y., and Zhang, D. (2022). Application of a hybrid ARIMA-LSTM model based on the SPEI for drought forecasting. *Environ. Sci. pollut. Res.* 29, 4128–4144. doi: 10.1007/s11356-021-15325-z

Xue, P., Liu, H., Zhang, M., Gong, H., and Cao, L. (2022). Nonlinear characteristics of NPP based on ensemble empirical mode decomposition from 1982 to 2015—A case study of six coastal provinces in southeast China. *Remote Sens.* 14, 15. doi: 10.3390/rs14010015

Yan, Y., Wang, J., Tian, D., Luo, Y., Xue, X., Peng, F., et al. (2022). Sustained increases in soil respiration accompany increased carbon input under long-term warming across global grasslands. *Geoderma* 428, 116157. doi: 10.1016/j.geoderma.2022.116157

Yan, M., Xue, M., Zhang, L., Tian, X., Chen, B., and Dong, Y. (2021). A decade's change in vegetation productivity and its response to climate change over Northeast China. *Plants* 10, 821. doi: 10.3390/plants10050821

Yang, H., Hu, D., Xu, H., and Zhong, X. (2020). Assessing the spatiotemporal variation of NPP and its response to driving factors in Anhui province, China. *Environ. Sci. pollut. Res.* 27, 14915–14932. doi: 10.1007/s11356-020-08006-w

Yuan, Y., Bao, A., Jiang, P., Hamdi, R., Termonia, P., De Maeyer, P., et al. (2022). Probabilistic assessment of vegetation vulnerability to drought stress in Central Asia. *J. Environ. Manage.* 310, 114504. doi: 10.1016/j.jenvman.2022.114504

Zhang, Z., Ju, W., Zhou, Y., and Li, X. (2022). Revisiting the cumulative effects of drought on global gross primary productivity based on new long-term series data, (1982–2018). *Global Change Biol.* 28, 3620–3635. doi: 10.1111/gcb.v28.11

Zhang, X., Xiao, W., Wang, Y., Wang, Y., Wang, H., Wang, Y., et al. (2020). Spatial-temporal changes in NPP and its relationship with climate factors based on sensitivity analysis in the Shiyang River Basin. *J. Earth System Sci.* 129, 1–13. doi: 10.1007/s12040-019-1267-6

Zhao, Y., Liu, H., Zhang, A., Cui, X., and Zhao, A. (2019b). Spatiotemporal variations and its influencing factors of grassland net primary productivity in Inner Mongolia, China during the period 2000–2014. *J. Arid Environments* 165, 106–118. doi: 10.1016/j.jaridenv.2019.01.004

Zhao, A., Zhang, A., Liu, J., Feng, L., and Zhao, Y. (2019a). Assessing the effects of drought and "Grain for Green" Program on vegetation dynamics in China's Loess Plateau from 2000 to 2014. *Catena* 175, 446–455. doi: 10.1016/j.catena.2019.01.013

Zhou, W., Gang, C., Zhou, F., Li, J., Dong, X., and Zhao, C. (2015). Quantitative assessment of the individual contribution of climate and human factors to desertification in northwest China using net primary productivity as an indicator. *Ecol. Indic.* 48, 560–569. doi: 10.1016/j.ecolind.2014.08.043

frontiers | Frontiers in Plant Science

TYPE Original Research
PUBLISHED 13 March 2025
DOI 10.3389/fpls.2025.1436439

OPEN ACCESS

EDITED BY
Sebastian Leuzinger,
Auckland University of Technology, New Zealand

REVIEWED BY
Xiang Liu,
Lanzhou University, China
Ya Fei Shi,
Gansu Agricultural University, China

*CORRESPONDENCE
Guangxin Lu
lugx74@qq.com

RECEIVED 22 May 2024
ACCEPTED 24 February 2025
PUBLISHED 13 March 2025

CITATION
Jin X, Deng A, Fan Y, Ma K, Zhao Y, Wang Y, Zheng K, Zhou X and Lu G (2025) Diversity, functionality, and stability: shaping ecosystem multifunctionality in the successional sequences of alpine meadows and alpine steppes on the Qinghai-Tibet Plateau. *Front. Plant Sci.* 16:1436439. doi: 10.3389/fpls.2025.1436439

Diversity, functionality, and stability: shaping ecosystem multifunctionality in the successional sequences of alpine meadows and alpine steppes on the Qinghai-Tibet Plateau

Xin Jin[1], Abby Deng[2], Yuejun Fan[3], Kun Ma[1], Yangan Zhao[1], Yingcheng Wang[1], Kaifu Zheng[1], Xueli Zhou[4] and Guangxin Lu[1]*

[1]College of Agriculture and Animal Husbandry, Qinghai University, Xining, China, [2]Enterprise High School, Redding, CA, United States, [3]Qinghai Vocational and Technical Institute of Animal Husbandry, Xining, China, [4]Qinghai Province Grassland Station, Xining, China

Recent investigations on the Tibetan Plateau have harnessed advancements in digital ground vegetation surveys, high temporal resolution remote sensing data, and sophisticated cloud computing technologies to delineate successional dynamics between alpine meadows and alpine steppes. However, these efforts have not thoroughly explored how different successional stages affect key ecological parameters, such as species and functional diversity, stability, and ecosystem multifunctionality, which are fundamental to ecosystem resilience and adaptability. Given this gap, we systematically investigate variations in vegetation diversity, functional diversity, and the often-overlooked dimension of community stability across the successional gradient from alpine meadows to alpine steppes. We further identify the primary environmental drivers of these changes and evaluate their collective impact on ecosystem multifunctionality. Our analysis reveals that, as vegetation communities progress from alpine meadows toward alpine steppes, multi-year average precipitation and temperature decline significantly, accompanied by reductions in soil nutrients. These environmental shifts led to decreased species diversity, driven by lower precipitation and reduced soil nitrate-nitrogen levels, as well as community differentiation influenced by declining soil pH and precipitation. Consequently, as species loss and community differentiation intensified, these changes diminished functional diversity and eroded community resilience and resistance, ultimately reducing grassland ecosystem multifunctionality. Using linear mixed-effects model and structural equation modeling, we found that functional diversity is the foremost determinant of ecosystem multifunctionality, followed by species diversity. Surprisingly, community stability also significantly influences ecosystem multifunctionality—a factor rarely highlighted in previous

studies. These findings deepen our understanding of the interplay among diversity, functionality, stability, and ecosystem multifunctionality, and support the development of an integrated feedback model linking environmental drivers with ecological attributes in alpine grassland ecosystems.

KEYWORDS

alpine meadow, diversity, functionality, stability, ecosystem multifunctionality

1 Introduction

Global biodiversity is declining unprecedentedly due to climate change and human activities, significantly impacting ecosystem multifunctionality (EMF)—the capacity of ecosystems to provide multiple functions and services simultaneously (Midgley, 2012). EMF is influenced by climatic factors, species diversity, and functional diversity (Wolf et al., 2021). For instance, in dryland ecosystems, mean annual precipitation strongly affects EMF, whereas mean annual temperature has a weaker impact (Delgado-Baquerizo et al., 2016). Conversely, on the QTP, precipitation does not significantly influence EMF, while temperature has a pronounced positive effect (Wu et al., 2022). These differences highlight that EMF mechanisms vary across ecosystems due to distinct interactions between environmental factors and biotic communities. Additionally, species and functional diversity are closely linked to EMF. Environmental stress reduces species diversity and forces vegetation functional traits to converge, decreasing functional diversity and thereby impairing ecosystem functioning (Biswas and Mallik, 2011). In grassland communities, disturbances often lead to the loss of certain species, while others compensate by increasing their abundance or functional roles, enhancing community resilience and stability (Wu et al., 2022). Consequently, the interactions among climate, species diversity, functional diversity, stability, and EMF are highly complex and ecosystem-specific.

Approximately half of the world's grassland ecosystems are currently undergoing degradation, with approximately five percent facing severe to extreme levels of deterioration (Wang et al., 2005). The Tibetan Plateau (QTP) is recognized as a crucial region for the conservation of high-altitude biodiversity, underscoring its global ecological significance (Chen et al., 2013; Myers et al., 2000). Within the QTP, alpine meadows are key contributors to species diversity (Wu et al., 2022); however, they exhibit relatively low stability, resistance, and resilience in the face of environmental stressors (Li et al., 2020; Yang et al., 2022). Extensive degradation driven by overgrazing and anthropogenic interference has compromised nearly one-third of the natural grassland area (Hou et al., 2022). This widespread deterioration not only threatens the unique biodiversity of the QTP but also undermines the essential ecosystem services provided by these high-altitude grasslands. Addressing these challenges is imperative for the sustainable conservation and restoration of grassland ecosystems on the Tibetan Plateau.

The complex topography and high spatial heterogeneity of the QTP, coupled with limited study durations, have constrained vegetation studies to small-area ground surveys. Previous research has primarily focused on degradation gradients at the spatial scale while neglecting the temporal dimensions of degradation succession (Liu et al., 2017). There is a prevalent view that alpine vegetation on the QTP tends to evolve towards a drier final ecosystem, transitioning from alpine swamp meadow through meadow, steppe, desert steppe, to desert (Qin and Ding, 2009). Vegetation on the Qinghai-Tibet Plateau was reported to be highly dependent on specific climatic conditions and extremely sensitive to climate change (Zhang et al., 1996). Correspondingly, local field studies have observed a shift from alpine steppe to alpine meadow under warmer and wetter conditions, driven by enhanced hydrothermal dynamics (Wang et al., 2022). Conversely, with decreases in precipitation and temperature, the plant community structure of alpine meadows becomes simplified, leading to a transition from alpine meadows to alpine steppes (Zhao et al., 2011; Wang et al., 2022b; Zong et al., 2019). Recent studies using multivariate data fusion and deep learning have identified a 40-year successional trend between alpine meadows and steppes. Under annual precipitation ≤400 mm, steppes were dominant from 1979 to 1990, shifting to meadows dominance from 2010 to 2018 (Wang et al., 2023b). Climate change primarily drives the conversion between adjacent successional stages of alpine meadows and steppes. However, these ecosystems are often studied independently, overlooking their successional relationship (Shuren et al., 2022; Wang et al., 2023). This approach limits our understanding of vegetation and community dynamics in alpine grasslands. Therefore, examining species and community differences and their driving factors within this successional sequence is essential for enhancing our theoretical understanding of changes in alpine meadows.

We hypothesize that the succession from alpine meadows to steppes results in declines in species diversity, functional diversity, and community stability, ultimately reducing EMF. We propose that vegetational succession alters habitat conditions by decreasing precipitation or increasing temperatures, which, in turn, reduces soil nutrient availability. These environmental changes are expected to decrease vegetation diversity and restructure community

composition, thereby diminishing functional diversity and stability. Ultimately, these ecological shifts are anticipated to impair EMF. This conceptual framework aims to clarify the complex responses of EMF to vegetation succession under changing climatic conditions on the Tibetan Plateau.

In this investigation, we examine alpine meadows and steppes in the Qilian Mountains of the QTP as a sequence of ecological degradation. Utilizing field surveys, we explore the interactions among climate factors, biodiversity, functional diversity, community stability, and EMF within these high-altitude ecosystems. Our objectives are to: 1) Characterize variations in habitat conditions, species diversity, community β-diversity, functional diversity, community stability, and EMF along the degradation gradient. 2) Identify the primary drivers of changes in species diversity, community β-diversity, functional diversity, and stability. 3) Elucidate the relationships between EMF and species diversity, community β-diversity, functional diversity, and community stability, thereby uncovering the key factors and regulatory pathways that influence EMF.

2 Materials and methods

2.1 Study area

The study was conducted in the Qilian Mountains, a key region of the QTP, where degraded grasslands comprise 72.4% of the total grassland area, indicating severe degradation (Luo et al., 2018). Previous research has utilized spatial sequences rather than temporal ones to investigate the succession from alpine swamp to meadows and ultimately to alpine steppe (Wu et al., 2022). This spatial approach facilitates long-term monitoring by comparing sites at different successional stages to infer ecological changes across degradation levels. Accordingly, we employed a spatial sequence method to examine the adjacent successional stages of Alpine meadows (AM) and alpine steppes (AS). Fieldwork was conducted during the peak biomass period from late July to early August 2021 across the Qilian Mountains region (97.252°E to 102.592°E, 36.693°N to 37.453°N), spanning 482.23 km (Supplementary Figure 1). The study area ranges in elevation from 2,510 to 4,045 meters, with average annual temperatures between -7.50°C and -0.39°C and annual precipitation from 236.18 mm to 550.34 mm (Supplementary Table 1).

2.2 Plant community survey and trait measurement

The sampling design was based on the BIODESERT survey method (Maestre, 2017) and adapted to the QTP's complex topography. To ensure representativeness, we maximized the number of alpine meadow plots to comprehensively capture alpine environmental characteristics. Alpine steppe plots were subsequently selected to retain key species from meadow communities, reflecting their successional sequence. Vegetation surveys were conducted during the peak biomass period (late July to early August 2021) across 32 sites, including 23 alpine meadows and 9 alpine steppes, each separated by at least 4.90 km. Within each site, a randomly designated 30 m × 30 m plot contained fifteen randomly placed 0.5 m × 0.5 m ecological quadrats. In each quadrat, we recorded species presence, abundance, cover (using the pin-prick method), and the average height of ten specimens. Unidentified plants were photographed in the field and later identified using the Chinese Plant Image Library (https://ppbc.iplant.cn/) and Flora of China (https://www.iplant.cn/frps). Subsequently, we collected all aboveground and belowground biomass from each quadrat. After oven-drying both components to a constant weight, we combined them to calculate the total biomass.

In each ecological plot, six well-developed specimens of each species were selected for trait measurements, following methodologies from previous grassland studies assessing functional traits across degradation gradients (Saruul et al., 2019). We identified ten key plant traits aligned with our study objectives, categorized under two resilience mechanisms: community resilience (ET) and community resistance (RT). Community resilience traits include lifespan, life form, flowering duration, leaf area, leaf dry matter content, and leaf phosphorus content. Community resistance traits encompass lifespan, leaf hair type, plant height, leaf dry matter content, leaf phosphorus content, leaf carbon-to-nitrogen ratio, and leaf lignin content. Notably, lifespan, leaf dry matter content, and leaf phosphorus content were highlighted as critical indicators of community resilience and stability (Saruul et al., 2019). Plant height and leaf area were measured in the field using a portable laser leaf area meter (LI-3000C, LI-COR). To ensure data accuracy, leaf phosphorus content, leaf carbon-to-nitrogen ratio, leaf dry matter content, and leaf lignin content were analyzed in the laboratory following the methods described by Saruul et al. (2019).

2.3 Soil characterization measurement

Following the vegetation survey, soil samples were collected, as primary physiological and biochemical activities in alpine grasslands occur mainly in the surface soil (Liu et al., 2018). Soil bulk density was measured using a 100 cm^3 ring knife on samples from the 0–15 cm layer. For soil physicochemical analysis, samples from the same layer were obtained with a 7 cm diameter auger, combining five samples per quadrat into a composite sample. The measured parameters included bulk density (BD), ammonium nitrogen (NH_4^+-N), nitrate nitrogen (NO_3^--N), total nitrogen (N), organic matter (OM), available phosphorus (AP), available potassium (AK), and soil pH (Tonin et al., 2019). Additionally, soil moisture (SM), soil temperature (ST), and soil electrical conductivity (EC) were measured in the field using a TDR 350 soil moisture meter, with five measurements per quadrat at a depth of 0–15 cm to match the soil sampling depth.

2.4 Geography, climate, topography and grazing

To address spatial autocorrelation and effectively analyze the geographic structure of the sampling sites, latitude and longitude

were decomposed into Moran eigenvectors (MEMs) using the dbmem function in the R software package "spatial" (Dray et al., 2017). A spatial vector representing broader geographic features (MEM3 was calculated, $P < 0.01$) was selected for data analysis.

Mean temperature and precipitation in Qilian Mountain National Park (1961–2020) have shown significant increasing trends ($P < 0.05$) (Wang et al., 2022a). Consequently, we used average annual temperature (MAT) and precipitation (MAP) to characterize the area's climate. Following the methodology of Saruul et al. (2019), we recorded the geographic coordinates of each sampling site using GPS. Climate factors were extracted for each site using ArcGIS 10.8 and climate raster data (2000–2021) with a 1 km spatial resolution, which is finer than the 4.90 km minimum distance between sampling points, ensuring data accuracy. Climate raster data were sourced from the National Earth System Science Data Sharing Service Platform (http://loess.geodata.cn).

The altitude of each sampling point was measured using the Global Positioning System (GPS). A 90-meter resolution Digital Elevation Model (DEM) was employed for the study area to ensure data accuracy, considering the minimum distance of 4.90 km between sampling sites. Using ArcGIS 10.8, two key topographic variables, aspect and slope, were extracted from the DEM (Saruul et al., 2019. The DEM was obtained from the National Glacial Tundra Desert Science Data Centre (http://www.ncdc.ac.cn).

Grazing pressure in the area was quantified as sheep units per unit area (Saruul et al., 2019). Using ArcGIS 10.8, cattle and sheep density data, as well as cool- and warm-season pastures, were extracted from livestock raster data based on the coordinates of the sampled area. Field observations were combined with this data to determine whether the sampling area corresponded to cool- or warm-season pastures. The livestock raster data, which cover rangeland extent and sheep and cattle populations on the Tibetan Plateau in 2020, were released in 2023 by the Second Tibetan Plateau Scientific Expedition and Research Program (TPSERP) and have a spatial resolution of 500 meters. This resolution is sufficient to meet the minimum 4.90 km distance between sampling sites, thereby ensuring data accuracy. Livestock density data were converted into standard sheep units (1 cattle = 5 sheep) to quantify grazing pressure as the number of sheep per unit area. The data are available as Geo TIFF files on the Zenodo platform: https://doi.org/10.5281/zenodo.7692064.

2.5 Diversity index, functional diversity and stability of plant communities

Species diversity was assessed using the Patrick index, Shannon–Wiener index, and Pielou index, with species importance values calculated based on their relative height, cover, and biomass (Zhang et al., 2018b).

The functional diversity of grasslands, determined by the abundance and functional traits of vegetation species, can be evaluated using key indicators such as Functional Richness (FRic) (Cornwell et al., 2006), Functional Evenness (FEve) (Mouillot et al., 2005), Functional Divergence (FDiv) (Mouillot et al., 2005), and Functional Dispersion (FDis) (Laliberté, and Legendre, 2010). These metrics are calculated using the FD package (Laliberté, and Legendre, 2010) within the R software.

Vegetation community stability was assessed using indicators of community resistance (RT), community resilience (ET), structural variability (St), and functional variability (Fu). These classifications were derived from 10 functional traits identified in our quadrat surveys, following approaches established in grassland studies (Cornelissen et al., 2003; Laliberté, and Legendre, 2010; Sterk et al., 2013). Among these traits, ET is determined by factors such as life cycle, life form, flowering duration, leaf area, and phosphorus content, while RT is influenced by traits including leaf hair type, plant height, carbon-to-nitrogen ratio, and lignin content. Data for life cycle, life form, leaf hair type, and flowering time were gathered through field observations and cross-referenced with the Flora of China (http://www.efloras.org/), with trait values assigned as per Saruul et al. (2019). Structural variability (St) was quantified using the mean Jaccard dissimilarity of species presence/absence, capturing the degree of variation in community composition (Pestana et al., 2019). Functional variability (Fu) was determined based on the spatial mean and standard deviation of plant biomass at each site (Tilman et al., 2006). The specific formulas for calculating RT, ET, St, and Fu were referenced from studies examining grassland degradation gradients (Bai et al., 2022).

2.6 Ecosystem multifunctionality of grassland

Traditional research often emphasizes single-scale indicators, capturing certain aspects of multifunctionality but failing to account for the interconnectedness of ecosystems as complex, multifaceted systems (Siwicka et al., 2021). This study investigates the effects of alpine meadows and alpine steppes, considered as contiguous successional sequences, on vegetation-related EMF. The analysis incorporates multiple factors, including vegetation biomass (both aboveground and belowground), plant diversity (encompassing species diversity (α-diversity), community diversity (β-diversity), and functional diversity), as well as community stability indicators. To address the issue of non-normal data distribution, all indicators were normalized to improve the accuracy and reliability of statistical analyses (Maestre et al., 2012), and Z-scores were subsequently calculated. EMF was quantified using the mean value method (Valencia et al., 2015).

2.7 Statistical analyses

Prior to performing two-sample t-tests to compare environmental parameters, productivity, species diversity, functional diversity, stability, and EMF, we first checked the data for normality and homogeneity of variances to ensure that the underlying t-test assumptions were met. Spearman correlations among species diversity, functional diversity, stability, and EMF were computed using the 'Hmisc' package, and chord diagrams produced with the

'circlize' package illustrated their interrelationships. Subsequently, vegetation communities were analyzed using principal coordinate analysis (PCoA) and biaxial non-metric multidimensional scaling (NMDS), both based on species' relative abundance and Bray–Curtis distances, implemented through the 'vegan' package (Oksanen, 2010). In addition, community dissimilarity, also derived from Bray–Curtis distances, was evaluated using permutation multivariate analysis of variance (PERMANOVA) and analysis of similarity (ANOSIM).

To determine key environmental factors influencing α-diversity (Patrick index) and β-diversity (Bray–Curtis dissimilarity) during succession (Lazzaro et al., 2020), we employed a linear mixed-effects model, in which vegetation type, climate, grazing, spatial, geographic, and soil parameters were included as fixed effects, and plot repetition was treated as a random effect. Variance inflation factors (VIF) were applied to address collinearity, excluding any predictor with a VIF greater than 10. The optimal model was selected via complete subset regression based on corrected Akaike Information Criterion (AICc) values using the MuMIn package (García-Palacios et al., 2018). Finally, hierarchical partitioning with the glmm.hp package was employed to quantify each predictor's relative contribution to explained variance, expressed as a percentage of the $_{Con}R^2$ (Conditional R^2) (Lai et al., 2023).

To clarify the key effects of environmental factors on variations in functional diversity and community stability, we performed Spearman correlation analyses between environmental factors and both functional diversity and community stability, presenting the results using heatmaps. The overall influence of environmental factors on functional and stability indices was assessed through multiple linear regression using the lm function and illustrated in bar charts. The significance of individual environmental factors was determined through variance decomposition analysis in conjunction with multiple linear regression models, computed with the calc.relimp function from the relaimpo package (Jiao et al., 2020), and depicted by the size of circles.

To prevent any single predictor (e.g., habitat, vegetation diversity, functional diversity, stability) from being overshadowed when identifying the drivers of EMF, each factor was analyzed separately (Manning et al., 2018). First, a random forest model, implemented with the rfPermute function, was used to pinpoint significant predictors of EMF, with their significance assessed through 999 random permutations. Subsequently, model importance was evaluated using the A3 package (Jiao et al., 2018). Building on these identified predictors, a linear mixed-effects model (in which vegetation type was included as a fixed effect, and plot repetition was treated as a random effect) was then developed to examine the relative influence of habitat, vegetation diversity, functional diversity, and stability on changes in EMF. To further clarify the contributions of each predictor, hierarchical partitioning in the glmm.hp package was applied, thereby quantifying each factor's contribution to the $_{Con}R^2$ (Conditional R^2) (Lai et al., 2023).

Finally, to understand the complex interplay among these factors, a mixed-effects piecewise structural equation model (SEM), treating different sampling points as random effects, was constructed. This allowed us to assess how habitat, vegetation diversity, functional diversity, stability, and their interactions jointly influence EMF. All statistical analyses and figure generation were performed using R 4.2.3 (R Development Core Team, 2023).

3 Results

3.1 Alterations in habitat

We identified 17 environmental variables representing climate, grazing, geography, and soil physicochemical properties as proxies for grassland habitats. These environmental indicators have changed throughout the ecological succession between alpine meadows (AM) and alpine steppes (AS). Specifically, the AM had a significantly higher MAP than the AS, with lower MAT, pH and altitude ($P < 0.05$). Moreover, there were increases in EC from AM to AS, while grazing, slope, NH_4^+-N, NO_3^-N, N, OM, AP, AK, BD, ST, and SM showed decreasing trends (Table 1).

3.2 Alterations and drivers of α diversity and β diversity in vegetation

The total biomass of vegetation was significantly higher in alpine meadows (AM) compared to alpine steppes (AS) ($P<0.001$, Supplementary Figure 2A). Additionally, the Patrick index, Pielou index and Shannon index for plants in AM were notably higher than those in AS ($P<0.001$, Supplementary Figures 2B, C; $P<0.01$, Supplementary Figure 2D). To examine changes in β diversity of plant communities between AM and AS, a Principal Coordinates Analysis (PCoA) based on Bray-Curtis distances was performed, revealing significant differences between AM and AS (PERMANOVA, $P<0.01$, Supplementary Figure 2E). Similarly, the Non-metric Multidimensional Scaling (NMDS) analysis (ANOSIM, $P<0.01$, Supplementary Figure 2F) supported the findings of the PCoA, showing notable changes in the plant communities during the succession.

In the study of vegetation diversity changes during the degradation succession between AM and AS, we found that key factors explained 67% of the variance in α-diversity ($_{Con}R^2 = 0.67$, $P<0.001$; Figure 1A), with soil factors contributing 51.11%, geographic factors 27.85%, and climatic factors 21.1%. Specifically, soil moisture (SM) and bulk density (BD) positively influenced α-diversity, while mean annual precipitation (MAP) and nitrate nitrogen (NO_3^--N) had significant positive effects. In contrast, altitude, slope, aspect, soil exchangeable potassium (AK), and soil electrical conductivity (EC) had significant negative impacts, with slope and the third principal component of the Moran's eigenvector map (MEM3) also exerting negative effects on α-diversity. Furthermore, climatic, geographic, and soil factors jointly explained 74% of the variation in vegetation β-diversity ($_{Con}R^2 = 0.74$, $P<0.001$; Figure 1B), with soil factors being the most influential (65.97%), followed by geographic factors (24.72%) and climatic factors (9.72%). Notably, altitude and EC significantly increased β-diversity, while MAP, pH, and BD had significant negative effects.

10.3389/fpls.2025.1436439

TABLE 1 The alteration of habitat factors in alpine meadows and alpine steppe.

Environmental factors	Variables	Alpine meadow (AM)	Alpine steppe (AS)
Climate	MAP (mm)	501.52 ± 36.65[a]	355.51 ± 19.90[b]
	MAT (°C)	-4.44 ± 2.12[b]	-3.37 ± 2.17[a]
Grazing	Grazing(sheep/ha)	18.24 ± 3.23[a]	5.76 ± 0.58[b]
Geography	Aspect (°)	167.31 ± 57.79[a]	217.55 ± 74.87[a]
	Slope (°)	9.19 ± 7.30[a]	4.67 ± 3.44[a]
	Altitude (m)	3381.24 ± 351.19[b]	3600 ± 106.49[a]
Soil physical-chemical factors	NH_4^+-N (mg/kg)	106.42 ± 43.21[a]	81.96 ± 22.21[a]
	NO_3-N (mg/kg)	86.53 ± 36.28[a]	83.40 ± 33.53[a]
	N (mg/kg)	6270.12 ± 2098.14[a]	5672.97 ± 2443.17[a]
	OM (%)	15.11 ± 7.82[a]	13.52 ± 8.70[a]
	AP (mg/kg)	31.45 ± 21.48[a]	25.96 ± 10.44[a]
	AK (mg/kg)	405.03 ± 176.58[a]	327.41 ± 85.88[a]
	pH	6.98 ± 0.58[b]	7.59 ± 0.39[a]
	BD (g/100cm^3)	0.83 ± 0.25[a]	0.80 ± 0.27[a]
	ST (°C)	21.63 ± 4.59[a]	21.50 ± 3.49[a]
	SM (%)	38.34 ± 13.41[a]	36.18 ± 12.58[a]
	EC (μS/cm)	0.43 ± 0.26[b]	0.52 ± 0.29[a]

The values in table represent mean ± SE. Comparisons were made between two treatments, AM (n = 69) and AS (n = 27), using an independent two-sample t-test (df = 94). MAP, Mean annual precipitation; MAT, Mean annual temperature; Grazing, Grazing; Aspect, Aspect; Slope, Slope; Altitude, Altitude; NH_4^+-N, Soil ammonium nitrogen; NO_3-N, Soil nitrate nitrogen; N, Soil total nitrogen; OM, Soil organic matter; AP, Soil available phosphorus; AK, Soil available kalium; pH, Soil pH; BD, Soil bulk density; ST, Soil temperature; SM, Soil moisture; EC, soil electrical conductivity. Different letters in the same row indicate that the variables differ significantly between grassland types, P <0.05.
Red indicates Climate factors, green indicates Grazing factors, blue indicates Geography factors, and peach indicates Soil physical-chemical factors.

3.3 Alterations and drivers of functional diversity and stability in vegetation

The functional dispersion index (Fdis), functional divergence index (Fdiv), functional richness (Fric), and functional evenness (Feve) were significantly higher in AM than in AS (P < 0.001; Supplementary Figures 3A–D). Similarly, the resilience (ET) and resistance (RT) of the community were significantly greater in AM compared to AS (P < 0.05; Supplementary Figures 3E, F). In contrast, both structural variability (St) and functional variability (Fu) were higher in AS than in AM, although these differences were not statistically significant (Supplementary Figures 3G, H).

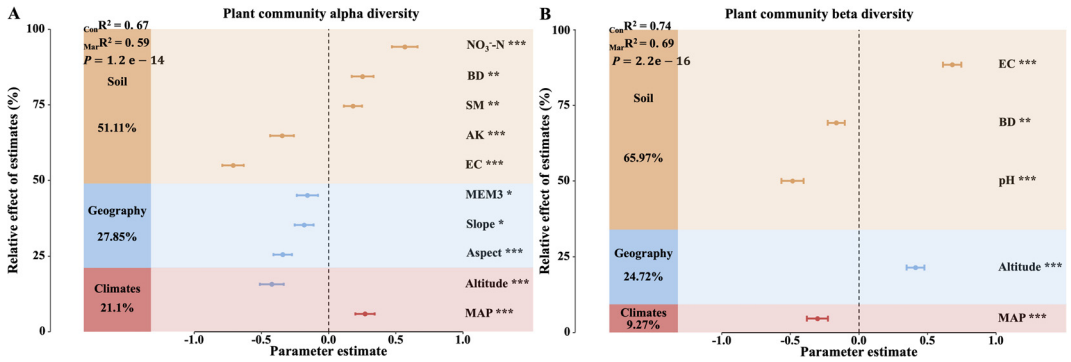

FIGURE 1
Drivers of differences in α-diversity and β-diversity between alpine meadows (AM) and alpine steppes (AS). **(A)** Relative contributions of habitat key factors to changes in α-diversity. **(B)** Relative contributions of habitat key factors to changes in β-diversity. $_{Mar}R^2$ (Marginal R^2) represents the proportion of variance explained by fixed effects alone, whereas $_{Con}R^2$ (Conditional R^2) denotes the variance explained by both fixed and random effects. The mean parameter estimates (standardized regression coefficients) of the predictors and their associated 95% confidence intervals, the relative importance of each predictor. MAP, Mean annual precipitation; Aspect, Aspect; Slope, Slope; Altitude, Altitude; MEM3, Spatial vector represents geography; NO_3^-N, Soil nitrate nitrogen; AK, Soil available kalium; pH, Soil pH; BD, Soil bulk density; SM, Soil moisture; EC, Soil electrical conductivity. Asterisks indicate the level of significance (*P < 0.05;**P < 0.01;***P < 0.001).

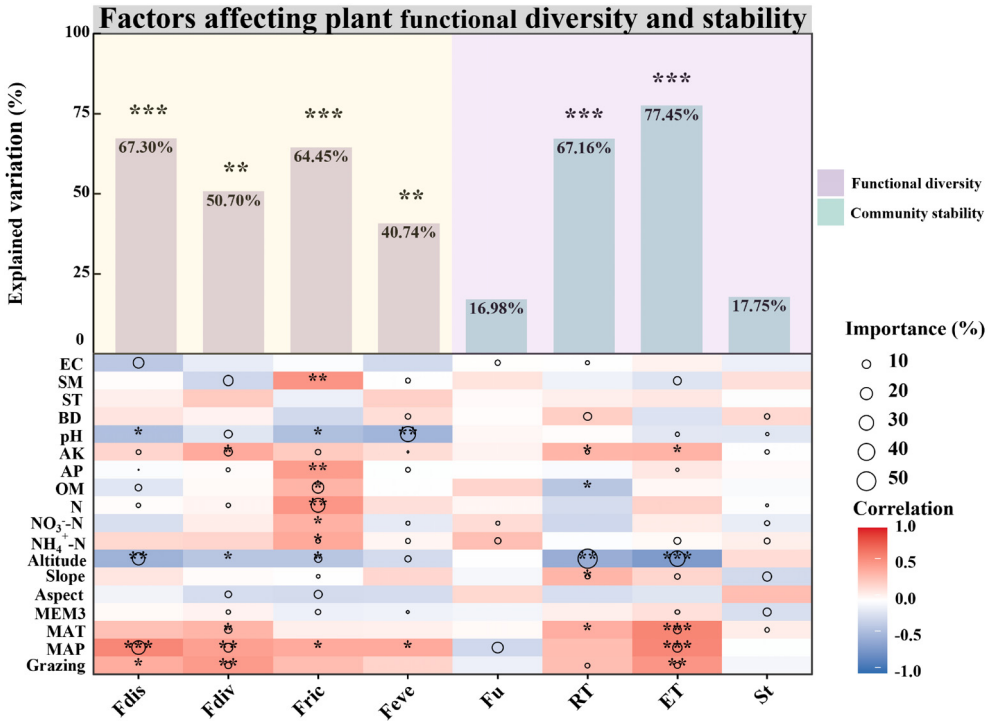

FIGURE 2
Drivers of differences in functional diversity and community stability between alpine meadows (AM) and alpine steppes (AS). Drivers of differences in functional diversity and community stability between alpine meadows (AM) and alpine steppes (AS). The bar chart represents the overall contributions of environmental factors, including specific contribution rates (%) and significance levels. The relative importance of each environmental factor is illustrated by the size of the circles in the diagram. Asterisks denote levels of statistical significance (*$P < 0.05$; **$P < 0.01$; ***$P < 0.001$). MAP, Mean annual precipitation; MAT, Mean annual temperature; Grazing, Grazing; MEM3, Spatial vector represents geography; Aspect, Aspect; Slope, Slope; Altitude, Altitude; NH_4^+-N, Soil ammonium nitrogen; NO_3^-N, Soil nitrate nitrogen; N, Soil total nitrogen; OM, Soil organic matter; AP, Soil available phosphorus; AK, Soil available kalium; pH, Soil pH; BD, Soil bulk density; ST, Soil temperature; SM, Soil moisture; EC, Soil electrical conductivity.

During the degradation succession, habitat factors significantly influenced the variability of vegetation community functional diversity indices (Figure 2). Specifically, habitat factors significantly affected the Fdis ($P < 0.001$), accounting for 67.30% of the variance, with dominant influences including MAP, Altitude, N, OM, AK and EC. Fdiv also showed significant habitat related variability ($P < 0.01$), explaining 50.70% of the variance with critical factors such as grazing, MAP, MAT, MEM3, Aspect, N, AP and AK. Fric was significantly shaped by habitat factors ($P < 0.001$), which explained 64.45% of the variation, primarily driven by MEM3, Aspect, Slope, Altitude, NH_4^+-N, N, OM and AK. Feve was significantly influenced by habitat ($P < 0.01$), which explained 40.74% of the variance. Altitude, NO_3^--N, pH, and SM had negative effects, while NH_4^+-N and BD exerted positive influences (Figure 2).

The variability in community resistance (RT) was significantly shaped by habitat factors ($P < 0.001$; Figure 2), accounting for 67.16% of the variance, where altitude negatively influenced it, while slope, AK, BD and SE had positive influences. Habitat significantly determined the variation in resilience (ET) ($P < 0.001$; Figure 2), explaining 77.45% of the variance, with positive influences from Grazing, MAP, MAT, MEM3 and slope, while negative impacts were associated with pH and altitude. Habitat factors exerted a minimal effect on the variability of community structure (St) and functional variability (Fu), explaining merely 17.75% and 16.98% of the variance, respectively (Figure 2).

3.4 Correlations and contributions of habitat, diversity, functionality, and stability to ecosystem multifunctionality

The analysis of EMF within grassland ecosystems revealed that AM exhibited significantly higher multifunctionality than AS ($P < 0.001$; Supplementary Figure 4A). As AM and AS represent adjacent stages along a degradation successional sequence, vegetation α-diversity was positively correlated with Fdis, Fric, Feve, and RT ($P < 0.05$; Supplementary Figure 4B). In contrast, β-diversity was negatively correlated with Fdis, Fdiv, ET, RT, and EMF ($P < 0.05$; Supplementary Figure 4B). EMF was positively correlated with α-diversity, Fdis, Fdiv, Fric, Feve, ET, and RT ($P < 0.05$; Supplementary Figure 4B). Additionally, Fdiv was positively related to both Feve and ET, while Feve and ET were also positively correlated ($P < 0.05$; Supplementary Figure 4B). Furthermore, ET showed a positive correlation with RT ($P < 0.05$; Supplementary Figure 4B), whereas RT was negatively correlated with Fu ($P < 0.05$; Supplementary Figure 4B).

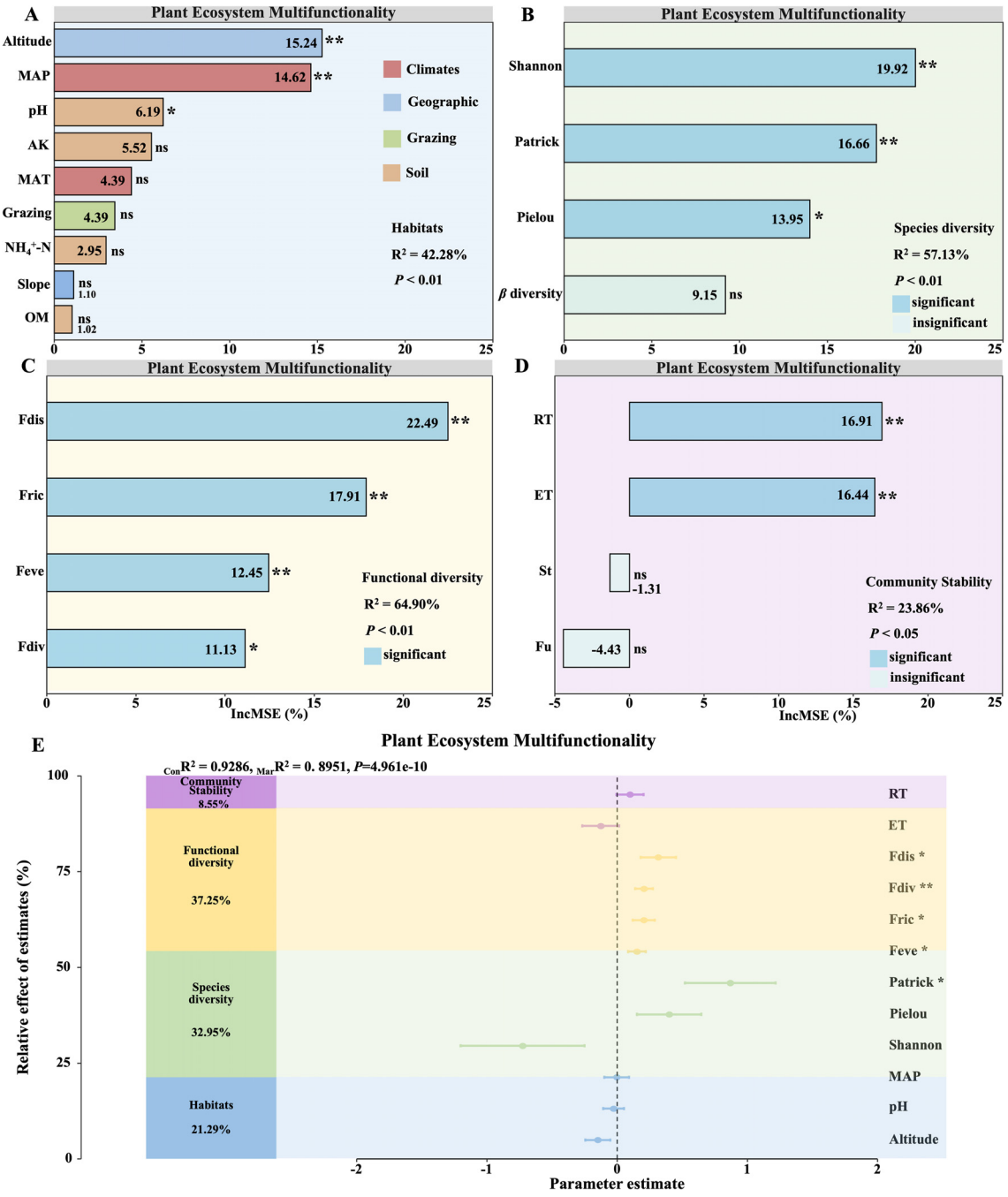

FIGURE 3
Determinants and contributions of key factors to grassland ecosystem multifunctionality. Random forest analysis reveals the major factors influencing ecosystem multifunctionality: Habitat **(A)**, Species diversity **(B)**, Functional diversity **(C)**, and Community Stability **(D)**. Panel **(E)** assesses key factors' relative contributions to changes in ecosystem multifunctionality (EMF). It includes R^2 values indicating model fit, mean parameter estimates with 95% confidence intervals, and the relative importance of predictors. $_{Mar}R^2$ (Marginal R^2) represents the proportion of variance explained by fixed effects alone, whereas $_{Con}R^2$ (Conditional R^2) denotes the variance explained by both fixed and random effects. Significance levels are denoted by asterisks (*P < 0.05; **P < 0.01).

Noteworthy contributors to EMF in alpine grassland ecosystems from habitat characteristics included MAP, altitude and pH (R^2 = 42.28%; P < 0.01; Figure 3A). Among diversity metrics, primary influences were observed from the Shannon, Patrick and Pielou indices (R^2 = 57.13%; P < 0.01; Figure 3B). Functional diversity indices (Fdis, Fdiv, Fric and Feve) were vital factors (R^2 = 64.90%; P < 0.01; Figure 3C). Regarding stability characteristics, major contributors included RT and ET (R^2 = 23.86%; P < 0.05; Figure 3D). This study further investigated the relative contributions of species diversity, functional diversity, and community stability to the variation in EMF (Figure 3E). The analysis revealed that habitat, species diversity, functional

diversity, and community stability collectively explained 92.86% ($_{Con}R^2$) of the variance in EMF. Specifically, habitat factors accounted for 21.29% of the variance, species diversity for 32.95%, functional diversity for 37.25%, and community stability for 8.55% (Figure 3E). Notably, Fdis, Fdiv, Fric, Feve, and the Patrick index exhibited significant linear relationships with EMF, whereas other indicators showed no such associations. These findings underscore the complex interplay of factors influencing EMF, suggesting that while individual factors may have limited effects, the combined contributions of key composite factors are substantial.

A structural equation model was developed using composite variables derived from the critical factors identified through random forest analysis. The results indicated that within habitat, increased precipitation, decreased altitude, and decreased pH exerted significantly positive effects on species diversity, functional diversity, community stability, and their interactions. Specifically, the habitat composite factor had the strongest effect on the interaction among species diversity, functional diversity, and community stability (0.66***), followed by functional diversity (0.651***), species diversity (0.5**), and community stability (0.44*) (Figure 4). In addition, the relationship between species diversity and functional diversity was the most pronounced (0.577***), followed by the interaction between functional diversity and community stability (0.144). The weakest correlation was between species diversity and community stability (0.085) (Figure 4). Notably, the interaction among species diversity, functional diversity, and community stability showed no significant linear effect on EMF. Among the composite factors, functional diversity exhibited the greatest influence on EMF (0.554***), followed by species diversity (0.48***), while community stability had a relatively weaker effect (0.2*) (Figure 4).

4 Discussion

4.1 Differences among habitat, diversity, functionality, stability, and ecosystem multifunctionality

The study examined alpine meadows and alpine steppes as contiguous successional sequences, revealing that higher temperatures and lower rainfall resulted in a warmer and drier climate transitioning from alpine meadows (AM) to alpine steppes (AS). Additionally, this climatic shift was accompanied by a decline in soil nutrients and a rise in altitude, leading to a decrease in vegetation α-diversity and a notable increase in β-diversity differences, ultimately decreasing ecosystem productivity significantly. Furthermore, the observations in this study align with other research, notably the transition from alpine marsh

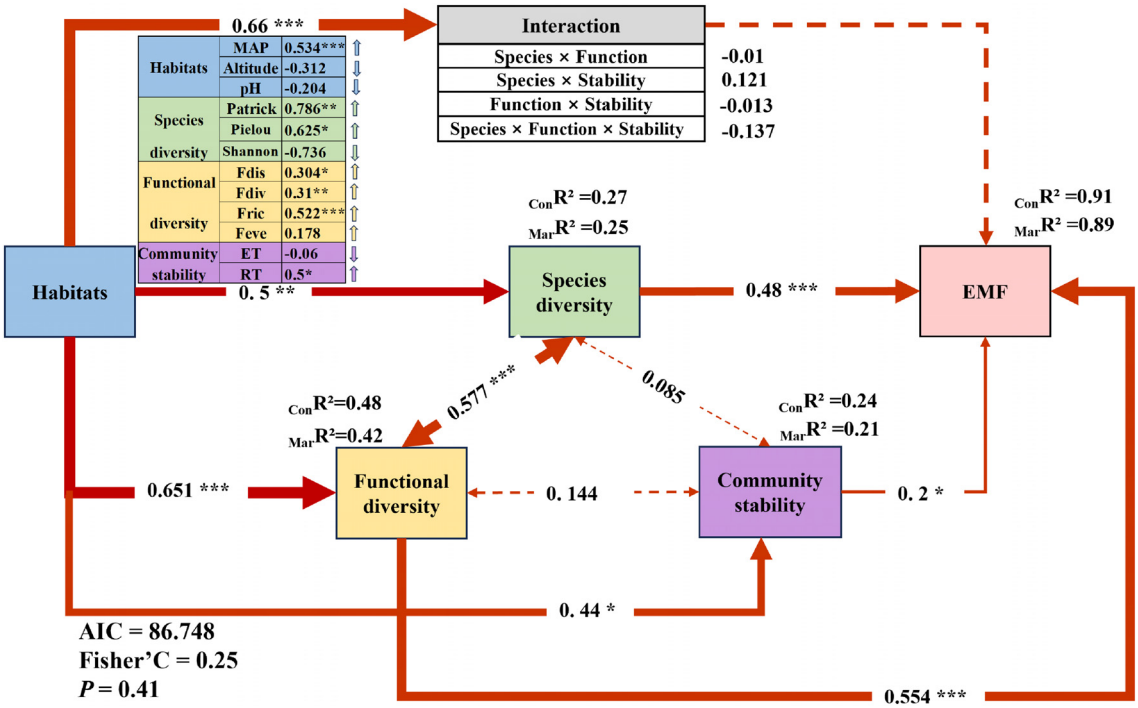

FIGURE 4
Ecosystem multifunctionality (EMF) and regulatory pathways in alpine grasslands. Structural equation modeling (SEM) reveals the direct and indirect effects of habitat, species diversity, functional diversity, and community stability on EMF. Path coefficients represent standardized effect sizes of these relationships. Red lines indicate positive effects, with line thickness reflecting the strength of the effect. Solid lines denote significant correlations, while dashed lines indicate non-significant correlations. $_{Mar}R^2$ (Marginal R^2) represents the proportion of variance explained by fixed effects alone, whereas $_{Con}R^2$ (Conditional R^2) denotes the variance explained by both fixed and random effects, with the random effects accounting for sampling points. Significance levels are denoted by asterisks: *P < 0.05, **P < 0.01, ***P < 0.001.

meadows to alpine meadows and then to alpine steppes, where decreases in precipitation and soil nutrients led to diminished productivity (Wang et al., 2023a). Functional diversity assesses how species within an ecosystem can substitute for or complement each other functionally, evaluating ecosystems' overall functional performance based on their traits (Díaz and Cabido, 2001). Research has suggested that plant functional traits may indicate ecosystem stability (Liu et al., 2021).

Our research findings revealed that as AM transitioned to AS, there was an apparent decrease in functional diversity indices (Fdis, Fdiv, Fric, Feve), RT and ET, accompanied by increased community St and Fu variability. This change may be attributed to environmental selection favoring species and functional traits adaptable to a warmer, drier climate, accompanied by a marked decline in species and functional diversity, leading to a homogenization of functional traits. Although there were simultaneous increases in the stability (St) and functionality (Fu) variability of AS, these did not fully compensate for the loss of diversity, ultimately resulting in reduced resilience (RT) and ecosystem functionality (ET) of the community (Moorselvan Moorsel et al., 2021). Although RT remains consistent across degradation gradients within the same type of grassland (Bai et al., 2022), we observed a significant decrease in RT during the succession between AM and AS. We hypothesize that different grass types exhibit distinct RT characteristics. While RT may fluctuate within a range during the degradation of a single grass type, transitioning between grassland types (between AM and AS) is associated with a significant decline in RT. Functional traits are a crucial link between plants and their environment, impacting ecosystem functions (Fry et al., 2018). Our study revealed a significant decrease in EMF as degradation succession progresses, consistent with the substantial declines in species and functional diversity observed in this research. This supports the notion that communities with higher species and functional diversity generally exhibit greater EMF (Fry et al., 2018).

4.2 Drivers of α and β diversity, functionality, and stability

Environmental change has profound impacts on long-term and extensive community assembly processes. These processes define appropriate habitats for species and shape their functional diversity (Brown and Milner, 2012). Our study revealed that environmental factors influence the species diversity (α-diversity) and community diversity (β-diversity) of the continuous successional sequences of alpine meadows and alpine steppes by 67% and 74%, respectively. This indicates that β-diversity is more influenced by environmental changes compared to α-diversity. Specifically, increased precipitation, soil water content, and soil nitrate-nitrogen levels were associated with higher plant species diversity. Conversely, higher altitudes, deteriorating topographic features like slope orientation and gradient, and reductions in available potassium were linked to decreased plant species diversity. Furthermore, altitude gains and higher soil conductivity enhanced community differentiation (β-diversity), while increases in precipitation, soil pH, and bulk density supported the consistency of plant communities. This pattern is likely due to altitude gains leading to diverse environmental conditions, prompting plant species to develop various adaptations and fostering community differentiation (Liu et al., 2020; Buckley et al., 2023). Additionally, higher soil conductivity may promote the aggregation of salt-tolerant plant communities, enhancing inter-community differentiation (Zhang et al., 2018a). Moreover, precipitation, soil pH, and bulk density improve plant community uniformity in this study.

Environmental factors significantly impact the functional diversity of communities (Portela et al., 2023). The study revealed that 67.30% of the variation in Functional Dispersion (Fdis) can be attributed to environmental factors, including mean annual precipitation (MAP), altitude, total nitrogen (TN), organic matter (OM), available potassium (AK), and electrical conductivity (EC). This implies that moisture, temperature, and soil nutrients play a crucial role in regulating the ecological niche differentiation of vegetation (Qi et al., 2015). Additionally, environmental variables explained 64.45% of the variance in Functional Richness (Fric), while Functional Divergence (Fdiv) and Evenness (Feve) explained 50.70% and 40.74%, respectively. Our findings show that the environment significantly influences the differentiation of vegetation ecological niches, followed by spatial utilization, ecological niche complementarity, and, to a lesser extent, resource use efficiency. Our study found that community resilience (ET) and resistance (RT) were significantly affected by environmental factors ($P < 0.001$). It was observed that environmental factors had a greater impact on ET (77.45% explained) than on RT (67.16% explained), indicating the crucial influence of environmental changes on ET. Subsequent analyses showed that higher mean annual temperature (MAT) and annual precipitation (MAP) increased the variability of community ET. Simultaneously, altitude was found to decrease the variability of community ET and RT.

4.3 Factors influencing the ecosystem multifunctionality of plant communities

Our research found a strong positive correlation between α-diversity and Fdis, Fric, Feve, RT, and EMF. This suggests higher species diversity enhances functional diversity, RT, and EMF. Conversely, greater community differences (β-diversity) showed a significant negative correlation with Fdis, Fdiv, ET, RT, and EMF, indicating that increased differences among communities can weaken functional diversity, ET, and RT, ultimately reducing EMF. Furthermore, functional diversity, ET, and RT affected EMF significantly and positively. Fdis had the highest impact (0.81***), followed by α-diversity (0.78***), RT (0.63***) and ET (0.59***) (Supplementary Table 2). Additionally, Fric, Feve and Fdiv were noted to impact EMF positively. The results suggest that high levels of niche differentiation within communities have the most significant positive impact on EMF, followed by species diversity. Our study also found that functional diversity reflects EMF more than species diversity under the degradation succession between AM and AS, supporting previous research findings (Zirbel et al.,

2019). Moreover, the study found that Fdis had a stronger positive impact on RT than α-diversity. This suggests that functional diversity is a better indicator of community stability than species diversity during degradation succession. The results support the notion that increased diversity can protect against external threats, highlighting the importance of functional diversity over species diversity in ensuring community stability (Kraft et al., 2015). These findings enhance our understanding of the interactions among species diversity, functional diversity, community stability, and EMF throughout community degradation succession.

EMF describes an ecosystem's capacity to provide functions such as productivity, nutrient cycling, and decomposition, assessing ecosystem health, and enhancing management and conservation efforts (Hölting et al., 2019; Van der Plas, 2019). Previous research has examined how species diversity, functional diversity, and climate independently influence changes in EMF (Jing et al., 2015; Steudel et al., 2016; Hertzog et al., 2019). However, the multifaceted nature of EMF drives the complexity of their underlying mechanisms, which are affected by multiple factors, making research more difficult (Giling et al., 2019). Consequently, it becomes increasingly imperative to elucidate the mechanisms underlying the multifunctionality of ecosystems. For our investigation, we considered various predictor variables such as habitat characteristics, species diversity, functional diversity, and community stability. Utilizing the random forest algorithm to identify the most important factors that influence changes in EMF. Based on the crucial factors identified and constructed, a mixed linear model was used to quantitatively assess their specific contributions to changes in EMF. The results showed that these factors explained 92.86% of the variations in EMF. Specifically, habitat factors accounted for 21.29% of the observed changes, while species diversity explained 32.95%, functional diversity 37.25%, and community stability 8.55% (Figure 3E). Significant linear correlations were found between Fdis, Fdiv, Fric, Feve, Patrick, and EMF. However, no other indicators showed any significant linear relationships. EMF is a complex phenomenon, so only a few single factors displayed significant linear correlations with it. Instead, composite factors such as climate, geography, and soil contribute more substantially to explaining changes in EMF.

In this study, we found that precipitation is a significant environmental differentiator between alpine meadows and alpine steppes in a continuous successional sequence. Precipitation was closely associated with EMF dynamics, as revealed by random forest analysis (Figure 3A). Meanwhile climate explaining 21.29% of the observed variation in EMF (Figure 3E). Notably, in our SEM, precipitation showed a strong positive correlation with EMF (0.543***) (Figure 4), suggesting that when precipitation is the dominant factor, changes in EMF within grassland ecosystems align with global dryland patterns—higher moisture availability enhances EMF in drylands globally (Maestre et al., 2012). Moreover, compared to temperature and nutrient changes, the impact of precipitation on dryland EMF was found to be more pronounced (Delgado-Baquerizo et al., 2017).

Our findings also highlighted that both functional diversity and species diversity significantly explained community EMF variation, with functional diversity (R^2 = 64.90%, $P < 0.01$; Figure 3C) and species diversity contributing (R^2 = 57.13%, $P < 0.01$; Figure 3B), respectively. These results align with previous studies showing that multiple dimensions of diversity—species, functional, and phylogenetic—are significantly correlated with EMF (De Bello et al., 2010; Zavaleta et al., 2010). Importantly, our research emphasizes that functional diversity has a greater influence on community EMF compared to species diversity (37.25% > 32.95%, Figure 3E). This is further supported by our SEM, where functional diversity (0.554***) exerted a stronger effect on EMF than species diversity (0.48***) (Figure 4). Our findings corroborate previous studies, which have emphasized that higher levels of species diversity are essential to maintain multiple ecosystem functions and that functional traits are more responsive to environmental changes, making them better predictors of EMF (Isbell et al., 2011; Pérez-Harguindeguy et al., 2013; Steudel et al., 2016; Zavaleta et al., 2010). These results align with findings from studies in Inner Mongolia, where drought significantly affected grassland vegetation, demonstrating that plant functional diversity, particularly traits such as plant height and leaf characteristics, explains EMF more effectively, while phylogenetic diversity contributes the least (Yan et al., 2020). Our study further supports previous findings that, under naturally assembled communities, functional diversity is a stronger driver of ecosystem multifunctionality compared to species diversity (Van der Plas, 2019). This can be attributed to the fact that functional diversity is directly linked to ecosystem functions and reflects the interactions between species and the environment, thereby best representing the influence of organisms on ecosystem processes (Steudel et al., 2016). For example, Gross found that skewness–kurtosis models incorporating trait abundance distributions outperformed species richness in predicting ecosystem multifunctionality, highlighting functional diversity as a major driver of ecosystem functions (Gross et al., 2017). Moreover, they observed that ecosystem multifunctionality reached its peak when the skewness of trait abundance distribution was zero. In summary, our findings indicate that in precipitation-driven vegetation ecosystems, functional diversity has a greater impact on EMF than species diversity. This underscores the importance of considering trait-based measures to better understand and predict ecosystem responses to environmental changes.

Furthermore, the study found a significant positive relationship between species diversity and functional diversity (0.577***) (Figure 4), supporting the notion that greater species diversity leads to a wider array of traits, enhancing functional trait diversity (Díaz and Cabido, 2001). Interestingly, our findings indicated that species and functional diversity had a positive yet insignificant effect on community stability. We speculate that the following processes might be involved: 1) Under favorable environmental conditions, species diversity and functional diversity might contribute insignificantly to stability due to high redundancy (Mori et al., 2013). 2) Conversely, under unfavorable environmental conditions —such as low soil nutrient levels, moisture, and temperature availability—the contribution of species diversity and functional diversity to stability may be limited (Jing et al., 2022; Pennekamp et al., 2018; Jing et al., 2022).

In addition, our study found that community stability explained 8.55% of the variance in grassland EMF (Figure 3E). The SEM further demonstrated that community stability had a significant positive effect on EMF (0.2*), specifically through community resistance (RT), which exhibited a notable positive effect (0.5*) on EMF (Figure 4). This finding was somewhat unexpected, revealing that community stability may play a more crucial role in maintaining grassland ecosystem multifunctionality than previously recognized. Previous studies have rarely explored the relationship between community stability and EMF. According to the biodiversity–stability hypothesis (Tilman and Downing, 1996), increased biodiversity is generally linked to enhanced ecosystem stability and functionality. We hypothesize that stable communities may more efficiently utilize resources, thereby minimizing niche overlap and enhancing overall ecosystem performance (Cardinale et al., 2012). Furthermore, community stability may help buffer against ecological disturbances, maintaining ecosystem function under varying conditions (Isbell et al., 2015). In response to environmental stressors such as drought or pest outbreaks, stable communities could rely on inherent resistance mechanisms to sustain ecological functions without significant impact. Interestingly, our findings diverge from previous research, which suggested that stability influences EMF indirectly through functional diversity (Glidden et al., 2023; Jia et al., 2023). In the specific context of alpine meadows and alpine steppes, which represent a continuous successional sequence, we observed that community stability directly affects EMF, challenging these earlier conclusions.

5 Conclusions

Our findings demonstrate that the successional transition from alpine meadows to alpine steppes is characterized by a marked reduction in species diversity, functionality, and stability, driven primarily by declining precipitation, soil nutrient depletion, and shifting soil acidity. These environmental perturbations orchestrate a complex restructuring of community composition and functional traits, affecting community resilience and resistance, and ultimately constraining ecosystem multifunctionality. Surprisingly, alongside the pivotal role of functional diversity and species richness, community stability emerges as a previously underappreciated but significant determinant of ecosystem multifunctionality.

Building on these insights, our results highlight the urgency of conserving not only species richness but also the functional attributes and stability of alpine grassland communities. This broader perspective will be essential for sustaining the integrated suite of ecosystem processes under intensifying climatic pressures. Future research should further elucidate the complex feedbacks among environmental drivers, community assembly, and multifunctionality, both within alpine systems and across other vulnerable biomes. Ultimately, these efforts will guide more effective management interventions that bolster ecological resilience and safeguard the biodiversity and productivity essential for sustaining ecosystem function under changing environmental conditions.

Data availability statement

The raw data supporting the conclusions of this article will be made available by the authors, without undue reservation.

Author contributions

XJ: Formal Analysis, Visualization, Writing – original draft. AD: Investigation, Data curation, Writing – review & editing, Methodology. YF: Data curation, Writing – review & editing. KM: Data curation, Writing – review & editing. YZ: Data curation, Writing – review & editing. YW: Methodology, Writing – review & editing. KZ: Writing – review & editing. XZ: Writing – review & editing. GL: Supervision, Writing – review & editing.

Funding

The author(s) declare that financial support was received for the research and/or publication of this article. This research was funded by International Scientific and Technological Cooperation of China (2023-HZ-803).

Conflict of interest

The authors declare that the research was conducted in the absence of any commercial or financial relationships that could be construed as a potential conflict of interest.

Publisher's note

Supplementary material

The Supplementary Material for this article can be found online at: https://www.frontiersin.org/articles/10.3389/fpls.2025.1436439/full#supplementary-material

References

Bai, X., Zhao, W., Wang, J., and Ferreira, C. S. S. (2022). Reducing plant community variability and improving resilience for sustainable restoration of temperate grassland. *Environ. Res.* 207, 112149. doi: 10.1016/j.envres.2021.112149

Biswas, S. R., and Mallik, A. U. (2011). Species diversity and functional diversity relationship varies with disturbance intensity. *Ecosphere* 2, 1–10. doi: 10.1890/ES10-00206.1

Brown, L. E., and Milner, A. M. (2012). Rapid loss of glacial ice reveals stream community assembly processes. *Global Change Biol.* 18, 2195–2204. doi: 10.1111/j.1365-2486.2012.02675.x

Buckley, J., Widmer, A., Mescher, M. C., and De Moraes, C. M. (2023). Experimental warming increases the vulnerability of high-elevation plant populations to a specialist herbivore. *Funct. Ecol.* 37, 1536–1552. doi: 10.1111/1365-2435.14324

Cardinale, B. J., Duffy, J. E., Gonzalez, A., Hooper, D. U., Perrings, C., Venail, P., et al. (2012). Biodiversity loss and its impact on humanity. *Nature* 486, 59–67. doi: 10.1038/nature11148

Chen, H., Zhu, Q. A., Peng, C. H., Wu, N., Wang, Y. F., Fang, X. Q., et al. (2013). The impacts of climate change and human activities on biogeochemical cycles on the qinghai-tibetan plateau. *Global Change Biol.* 19, 2940–2955. doi: 10.1111/gcb.12277

Cornelissen, J. H. C., Lavorel, S., Garnier, E., Díaz, S. M., Buchmann, N., Gurvich, D. E., et al. (2003). A handbook of protocols for standardised and easy measurement of plant functional traits worldwide. *Aust. J. Bot.* 51, 335–380. doi: 10.1071/bt02124

Cornwell, W. K., Schwilk, D. W., and Ackerly, D. D. (2006). A trait-based test for habitat filtering: convex hull volume. *Ecology* 87, 1465–1471. doi: 10.1890/0012-9658(2006)87[1465:ATTFHF]2.0.CO;2

De Bello, F., Lavorel, S., Díaz, S., Harrington, R., Cornelissen, J. H. C., Bardgett, R. D., et al. (2010). Towards an assessment of multiple ecosystem processes and services via functional traits. *Biodivers. Conserv.* 19, 2873–2893. doi: 10.1007/s10531-010-9850-9

Delgado-Baquerizo, M., Maestre, F. T., Eldridge, D. J., Bowker, M. A., Ochoa, V., Gozalo, B., et al. (2016). Biocrust-forming mosses mitigate the negative impacts of increasing aridity on ecosystem multifunctionality in drylands. *New Phytol.* 209, 1540–1552. doi: 10.1111/nph.13688

Delgado-Baquerizo, M., Trivedi, P., Trivedi, C., Eldridge, D. J., Reich, P. B., Jeffries, T. C., et al. (2017). Microbial richness and composition independently drive soil multifunctionality. *Funct. Ecol.* 31, 2330–2343. doi: 10.1111/1365-2435.12924

Díaz, S., and Cabido, M. (2001). Vive la difference:: plant functional diversity matters to ecosystem processes. *Trends Ecol. Evol.* 16, 646–655. doi: 10.1016/s0169-5347(01)02283-2

Dray, S., Blanchet, G., Borcard, D., et al. (2017). adespatial: multivariate multiscale spatial analysis. Available online at: https://CRAN.R-project.org/package=adespatial.

Fry, E. L., Savage, J., Hall, A. L., Oakley, S., Pritchard, W. J., Ostle, N. J., et al. (2018). Soil multifunctionality and drought resistance are determined by plant structural traits in restoring grassland. *Ecology* 99, 2260–2271. doi: 10.1002/ecy.2437

García-Palacios, P., Gross, N., Gaitán, J., and Maestre, F. T. (2018). Climate mediates the biodiversity–ecosystem stability relationship globally. Proc. *Natl. Acad. Sci.* 115, 8400–8405. doi: 10.1073/pnas.1800425115

Giling, D. P., Beaumelle, L., Phillips, H. R. P., Cesarz, S., Eisenhauer, N., Ferlian, O., et al. (2019). A niche for ecosystem multifunctionality in global change research. *Global Change Biol.* 25, 763–774. doi: 10.1111/gcb.14528

Glidden, A. J., Sherrard, M. E., Meissen, J. C., Myers, M. C., Elgersma, K. J., and Jackson, L. L. (2023). Planting time, first-year mowing, and seed mix design influence ecological outcomes in agroecosystem revegetation projects. *Restor. Ecol.* 31, e13818. doi: 10.1111/rec.13818

Gross, N., Bagousse-Pinguet, Y. L., Liancourt, P., Berdugo, M., Gotelli, N. J., and Maestre, F. T. (2017). Functional trait diversity maximizes ecosystem multifunctionality. *Nat. Ecol. Evol.* 1, 132. doi: 10.1038/s41559-017-0132

Hertzog, L. R., Boonyarittichaikij, R., Dekeukeleire, D., de Groote, S. R. E., van Schrojenstein Lantman, I. M., Sercu, B. K., et al. (2019). Forest fragmentation modulates effects of tree species richness and composition on ecosystem multifunctionality. *Ecology* 100, e02653. doi: 10.1002/ecy.2653

Hölting, L., Beckmann, M., Volk, M., and Cord, A. F. (2019). Multifunctionality assessments – more than assessing multiple ecosystem functions and services? A quantitative literature review. *Ecol. Indic.* 103, 226–235. doi: 10.1016/j.ecolind.2019.04.009

Hou, Q., Ji, Z., Yang, H., and Yu, X. (2022). Impacts of climate change and human activities on different degraded grassland based on NDVI. *Sci. Rep.* 12, 15918. doi: 10.1038/s41598-022-19943-6

Isbell, F., Calcagno, V., Hector, A., Connolly, J., Harpole, W. S., Reich, P. B., et al. (2011). High plant diversity is needed to maintain ecosystem services. *Nature* 477, 199–202. doi: 10.1038/nature10282

Isbell, F., Craven, D., Connolly, J., Loreau, M., Schmid, B., Beierkuhnlein, C., et al. (2015). Biodiversity increases the resistance of ecosystem productivity to climate extremes. *Nature* 526, 574–U263. doi: 10.1038/nature15374

Jia, Y. Y., Qin, W. H., Zhang, T., and Feng, G. (2023). Progress on mechanisms underlying arbuscular mycorrhizal fungi maintaining desert ecosystem stability under climate change. *Chin. Sci. Bull.-chin.* 68, 3172–3184. doi: 10.1360/TB-2023-0057

Jiao, S., Chen, W., Wang, J., Du, N., Li, Q., and Wei, G. (2018). Soil microbiomes with distinct assemblies through vertical soil profiles drive the cycling of multiple nutrients in reforested ecosystems. *Microbiome* 6, 146. doi: 10.1186/s40168-018-0526-0

Jiao, S., Yang, Y., Xu, Y., Zhang, J., and Lu, Y. (2020). Balance between community assembly processes mediates species coexistence in agricultural soil microbiomes across eastern China. *ISME J.* 14, 202–216. doi: 10.1038/s41396-019-0522-9

Jing, X., Sanders, N. J., Shi, Y., Chu, H., Classen, A. T., Zhao, K., et al. (2015). The links between ecosystem multifunctionality and above- and belowground biodiversity are mediated by climate. *Nat. Commun.* 6, 8159. doi: 10.1038/ncomms9159

Jing, Z. W., Wang, J., Bai, Y., and Ge, Y. (2022). Faunal communities mediate the effects of plant richness, drought, and invasion on ecosystem multifunctional stability. *Commun. Biol.* 5, 1–10. doi: 10.1038/s42003-022-03471-0

Kraft, N. J. B., Adler, P. B., Godoy, O., James, E. C., Fuller, S., and Levine, J. M. (2015). Community assembly, coexistence and the environmental filtering metaphor. *Funct. Ecol.* 29, 592–599. doi: 10.1111/1365-2435.12345

Lai, J., Zhu, W., Cui, D., and Mao, L. (2023). Extension of the glmm.hp package to zero-inflated generalized linear mixed models and multiple regression. J. *Plant Ecol.* 16, rtad038. doi: 10.1093/jpe/rtad038

Laliberté, E., and Legendre, P. (2010). A distance-based framework for measuring functional diversity from multiple traits. *Ecology* 91, 299–305. doi: 10.1890/08-2244.1

Lazzaro, L., Lastrucci, L., Viciani, D., Benesperi, R., Gonnelli, V., and Coppi, A. (2020). Patterns of change in α and β taxonomic and phylogenetic diversity in the secondary succession of semi-natural grasslands in the northern apennines. *PeerJ* 8, e8683. doi: 10.7717/peerj.8683

Li, M., Zhang, X., He, Y., Niu, B., and Wu, J. (2020). Assessment of the vulnerability of alpine grasslands on the qinghai-tibetan plateau. *PeerJ* 8, e8513. doi: 10.7717/peerj.8513

Liu, C., Li, Y., Yan, P., and He, N. (2021). How to improve the predictions of plant functional traits on ecosystem functioning? *Front. Plant Sci.* 12. doi: 10.3389/fpls.2021.622260

Liu, H., Mi, Z., Lin, L., Wang, Y., Zhang, Z., Zhang, F., et al. (2018). Shifting plant species composition in response to climate change stabilizes grassland primary production. *Proc. Natl. Acad. Sci. U. S. A.* 115, 4051–4056. doi: 10.1073/pnas.1700299114

Liu, S., Zhang, C., Zhang, Y., Wang, T., Zhao, A., Zhou, T., et al. (2017). "Miniaturized spectral imaging for environment surveillance based on UAV platform," in *AOPC 2017: optical spectroscopy and imaging* (Bellingham, WA, USA: SPIE), 420–429. doi: 10.1117/12.2285543

Liu, W., Zheng, L., and Qi, D. (2020). Variation in leaf traits at different altitudes reflects the adaptive strategy of plants to environmental changes. *Ecol. Evol.* 10, 8166–8175. doi: 10.1002/ece3.6519

Luo, G., Rensing, C., Chen, H., Liu, M., Wang, M., Guo, S., et al. (2018). Deciphering the associations between soil microbial diversity and ecosystem multifunctionality driven by long-term fertilization management. *Funct. Ecol.* 32, 1103–1116. doi: 10.1111/1365-2435.13039

Maestre, F. T. (2017). *The BIODESERT Survey:assessing the impacts of grazing and climate change in global drylands* (Spain: Rey Juan Carlos Unieversity, Dryland Ecology and Global Change Lab). Available at: https://biodesert.maestrelab.com.

Maestre, F. T., Quero, J. L., Gotelli, N. J., Escudero, A., Ochoa, V., Delgado-Baquerizo, M., et al. (2012). Plant species richness and ecosystem multifunctionality in global drylands. *Science* 335, 214–218. doi: 10.1126/science.1215442

Manning, P., van der Plas, F., Soliveres, S., Allan, E., Maestre, F. T., Mace, G., et al. (2018). Redefining ecosystem multifunctionality. *Nat. Ecol. Evol.* 2, 427–436. doi: 10.1038/s41559-017-0461-7

Midgley, G. F. (2012). Biodiversity and ecosystem function. *Science* 335, 174–175. doi: 10.1126/science.1217245

Moorselvan Moorsel, S. J., Hahl, T., Petchey, O. L., Ebeling, A., Eisenhauer, N., Schmid, B., et al. (2021). Co-occurrence history increases ecosystem stability and resilience in experimental plant communities. *Ecology* 102, e03205. doi: 10.1002/ecy.3205

Mori, A. S., Furukawa, T., and Sasaki, T. (2013). Response diversity determines the resilience of ecosystems to environmental change. *Biol. Rev.* 88, 349–364. doi: 10.1111/brv.12004

Mouillot, D., Mason, W. H. N., Dumay, O., and Wilson, J. B. (2005). Functional regularity: a neglected aspect of functional diversity. *Oecologia* 142, 353–359. doi: 10.1007/s00442-004-1744-7

Myers, N., Mittermeier, R. A., Mittermeier, C. G., da Fonseca, G. A. B., and Kent, J. (2000). Biodiversity hotspots for conservation priorities. *Nature* 403, 853–858. doi: 10.1038/35002501

Oksanen, J. (2010). Vegan: community ecology package. Available online at: http://vegan.r-forge.r-proj.org/.

Pennekamp, F., Pontarp, M., Tabi, A., Altermatt, F., Alther, R., Choffat, Y., et al. (2018). Biodiversity increases and decreases ecosystem stability. *Nature* 563, 109–112. doi: 10.1038/s41586-018-0627-8

Pérez-Harguindeguy, N., Díaz, S., Garnier, E., Lavorel, S., Poorter, H., Jaureguiberry, P., et al. (2013). New handbook for standardised measurement of plant functional traits worldwide. *Aust. J. Bot.* 61, 167–234. doi: 10.1071/BT12225

Pestana, C. J., Capelo-Neto, J., Lawton, L., Oliveira, S., Carloto, I., and Linhares, H. P. (2019). The effect of water treatment unit processes on cyanobacterial trichome integrity. *Sci. Total Environ.* 659, 1403–1414. doi: 10.1016/j.scitotenv.2018.12.337

Portela, A. P., Durance, I., Vieira, C., and Honrado, J. (2023). Environmental filtering and environmental stress shape regional patterns of riparian community assembly and functional diversity. *Freshw. Biol.* 68, 1428–1441. doi: 10.1111/fwb.14138

Qi, W., Zhou, X., Ma, M., Knops, J. M. H., Li, W., and Du, G. (2015). Elevation, moisture and shade drive the functional and phylogenetic meadow communities' assembly in the northeastern tibetan plateau. *Community Ecol.* 16, 66–75. doi: 10.1556/168.2015.16.1.8

Qin, D. H., and Ding, Y. (2009). Cryospheric changes and their impacts: present, trends and key issues. *Adv Clim Change Res.* 5, 187–195. doi: 10.1016/S1003-6326(09)60084-4

Saruul, K., Jiangwen, L., Jianming, N., Qing, Z., Xuefeng, Z., Guodong, H., et al. (2019). Typical steppe ecosystems maintain high stability by decreasing the connections among recovery, resistance, and variability under high grazing pressure. *Sci. Total Environ.* 659, 1146–1157. doi: 10.1016/j.scitotenv.2018.12.447

Shuren, W., Jiao, C., Zhao, D., Zeng, J., Xing, P., Liu, Y., et al. (2022). Disentangling the assembly mechanisms of bacterial communities in a transition zone between the alpine steppe and alpine meadow ecosystems on the Tibetan Plateau. *Sci. Total Environ.* 847, 157446. doi: 10.1016/j.scitotenv.2022.157446

Siwicka, E., Gladstone-Gallagher, R., Hewitt, J. E., and Thrush, S. F. (2021). Beyond the single index: investigating ecological mechanisms underpinning ecosystem multifunctionality with network analysis. *Ecol. Evol.* 11, 12401–12412. doi: 10.1002/ece3.7987

Sterk, M., Gort, G., Klimkowska, A., van Ruijven, J., van Teeffelen, A. J. A., and Wamelink, G. W. W. (2013). Assess ecosystem resilience: linking response and effect traits to environmental variability. *Ecol. Indic.* 30, 21–27. doi: 10.1016/j.ecolind.2013.02.001

Steudel, B., Hallmann, C., Lorenz, M., Abrahamczyk, S., Prinz, K., Herrfurth, C., et al. (2016). Contrasting biodiversity–ecosystem functioning relationships in phylogenetic and functional diversity. *New Phytol.* 212, 409–420. doi: 10.1111/nph.14054

Tilman, D., and Downing, J. A. (1996). Biodiversity and stability in grasslands. *Nature* 367, 363–365. doi: 10.1038/367363a0

Tilman, D., Reich, P. B., and Knops, J. M. H. (2006). Biodiversity and ecosystem stability in a decade-long grassland experiment. *Nature* 441, 629–632. doi: 10.1038/nature04742

Tonin, R., Gerdol, R., Tomaselli, M., Petraglia, A., Carbognani, M., and Wellstein, C. (2019). Intraspecific functional trait response to advanced snowmelt suggests increase of growth potential but decrease of seed production in snowbed plant species. *Front. Plant Sci.* 10. doi: 10.3389/fpls.2019.00289

Valencia, E., Maestre, F. T., Le-Bagousse-Pinguet, Y., Quero, J. L., Tamme, R., Börger, L., et al. (2015). Functional diversity enhances the resistance of ecosystem multifunctionality to aridity in Mediterranean drylands. *New Phytol.* 206, 660–671. doi: 10.1111/nph.13268

Van der Plas, F. (2019). Biodiversity and ecosystem functioning in naturally assembled communities. *Biol. Rev.* 94, 1220–1245. doi: 10.1111/brv.12499

Wang, X. G., Han, J. G., and Dong, Y. P. (2005). Recent grassland policies in China - an overview. *Outlook Agric.* 34, 105–110. doi: 10.5367/0000000054224319

Wang, Y., Li, D., Lu, G., and Huang, P. (2022a). Characteristics of climate change and its impacts on water resources in qilian mountains, China. *J. Appl. Ecol.* 33, 2805–2812. doi: 10.13287/j.1001-9332.202210.024

Wang, Y., Ning, D., Kai, F., Junbang, W., Xin, J., Yao, S., et al. (2023a). Grass-microbial inter-domain ecological networks associated with alpine grassland productivity. *Front. Microbiol.* 14. doi: 10.3389/fmicb.2023.1109128

Wang, Y., Sun, J., He, W., Ye, C., Liu, B., Chen, Y., et al. (2022b). Migration of vegetation boundary between alpine steppe and meadow on a century-scale across the Tibetan Plateau. *Ecol. Indic.* 136, 108599. doi: 10.1016/j.ecolind.2022.108599

Wang, Y., Xue, K., Hu, R., Ding, B., Zeng, H., Li, R., et al. (2023b). Vegetation structural shift tells environmental changes on the Tibetan Plateau over 40 years. *Sci. Bull.* 68, 1928–1937. doi: 10.1016/j.scib.2023.07.035

Wolf, A. A., Funk, J. L., Selmants, P. C., Morozumi, C. N., Hernández, D. L., Pasari, J. R., et al. (2021). Trait-based filtering mediates the effects of realistic biodiversity losses on ecosystem functioning. *Proc. Natl. Acad. Sci. U.S.A.* 118, e2022757118. doi: 10.1073/pnas.2022757118

Wu, M.-H., Xue, K., Wei, P.-J., Jia, Y.-L., Zhang, Y., and Chen, S.-Y. (2022). Soil microbial distribution and assembly are related to vegetation biomass in the alpine permafrost regions of the Qinghai-Tibet Plateau. *Sci. Total Environ.* 834, 155259. doi: 10.1016/j.scitotenv.2022.155259

Yan, Y., Zhang, Q., Buyantuev, A., Liu, Q., and Niu, J. (2020). Plant functional β diversity is an important mediator of effects of aridity on soil multifunctionality. *Sci. total Environ.* 726, 138529. doi: 10.1016/j.scitotenv.2020.138529

Yang, Y., Sun, Y., Niu, B., Feng, Y., Han, F., and Li, M. (2022). Increasing connections among temporal invariability, resistance and resilience of alpine grasslands on the Tibetan Plateau. *Front. Plant Sci.* 13. doi: 10.3389/fpls.2022.1026731

Zavaleta, E. S., Pasari, J. R., Hulvey, K. B., and Tilman, G. D. (2010). Sustaining multiple ecosystem functions in grassland communities requires higher biodiversity. *Proc. Natl. Acad. Sci. U. S. A.* 107, 1443–1446. doi: 10.1073/pnas.0906829107

Zhang, R., Liu, W., and Xu, H. (2018b). Effects of plateau pika (ochotona curzoniae) on alpine meadow phytocoenosium and analysis of the strategy it uses to expand habitat. *Acta Ecol. Sin.* 38, 48–52. doi: 10.1016/j.chnaes.2018.01.008

Zhang, X., Yang, D., Zhou, G., Liu, C., and Zhang, J. (1996). "Model expectation of impacts of global climate change on biomes of the Tibetan Plateau," in *Climate change and plants in east asia* (Springer Japan, Tokyo), 25–38. doi: 10.1007/978-4-431-66899-2_3

Zhang, D. M., Zhao, W. Z., and Zhang, G. F. (2018a). Soil moisture and salt ionic composition effects on species distribution and diversity in semiarid inland saline habitats, northwestern China. *Ecol. Res.* 33, 505–515. doi: 10.1007/s11284-018-1570-8

Zhao, D., Wu, S., Yin, Y., and Yin, Z. (2011). Vegetation distribution on Tibetan Plateau under climate change scenario. *Reg. Environ. Change* 11, 905–915. doi: 10.1007/s10113-011-0228-7

Zirbel, C. R., Grman, E., Bassett, T., and Brudvig, L. A. (2019). Landscape context explains ecosystem multifunctionality in restored grasslands better than plant diversity. *Ecology* 100, e02634. doi: 10.1002/ecy.2634

Zong, N., Zhao, G., and Shi, P. (2019). Different sensitivity and threshold in response to nitrogen addition in four alpine grasslands along a precipitation transect on the northern Tibetan Plateau. *Ecol. Evol.* 9, 9782–9793. doi: 10.1002/ece3.5514

frontiers | Frontiers in Plant Science

TYPE Original Research
PUBLISHED 06 June 2025
DOI 10.3389/fpls.2025.1562363

OPEN ACCESS

EDITED BY
Xiali Guo,
Guangxi University, China

REVIEWED BY
Guilin Wu,
Chinese Academy of Sciences (CAS), China
Shujun Zhang,
Xinjiang University, China

*CORRESPONDENCE
Yaoming Li
lym@ms.xjb.ac.cn
Yingzhi Gao
gaoyz108@nenu.edu.cn

RECEIVED 17 January 2025
ACCEPTED 15 May 2025
PUBLISHED 06 June 2025

CITATION
Ma X, Fan L, Yang M, Li J, Yan M, Yang Z, Chen X, Zhang B, Li Y and Gao Y (2025) Allocation strategy of nonstructural carbohydrates in *Spiraea* L. across different grassland types in the Altai Mountains. *Front. Plant Sci.* 16:1562363. doi: 10.3389/fpls.2025.1562363

Allocation strategy of nonstructural carbohydrates in *Spiraea* L. across different grassland types in the Altai Mountains

Xuexi Ma[1,2,3,4], Lianlian Fan[1,3,4], Meiniu Yang[1,3], Jiangyue Li[1,3], Meng Yan[2], Ziyue Yang[1,2], Xi Chen[1,3], Bo Zhang[1], Yaoming Li[1,3,4]* and Yingzhi Gao[2,5]*

[1]Key Laboratory of Ecological Safety and Sustainable Development in Arid Lands, Xinjiang Institute of Ecology and Geography, Chinese Academy of Sciences, Urumqi, China, [2]College of Grassland Science, Xinjiang Agricultural University, Key Laboratory of Grassland Resources and Ecology of Western Arid Desert Area of the Ministry of Education, Urumqi, China, [3]Chinese Academy of Sciences (CAS) Research Center for Ecology and Environment of Central Asia, Urumqi, China, [4]Bayinbuluk Alpine Grassland Observation and Research Station of Xinjiang, Bayinbuluk, Xinjiang, China, [5]Institute of Grassland Science, Northeast Normal University, Key Laboratory of Vegetation Ecology of the Ministry of Education, State Environmental Protection Key Laboratory of Wetland Ecology and Vegetation Restoration, Changchun, China

Global climate change and overgrazing have exacerbated shrub encroachment in arid and semi-arid grasslands and risking the stability and multifunctionality of grassland ecosystems. This shift between shrub and grassland raises a great concern to explicitly analyze the distribution of shrubs into arid and semi-arid grasslands and related environmental adaptation by using their nonstructural carbohydrates (NSCs) concentrations, and assess their allocation strategies and key determinants of these strategies. This research study was conducted in the Altai mountains of northwest of China and specifically focused on *Spiraea*, a dominant shrub in this region, and analyzed the NSCs component concentrations and their allocation in *Spiraea* leaves across different grassland types. The results showed significant variations in the NSCs concentrations, components, and allocation in *Spiraea* leaves across various grassland types, demonstrating higher overall values in meadows rather than grasslands ($p < 0.05$). Moreover, the total NSCs concentrations(the sum of soluble sugar and starch concentrations, and the ratio of soluble sugar to starch) exhibited consistent responses to environmental changes, and indicated increasing trends with elevation, soil water content (SWC), and soil total nitrogen concentrations (TN), while decreasing with mean annual temperature (MAT). Notably, MAT and SWC were emerged as the factors with the highest influence on NSCs concentrations and allocation in *Spiraea* leaves. These findings indicate that *Spiraea* in the Altai mountains can rapidly adapt to environmental changes

across different grassland types by calibrating their NSCs concentrations and composition. These findings also present an insightful theoretical foundation for managing shrub-grassland encroachments in the Altai mountains region and other arid and semi-arid regions.

KEYWORDS

grassland shrub encroachment, Altai Mountains, nonstructural carbohydrates, soluble sugars, starch

1 Introduction

Nonstructural carbohydrates (NSCs) are crucial energy sources and osmotic adjustment substances in plants that sustain plant growth and facilitate survival under stressful conditions (Hartmann and Trumbore, 2016; Yin et al., 2021)., NSCs include starch (energy storage) and soluble sugars (direct energy and osmotic adjustment) These two components can interconvert under specific environmental conditions to help plants adapt to diverse environments (McDowell, 2011; Zhang et al., 2023). For instance, under similar growth conditions, plants with higher NSCs concentrations tend to have higher chances of survival and better ability to do so (Blumstein et al., 2023; O'Brien et al., 2014). Therefore, NSCs storage can shield plants against carbon supply deficiencies, allowing them to cope with abiotic and biotic stresses. Consequently, NSCs storage is an important physiological indicator for assessing plant responses to environmental changes (Barker Plotkin et al., 2021; Martínez-Vilalta et al., 2016). Thus, explaining not only the concentrations of starch and soluble sugars within plants but also their allocation strategies is necessary to understand how plants adapt to diverse environmental conditions.

The factors influencing NSCs concentrations and allocation strategy include precipitation, temperature, and soil physicochemical properties (Guo et al., 2020; O'Brien et al., 2014; Zhang et al., 2024a). Increased drought intensity and duration correspond with a decline in the starch content in most woody plant organs and a rise in the concentration of soluble sugars, causing an increase in the ratio of soluble sugar to starch. Consequently, plants convert more starch into soluble sugars for osmotic adjustment, thereby maintaining cell osmotic pressure and ensuring plant growth and survival under drought conditions (He et al., 2020; Liu et al., 2019). Similarly, plants demonstrate analogous responsive characteristics in response to temperature stress, where high or low temperatures trigger starch hydrolase activity, prompting the conversion of starch into soluble sugars (Thalmann and Santelia, 2017; Yin and Zhang, 2016). In their study on alpine coniferous forests in the Qinghai–Tibet Plateau, Zhang et al. (2024a) argued that plant NSCs, especially those found in aboveground leaves, are mainly influenced by the combined effects of temperature and precipitation. Along with hydrothermal conditions, soil nutrient supply is a key factor affecting NSCs concentrations and allocation in plants. As a result of continuous climate changes and shifts in regional precipitation patterns, northwestern China is transitioning toward a warmer and wetter climate. In this context, soil nitrogen and phosphorus supply can promote plant growth and stressor resistance, thereby compensating for any adverse conditions such as drought and, subsequently, influencing NSCs concentrations and dynamics in plants (Zhang et al., 2024b; Zhou et al., 2011). Therefore, the concentration and allocation dynamics of plant NSCs demonstrate strong species- and region-specific characteristics.

The Altai mountains are a transitional zone between the Taiga biogeographical community and the arid desert biogeographical community. This adds to the significance of their grasslands as far as northern China is concerned. However, human activities such as overgrazing have contributed to severe degradation of the grassland ecosystem in the Altai mountains (Li et al., 2024). Moreover, the coverage and diversity of herbaceous plants in the grassland have steadily decreased. In contrast, the coverage of shrubs has rapidly increased, gradually replacing herbaceous plants as the dominant species in the region, causing grassland shrub encroachment (Ding and Eldridge, 2023; Moore et al., 2020; Ma and Gao, 2025). This has reduced the grassland ecosystem's productivity, carbon sequestration capacity, nutrient cycling, and water-holding capacity, threatening its multifunctionality (Eldridge et al., 2011; Pierce et al., 2019). The shrub species of the genus *Spiraea*, with their developed root systems and better drought and nutrient-poor tolerance than those of herbaceous plants, are widely distributed in the Altai mountains grassland. They have become the dominant species in the region's grassland shrub encroachment. However, the exact mechanisms underlying the adaptation of *Spiraea* to the Altai mountains' diverse climatic conditions in terms of NSCs composition and allocation remain shrouded in uncertainty shrouded in concentration and their response to environmental gradients are poorly understood. Hence, the present study proposed two scientific hypotheses. First, a decrease in precipitation and temperature will cause a corresponding decrease in plant starch concentration and a corresponding increase in the ratio of soluble sugar to starch. Second, how do climatic and edaphic variables across grassland types influence the NSC allocation strategy of Spiraea, and which factors most strongly drive variation? To

validate these hypotheses, this study selected the Altai mountains as the research area and focused on the dominant shrub species, *Spiraea*, as the subject of investigation. By systematically collecting samples of *Spiraea* from various grassland types and thoroughly analyzing the NSCs concentrations and proportions in their leaves, the study aimed to explore the NSCs concentrations and allocation patterns within *Spiraea* foliage under different environmental conditions. Further, it attempted to identify the key factors influencing NSCs in *Spiraea* leaves, thus presenting crucial scientific evidence for the stability and informed management of grassland ecosystems amid global climate change. This study is the first to quantify leaf NSC concentrations in Spiraea across Altai mountain grasslands, revealing how shrub encroachment influences ecosystem responses to climate change.

2 Materials and methods

2.1 Study area

The Altai mountains, which stretch nearly 1,200 km in a northwest direction along the borders of Russia, China, and Mongolia, reach a maximum elevation of 4,374 m. The Chinese segment of the Altai mountains (44°11'~46°20'N, 84°31'~90°00'E) is situated in the heart of the Eurasian continent. It occupies the middle southern slope of the mountain range, running in a northwest–southeast direction and gradually descending. This region is a significant climatic and natural boundary influenced by the Pacific and Atlantic Oceans that is marked by a continental temperate climate, boasting cold winters and abundant snowfall. The annual precipitation averages around 300 mm, demonstrating a vertical zonation pattern ranging from 100 mm in the lower mountainous regions to 600 mm in the higher alpine areas. Additionally, the annual mean temperature varies between -3.6°C and 1.8°C (Huang et al., 2015).

The Altai mountains region demonstrates complete vertical vegetation zonation, with the grassland zone primarily condensed at elevations between 800 and 1,800 m. Recently, the grasslands in this region have revealed a marked tendency toward shrub encroachment in response to global climate change and overgrazing. In this context, the dominant shrubs belong to the genus *Spiraea* (*Spiraea salicifolia* L.), including species such as *Spiraea hypericifolia* L., *Spiraea media* Schmidt, and *Lonicera japonica* Thunb (Ma et al., 2025).

2.2 Experimental design

In July 2023, we collected leaves from five healthy *Spiraea* plants across different grassland types in the Altai mountains (Figure 1). These grassland types included temperate steppe desert (TSD), constituting one site; temperate desert steppe (TDS), constituting three sites; temperate steppe (TS), constituting 10 sites; temperate meadow steppe (TMS), constituting five sites; and mountain meadow (MM), constituting four sites (Figure 1). The mean annual precipitation (MAP) gradient across the sampling sites ranged from 155 mm to 354 mm, whereas the mean annual temperature (MAT) gradient ranged from -2.92°C to 5.31°C. For each sampling site, a large plot of 100 m × 100 m was established, within which five small plots of 10 m × 10 m were set up following a

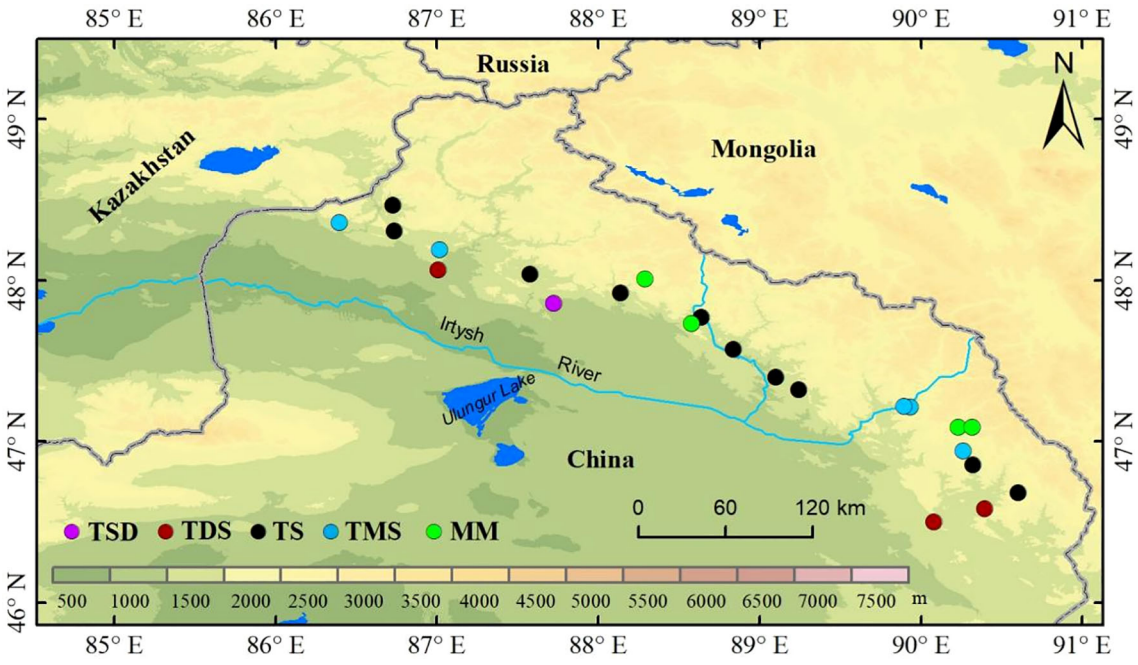

FIGURE 1
Distribution map of sample points.

five-point sampling method. Further, within each small plot, leaves from five healthy *Spiraea* plants were randomly collected between 11:00 and 16:00 to minimize diurnal variation in NSC concentrations and mixed to form one sample, with five replicate samples in total. We transported samples to the laboratory and fixed them at 105°C for 10 minutes. Subsequently, they were dried at 65°C to constant weight before being pulverized in a ball mill for future use.

Concurrently, soil samples were collected from the 0–10 cm layer using a soil auger within each small plot at each site, with five replicates per site. The collected soil samples were sieved through a 2 mm mesh to remove large debris or roots. Then, they were divided into two portions. While one was air-dried to determine soil organic carbon (SOC), total nitrogen (TN), total phosphorus (TP), available phosphorus (AP), pH, and electrical conductivity (EC), the other was refrigerated at 4°C and analyzed for soil water content (SWC) and available nitrogen (AN) within one week.

2.3 Determination of NSCs concentrations

Primarily, NSCs comprise starch and total soluble sugars, as these two components account for over 90% of the total NSCs concentrations. Therefore, in the present study, the total NSCs concentrations were calculated as the sum of soluble sugars and starch—both of which were measured through the traditional anthrone–sulfuric acid method (Zhang et al., 2023). Using this method, 0.15 g of dried and powdered plant leaf samples were accurately weighed and placed in 10 mL of 80% absolute ethanol. Afterward, the mixture was extracted in a boiling water bath for 10 minutes. This mixture was then centrifuged at 4,000 $r{\cdot}min^{-1}$ for 10 minutes to collect the supernatant as the extract of soluble sugars. Subsequently, 10 mL of 30% (v/v) perchloric acid was added to the centrifuged precipitate, and the mixture was allowed to stand overnight. After accurate extraction in a water bath at 80°C for 10 minutes to ensure complete hydrolysis of starch, the mixture was cooled and centrifuged again at 4,000 $r{\cdot}^{-1}$ for 10 minutes. Following this, the supernatant was used to determine the starch concentration.

2.4 Collection and measurement of environmental factors

The gravimetric method was used to determine SWC. Under this method, fresh soil samples were dried in an oven at 105°C for 48 hours until a constant weight was achieved, followed by weighing. The pH value and EC were measured using the potentiometric method, with soil-to-water ratios of 1:2.5 and 1:5, respectively. Moreover, SOC was determined using the HCl titration-combustion method on a carbon-nitrogen analyzer (Multi 3100C/N, Analytik Jena AG, Germany). Furthermore, using a fully automated flow analyzer, the TN and TP concentrations in the soil were measured after digestion with concentrated sulfuric acid, perchloric acid, and hydrofluoric acid, and AP concentration was extracted with 0.5 mol L^{-1} $NaHCO_3$ solution (Bran Luebbe, AA3, Germany). The Kjeldahl method was employed for TN determination, while the molybdenum-antimony anti-colorimetry method was used for both TP and AP. Additionally, the AN concentration in the soil was determined using the alkaline hydrolysis diffusion method (Yin et al., 2024).

2.5 Statistical analysis

To begin with, the obtained data were subjected to normality and homogeneity of variance tests. The differences in soluble sugars, starch, soluble sugar/starch ratio, and total NSCs among different grassland types were compared using a one-way analysis of variance (ANOVA), followed by the least significant difference (LSD) test. Additionally, the graphics were created using the ggplot2 package in R 4.2.1; Spearman correlation analysis and random forest modeling were conducted using the randomForest and linkET packages in R 4.1.3 to assess the impact of abiotic factors on soluble sugars, starch, soluble sugar/starch ratio, and total NSCs. Furthermore, regression analyses were performed between key abiotic factors and these NSCs components to identify potential abiotic factors influencing their concentrations. To explain the complex relationships between environmental factors and NSCs in *Spiraea*, a piecewise structural equation model (SEM) was constructed using the "piecewiseSEM" package in R 4.2.1, which was used to determine the direct and indirect effects of climatic factors and soil physicochemical properties on NSCs. Model evaluation was based on Fisher's C significance ($0.05 < p < 1$) and the AIC, with stepwise refinement of the model as per the significance of path coefficients (Tian et al., 2022). Throughout the analysis and visualization process, various packages were utilized, including "dplyr," "ggplot2," "patchwork," "tidyverse," and "vegan."

3 Results

3.1 Effects of different grassland types on physical and chemical properties of soil

Notable differences were observed in the soil physicochemical properties across grassland types. The SWC, SOC, TN, and AN levels were higher in TMS and MM soils than in TDS and TS soils (Figure 2, $p < 0.05$). Conversely, the soil pH and AP concentrations were significantly lower in TMS and MM soils than in TDS and TS soils ($p < 0.05$).

3.2 Characteristics of differences in NSCs concentrations of *Spiraea* across different grassland types

Significant differences were observed in the total soluble sugars, starch, total NSCs concentrations, and the ratio of soluble sugar to starch of *Spiraea* across different grassland types. The soluble sugar,

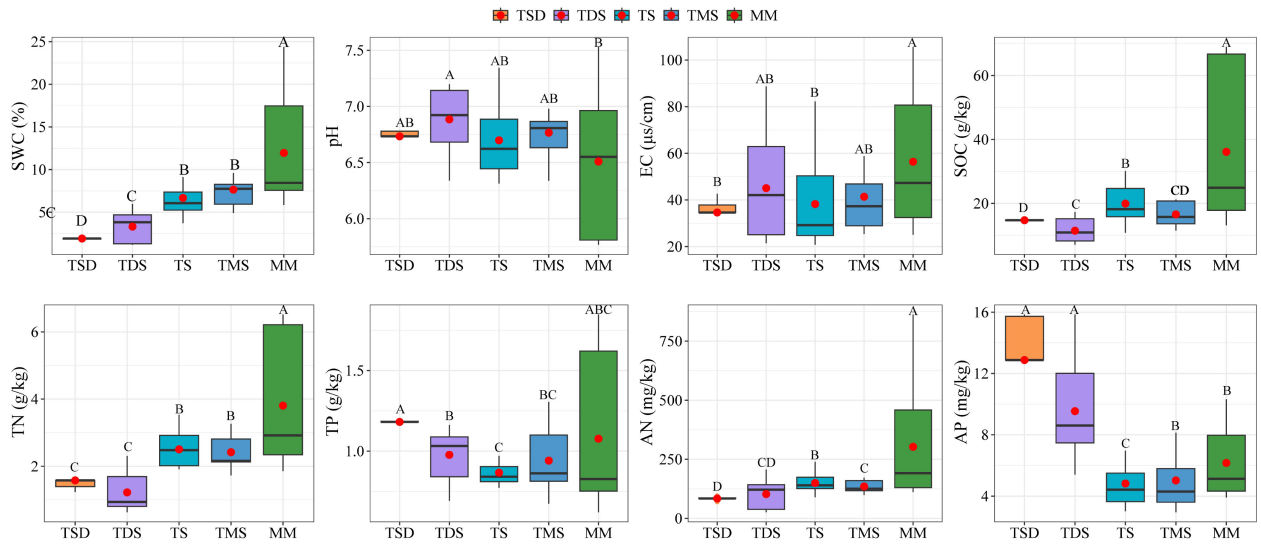

FIGURE 2
Effects of different grassland types on soil physicochemical properties; the different letters indicate significant differences between treatments at $p < 0.05$.

starch, NSCs concentrations, and soluble sugar/starch ratio in *Spiraea* from TMS and MM soils were significantly higher than those from TDS and TS soils (Figure 3, $p < 0.05$). Further, the soluble sugar concentration in *Spiraea* from TSD soils was significantly lower than that from TMS and MM soils ($p < 0.05$), while no significant differences were found in starch and NSCs concentrations ($p > 0.05$).

3.3 Relationship between NSCs concentrations in *Spiraea* and environmental factors

The random forest analysis found that climate and soil environmental factors explained a significantly higher proportion of the variation in total soluble sugar concentration (37.95%) and total NSCs concentrations (27.99%) than starch concentration (2.84%) and the ratio of soluble sugar to starch (5.82%). As seen in Figure 4A, elevation, MAT, SWC, and TN were identified as the most important predictors influencing the variation in NSCs and their component concentrations in *Spiraea* leaves (Figure 4A). Moreover, as Figure 4B illustrates, NSCs and their individual component concentrations in *Spiraea* leaves significantly increased with increasing elevation, SWC, and TN while significantly decreasing with increasing MAT.

3.4 Key determinants influencing the NSCs concentrations in *Spiraea*

As Figure 5 illustrates, we employed piecewise SEM to analyze how climate, soil particle size, and physicochemical properties directly and indirectly influence the spatial variation of total NSCs in *Spiraea*. The results suggest that MAT, soil particle size, and physicochemical properties collectively explain 33% of the spatial variation in NSCs in *Spiraea*. Notably, MAT emerged as the primary factor influencing the spatial variation of NSCs, exerting a negative effect primarily through its indirect impacts on SWC, soil particle size, and physicochemical properties. Further, SWC had a secondary but significant impact on its spatial variation. In contrast, soil particle size exhibited the least influence.

4 Discussion

4.1 Influence of hydrothermal conditions on the NSCs concentrations of *Spiraea*

Hydrothermal conditions limit plant productivity and growth in various ecosystem types within arid regions, exerting direct and indirect influences on plant physiological metabolism (Dickman et al., 2019; Zhao et al., 2022). As organs highly sensitive to environmental changes, plant leaves can reflect adaptive responses through timely changes in NSC concentrations. This study revealed that MAT and SWC significantly impact the total NSCs, their individual component concentrations, and the ratio of soluble sugar to starch in different grassland types of the Altai Mountains, which aligns with our hypothesis. Under the higher SWC conditions, *Spiraea* can enhance its metabolic activities and carbon reserve synthesis by acquiring more water, thereby increasing the concentrations of soluble sugars and starch (O'Brien et al., 2014; Zhang et al., 2024a). Moreover, a meta-analysis indicates that NSCs accumulate under moderate water stress, whereas severe or prolonged drought may cause net carbon reserve losses (He et al.,

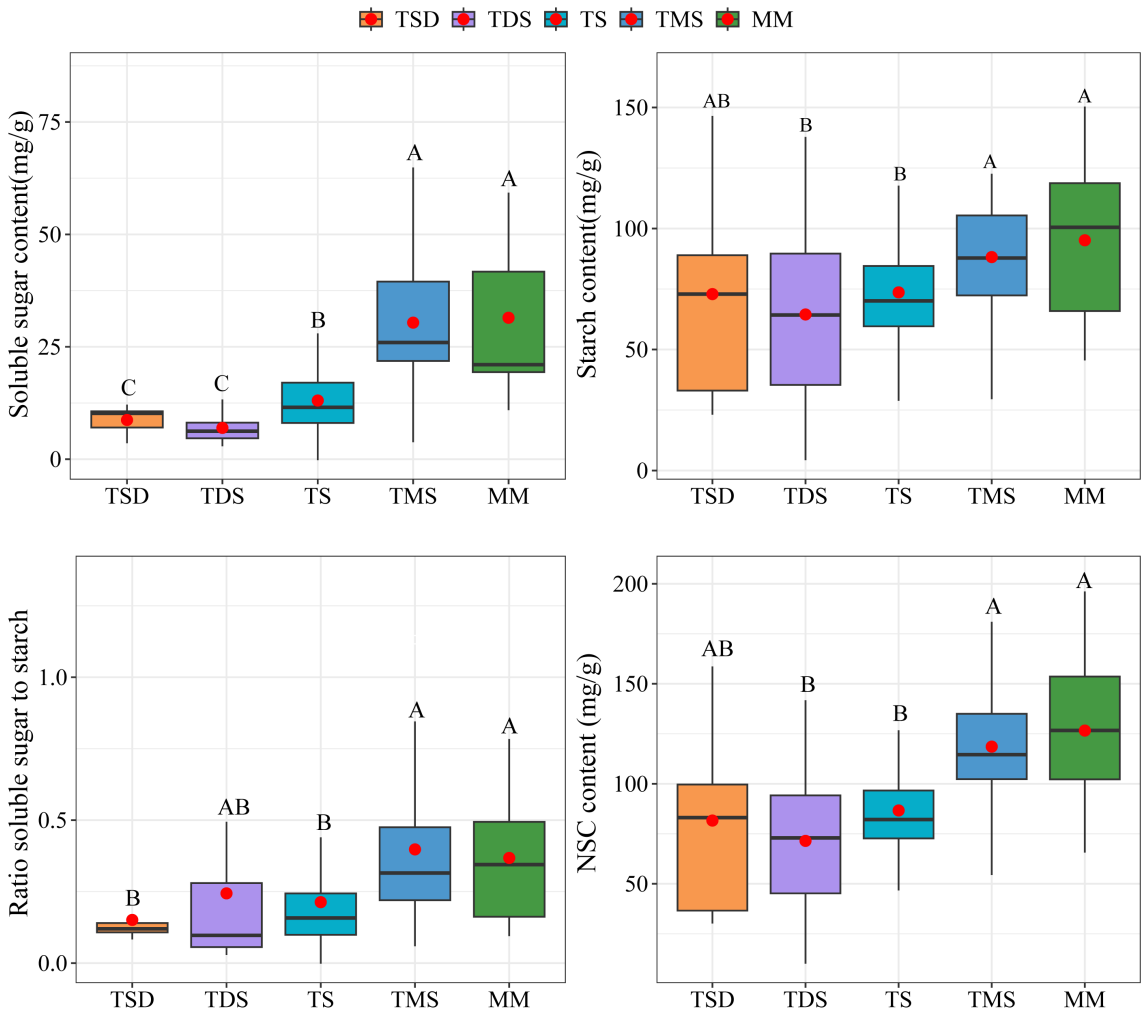

FIGURE 3
Differences in NSCs and their components of *Spiraea* across various grassland types; different letters indicate significant differences between treatments at $p < 0.05$.

2020). This suggests that along with altitudinal gradients, plants balance temperature and water availability. This trade-off in resource utilization determines the distribution and concentration variations of carbohydrates in *Spiraea*.

As the factor limiting plant growth in arid regions the most, water directly influences photosynthesis, as well as the synthesis and allocation of NSCs in plants (Adams et al., 2017; Sevanto et al., 2014). Precipitation in mountainous areas is more unevenly distributed than in plain ecosystems, leaving plants more susceptible to water limitations during their growth process. Subsequently, this affects photosynthetic carbon fixation. Generally, plants growing in arid environments retain high NSCs reserves and allocate a larger proportion of these reserves as soluble sugars, thus reducing water potential during turgor loss and promoting their survival during droughts (Wiley and Helliker, 2012). Our results indicate that the NSCs concentrations in *Spiraea* are influenced more by SWC than by precipitation, which contradicts both our hypothesis and previous findings. This discrepancy is caused by the region's soil texture and topographical environment, where precipitation in mountainous areas is more vulnerable to runoff and less likely to infiltrate the soil. Notably, SWC is a crucial factor here as it is more accessible to plants. An increase in SWC corresponds with an increase in the total NSCs concentrations and its components in *Spiraea* plants. Under adequate water conditions, Spiraea efficiently fixes soluble sugars and starch through photosynthesis, likely as a strategy to endure harsh winter periods (Jang and Sheen, 1994; Yin et al., 2021).

Temperature exerts a more significant influence than SWC on the composition of NSCs in different grassland types of the Altai Mountains. This may be because of the regional climate, where the Altai Mountains, located at a higher latitude and in a mountainous area, receive more precipitation (approximately 300 mm) than other arid grasslands at similar latitudes. Further, the lower temperatures lead to slower water evaporation and higher water availability. Several studies have found that plant carbon allocation efficiency and growth rate are temperature-dependent, especially in high-latitude regions (García-Carreras et al., 2018). Moreover,

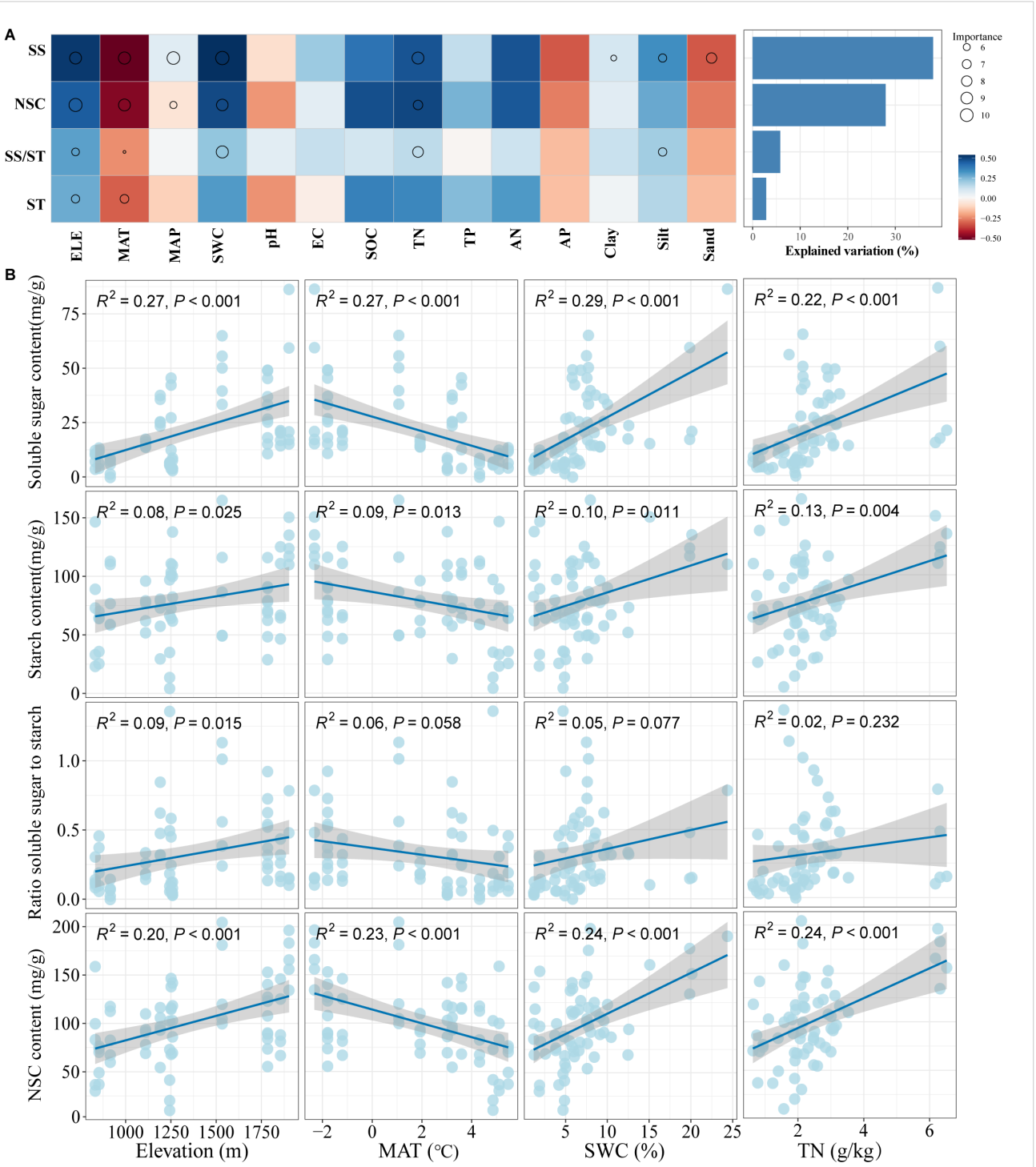

FIGURE 4
(A) Random forest analysis of key factors influencing the concentrations of NSCs and their components in *Spiraea* leaves; **(B)** Relationship between the concentrations of NSCs and their components in *Spiraea* leaves and environmental variables; here, SS represents total soluble sugars, ST represents the starch concentration in *Spiraea* leaves, and ELE represents elevation.

soluble sugars, as important energy sources and osmotic adjustment substances in plants, amass in response to environmental stresses such as low temperatures, thereby enhancing the plant's resistance (Rodríguez-Calcerrada et al., 2011; Klopotek and Kläring, 2014). Therefore, as temperatures decrease, *Spiraea*, under low-temperature stress, increases its NSCs concentrations, particularly soluble sugars, to elevate leaf osmotic pressure. Additionally, they secrete starch-hydrolyzing enzymes to hydrolyze part of the starch into soluble sugars, thus maintaining normal metabolic activities (Yin and Zhang, 2016; Michaletz, 2018; He et al., 2023).

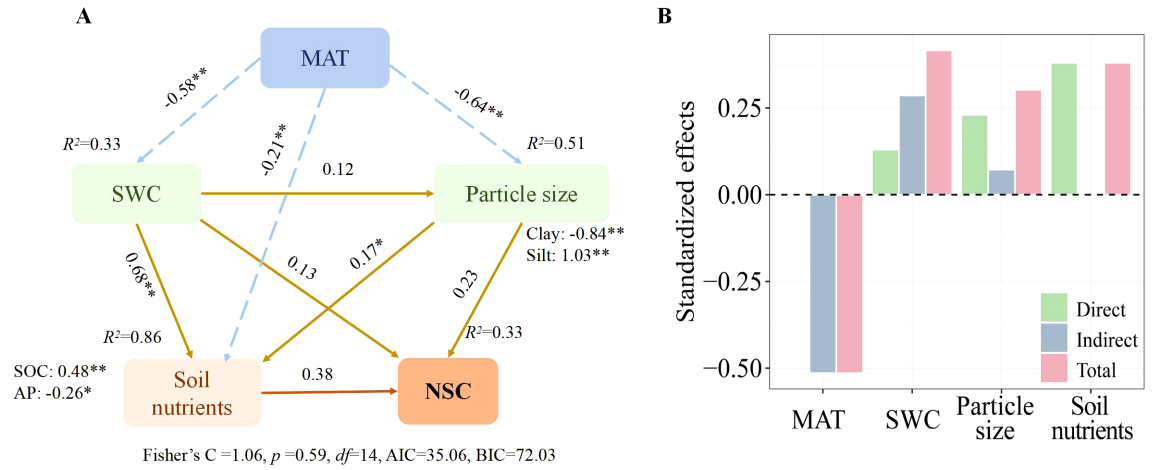

FIGURE 5
(A) A piecewise SEM calculating the direct and indirect effects of climatic factors, soil nutrients, SWC, and soil particle size on the NSCs in *Spiraea*; **(B)** The overall effects of all predictors on NSCs concentrations in *Spiraea*; here, the dashed lines indicate negative effects, while solid lines indicate positive effects; ** and * denote significance levels of $p < 0.01$ and $p < 0.05$, respectively.

4.2 Impact of grassland type on the NSCs concentrations of *Spiraea*

This study's findings validate our hypothesis that different grassland types significantly impact the NSCs and their component concentrations in *Spiraea*. We found that the concentrations of soluble sugars and total NSCs in *Spiraea* from high-altitude MMs and TMSs are significantly higher than those in other grassland types. This variation may be because of the low-temperature conditions at higher altitudes, which slow down plant metabolic rates (Körner, 2007), reducing the rate of carbon reserve decomposition. Simultaneously, the higher SWC and nutrient supply (such as SOC and TN) enhance plant photosynthetic efficiency and promote carbohydrate accumulation (Hoch and Körner, 2009; Blumstein et al., 2023). Conversely, in low-altitude TDSs and TSDs, plants experience greater environmental stress due to higher temperatures and the scarcity of SWC and nutrients. Moreover, the more frequent utilization of their carbohydrates for maintaining basic metabolism and survival adaptations results in significantly lower NSCs concentrations, with the lowest soluble sugar/starch ratio (Moore et al., 2021; Ryhti et al., 2022). This suggests that changes in altitude, hydrothermal conditions, and soil nutrients jointly drive significant differences in the resource allocation strategies of *Spiraea*, gradually transitioning from a rapid growth mode to an adaptation mode focused on storage.

Differences in grassland types significantly alter soil physicochemical properties, indirectly influencing the variation in plant NSCs and their component concentrations (Zhang et al., 2023), with SOC and TN being especially important in this process. While SOC functions as a carbon source for soil microbial activity and plant metabolism that enhances the plant's carbon fixation and storage capacity (Huang et al., 2024), nitrogen is a key limiting factor for plant growth in arid and semi-arid regions that promotes NSCs accumulation by enhancing plant nitrogen uptake and protein synthesis capabilities, which, in turn, increases enzyme activity related to photosynthesis and carbon metabolism. This promotes water utilization and transport, enhancing carbon utilization strategies (Schimel et al., 2004; Garnett et al., 2009; Wang et al., 2022). This was further confirmed in the present study, where SEM revealed that soil nitrogen significantly influences the NSCs concentrations in *Spiraea* that grows in the Altai Mountains. As soil TN content increases, there is a corresponding increase in plant soluble sugars, total NSCs, and the ratio of soluble sugar to starch. This trend reflects nitrogen supply, which alleviates limitation in plants, enhancing photosynthetic activity and promoting the accumulation of soluble sugars and other substances (Zhou et al., 2011; Xie et al., 2018). Furthermore, the availability of these nutrients is not only related to their concentration but also regulated by soil particle composition, such as the proportion of clay and sand particles. A high proportion of clay particles aids in nutrient retention, whereas a high concentration of sand particles may lead to nutrient loss, particularly in mountainous regions (Wang et al., 2020). Therefore, soil nutrients directly influence plant physiological metabolic processes and resource allocation strategies, driving the dynamic changes in NSCs and their components in *Spiraea*.

5 Conclusion

Spiraea in the Altai Mountains can adapt to diverse grassland environments by regulating the concentrations and composition of NSCs. This study found that SWC, MAT, soil TNC, and altitude can directly or indirectly affect NSCs concentrations and distribution. Among these factors, MAT and SWC most significantly influence the NSCs concentrations and components of *Spiraea* in different

grassland types. As MAT decreases and SWC and soil TNC increase, the soluble sugars, starch, and total NSCs concentrations in *Spiraea* leaves show an upward trend. Thus, these findings offer physiological and ecological insights into why *Spiraea* has become a dominant species in the grassland shrub encroachment of this region, offering theoretical support for scientifically managing grassland shrub encroachment in this area. However, further research is necessary to investigate the NSCs allocation strategies of *Spiraea* above and below ground, as well as their variation patterns during different growth stages.

Data availability statement

The original contributions presented in the study are included in the article/supplementary material. Further inquiries can be directed to the corresponding authors.

Author contributions

XM: Formal Analysis, Investigation, Methodology, Software, Validation, Writing – original draft, Writing – review & editing. LF: Conceptualization, Investigation, Writing – review & editing. MY: Investigation, Software, Visualization, Writing – original draft. JL: Formal Analysis, Visualization, Writing – original draft. MY: Data curation, Visualization, Writing – original draft. ZY: Investigation, Methodology, Writing – original draft. XC: Conceptualization, Funding acquisition, Writing – review & editing. BZ: Conceptualization, Writing – review & editing, Resources. YL: Conceptualization, Methodology, Supervision, Writing – review & editing. YG: Conceptualization, Formal Analysis, Methodology, Supervision, Writing – review & editing.

Funding

The author(s) declare that financial support was received for the research and/or publication of this article. This research was supported by the National Natural Science Foundation of China (W2412123), the Tianshan Talent Project of Xinjiang Uygur Autonomous Region, China (2022TSYCLJ0056), the Third Xinjiang Scientific Expedition Program (2021xjkk0603) and the Xinjiang Agricultural University Graduate School-level Scientific Research and Innovation Program (XJAUGRI2024001).

Conflict of interest

The authors declare that the research was conducted in the absence of any commercial or financial relationships that could be construed as a potential conflict of interest.

Generative AI statement

The author(s) declare that no Generative AI was used in the creation of this manuscript.

Publisher's note

References

Adams, H. D., Zeppel, M. J., Anderegg, W. R., Hartmann, H., Landhäusser, S. M., Tissue, D. T., et al. (2017). A multi-species synthesis of physiological mechanisms in drought-induced tree mortality. *Nat. Ecol. Evol.* 1, 1285–1291. doi: 10.1038/s41559-017-0248-x

Barker Plotkin, A., Blumstein, M., Laflower, D., Pasquarella, V. J., Chandler, J. L., Elkinton, J. S., et al. (2021). Defoliated trees die below a critical threshold of stored carbon. *Funct. Ecol.* 35, 2156–2167. doi: 10.1111/1365-2435.13891

Blumstein, M., Gersony, J., Martínez-Vilalta, J., and Sala, A. (2023). Global variation in nonstructural carbohydrate stores in response to climate. *Global Change Biol.* 29, 1854–1869. doi: 10.1111/gcb.16573

Dickman, L. T., McDowell, N. G., Grossiord, C., Collins, A. D., Wolfe, B. T., Detto, M., et al. (2019). Homoeostatic maintenance of nonstructural carbohydrates during the 2015–2016 El Niño drought across a tropical forest precipitation gradient. *Plant Cell Environ.* 42, 1705–1714. doi: 10.1111/pce.13501

Ding, J., and Eldridge, D. (2023). The success of woody plant removal depends on encroachment stage and plant traits. *Nat. Plants* 9, 58–67. doi: 10.1038/s41477-022-01307-7

Eldridge, D. J., Bowker, M. A., Maestre, F. T., Roger, E., Reynolds, J. F., and Whitford, W. G. (2011). Impacts of shrub encroachment on ecosystem structure and functioning: towards a global synthesis. *Ecol. Lett.* 14, 709–722. doi: 10.1111/j.1461-0248.2011.01630.x

García-Carreras, B., Sal, S., Padfield, D., Kontopoulos, D. G., Bestion, E., Schaum, C. E., et al. (2018). Role of carbon allocation efficiency in the temperature dependence of autotroph growth rates. *Proc. Natl. Acad. Sci.* 115, E7361–E7368. doi: 10.1073/pnas.1800222115

Garnett, T., Conn, V., and Kaiser Brent, N. (2009). Root based approaches to improving nitrogen use efficiency in plants. *Plant Cell Environ.* 32, 1272–1283. doi: 10.1111/j.1365-3040.2009.02011.x

Guo, J. S., Gear, L., Hultine, K. R., Koch, G. W., and Ogle, K. (2020). Non-structural carbohydrate dynamics associated with antecedent stem water potential and air temperature in a dominant desert shrub. *Plant Cell Environ.* 43, 1467–1483. doi: 10.1111/pce.13749

Hartmann, H., and Trumbore, S. (2016). Understanding the roles of nonstructural carbohydrates in forest trees–from what we can measure to what we want to know. *New Phytol.* 211, 386–403. doi: 10.1111/nph.2016.211.issue-2

He, R., Shi, H., Hu, M., Zhou, Q., Zhang, Q., and Dang, H. (2023). Divergent effects of warming on nonstructural carbohydrates in woody plants: a meta-analysis. *Physiologia Plantarum* 175, e14117. doi: 10.1111/ppl.v175.6

He, W., Liu, H., Qi, Y., Liu, F., and Zhu, X. (2020). Patterns in nonstructural carbohydrate contents at the tree organ level in response to drought duration. *Global Change Biol.* 26, 3627–3638. doi: 10.1111/gcb.15078

Hoch, G., and Körner, C. (2009). Growth and carbon relations of tree line forming conifers at constant vs. variable low temperatures. *J. Ecol.* 97, 57–66. doi: 10.1111/j.1365-2745.2008.01447.x

Huang, L., Gao, Y., Li, Y., Zhang, T., Hu, D., and Wang, L. (2015). Growth of Siberia larch in the middle east of Altay Mountains and its response to climate change. *Arid Land Geography* 38, 1169–1178. doi: 10.13826/j.cnki.cn65-1103/x.2015.06.010

Huang, Q., Wang, B., Shen, J., Xu, F., Li, N., Jia, P., et al. (2024). Shifts in C-degradation genes and microbial metabolic activity with vegetation types affected the surface soil organic carbon pool. *Soil Biol. Biochem.* 192, 109371. doi: 10.1016/j.soilbio.2024.109371

Jang, J. C., and Sheen, J. (1994). Sugar sensing in higher plants. *Plant Cell* 6, 1665–1679. doi: 10.1016/S1360-1385(97)89545-3

Klopotek, Y., and Kläring, H. P. (2014). Accumulation and remobilisation of sugar and starch in the leaves of young tomato plants in response to temperature. *Scientia Hortic.* 180, 262–267. doi: 10.1016/j.scienta.2014.10.036

Körner, C. (2007). The use of 'altitude' in ecological research. *Trends Ecol. Evol.* 22, 569–574. doi: 10.1016/j.tree.2007.09.006

Li, Y., Zhang, Z., Zhou, X., Gao, M., Duan, J., Xue, Y., et al. (2024). Transformation and mechanisms of climate wet/dry change on the northern Tibetan Plateau under global warming: A perspective from paleoclimatology. *Sci. China Earth Sci.* 67, 1932–1951. doi: 10.1007/s11430-023-1260-6

Liu, H., Shangguan, H., Zhou, M., Airebule, P., Zhao, P., He, W., et al. (2019). Differentiated responses of nonstructural carbohydrate allocation to climatic dryness and drought events in the Inner Asian arid timberline. *Agric. For. Meteorology* 271, 355–361. doi: 10.1016/j.agrformet.2019.03.008

Ma, X., Fan, L., Fakher, A., Li, Y., Mao, J., Yang, M., et al. (2025). Shrub encroachment: A catalyst for enhanced soil nutrients storage in the Altai Mountains. *Plants* 14, 623. doi: 10.3390/plants14040623

Ma, X., and Gao, Y. (2025). Impact of shrub encroachment on soil hydrological processes in grassland. *Acta Prataculturae Sin.* 34, 212–222. doi: 10.11686/cyxb2024201

Martínez-Vilalta, J., Sala, A., Asensio, D., Galiano, L., Hoch, G., Palacio, S., et al. (2016). Dynamics of non-structural carbohydrates in terrestrial plants: a global synthesis. *Ecol. Monogr.* 86, 495–516. doi: 10.1002/ecm.1231

McDowell, N. G. (2011). Mechanisms linking drought, hydraulics, carbon metabolism, and vegetation mortality. *Plant physiol.* 155, 1051–1059. doi: 10.1104/pp.110.170704

Michaletz, S. T. (2018). Evaluating the kinetic basis of plant growth from organs to ecosystems. *New Phytol.* 219, 37–44. doi: 10.1111/nph.2018.219.issue-1

Moore, T. E., Jones, C. S., Chong, C., and Schlichting, C. D. (2020). Impact of rainfall seasonality on intraspecific trait variation in a shrub from a Mediterranean climate. *Funct. Ecol.* 34, 865–876. doi: 10.1111/1365-2435.13533

Moore, C. E., Meacham-Hensold, K., Lemonnier, P., Slattery, R. A., Benjamin, C., Bernacchi, C. J., et al. (2021). The effect of increasing temperature on crop photosynthesis: from enzymes to ecosystems. *J. Exp. Bot.* 72, 2822–2844. doi: 10.1093/jxb/erab090

O'Brien, M., Leuzinger, S., Philipson, C., Tay, J., and Hector, A. (2014). Drought survival of tropical tree seedlings enhanced by nonstructural carbohydrate levels. *Nat. Climate Change* 4, 710–714. doi: 10.1038/nclimate2281

Pierce, N. A., Archer, S. R., and Bestelmeyer, B. T. (2019). Competition suppresses shrubs during early, but not late, stages of arid grassland-shrubland state transition. *Funct. Ecol.* 33, 1480–1490. doi: 10.1111/1365-2435.13336

Rodríguez-Calcerrada, J., Shahin, O., Del Rey, M. D. C., and Rambal, S. (2011). Opposite changes in leaf dark respiration and soluble sugars with drought in two Mediterranean oaks. *Funct. Plant Biol.* 38, 1004–1015. doi: 10.1071/FP11135

Ryhti, K., Schiestl-Aalto, P., Tang, Y., Rinne-Garmston, K. T., Ding, Y., Pumpanen, J., et al. (2022). Effects of variable temperature and moisture conditions on respiration and nonstructural carbohydrate dynamics of tree roots. *Agric. For. Meteorology* 323, 109040. doi: 10.1016/j.agrformet.2022.109040

Schimel, J. P., Bilbrough, C., and Welker, J. A. (2004). Increased snow depth affects microbial activity and nitrogen mineralization in two Arctic tundra communities. *Soil Biol. Biochem.* 36, 217–227. doi: 10.1016/j.soilbio.2003.09.008

Sevanto, S., McDowell, N. G., Dickman, L. T., Pangle, R., and Pockman, W. T. (2014). How do trees die? A test of the hydraulic failure and carbon starvation hypotheses. *Plant Cell Environ.* 37, 153–161. doi: 10.1111/pce.2014.37.issue-1

Thalmann, M., and Santelia, D. (2017). Starch as a determinant of plant fitness under abiotic stress. *New Phytol.* 214, 943–951. doi: 10.1111/nph.2017.214.issue-3

Tian, P., Zhao, X., Liu, S., Sun, Z., Jing, Y., and Wang, Q. (2022). Soil microbial respiration in forest ecosystems along a north-south transect of eastern China: Evidence from laboratory experiments. *Catena* 211, 105980. doi: 10.1016/j.catena.2021.105980

Wang, J., Qu, F., Liang, J., Yang, M., and Hu, X. (2022). Bacillus velezensis SX13 promoted cucumber growth and production by accelerating the absorption of nutrients and increasing plant photosynthetic metabolism. *Scientia Hortic.* 301, 111151. doi: 10.1016/j.scienta.2022.111151

Wang, R., Wu, H., Sardans, J., Li, T., Liu, H., Peñuelas, J., et al. (2020). Carbon storage and plant-soil linkages among soil aggregates as affected by nitrogen enrichment and mowing management in a meadow grassland. *Plant Soil* 457, 407–420. doi: 10.1007/s11104-020-04749-0

Wiley, E., and Helliker, B. (2012). A re-evaluation of carbon storage in trees lends greater support for carbon limitation to growth. *New Phytol.* 195, 285–289. doi: 10.1111/j.1469-8137.2012.04180.x

Xie, H., Yu, M., and Cheng, X. (2018). Leaf non-structural carbohydrate allocation and C: N: P stoichiometry in response to light acclimation in seedlings of two subtropical shade-tolerant tree species. *Plant Physiol. Biochem.* 124, 146–154. doi: 10.1016/j.plaphy.2018.01.013

Yin, B., Li, J., Zhang, Q., Wu, N., Zhang, J., Rong, X., et al. (2021). Freeze-thaw cycles change the physiological sensitivity of *Syntrichia caninervis* to snow cover. *J. Plant Physiol.* 266, 153528. doi: 10.1016/j.jplph.2021.153528

Yin, B., Li, J., Zhang, Q., Zhang, S., Liu, Z., Zhou, X., et al. (2024). Snow depth has greater influence on moss biocrusts' soil multifunctionality than the number of freeze-thaw cycles. *Appl. Soil Ecol.* 199, 105420. doi: 10.1016/j.apsoil.2024.105420

Yin, B. F., and Zhang, Y. M. (2016). Physiological regulation of *Syntrichia caninervis* Mitt. in different microhabitats during periods of snow in the Gurbantünggüt Desert, northwestern China. *J. Plant Physiol.* 194, 13–22. doi: 10.1016/j.jplph.2016.01.015

Zhang, P., Ding, J., Wang, Q., McDowell, N. G., Kong, D., Tong, Y., et al. (2024a). Contrasting coordination of non-structural carbohydrates with leaf and root economic strategies of alpine coniferous forests. *New Phytol.* 243, 580–590. doi: 10.1111/nph.v243.2

Zhang, S., Yang, A., Zang, Y., Guo, K., Zhou, X., Rong, X., et al. (2024b). Slope position affects nonstructural carbohydrate allocation strategies in different types of biological soil crusts in the Gurbantunggut Desert. *Plant Soil*, 1–14. doi: 10.1007/s11104-024-06951-w

Zhang, S., Zhang, Q., Li, Y., Lu, Y., Zhou, X., Yin, B., et al. (2023). Shrubs have a greater influence on the nonstructural carbohydrates of desert mosses along precipitation decreased. *Environ. Exp. Bot.* 216, 105530. doi: 10.1016/j.envexpbot.2023.105530

Zhao, L., Chen, H., Chen, B., Wang, Y., and Sun, H. (2022). Drought shapes photosynthetic production traits and water use traits along with their relationships with leaves of typical desert shrubs in Qaidam. *Forests* 13, 1652. doi: 10.3390/f13101652

Zhou, X., Zhang, Y., Ji, X., Downing, A., and Serpe, M. (2011). Combined effects of nitrogen deposition and water stress on growth and physiological responses of two annual desert plants in northwestern China. *Environ. Exp. Bot.* 74, 1–8. doi: 10.1016/j.envexpbot.2010.12.005

frontiers | Frontiers in Plant Science

TYPE Original Research
PUBLISHED 30 July 2025
DOI 10.3389/fpls.2025.1577533

OPEN ACCESS

EDITED BY
Sebastian Leuzinger,
Auckland University of Technology,
New Zealand

REVIEWED BY
Dengpan Xiao,
Hebei Normal University, China
Can Wang,
Southwest Jiaotong University, China

*CORRESPONDENCE
Vladimir Camel
vcamelpa@ucv.edu.pe

RECEIVED 16 February 2025
ACCEPTED 26 June 2025
PUBLISHED 30 July 2025

CITATION
Camel V, Pillpa F, Colqui V, Ataucusi J, Quispe-Huañahue J, Felix E, Ninanya-Parra Z, Maravi-Hinostroza K, Caysahuana K and Cabello-Torres R (2025) Mortality, structure, propagation, and microhabitat characterization of *Haageocereus acranthus*: a case study on coastal lomas. *Front. Plant Sci.* 16:1577533. doi: 10.3389/fpls.2025.1577533

Mortality, structure, propagation, and microhabitat characterization of *Haageocereus acranthus*: a case study on coastal lomas

Vladimir Camel*, Freddy Pillpa, Virginia Colqui, Jose Ataucusi, July Quispe-Huañahue, Edwin Felix, Zulema Ninanya-Parra, Key Maravi-Hinostroza, Keiko Caysahuana and Rita Cabello-Torres

Grupo de Investigación en Ecofisiología Vegetal y Restauración de Ecosistemas Degradados, Escuela de Ingeniería Ambiental, Universidad Cesar Vallejo, Lima, Peru

The *Haageocereus* genus includes endemic species found in the coastal region of Peru and is characterized by varying ploidy levels that influence its shape and adaptability. It establishes itself in coastal lomas and desert ecosystems, capturing moisture from fog and reproducing through stem fragmentation and seeds to survive. Ecologically, it helps stabilize the soil and provides shelter and food for wildlife. The study aimed to propagate, evaluate mortality and structure, and characterize the microhabitat of *Haageocereus acranthus* in the coastal lomas of Mangomarca, Lima, Peru. To achieve this, three transects were established across an altitudinal gradient. The abundance, morphological data, and environmental factors (pH, cover, slope, organic matter, etc.) were assessed, and living and dead colonies were counted. Consequently, the stems grow approximately 4.8 cm per year under nursery conditions, while the roots develop 4.42 cm in 45 days. In a 4.41 ha area, 94 colonies were recorded, comprising 1,801 stems; 37.89% of the individuals had lengths between 20 and 40 cm. The largest stem reached a diameter of 8 cm and a length of 169 cm. Additionally, around 1,788 living colonies and 14,741 dead colonies were counted across all the lomas. The death of the cacti may be linked to anthropogenic pressure that has altered the soil from acidic to basic, increasing electrical conductivity while reducing the availability of organic matter and nutrients. Our research has also shown that pH and altitude influence the phenotypic characteristics of *H. acranthus* stems. At higher elevations, the size of the cacti increased alongside the amount of organic matter, while the concentration of carbonates decreased. Ultimately, mortality rates will likely rise due to severe human impacts, increasing temperatures, and prolonged droughts. Therefore, it is crucial to closely monitor and implement conservation and restoration measures for these coastal lomas endemic to South America.

KEYWORDS

arid ecosystems, Cactaceae, cytometry, degraded soils, ecological restoration

1 Introduction

Cacti have their center of origin and most abundant diversity in the American continent, and they are used as a model to understand the origin of arid biomes. Suggesting that the most extensive cactus lineages were established in the context of climate change and the expansion of arid and semi-arid habitats (Arakaki et al., 2011). Cacti are dicotyledonous, xerophytic plants that are resistant to extreme climatic conditions. Their roots are shallow, and their metabolism is CAM-type. They live in saline or slightly acidic soils (Lim et al., 2019). There are 262 species in 40 genera in Peru (Ostolaza, 2014). Most of these taxa are distributed between 0 and 4,500 meters above sea level and mainly inhabit desert shrublands, grasslands, lomas, and coastal deserts (Arakaki et al., 2006). Currently, little is known about the conservation status of Cactaceae, which is why it is important to develop ecological studies on their structure, functioning, and restoration (Winchell et al., 2022). Various cactus species are experiencing changes in their populations. Even though they are growing, there remains a risk of increased mortality if natural regeneration rates are impacted by climatic variations and human pressures such as fragmentation, roads, particulate matter, mining activity, and urban expansion (Flores and Van Meerbeek, 2024). Therefore, given the importance of the ecosystem services they provide and their evident degradation, the regional government of Lima, Peru (2012-2025) has established as a primary objective the conservation, protection, and restoration of the urban ecosystems that constitute the ecological structure of Lima, affirming the sustainable use and recovery of degraded environments populated by abundant herbaceous, xerophytic, and stationary vegetation (Flood Chávez and Niewiadomski, 2022).

In this research, we address the genus *Haageocereus*, which includes 20 accepted species, of which seven are endangered. They also have different ploidy levels. *Haageocereus tenuis* F. Ritter (2 N = 3 x = 33) and *H. repens* Rauh and Backeb. (2 N = 2 x = 22) have a single population near the city of Lima. While *H. acranthus* (Vaup.) Backeb. (2 N = 4 x = 44) and *H. pseudomelanostele* (Werdermann and Backeb.) Backeb. (2 N = 2 x = 22) have several large populations (Arakaki et al., 2007). Its biogeographic distribution is restricted to the Pacific basin of the Andes. They are species that adapt to extremely harsh living conditions, tolerating thermal, water (annual rainfall of 18–100 mm), and radiation stress (Calderón et al., 2007).

In general, cacti efficiently absorb large amounts of carbon dioxide quickly, showing great potential as carbon sinks (Torre, 2017). Ecologically, their spines capture humidity from the air and transfer it by osmosis to their tissues. Physiologically, their stomata close during the day and open at night to prevent water loss (Calhoun, 2012), thus optimizing their photosynthetic processes. Furthermore, cacti can be utilized in the food industry, as well as for vegetable fiber, cosmetics, and more (Ostolaza, 2014). In this context (Simpalo et al., 2020), reported that the vitamin C content (66.73 mg/100 g) of the fruit of *H. pseudomelanostele* is higher than that of other fruits with similar structure, such as aguaymanto, sanqui, and tuna.

Regarding ecology, studies report that for the species *Haageocereus pseudomelanostele*, *Melocactus peruvianus*, *Mila nealeana*, and *Neoraymondia arequipensis*, rocks acted as nurses in coastal ecosystems by providing a temperature lower than 1.2°C compared to bare soil, extending the soil moisture period, accumulating more organic matter, and protecting against intense solar radiation (Pisco, 2016). This created a favorable microclimate for the seeds of these species to germinate and establish themselves or for seedlings to survive the extreme conditions of the arid ecosystem (Castro-Cepero et al., 2006). Likewise, microorganisms in the rhizosphere promote the growth of cacti (Villanueva, 2018); they are involved in seed germination and flowering processes (Chávez et al., 2016); and they assist in tolerating water and salt stress (Sánchez et al., 2023). On the other hand, recent studies in coastal lomas indicate that the percentages of organic matter, nitrogen, phosphorus, and potassium in the soil are abruptly altered by human activities, which convert acidic soils into basic ones, raising the levels of electrical conductivity due to an increase in Mg and Ca (Camel et al., 2024). This phenomenon could be linked to the death of cacti and other species typical of coastal lomas.

On the other hand, regarding the reproduction of some triploid species (*H. tenuis*) within the genus *Haageocereus*, it is essential to note that they mainly reproduce through stem fragmentation and agamospermy, producing viable seeds without sexual fertilization (Arakaki et al., 2013). This indicates that all individuals are genetically identical, suggesting that the population represents a single clone. This process is crucial for plants that colonize specific areas or face adverse conditions, as it ensures genetic stability. Conversely, *H. repens* is endangered and limited to a single population (Arakaki et al., 2007). In contrast, the widely distributed species *H. pseudomelanostele* (diploid) and *H. acranthus* (tetraploid) exhibit high genetic diversity, indicating potential gene flow influenced by insects, bats, and hummingbirds (Arakaki, 2008). Additionally, the seed propagation of *H. pseudomelanostele* shows a high germination rate and healthy development under shaded conditions (Castro-Cepero et al., 2006).

Therefore, it is essential to propose restoration models for coastal lomas since they are fragile ecosystems (Balaguer et al., 2011). In this way, desertification processes can be slowed down, in addition to avoiding the extinction of endemic species under some threat. To do this, it is crucial to know the behavior of native species, such as their propagation and climatic and edaphic conditions of their microsite, and evaluate the development, physiology, and plant-microorganism interaction (Cordero et al., 2017). For this reason, the present work aims to propagate, evaluate mortality and structure, and characterize the microhabitat of *Haageocereus acranthus* in the coastal lomas of Mangomarca, Lima-Peru.

2 Materials and methods

2.1 Study area

This study was conducted in the lomas of Mangomarca, situated in the district of San Juan de Lurigancho-Lima, Peru, and encompasses an area of 516.10 hectares. It is regarded as a fragile

ecosystem threatened by human activities since pre-Inca times (Marcone et al., 2024), The Ichma culture, which flourished near the lomas of Mangomarca, along with the archaeological findings, indicates that they utilized resources such as granite rocks (composed of ferromagnesian minerals, calcium-sodium feldspars, alkali feldspars, and quartz), wood, and fruits (Eeckhout, 2004). The lomas of Mangomarca are characterized by ravines and slopes exceeding 30 degrees. They are found between 180 and 850 meters above sea level and are noted for their rocky outcrops (Camel et al., 2024). Furthermore, in the coastal lomas, the existence of animals (lizards, birds, bats, and rodents) is intricately linked to perennial plants (*Solanum peruvianum*, *Trixis cacalioides*, *Atriplex rotundifolia*, *Haagacereus* sp.), which play a crucial role in their diet. These animals feed on the stems, fruits, leaves, and juicy fleshy roots. In return, they are valuable for pollinating flowers and propagating seeds (Bugaret, 2010).

2.2 Inventory and population structure of *Haageocereus acranthus*

To conduct the inventory of the *H. acranthus* cactus, three transects were established throughout the study area to analyze the structural and environmental characteristics (Figure 1c). Each transect was 100 m wide, with a line perpendicular to the slope established along its length. Additionally, the transects were set up at different elevation levels: T1 (0.90 ha, from 448 to 523 m asl), T2 (1.79 ha, from 674 to 769 m asl), and T3 (1.72 ha, from 760 to 841 m asl)

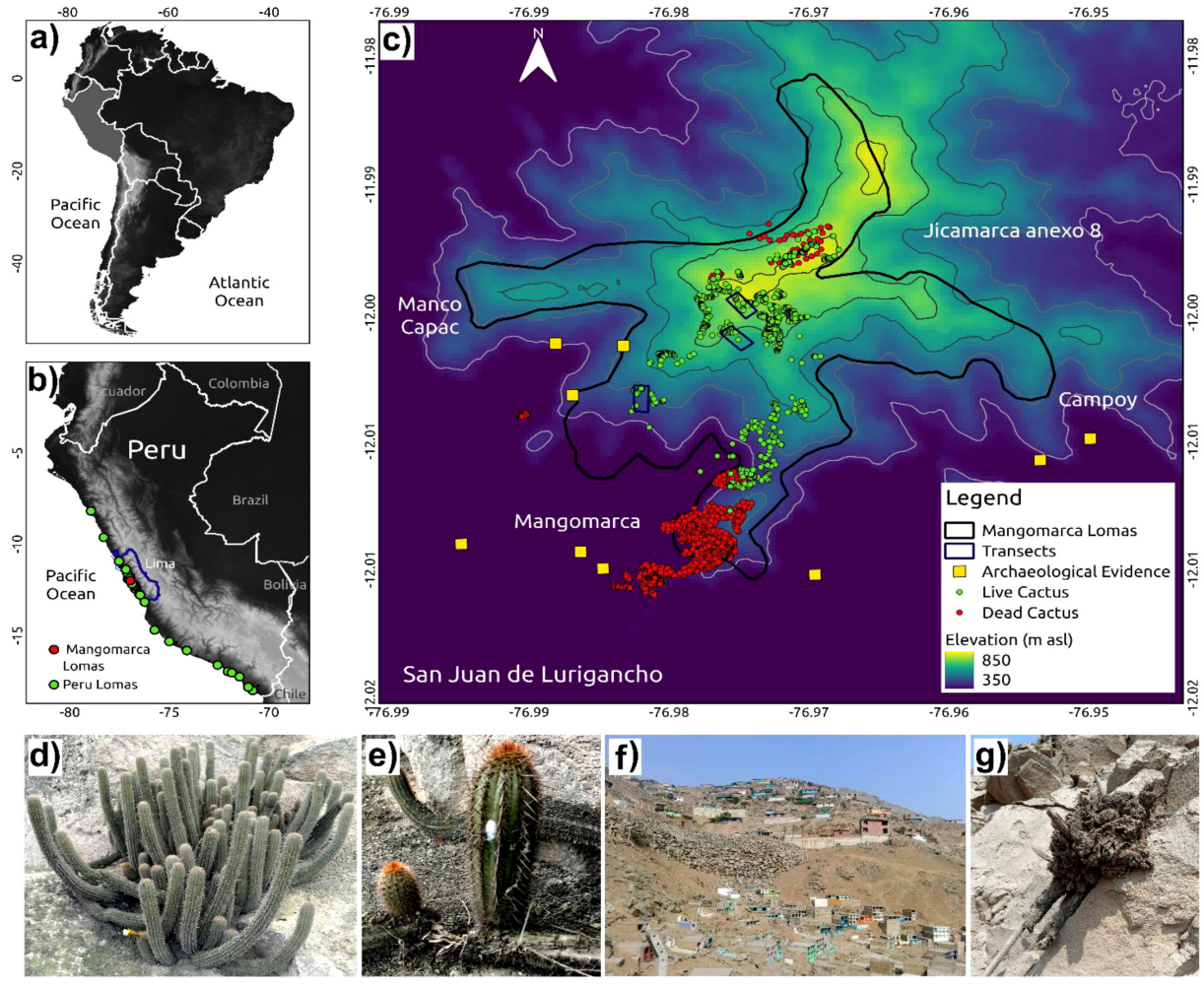

FIGURE 1
Location of coastal lomas ecosystems in Peru and spatial distribution of *H. acranthus* colonies. **(a)** Geographic location of Peru in the South American continent. **(b)** Distribution of lomas in Peru: the green dots indicate the location of other coastal lomas, and the red dots indicate the position of the Mangomarca Lomas. **(c)** Distribution of *H. acranthus* in Mangomarca Lomas: the red dots represent dead cacti, and the green dots indicate living cacti. **(d)** A colony of the Cactus *H. acranthus*, featuring 77 stems, is located within the preserved area of the Mangomarca Coastal Lomas. **(e)** Asexual reproduction of *H. acranthus*: the stem detaches from the parent plant and continues the natural rooting process. **(f)** A coastal lomas area that is being degraded by human activities. The primary activities include housing and road construction, illegal granite mining, planting exotic plants, increased animals (such as dogs) that trample the biological crust, and rising amounts of solid waste. **(g)** Dead *H. acranthus*, with visible signs of deterioration and decomposition.

with a slope greater than 30% (Figure 1c). The layout of the transects aims to inventory the cacti about altitude and slope, their variation due to the presence of rocks, and areas devoid of vegetation. Data collection was conducted *in situ*, with location coordinates recorded at a spatial level alongside slope and elevation. Furthermore, the height and diameter of the cactus stems by colony were measured. To evaluate the soil cover around each colony, the following variables were recorded: distance to rock cover, soil depth, presence or absence of trails, presence or absence of lichen, and presence or absence of solid waste. Likewise, soil samples were collected from each sampled cactus live colony. On the other hand, 50 soil samples were collected from dead cacti along the roadside, and their geographic coordinates (UTM) were recorded. And later, in the biotechnology laboratory of Cesar Vallejo University, the pH value, humidity, percentage of organic matter, and percentage of carbonates were determined.

On the other hand, to spatially locate all the living and dead cactus colonies in the lomas of Mangomarca, Aster satellite images and the GPS Garmin 76SX were utilized. All maps were processed using the QGIS program.

2.3 Rooting, growth, and genome size estimation

First, individuals were collected near the roads and plants that were found under anthropic pressure due to the presence of particulate matter. Subsequently, the cacti were washed to remove dust residues; the wounds were cauterized at room temperature in the shade. After 30 days, the rooting process was carried out on bare soil using the Premix5 substrate, which is composed of Canadian Sphagnum peat moss (75 - 85% approx.), perlite (20% approx.), dolomite, gypsum, silicon dioxide (0.25%), soluble silicon (0.12%), with a pH between 5.5 and 6.0, and electrical conductivity between 0.75-1.0 dS m^{-1}. After 45 days, the plants were carefully extracted and transferred to pots with substrates of black soil, blond peat, and stones in a 3:2:1 ratio. On the other hand, growth measurements were made for 1 year. Flow cytometry analysis was conducted in the cereals and native grains program laboratory at the National Agrarian University La Molina. Three samples were analyzed following the protocols described by Doležel et al. (2007) and Salcedo (2022). In a cold Petri dish, 1 ml of OTTO I (100 mM citric acid, 0.50% (v/v) +/Tween 20; pH 2-3), 1 g of fresh tissue from the apical part of the *H. acranthus* stem, and 1 cm^2 of fresh *Physalis peruviana* L. tissue was placed as a reference standard. The entire sample was then mechanically homogenized with a double-edged blade. Next, it was filtered using a 40 µm nylon mesh and centrifuged at 1500 rpm at 5°C for 5 minutes. The supernatant was discarded, and the pellets were resuspended in 500 µl of OTTO I, followed by the addition of 500 µl of OTTO II (400 mM $Na_2PO_4{\cdot}12H_2O$, pH 8–9) supplemented with 50 µg/ml of propidium iodide (Sigma-Aldrich Company, USA) and 50 µg/ml of RNAse (Sigma-Aldrich Company, USA). The resuspension was incubated at 5°C for 10 minutes and analyzed using an Attune Nxt flow cytometer (Thermo Fisher Scientific) (Salcedo, 2022).

2.4 Data analysis

A linear model was used to evaluate the correlation between chromosome number and genome size. To do this, the genome size of *H. acranthus* in the Lomas de Mangomarca was estimated and complemented by other scientific reports identified through text mining. On the other hand, the correlation of root growth with the diameter and height of the stems was analyzed using generalized linear models. Next, we utilized mixed effects models to compare MO, EC, and pH in Lomas Coastal soils (disturbed and undisturbed). To account for the possible lack of independence between soil samples, we included the state of soil (perturbed and non-perturbed) as a random factor (Bolker et al., 2009). A Gaussian error distribution with an identity link function was used as the model due to the normality tested by the Shapiro–Wilk test. A Kruskal–Wallis with Bonferroni–Dunn *post hoc* test ($p < 0.05$) was used to compare differences (Matter organic, electric conductivity, and pH) between samples for perturbed and non-perturbed. We used generalized linear models to examine the correlation between the closest road distance to live (conserved area) and dead (disturbed area) cacti, with their respective pH values. To understand the structure of *H. acranthus*, a stacked bar histogram was made where the different colors represented the transects. The total height (cm) was considered a class because it is the most differentiated morphological trait among the other stems in the colonies. Likewise, I would like to analyze the relationship between structure, environmental variables, and anthropogenic effects. A multi-model inference approach was utilized to achieve this. Structural components, such as the number of stems per colony, diameter, and total height, were treated as response variables. Conversely, environmental conditions (including altitude, distance to the rocks, slope, humidity, soil pH, and organic matter) and anthropogenic impacts (the presence or absence of trails and solid waste) were considered explanatory variables. Transects were considered a random effect. Based on Akaike's information criterion (AIC), we ranked the models from the best to the worst and considered the set of models with $\Delta AICc < 2$ as equally well supported (Burnham et al., 2010). Since the response variable was a ratio, we applied a log-normal distribution.

Finally, generalized linear models were employed to assess the relationship between elevation (m asl) and variables such as stem diameter (cm), total stem height (cm), organic matter (%), carbonates (%), relative soil humidity (%), and pH. All the analyses were conducted using the R-Project software (R Core team, 2024); for the GLMM, we employed the lme4 package (effects and lmerTest) (Bates et al., 2015; Kuznetsova et al., 2017), MuMIn package for multi-model inference (Bartoń, 2010), and ggplot2 package for plots in general (Wickham, 2013).

3 Results

3.1 Determining the genome size of *H. acranthus*

The chromosome number and genome size of three *Haageocereus* species (*H. versicolor*, *H. pseudomelanostele*, and *H. acranthus*) have been recorded (Table 1). Figure 2a indicates that the genome size of *H. acranthus* from lomas of Mangomarca reached 7.94 ± 0.01 pg of DNA, confirming the correct genome size estimation for 4X tetraploid individuals with 44 chromosome pairs (Figure 2b).

3.2 Rooting and longitudinal growth of *H. acranthus*

Under nursery conditions, *H. acranthus* stems grew an average of 4.80 ± 0.2 cm over one year (Figure 3a). Likewise, during the rooting process, *H. acranthus* individuals developed primary roots measuring 4.42 cm in 45 days. However, correlation analyses show that the diameter and height of the stems do not significantly affect root growth (Figures 3b, c).

3.3 Inventory and population structure of *H. acranthus*

Approximately 1,788 living cactus colonies and 14,741 dead colonies of *Haageocereus acranthus* were identified, spread over an area of 270.10 hectares within an altitudinal range of 228 to 852 meters above sea level (m asl). The highest concentration of living *H. acranthus* was observed at altitudes ranging from 500 to 800 m asl (Figure 1), while the dead individuals were found between 250 and 500 m asl near the human population. Additionally, Figure 1 shows a limited presence of *H. acranthus* individuals at the northern and eastern ends of the Mangomarca hills. The results also indicate that the species primarily reproduces from stems and shows no evidence of plant propagation from seeds.

On the other hand, the differences between the soils (electrical conductivity, pH, and organic matter) of living and dead cacti were analyzed (Figure 4). The results indicate that human impact significantly affected all three parameters. Regarding EC and pH, there was an increase from 1.5 to 8 dS m^{-1} and from 6.54 to 7.68, respectively, while the percentage of organic matter decreased from 14% to 5% (Figure 4). We also demonstrated that the soil pH level in coastal lomas changes from acidic to alkaline as it approaches trails and roads (Figure 4d).

TABLE 1 Chromosome numbers, genome sizes, and seed measurements of the genus *Haageocereus*.

Species	Ploidy	CN	GS (pg)	Seed size (mm)	Seed weight (mg)	References
Haageocereus acranthus (Vaupel) Backeb.	Tetraploide	44	7.94	1.51	0.53	(Arakaki, 2008; Results by V.C.)
Haageocereus acranthus (Vaupel) Backeb.	Tetraploide	44	7.69	1.41	0.51	(Arakaki, 2008; Silva, 2015)
Haageocereus pseudomelanostele (Werderm. & Backeb.) Backeb.	Diploide	22	3.97	1.28	0.33	(Arakaki, 2008; Silva, 2015)
Haageocereus versicolor (Werderm. & Backeb.) Backeb.	Diploide	22	4.2	1.21	0.37	(Arakaki, 2008; Silva, 2015)
Haageocereus australis Backeb.	Diploide	22				(Arakaki, 2008)
Haageocereus chalaensis F. Ritter	Tetraploide	44				(Arakaki, 2008)
Haageocereus decumbens (Vaupel) Backeb.	Diploide	22				(Arakaki, 2008)
Haageocereus fulvus var. *yautanensis*	Tetraploide	44				(Arakaki, 2008)
Haageocereus horrens Rauh & Backeb.	Diploide	22				(Arakaki, 2008)
Haageocereus icosagonoides Rauh & Backeb.	Diploide	22				(Arakaki, 2008)
Haageocereus multangularis (Willd.) F. Ritte	Diploide	22				(Arakaki, 2008)
Haageocereus multicolorispinus Buining	Tetraploide	44				(Arakaki, 2008)
Haageocereus pacalaensis subsp. repens (Rauh & Backeb.) Ostolaza	Diploide	22		1.2		(Arakaki, 2008)
Haageocereus platinospinus (Werderm. & Backeb.) Backeb.	Diploide	22			0.2	(Arakaki, 2008; Jara-Peña, 2024)
Haageocereus pseudoversicolor Rauh & Backeb.	Diploide	22				(Arakaki, 2008)
Haageocereus tenuis F. Ritter	Triploide	33		1.415		(Arakaki, 2008; Alcalá, 2021)

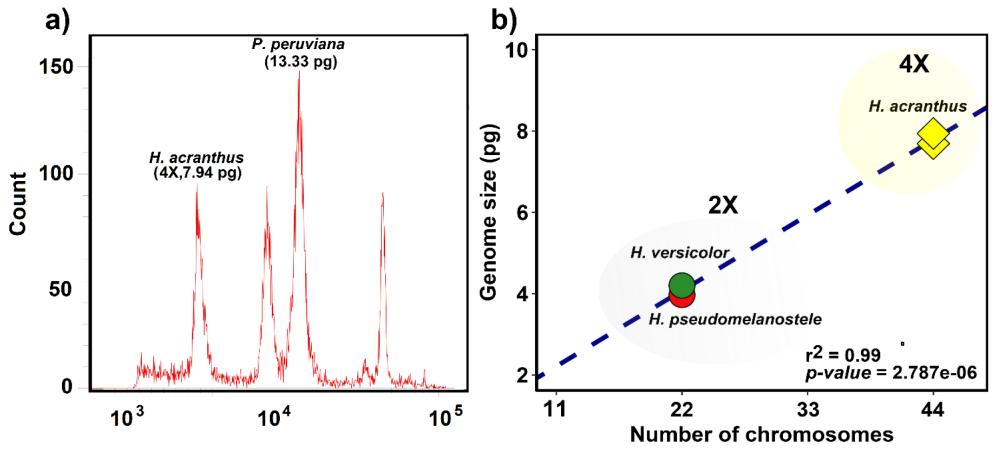

FIGURE 2
Estimating the absolute amount of nuclear DNA (genome size) in *H. acranthus* individuals. **(a)** Comparison of the G1 peak between *Physalis peruviana* and the tetraploid genotype of *H. acranthus*. **(b)** Correlation between chromosome number and genome size in three species of the genus *Haageocereus*.

The inventory of colonies and stem numbers across three transects (Figure 5) shows that transect 1 (0.9 ha) contains 33 colonies with 429 stems, and transect 2 (1.79 ha) has 30 colonies with 788 stems. Transect 3 (1.72 ha) records 31 colonies with 584 stems. The frequency of total height classes indicates that 37.89% of the plants fall between 20 and 40 cm, followed by those smaller than 20 cm at 24.82% (Figure 5). Furthermore, individuals exceeding one meter in height were observed in the higher elevation transects T2 (between 674 and 769 m asl) and T3 (between 760 and 841 m asl).

3.4 The influence of environmental factors on the development of the species *Haageocereus acranthus*

The lomas of Mangomarca have an average slope of 46.6%. Its soil properties include a depth of 6.8 cm (between soil and organic matter) and an average pH of 6.36, with humidity reaching 10.37% in May. In terms of organic matter, it contains 12.36% (Supplementary Material Table 1). The results regarding the relationship between

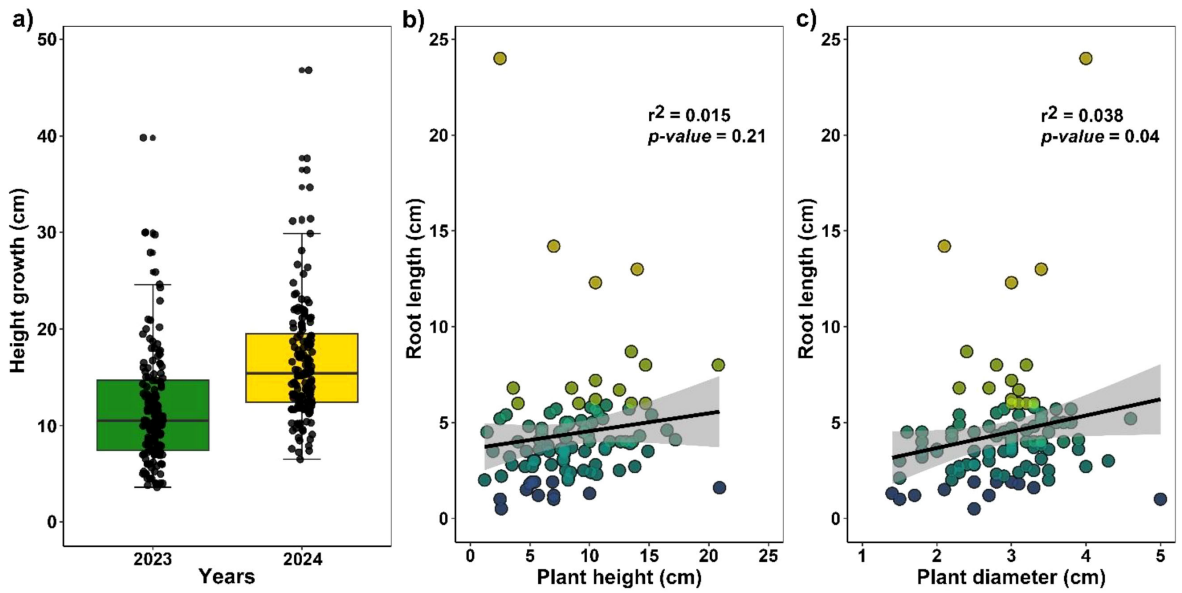

FIGURE 3
(a) Annual growth of cactus stem length. **(b)** Correlation between *H. acranthus* stem size and root length. **(c)** Correlation of *H. acranthus* stem diameter with root length. The rooting process occurred in bare soil for 45 days.

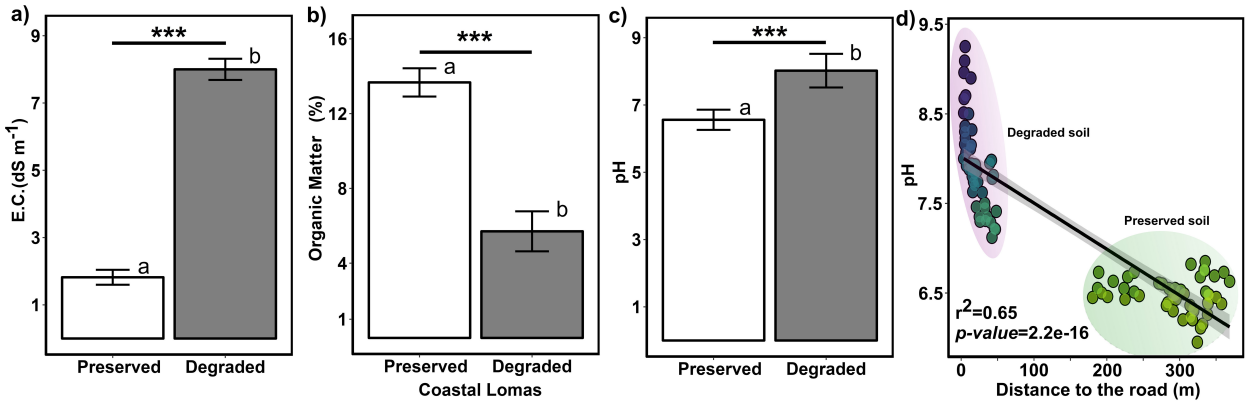

FIGURE 4
Comparison of soil properties between conserved and degraded soils. **(a)** electrical conductivity. **(b)** pH levels. **(c)** organic matter content. **(d)** Correlation between the distance of living and deceased individuals of H. acranthus to the nearest road and soil pH. The asterisks indicate significant differences between preserved and degraded soil: "*" $p \leq 0.05$; "**" $p \leq 0.01$; and "***" $p \leq 0.001$. The letters (a, b) indicate that treatments differ significantly from each other ($p < 0.05$). Therefore, degradation significantly affects these soil properties (pH, E.C., and O.M.) in the Coastal Lomas.

environmental and anthropogenic factors and the height, diameter, and number of stems per colony (Figure 6) indicate that pH significantly influences the structure of *H. acranthus* in the lomas of Mangomarca. Figure 6a shows that an increase in pH negatively impacts the total height of the evaluated cactus stems. Additionally, the findings suggest that as pH (*p-value* = 0.0380) and relative soil humidity (*p-value* = 5e-07) increase, the number of *H. acranthus* stems per colony decreases (Figure 6c). Conversely, stem diameter remained unaffected by any evaluated parameter (Figure 6b). Furthermore, factors such as % OM, slope, distance to rock, presence of lichen, and biological crust did not show significant relationships with the abundance of stems and phenotypic traits (height and diameter).

On the other hand, Figure 7 illustrates a positive correlation between stem diameter and height (r^2 = 0.33, p-value = 1.199e-11). It is also reported that under the environmental conditions of the Lomas of Mangomarca, the maximum stem diameters and heights were 8 cm and 169 cm, respectively. Furthermore, it was observed that stems exceeding these reported maximum sizes tend to fall to the ground to continue their asexual reproduction processes. Additionally, correlations based on elevation indicate that more large cacti are found at higher altitudes (r^2 = 0.18, *p-value* = 4.849e-06), along with a higher concentration of organic matter (r^2 = 0.20, *p-value* = 2.249e-06) (Figure 7). In contrast, the percentage of carbonates decreases with increasing altitude (r^2 = 0.53, *p-value* = 2.2e-16) (Figure 7). These factors do not vary with elevation regarding stem diameter, pH, and soil moisture percentage.

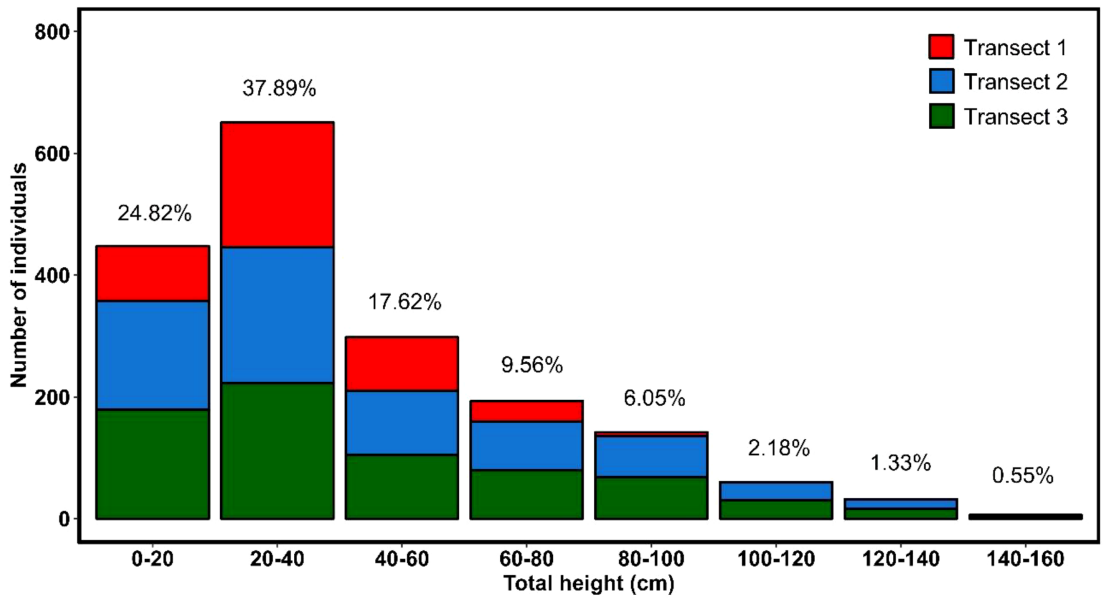

FIGURE 5
Distribution of *Haageocereus acranthus* individuals by height category across the three study transects.

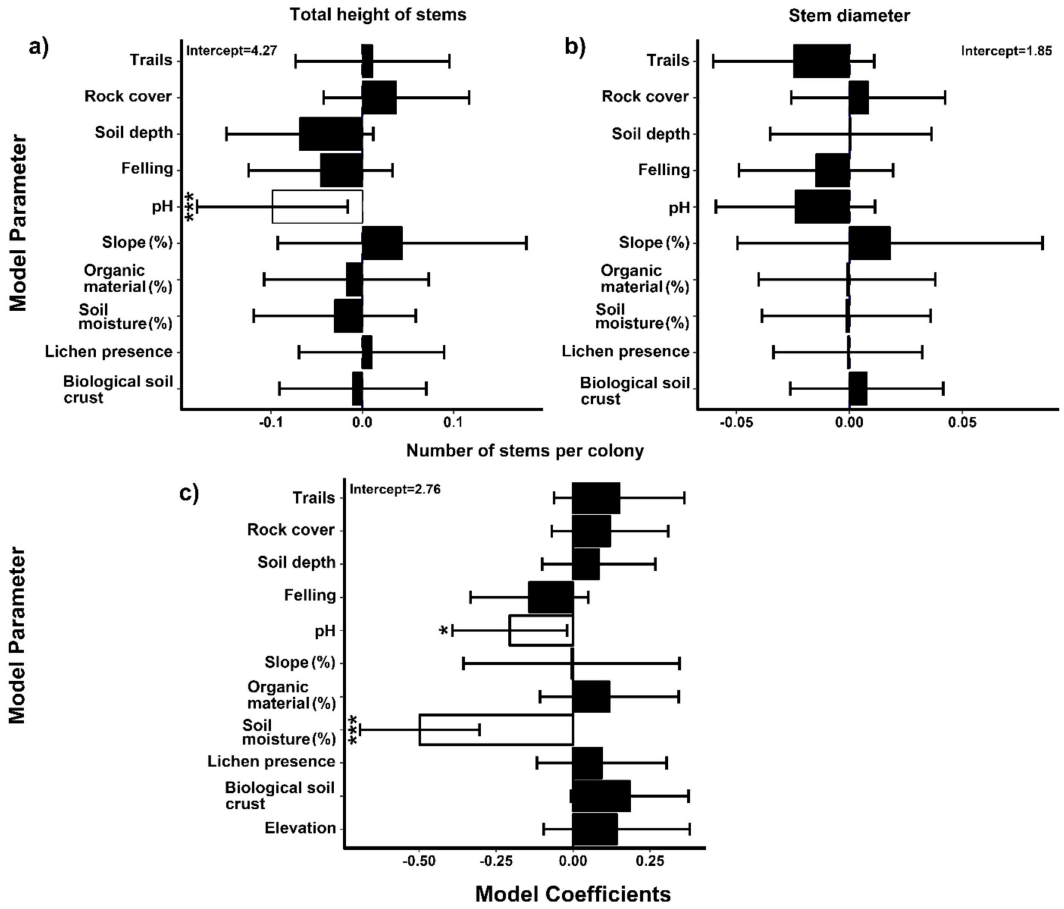

FIGURE 6
A generalized linear mixed model assesses the effects of environmental factors on the number of *H. acranthus* individuals in the study area concerning soil depth (SD), biological crust (BC), pruning, slope, organic matter (OM), humidity, presence of lichen, and altitude. **(a)** Total height of stems. **(b)** Stem diameter. **(c)** Number of stems in the colony. The error bars represent 95% confidence intervals. The white boxes with asterisks indicate significant effects on the structural parameters ($p < 0.05$): "*" $p \leq 0.05$; "**" $p \leq 0.01$; and "***" $p \leq 0.001$.

4 Discussions

In this study, we report information on the spread, abundance, mortality, and structure of the *H. acranthus* species in a coastal lomas ecosystem. The results are concerning; despite the lomas of Mangomarca being considered a protected ecosystem, we counted approximately 14,741 dead colonies (Figure 1) and 1,801 living colonies over a total area of 3.79 ha along the altitudinal gradient (448 to 841 m asl) (Figure 5). Although the exact causes of death remain unknown, evidence suggests direct and indirect impacts of human activity, as the dead cacti were found at lower elevations and in areas near the city (Figure 1). Furthermore, human activities have intensified over the past 19 years, particularly due to the invasion. In 2020, they impacted 97.5 hectares out of 516.10 hectares (SERFOR, 2014), leading to a 46.9% reduction in vegetation cover (Bolivar and Velasquez, 2021). This has altered soil conditions, resulting in the death of many *H. acranthus* individuals, sensitive to changes in characteristics such as pH, EC, and OM (Figure 4), which have been drastically changed. Recent studies by Camel et al. (2024) also indicate that degraded soils affect the concentrations of Ca, Mg, K, and P, primarily due to soil disturbance from trampling by animals (packs of dogs), road opening, house construction, and other activities. Other studies also mention that cacti mortality is primarily due to prolonged periods of drought and extreme temperatures, such as frost (Orum et al., 2016), emphasizing the importance of nurse plants that protect against extreme temperatures and solar radiation. Similarly, our results indicate that at higher elevations, there is a greater concentration of organic matter and more prominent *H. acranthus* individuals; conversely, the lower areas exhibited a higher concentration of carbonates. These results align with previous studies, which indicate that as elevation increases in coastal lomas, the percentage of humidity rises (Dillon and Rundel, 1990), along with canopy cover, photosynthetic activity, and organic matter in the soil (Rolando et al., 2017). This facilitates the germination and growth of annual plants (Tovar et al., 2018), thereby boosting the nutrient cycle, particularly the organic matter cycle (Fabre et al., 2006). Furthermore, it is worth noting that *H. acranthus* individuals were found near rocks, as they play an essential role as nurse plants, capturing more humidity, reducing the temperature, preventing erosion, and providing micronutrients to other plants (Ángel et al., 2021).

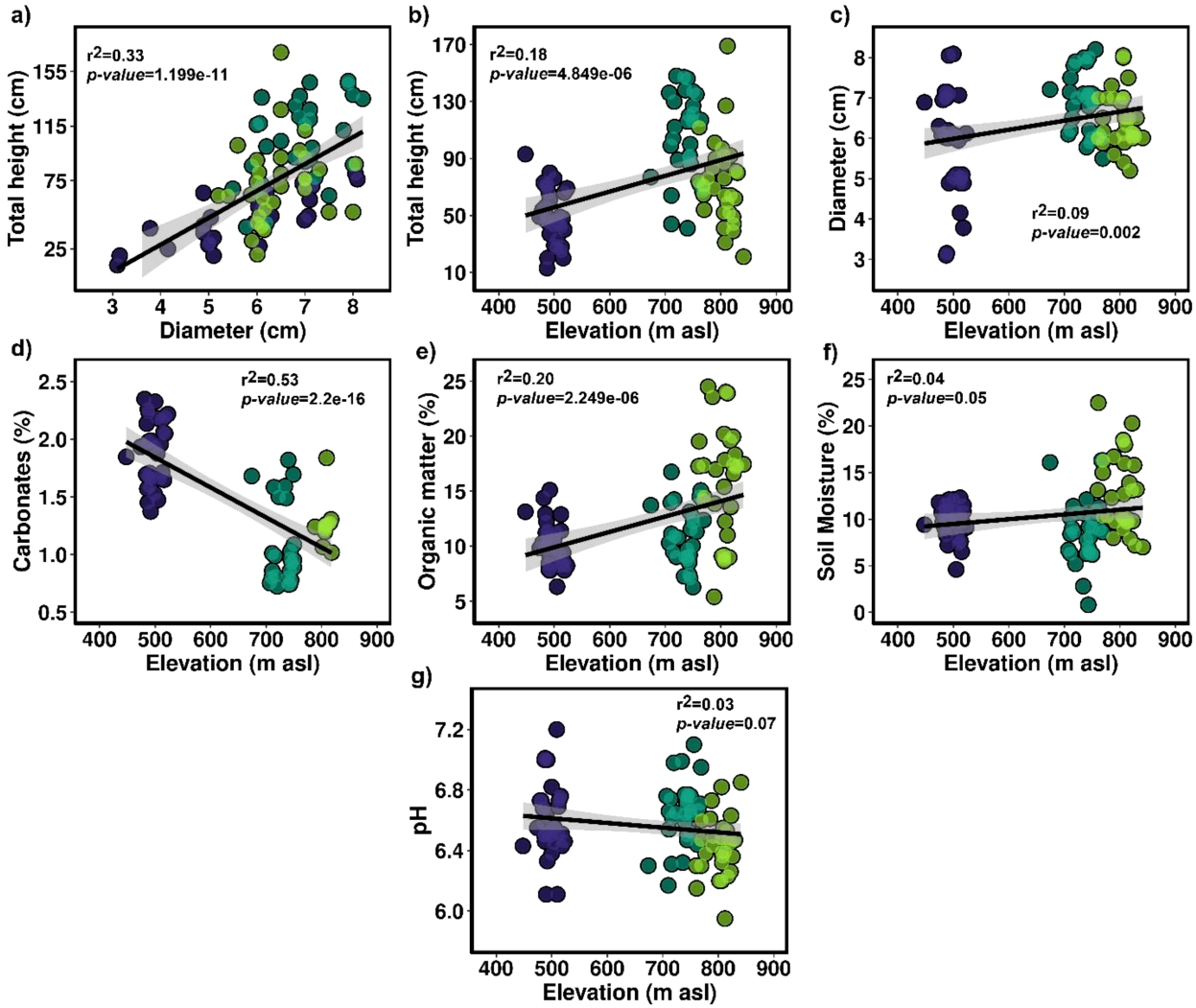

FIGURE 7
(a) Correlations between the diameter and total height of *H. acranthus*. **(b)** Correlations between elevation and the total height of *H. acranthus*. **(c)** Correlations between elevation and diameter. **(d)** Relationship between elevation and percentage of carbonates. **(e)** Correlation between altitude and organic matter. **(f)** Correlation between elevation and percentage of soil moisture. **(g)** Correlation between elevation and soil pH.

Another important aspect is the adequate soil depth and presence of organic matter; according to our measurements, its average is 6.8 cm and is accompanied by small, non-rounded stone fragments mixed with gravel and coarse sand (Kalicki and Kalicki, 2020). This type of soil provides better access for establishing cacti, which have small roots. At a certain point, this also explains the scarcity of trees in the upper part of the lomas of Mangomarca. Similarly, another crucial variable negatively affecting the area is the pH; the results indicate that an increase in pH impacts the total size and the number of stems per colony. At lower elevations, there is more significant anthropic pressure due to illegal land invasions (Camel et al., 2024), and it is essential to note that packs of dogs have been observed inhabiting and moving through the hills (per. observation). During dry periods, substantial particulate matter rises, is carried by the wind, and settles on perennial plants' biological soil crust (BSC) and the leaves and stems. These factors may alter the soil pH, leading to the progressive death of its biological organisms (Figure 4). Likewise, other studies (Gong et al., 2024; Sun et al., 2023) indicate that increased droughts and human activities negatively impact the characteristic pH of a soil type, altering the functionality of biodiversity (microorganisms, plants, animals, etc.) (Gong et al., 2024). Similarly, our results indicate that the soils of Coastal Lomas nearest to the road shift from acidic to alkaline pH, raising cacti mortality (Figures 1c, 4d). The most concerning aspect is the death of BSC microorganisms, as they are linked to the decline in soil pH; this occurs because they release protons (H^+) during photosynthesis (Jung et al., 2019), decompose organic matter (Chamizo et al., 2012), produce organic acids (such as oxalic and citric acid), and convert ammoniacal compounds into nitrates (Guida et al., 2023) all factors that contribute to acidification, especially in arid and semi-arid environments.

Despite the higher mortality rate recorded, structural studies enabled us to identify that in all colonies, there is a more significant number of stems between 20 and 40 cm, followed closely by those less than 20 cm (Figure 5). Additionally, in the highest areas, stems

exceeding 1 meter were inventoried. At the same time, the diameter averaged a maximum of 8 cm. On the other hand, unlike adult trees that reach defined heights and experience a constant increase in diameter (Kessler et al., 2014), the *H. acranthus* species maintains a defined diameter even as the longitudinal size continues to grow until it reaches the length that allows it to lean parallel to the ground, thereby reproducing in an agamic manner (Arakaki et al., 2013). We consider this an essential strategy for the species to colonize new spaces, as they can root swiftly under suitable humidity conditions. Under experimental conditions, over 45 days, the stems rooted by 4.42 cm and grew an average of 4.80 cm for a year. This could be a significant strategy for expanding the production of *H. acranthus* individuals in nurseries. Moreover, it is essential to implement strategies for exchanging individuals between different coastal lomas to enhance genetic variability within the ecosystem (Arakaki et al., 2013). It should be noted that studies on *H. acranthus* plantations regard it as a potential bioremediation agent for arid soils, effectively reducing heavy metals such as zinc, antimony, and molybdenum from the soil, and may be beneficial in restoring coastal lomas ecosystems.

On the other hand, while polyploidy in the genus *Haageocereus* may help explain the phenotypic differences, life cycle, and development among species (Arakaki et al., 2007), further research is necessary to determine its reproductive mechanisms (Cota-Sánchez and Bomfim-Patrício, 2010). Recent findings suggest that in cacti, increasing seed size is closely associated with polyploid cytotypes (Cota-Sánchez and Bomfim-Patrício, 2010). Our reports on genome and seed size indicate that *H. acranthus* (2N = 4x = 44) contained 7.94 pg of DNA (Figure 2), while the seeds measured 1.51 mm in size and weighed 0.534 mg; these results were similar to those reported by Silva (2015). In contrast, the species *H. pseudomelanostele* (2N = 2x = 22) and *H. versicolor* (2N = 2x = 22) showed smaller seeds and lower amounts of DNA in pg (Arakaki et al., 2007; Silva, 2015). Future seed studies could support this hypothesis and provide additional information on recruitment, germination, and genetic diversity, among other factors. Finally, the results of the present study offer insight into the current state of conservation of the Mangomarca hills, highlighting the importance of propagating native species for the recovery of degraded areas. This way, the various species that depend on them can be protected.

5 Conclusions

This is the first study to document a species' mortality levels and structure within the genus Haageocereus. In the Coastal Lomas of Mangomarca, 94 colonies were recorded across 4.41 ha, encompassing 1,801 stems. Of these, 37.89% of individuals had lengths between 20 and 40 cm, followed by plants smaller than 20 cm (24.82%). The largest stems of *H. acranthus* reached a diameter of 8 cm and a length of 169 cm. Across all hills, approximately 1,788 living cactus colonies and 14,741 dead colonies were counted. The mortality of cacti is likely attributed to anthropogenic impacts, as these modify the chemical and biological structure of the soil, changing its composition from acidic to basic, increasing electrical conductivity, and reducing both organic matter and nutrients. We also demonstrated that pH and altitude influence the phenotypic characteristics of *H. acranthus* stems. At higher elevations, the size of the cacti increased, along with the percentage of organic matter. At the same time, the concentration of carbonates decreased, likely due to the enhanced dynamics of annual plants during the southern winter. Additionally, *H. acranthus* has a genome size of 7.94 pg of DNA, with seeds averaging 1.51 mm in length and 0.53 mg in weight. Under nursery conditions, established stems grow approximately 4.8 cm per year, while the roots can develop up to 4.42 cm in just 45 days. Finally, mortality levels are expected to rise due to anthropogenic impacts' severity, temperature increases and decreases in precipitation resulting from climate change. Therefore, careful monitoring is necessary, and conservation and restoration actions must be proposed for these coastal lomas that are endemic to South America.

Data availability statement

The raw data supporting the conclusions of this article will be made available by the authors, without undue reservation.

Author contributions

VCa: Conceptualization, Data curation, Formal analysis, Funding acquisition, Investigation, Methodology, Project administration, Resources, Software, Supervision, Validation, Visualization, Writing – original draft, Writing – review & editing. FP: Conceptualization, Funding acquisition, Investigation, Project administration, Resources, Writing – original draft, Writing – review & editing. VCo: Investigation, Methodology, Validation, Writing – review & editing, Writing – original draft. JA: Investigation, Methodology, Validation, Writing – review & editing, Writing – original draft. JQ-H: Formal analysis, Investigation, Software, Supervision, Validation, Writing – review & editing, Writing – original draft. EF: Data curation, Investigation, Supervision, Writing – review & editing, Writing – original draft. ZN-P: Formal analysis, Investigation, Supervision, Validation, Writing – review & editing, Writing – original draft. KM-H: Data curation, Investigation, Supervision, Writing – review & editing, Writing – original draft. KC: Data curation, Investigation, Software, Supervision, Writing – review & editing, Writing – original draft. RC-T: Conceptualization, Data curation, Funding acquisition, Investigation, Resources, Supervision, Writing – review & editing, Writing – original draft.

Funding

The author(s) declare that financial support was received for the research and/or publication of this article. Universidad Cesar Vallejo funded this research. Code "P-2023-103", resolution number 185-2023-VI-UCV.

Acknowledgments

We thank the Lomas de Mangomarca Association for tireless efforts to conserve this habitat. We also thank and acknowledge the current administration of the Municipality of San Juan de Lurigancho (2023-2026) for controlling direct encroachment into an area of cultural and environmental interest, such as Lomas de Mangomarca. Finally, we thank Servicio Nacional Forestal y de Fauna Silvestre (SERFOR) for providing suggestions and corrections for a project aimed at conserving and restoring the Lomas de Mangomarca using the *H. acranthus* species, under the resolution codes "RD N° D000124-2025-MIDAGRI-SERFOR-DGGSPFFS-DGSPF, and RA N° D000103-2025-MIDAGRI-SERFOR-ATFFS LIMA.

Conflict of interest

The authors declare that the research was conducted in the absence of any commercial or financial relationships that could be construed as a potential conflict of interest.

Generative AI statement

The author(s) declare that no Generative AI was used in the creation of this manuscript.

Publisher's note

All claims expressed in this article are solely those of the authors and do not necessarily represent those of their affiliated organizations, or those of the publisher, the editors and the reviewers. Any product that may be evaluated in this article, or claim that may be made by its manufacturer, is not guaranteed or endorsed by the publisher.

Supplementary material

The Supplementary Material for this article can be found online at: https://www.frontiersin.org/articles/10.3389/fpls.2025.1577533/full#supplementary-material

References

Alcalá, B. (2021). *Nueva localidad de Haageocereus tenuis F. Ritter en el distrito de Ancón (Lima, Perú).*

Ángel, R.-R., Lauro, L.-M., and Juan Antonio, C.-R. (2021). Rocks are safe sites for establishment of Bursera seedlings in a seasonally dry tropical forest of Mexico. *J. Arid Environments* 186, 104395. doi: 10.1016/j.jaridenv.2020.104395

Arakaki, (2008). *Systematics of tribe Trichocereeae and population genetics of Haageocereus (Cactaceae)* (Gainesville, FL, USA: University of Florida).

Arakaki, M., Christin, P.-A., Nyffeler, R., Lendel, A., Eggli, U., Ogburn, R. M., et al. (2011). Contemporaneous and recent radiations of the world's major succulent plant lineages. *Proc. Natl. Acad. Sci.* 108, 8379–8384. doi: 10.1073/pnas.1100628108

Arakaki, M., Ostolaza, C., Cáceres, F., and Roque, J. (2006). Cactaceae endémicas del Perú. *Rev. Peruana Biología* 13, 193s–219s. doi: 10.15381/rpb.v13i2.1821

Arakaki, M., Soltis, D. E., and Speranza, P. (2007). New chromosome counts and evidence of polyploidy in Haageocereus and related genera in tribe Trichocereeae and other tribes of Cactaceae. *Brittonia* 59, 290–297. doi: 10.1663/0007-196X

Arakaki, M., Speranza, P., Soltis, P. S., and Soltis, D. E. (2013). Genetic variability of an unusual apomictic triploid cactus—Haageocereus tenuis ritter—From the coast of central Peru. *J. Heredity* 104, 127–133. doi: 10.1093/jhered/ess072

Balaguer, L., Arroyo-García, R., Jiménez, P., Jiménez, M. D., Villegas, L., Cordero, I., et al. (2011). Forest restoration in a fog oasis: evidence indicates need for cultural awareness in constructing the reference. *PLoS One* 6, e23004. doi: 10.1371/journal.pone.0023004

Bartoń, K. (2010). *MuMIn: Multi-Model Inference*. (R package version 0.12). Vienna, Austria: R Foundation for Statistical Computing. 1.48.11. doi: 10.32614/CRAN.package.MuMIn

Bates, D., Mächler, M., Bolker, B., and Walker, S. (2015). Fitting linear mixed-effects models using lme4. *J. Stat. Software*, 67(1):1–48. doi: 10.18637/jss.v067.i01

Bolivar, S., and Velasquez, R. (2021). *Variación de cobertura vegetal y suelo por la expansión urbana, aplicando teledetección, Lomas de Mangomarca, San Juan de Lurigancho 2000-2020* (Trujillo, Perú: Universidad Cesar Vallejo). Available online at: https://repositorio.ucv.edu.pe/handle/20.500.12692/93057 (Accessed July 7, 2025).

Bolker, B. M., Brooks, M. E., Clark, C. J., Geange, S. W., Poulsen, J. R., Stevens, M. H. H., et al. (2009). Generalized linear mixed models: A practical guide for ecology and evolution. *Trends Ecol. Evol.* 24, 127–135. doi: 10.1016/j.tree.2008.10.008

Bugaret, F. (2010). *Cactus et plantes succulentes du monde*, Versailles, Francia: Quae, Ed.

Burnham, K. P., Anderson, D. R., and Anderson, D. R. (2010). *Model selection and multimodel inference: A practical information-theoretic approach. 2. ed* (New York, NY, USA: Springer).

Calderón, N., Zappi, D., Taylor, N., and Ceroni, A. (2007). Taxonomy and conservation of haageocereus backeb. (Cactaceae) in Peru. *BioOne* 25, 45–124. doi: 10.25223/brad.n25.2007.a8

Calhoun, S. (2012). *The Gardener´s Guide to Cactus* (Portland, OR, USA: Timber_Press).

Camel, V., Quispe-Huañahue, J., Felix, E., Ninanya-Parra, Z., Mendoza, Y., Peralta-Yalta, S., et al. (2024). Effect of environmental and anthropic conditions on the development of solanum Peruvianum: A case of the coastal lomas, lima-peru. *Plants* 13, 2683. doi: 10.3390/plants13192683

Castro-Cepero, V., Eyzaguirre-Pérez, R., and Ceroni-Stuva, A. (2006). SUPERVIVENCIA DE PLÁNTULAS DE Melocactus Peruvianus Vaupel y Haageocereus pseudomelanostele subsp. Aureispinus (Rauh & Backeberg) Ostolaza, EN CONDICIONES EXPERIMENTALES. CERRO UMARCATA, VALLE DEL RÍO CHILLÓN, LIMA. *Ecología Aplicada* 5, 61. doi: 10.21704/rea.v5i1-2.318

Chamizo, S., Cantón, Y., Miralles, I., and Domingo, F. (2012). Biological soil crust development affects physicochemical characteristics of soil surface in semiarid ecosystems. *Soil Biol. Biochem.* 49, 96–105. doi: 10.1016/j.soilbio.2012.02.017

Chávez, L., Hernández, A., and Cabrera, J. (2016). Aislados de Bacillus provenientes de la rizósfera de cactus incrementan la germinación y la floración en Mammillaria spp. (Cactaceae). *Rev. Argent. Microbiología* 8, 318–325. doi: 10.1016/j.ram.2016.09.001

Cordero, I., Ruiz-Díez, B., Balaguer, L., Richter, A., Pueyo, J. J., and Rincón, A. (2017). Rhizospheric microbial community of Caesalpinia spinosa (Mol.) Kuntze in conserved and deforested zones of the Atiquipa fog forest in Peru. *Appl. Soil Ecol.* 114, 132–141. doi: 10.1016/j.apsoil.2017.02.015

Cota-Sánchez, J. H., and Bomfim-Patrício, M. C. (2010). *Seed morphology, polyploidy and the evolutionary history of the epiphytic cactus Rhipsalis baccifera* (Ciudad de México, México: Universidad Nacional Autónoma de México). doi: 10.17268/sci.agropecu.2023.002

Dillon, M. O., and Rundel, P. W. (1990). "The botanical response of the atacama and Peruvian desert floras to the 1982–83 el niño event," in *En* Elsevier Oceanography Series, vol. 52. (Amsterdam, Países Bajos: Elsevier), 487–504. doi: 10.1016/S0422-9894(08)70047-3

Doležel, J., Greilhuber, J., and Suda, J. (2007). Estimation of nuclear DNA content in plants using flow cytometry. *Nat. Protoc.* 2, 2233–2244. doi: 10.1038/nprot.2007.310

Eeckhout, P. (2004). La sombra de Ychsma. Ensayo introductorio sobre la arqueología de la costa central del Perú en los períodos tardíos. *Bulletin de l'Institut français d'études andines*. 33 (3), 403–423.

Fabre, A., Gauquelin, T., Vilasante, F., Ortega, A., and Puig, H. (2006). Phosphorus content in five representative landscape units of the Lomas de Arequipa (Atacama Desert-Peru). *CATENA* 65, 80–86. doi: 10.1016/j.catena.2005.10.004

Flood Chávez, D. I., and Niewiadomski, P. (2022). The urban political ecology of fog oases in Lima, Peru. *Geoforum* 129, 1–12. doi: 10.1016/j.geoforum.2022.01.001

Flores, S., and Van Meerbeek, K. (2024). Endangered Lomas plant communities and their potential on green roofs in Peru. *Landscape Urban Plann.* 247, 105061. doi: 10.1016/j.landurbplan.2024.105061

Gong, J., Yang, G., Zhang, S., Zhang, W., Dong, X., Zhang, S., et al. (2024). Human activities weaken the positive effects of soil abiotic factors and biodiversity on ecosystem multifunctionality more than drought: A case study in China's West Liao River Basin. *Sci. Total Environ.* 957, 177564. doi: 10.1016/j.scitotenv.2024.177564

Guida, G., Nicosia, A., Settanni, L., and Ferro, V. (2023). A review on effects of biological soil crusts on hydrological processes. *Earth-Science Rev.* 243, 104516. doi: 10.1016/j.earscirev.2023.104516

Jara-Peña, E., Quiroz, A., and Vela, A. (2024). Influencia de la luz en la germinación de semillas de 14 especies de cactáceas del Perú. *Acta Botanica Mexicana* 131. doi: 10.21829/abm131.2024.2273

Jung, P., Emrich, D., Briegel-Williams, L., Schermer, M., Weber, L., Baumann, K., et al. (2019). Ecophysiology and phylogeny of new terricolous and epiphytic chlorolichens in a fog oasis of the Atacama Desert. *MicrobiologyOpen* 8, e894. doi: 10.1002/mbo3.894

Kalicki, T., and Kalicki, P. (2020). Fluvial activity in the Lomas de Lachay during the upper Pleistocene and Holocene. *Geomorphology* 357, 107087. doi: 10.1016/j.geomorph.2020.107087

Kessler, M., Toivonen, J. M., Sylvester, S. P., Kluge, J., and Hertel, D. (2014). Elevational patterns of Polylepis tree height (Rosaceae) in the high Andes of Peru: Role of human impact and climatic conditions. *Front. Plant Sci.* 5. doi: 10.3389/fpls.2014.00194

Kuznetsova, A., Brockhoff, P. B., and Christensen, R. H. B. (2017). lmerTest package: tests in linear mixed effects models. *J. Stat. Software* 82, 1–26. doi: 10.18637/jss.v082.i13

Lim, S. D., Lee, S., Choi, W.-G., Yim, W. C., and Cushman, J. C. (2019). Laying the foundation for crassulacean acid metabolism (CAM) biodesign: expression of the C4 metabolism cycle genes of CAM in arabidopsis. *Front. Plant Sci.* 10. doi: 10.3389/fpls.2019.00101

Marcone, G., Huertas, G., Zimmer-Dauphinee, J., Van Valkenburgh, P., Moat, J., and Wernke, S. A. (2024). Late pre-Hispanic fog oasis settlements and long-term human occupation on the Peruvian central coast from satellite imagery. *Antiquity* 98, 211–228. doi: 10.15184/aqy.2023.179

Orum, T. V., Ferguson, N., and Mihail, J. D. (2016). Saguaro (Carnegiea gigantea) mortality and population regeneration in the cactus forest of saguaro national park: seventy-five years and counting. *PLoS One* 11, e0160899. doi: 10.1371/journal.pone.0160899

Ostolaza, C. (2014). *Todos los Cactus del Perú* (Lima, Perú: Ministerio del Ambiente).

Pisco, A. (2016). *Asociación Cactacea-Roca en el cerro Umarcata, valle del río chillón, Lima* (Lima, Perú: Universidad Nacional Agraria La Molina).

R Core team (2024). *R: a languague and enviroment for statistical computing* (Vienna: R Foundation for Statistical Computing). Available online at: https://www.R-project.org/ (Accessed July 7, 2025).

Rolando, J. L., Castillo, J. D. D., Padilla, D., Quinteros, Z., and Sánchez, E. (2017). Annual seasonality and diversity patterns of the plant community in a fog oasis ecosystem in the city of Lima. *Trop. Ecol.* 58, 781–791.

Salcedo, G. C. C. (2022). *Niveles de ploidía de plantas androgénicas de aguaymanto (*Physalis Peruviana *L.) asociado a caracteres citogenéticos y morfológicos* (Lima, Perú: Universidad Nacional Agraria La Molina). Available online at: http://45.231.83.156/handle/20.500.12996/5332 (Accessed May, 2022).

Sánchez, M., Hernandez, J., Caro, J., and Carreño, C. (2023). Rhizospheric actinobacteria of Opuntia sp. " Prickly pear " with deaminase activity. *Scientia Agropecuaria* 14, 21–30.

Servicio Nacional Forestal y de Fauna Silvestre [SERFOR] (2014). "Municipalidad Distrital de San Juan de Lurigancho, & Asociación de Pobladores Villa Mangomarca," in *Ficha Técnica de Campo: Propuesta de Ecosistema Frágil Loma Mangomarca* (Lima, Perú: Ministerio de Agricultura y Riego – MINAGRI). Oficio N° 647-2014-MINAGRI-DGFFS/DGEFFS.

Silva, R. (2015). *Genome size of invasive and non-invasive succulent species*. (Coimbra, Portugal: Universidade de Coimbra).

Simpalo, W., Miñan, G., Galarreta, G., and Castillo, W. (2020). "Caracterización fisicoquímica de un fruto silvestre de cactaceae (Haageocereus pseudomelanostele). Deshidratado por diferentes métodos para la conservación de su contenido de vitamina C," in *18th LACCEI International Multi-Conference for Engineering, Education, and Technology*, July 2020. Latin American and Caribbean Consortium of Engineering Institutions, Virtual Edition, 27–31. doi: 10.18687/LACCEI2020.1.1.114

Sun, W., Li, S., Zhang, G., Fu, G., Qi, H., and Li, T. (2023). Effects of climate change and anthropogenic activities on soil pH in grassland regions on the Tibetan Plateau. *Global Ecol. Conserv.* 45, e02532. doi: 10.1016/j.gecco.2023.e02532

Torre, D. (2017). *Cactus*. Reaktion Books, London, UK (distributed by University of Chicago Press, Chicago, IL, USA)

Tovar, C., Sánchez Infantas, E., and Teixeira Roth, V. (2018). Plant community dynamics of lomas fog oasis of Central Peru after the extreme precipitation caused by the 1997–98 El Niño event. *PLoS One* 13, e0190572. doi: 10.1371/journal.pone.0190572

Villanueva, R. (2018). Germinación de semillas y crecimiento de plántulas de las especies de *cactáceas del ACP Lomas del Cerro Campana, Trujillo, Perú, 2018* (Trujillo, Perú: Universidad Nacional de Trujillo).

Wickham, H. (2013). *Ggplot2 Elegant Graphics for Data Analysis* (Cham, Suiza: Springer International Publishing). doi: 10.1007/978-3-319-24277-4

Winchell, C. S., Huyvaert, K. P., Doherty, P. F., Taylor, J. M., and Grant, T. J. (2022). Ecological correlates to habitat use in the Cactus Wren (*Campylorhynchus brunneicapillus*). *Wilson J. Ornithology* 133 (3), 408–416. doi: 10.1676/19-00145

frontiers | Frontiers in Plant Science

TYPE Original Research
PUBLISHED 21 October 2025
DOI 10.3389/fpls.2025.1641811

OPEN ACCESS

EDITED BY
Yuanrun Zheng,
Chinese Academy of Sciences (CAS), China

REVIEWED BY
Emad A. Farahat,
Helwan University, Egypt
Muhammad Zain,
Yangzhou University, China

*CORRESPONDENCE
Qiqing Cheng
chengqiqing0917@163.com

†These authors have contributed equally to this work

RECEIVED 05 June 2025
ACCEPTED 08 October 2025
PUBLISHED 21 October 2025

CITATION
Li X, Li P, Li S, Hu M, Li Y, Li Y, Wang S, Shu T, Yang M and Cheng Q (2025) Assessing the impact of climate change on habitat dynamics of *Hovenia dulcis* in China using the MaxEnt model.
Front. Plant Sci. 16:1641811.
doi: 10.3389/fpls.2025.1641811

Assessing the impact of climate change on habitat dynamics of *Hovenia dulcis* in China using the MaxEnt model

Xi Li[1†], Peiyao Li[1†], Shimeng Li[1], Mingli Hu[1,2], Yankun Li[1,2], Yuanxin Li[1], Shi Wang[1,2], Ting Shu[1,2], Mingrong Yang[3] and Qiqing Cheng[1,2*]

[1]School of Pharmacy, Xianning Medical College, Hubei University of Science and Technology, Xianning, Hubei, China, [2]Hubei Engineering Research Center of Traditional Chinese Medicine of South Hubei Province, Xianning, Hubei, China, [3]Faculty of Chinese Medicine and State Key Laboratory of Quality Research in Chinese Medicine, Macau University of Science and Technology, Macau, Macao SAR, China

Introduction: *Hovenia dulcis* Thunberg, a multifunctional medicinal plant native to East and Southeast Asia, has been introduced worldwide. However, the environmental factors that determine its habitat and its precise distribution in China remain incompletely characterized.

Methods: Therefore, the Maximum Entropy (MaxEnt) model integrated with, ArcGIS was employed to predict the potential distribution of *H. dulcis* in China, using 479 initial occurrence records (which were spatially filtered to 191 points) and 33 environmental variables (of which 15 were selected for the final analysis). Model performance was assessed via AUC-ROC, with key variables identified through permutation importance and response curves. Future projections were made under SSP126 and SSP585 scenarios for the 2050s and 2090s.

Results: The model demonstrated high accuracy (AUC = 0.934). The distribution of *H. dulcis* was primarily governed by annual precipitation (Bio12), the minimum temperature of the coldest month (Bio06), elevation, and the mean diurnal temperature range (Bio02). The optimal ranges for these variables were as follows: annual precipitation of 708.5–2,956.8 mm, a minimum temperature of the coldest month between -4.9 and 8.9 °C, elevation of 273.9–1,019.4 m, and a mean diurnal temperature range of 6.81–10.18 °C. At present, suitable habitats are concentrated in central and southwestern China. Future projections indicate a northward shift and altitudinal increase in suitable areas, with expansions in Beijing, Hebei, and Liaoning, but contractions in Guangxi and Shandong. Hunan, Jiangxi, Sichuan, and Guizhou remain core suitable regions. This northward shift is consistent with preference of *H. dulcis* for the warm temperatures and adequate humidity, highlighting both its vulnerability and its adaptive potential under global warming.

Discussion: *H. dulcis* is highly sensitive to climatic variables, particularly temperature and precipitation. Our findings provide a scientific basis for developing well-targeted conservation strategies, promoting sustainable utilization, and optimizing cultivation practices for *H. dulcis* under climate change.

KEYWORDS

Maximum Entropy model, *Hovenia dulcis*, environmental variable, contribution rate, confidence importance, potential distribution area

1 Introduction

Hovenia dulcis Thunberg, a member of the Rhamnaceae family, is a multifunctional plant with significant medicinal and economic value (De Godoi et al., 2021). It is native to East and Southeast Asia and has been introduced and naturalized in North America, Australia, and New Zealand (Sferrazza et al., 2021). It is worth noting that the species has fragrant flowers and possesses large leaves, which contributes to its considerable value in urban air regulation and make it a suitable candidate for street greening. Its fruits and seeds, known as "Zhijuzi" in traditional Chinese medicine, are well supported by evidence to have hepatoprotective effects (Hyun et al., 2010). For centuries, "Zhijuzi" has been used to treat health conditions such as fever, excessive thirst, alcohol poisoning, and urinary disorders. Pharmacological studies have confirmed its broad bioactive properties, especially its ability to reduce blood alcohol levels and enhance alcohol metabolism (Meng et al., 2020), while exhibiting significant antioxidant activity that mitigates alcohol-induced oxidative stress (Tomczyk et al., 2012). The phytochemical profile of *H. dulcis* is remarkably diverse, comprising constituents such as flavonoids, terpenoids, fatty acids, saponins, and polysaccharides, which exhibit potential therapeutic effects against a range of liver diseases, particularly those associated with alcohol consumption (Li et al., 2021; He et al., 2024).

Global warming profoundly affects ecosystems worldwide and threatens both the geographic distribution and long-term persistence of medicinal plant species. As climatic change increasingly accelerates in rate and magnitude, assessing its impacts has become an urgent matter that needs to be prioritized (Thomas et al., 2004). In China, changes in climatic conditions have intensified the occurrence of extreme meteorological events. The frequency and severity of such events are both on the rise, exerting a profound impact on the ecological environment and threatening the natural habitats of numerous plant species. Environmental variables, especially temperature, precipitation, and elevation, together with human activities, fundamentally shape the distribution and quality of medicinal plants. The prediction output of species distribution models under future climate scenarios largely depends on method selection (e.g., algorithm selection and predictor curation) and climatic uncertainties (e.g., divergent projection ranges and greenhouse gas trajectories) (Porfirio et al., 2014). Forecasting the potential geographical distribution of species under climate change conditions is essential for biodiversity conservation and the sustainable utilization of resources (Guisan and Thuiller, 2005).

Species distribution models (SDMs) offer critical insights into the exploration and prediction of species distribution and play an essential role in understanding and conserving global biodiversity (Niiya et al., 2024). Various SDMs are commonly used to assess potential species habitats, including Maximum Entropy (MaxEnt), Boosted Regression Trees (BRT), Random Forests (RF), Generalized Additive Model (GAMs), and Generalized Linear Model (GLMs) (Melo-Merino et al., 2020). According to statistical analyses, the MaxEnt model is the most widely used (Khan et al., 2022). Since its introduction in 2006, it has become a mainstream approach in species distribution modeling (Phillips et al., 2006). By applying the principle of maximum entropy, it effectively identifies the most influential environmental factors, even under complex ecological conditions (Cao et al., 2021). There are three main reasons why the MaxEnt model stands out. First of all, it is specifically designed for presence-only data, which is particularly valuable for medicinal plants with insufficient sampling. Secondly, it performs reliably with small sample sizes of as few as 25 records, while minimizing overfitting through built-in regularization (Phillips and Dudík, 2008). Finally, its logistic output generates continuous probability surfaces, facilitating the interpretation of protection planning. Therefore, MaxEnt has been widely applied in disciplines such as conservation biology and ecology (Kumar et al., 2022; Shen et al., 2023).

To examine the current and future distribution patterns of *H. dulcis* across China, this study integrates species occurrence records with climatic, soil and topographic variables. Using MaxEnt model in combination with ArcGIS spatial analysis, we reconstruct habitat suitability during the Last Glacial Maximum (LGM) and Mid-Holocene (MH) scenarios, evaluate current suitability from 1970 to 2000, and project future distributions for the 2050s and 2090s. The study aims to achieve four key objectives: (1) to simulate the current potential distribution and delineate suitable habitats of *H. dulcis*; (2) to identify the dominant ecological variables that control its geographical scope; (3) to forecast shifts in suitable habitats for

the 2050s and 2090s through analyses of response curves and permutation importance; and (4) to elucidate optimal growth conditions, thereby providing a theoretical foundation for conservation and sustainable utilization strategies.

Additionally, these findings will support the development of strategies for the protection, cultivation, and sustainable utilization of *H. dulcis*, thereby ensuring its long-term survival and ecological contributions under global warming. By delineating optimal habitats and identifying the dominant environmental variables, the study elucidates both the most favorable growth conditions and the potential impacts of climate change (Li and Park, 2020). These insights will strengthen the conservation and management of *H. dulcis* resources, ensuring their continuous availability for both medicinal and economic applications.

2 Materials and methods

2.1 Acquisition and screening of *H. dulcis* distribution data

To systematically investigate the distribution of *H. dulcis*, occurrence data were retrieved from major online botanical databases, including the Chinese Virtual Herbarium (CVH, https://www.cvh.ac.cn/) and the China National Specimen Information Infrastructure (NSII, http://www.nsii.org.cn/). A total of 479 occurrence records across China were compiled (Supplementary Table S1). To remove duplicate and ambiguous entries, records lacking precise geographical coordinates were georeferenced using the Baidu Coordinate Pickup System (http://api.map.baidu.com/lbsapi/getpoint/index.html) (Fan et al., 2014). This process resulted in 254 accurately georeferenced occurrence points (Supplementary Table S2). To reduce overfitting caused by sampling bias, spatial filtering was performed in ArcGIS 10.4.1. A 10 km buffer was generated around each point, and within every 20 km diameter circle, a single presence record was randomly retained. The filtering procedure was determined primarily by three considerations: the ecological traits of *H. dulcis*, a deciduous tree with animal-assisted seed dispersal, which justify the use of a 10 km buffer to account for local clustering (Zhou et al., 2013); the spatial resolution of environmental variables, such as bioclimatic, soil and topographic variables exhibits spatial autocorrelation within 10 km, making a 20 km zone appropriate for capturing environmental variation (Pokharel et al., 2016); methodological consistency, as similar filtering thresholds of 10–20 km have been widely applied to medicinal plants such as *Panax notoginseng*, *Piper kadsura*, and *Magnolia biondii* to balance ecological accuracy with bias control (Guo et al., 2025; Li et al., 2025). This procedure yielded 191 validated occurrence points (Figure 1; Supplementary Table S3), which were formatted into a CSV file containing the species name, longitude, and latitude for subsequent modeling. According to the NSII platform and Flora of China, these records were primarily distributed across central, eastern and southwestern China. The highest numbers of records were from Henan (66 points), Jiangxi (64 points), Guizhou (40 points), Shandong (33 points), Shaanxi (28 points), Hebei (23 points), Sichuan (22 points), Hunan (20 points), Guangxi (19 points), Fujian and Zhejiang (17 points each), Anhui (16 points), and Hubei (13 points).

2.2 Acquisition and screening of environmental variables influencing suitable habitats

Nineteen bioclimatic variables were obtained from the WorldClim database (http://www.worldclim.org). The soil variables utilized in our study were collected from the World Soil Database hosted on the FAO Soils Portal (http://www.fao.org/soils-portal/data-hub/en/), totaling 11 distinct parameters. The topographic variables were sourced from the WorldClim website (https://www.worldclim.org/), amounting to 3 variables (Ouyang et al., 2022). Overall, these 33 independent environmental variables form a comprehensive dataset that has been carefully selected and prepared for the ecological analyses outlined in Table 1. We adopted the 1970–2000 climate dataset as our baseline, supplemented with historical climate data from LGM and MH scenarios, as well as future climate projections for 2041–2060 and 2081–2100 under different emission scenarios. For future climate projections, we used the CMIP6-based Shared Socioeconomic Pathways (SSPs) framework, which defines alternative socio-economic and climate change scenarios. Among them, SSP126 represents a low-emission scenario and SSP585 represents a high-emission scenario, both are widely used to predict climate change impacts on species distributions (Karuppaiah et al., 2023). These scenarios have been employed in numerous ecological predictions, including the research on medicinal plants such as *Zingiber striolatum* and various pests and plants (Huang et al., 2024; Mao et al., 2024). While intermediate scenarios aid in a more comprehensive understanding of impacts across different emission trajectories, many studies (including ours) have chosen extreme scenarios to simplify analysis and conserve computational resources (Zheng et al., 2022).

2.3 Correlation analysis and determination of key environmental variables for adaptation

To mitigate multicollinearity among environmental variables and reduce the risk of overfitting, we calculated Spearman's rank correlations in SPSS 26.0. We excluded any variable that exhibited $|r| > 0.8$ with another variable and whose permutation-based variable importance score contributed < 5% to the ensemble model. According to the describe screening procedure (Zhang et al., 2020), 15 variables for the *H. dulcis* distribution model were finally selected. It included 7 bioclimatic variables (Bio_2, Bio_3, Bio_4, Bio_6, Bio_8, Bio_10, and Bio_12), 5 edaphic variables (top-soil organic carbon, sub-soil organic carbon, calcium carbonate content, sand, and clay fractions), and 3 topographic variables (elevation, slope, and aspect).

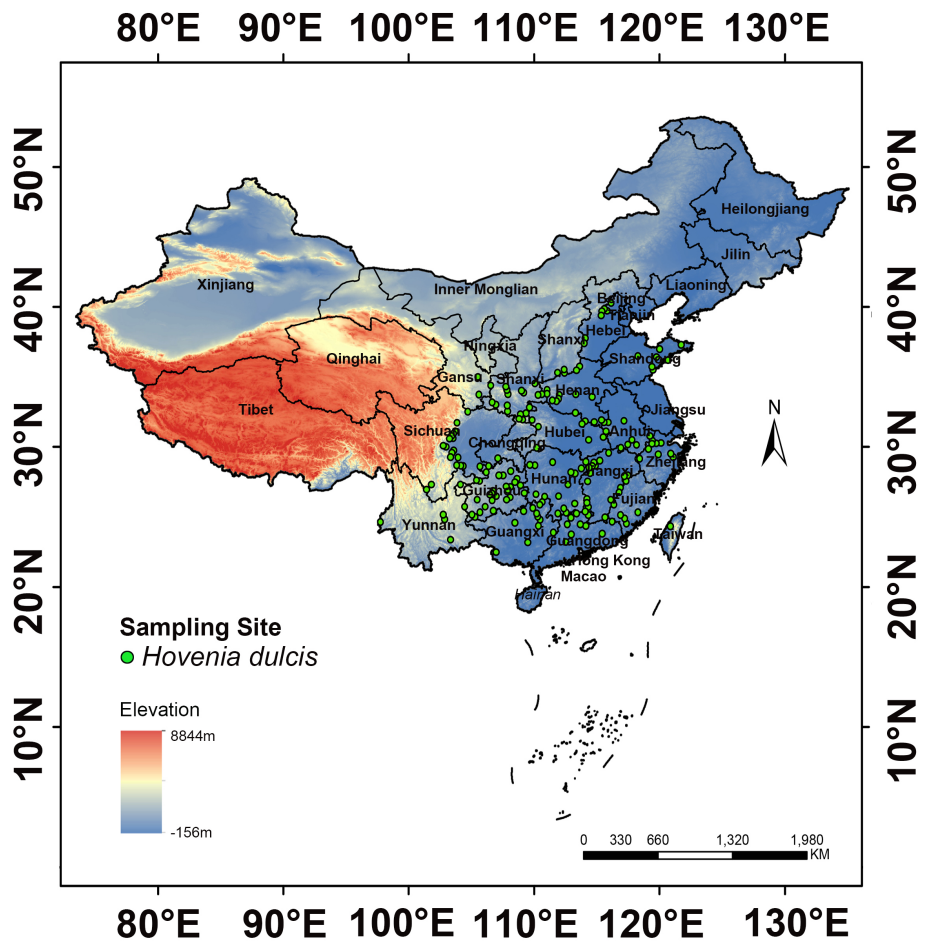

FIGURE 1
Distribution map of *H. dulcis*.

2.4 Construction of the MaxEnt model

Climate variables and species-occurrence records of *H. dulcis* were inputted into MaxEnt, with the parameters set as: bootstrap resampling, logistic output, and the default regularization multiplier of 1. This follows common practices in similar studies when lacking species-specific tuning data, and preliminary tests showed no significant performance improvement with adjustments (Zhan et al., 2022). Although the logistic output was optional in MaxEnt, it yielded an estimate of occurrence probability that is more readily interpretable (Elith et al., 2011). And 75% of the occurrence records were randomly selected as the training set, and the remaining 25% were used as the test set to evaluate the model performance. Each bootstrap replicate was run for 1000 iterations, which was consistent with the default setting commonly used in species distribution modeling studies (Pischl et al., 2020), and the ensemble average of 10 replicates was adopted as the final prediction (Syfert et al., 2013).

Raster outputs for *H. dulcis* were imported into ArcMap 10.4.1 and reclassified using the natural-breaks method (Bergamin et al., 2022). Subsequently, the area under the receiver operating characteristic curve (AUC-ROC) was used to evaluate the validity of the model. As a threshold-independent metric, AUC-ROC has been emphasized in recent studies for evaluating the MaxEnt model (Ahmadi et al., 2023). The predictive accuracy of model was classified according to standard AUC thresholds, <0.6 indicated failure, 0.6–0.7 represented poor, 0.7–0.8 showed moderate, 0.8–0.9 demonstrated good, and 0.9–1.0 means excellent predictive performance (Ottó and Végvári, 2022).

2.5 Model evaluation and habitat classification

The Jackknife method was used to evaluate the relative influence of individual environmental variables on the distribution of *H. dulcis* (Hong et al., 2021). Response curves of the most influential variables were generated to visualize the environmental preferences of species (Yan et al., 2020; Son et al., 2023). Ranking importance quantified model sensitivity to each variable by randomly changing its values across training and background data, with higher values indicating greater influence (Ma et al., 2024).

In species distribution modeling and habitat classification, the Maximum Test Sensitivity plus Specificity (MTSPS) threshold was widely applied to distinguish suitable from unsuitable habitats

TABLE 1 Description of environmental variables.

Variable	Description	Variable	Description
Bio1	Annual average temperature (°C)	Bio18	Precipitation of warmest quarter (mm)
Bio2	Mean diurnal range (mean of monthly (max temp - min temp)) (°C)	Bio19	Precipitation of coldest quarter (mm)
Bio3	Isothermality (bio2/bio7) (× 100)	awc_class	Soil available water content
Bio4	Temperature seasonality (standard deviation × 100)	s_caco3	Topsoil calcium Carbonate (%wt)
Bio5	Max temperature of warmest month (°C)	s_clay	Substrate-soil clay content (%wt)
Bio6	Min temperature of coldest month (°C)	s_oc	Substrate-soil organic carbon (%wt)
Bio7	Annual temperature span (bio5-bio6) (°C)	s_ph_h2o	Substrate-soil pH
Bio8	Mean temperature of wettest quarter (°C)	s_sand	Sediment content in the subsoil (%wt)
Bio9	Mean temperature of driest quarter (°C)	t_caco3	Topsoil carbonate or lime content (%wt)
Bio10	Mean temperature of warmest quarter (°C)	t_clay	Clay content in the upper soil (%wt)
Bio11	Mean temperature of coldest quarter (°C)	t_oc	Topsoil organic carbon (%wt)
Bio12	Annual precipitation (mm)	t_ph_h2o	Topsoil pH
Bio13	Precipitation of wettest month (mm)	t_sand	Sand content (%wt)
Bio14	Precipitation of driest month (mm)	aspect	Aspect
Bio15	Precipitation variability (coefficient of variation)	elev	Elevation (m)
Bio16	Rainfall of wettest quarter (mm)	slope	Slope (°)
Bio17	Precipitation of driest quarter (mm)		

because of its practicality and effectiveness. The mean of the ten MTSPS values was then adopted as the determination threshold, and habitat suitability was classified into four categories: unsuitable (0–MTSPS), low suitability (MTSPS–0.3), medium suitability (0.3–0.5), and high suitability (0.5–1) (Aligaz et al., 2024). This procedure ensured that the threshold is derived exclusively from data not used in training, minimizing overfitting and ensuring the objectivity and generalizability of the classification criterion, in line with best-practice recommendations in species-distribution modeling. The occurrence probability of *H. dulcis* was projected throughout China. Furthermore, the suitability models were applied to seven different scenarios to generate corresponding distribution maps, including the Last Glacial Maximum (LGM), Mid-Holocene (MH), current, and future projections for the 2050s and 2090s under both SSP126 and SSP585. Based on the MTSPS classification standard, the areas of medium- and high-suitability habitats were calculated, and their sum was determined as the total suitable habitat area (Zhang et al., 2023; Yang et al., 2024).

2.6 Analysis of the area changes of the suitable habitat of different provinces in China

The provincial boundary shapefile of China (Review Map No.: GS(2019)1822) was imported into ArcMap 10.4.1. Habitat suitability rasters (.asc) for each period were converted to GeoTIFF (.tif) format with FLOAT data type. After assigning the WGS_1984 geographical coordinate system, the data were projected to WGS_1984_Albers for accurate area measurement. Provincial attribute tables were updated with the corresponding province names. Then, the continuous suitability data were reclassified into four categories: unsuitable, low suitability, medium suitability, and high suitability. The regional geometry tool calculated categorical areas within each province. The results were exported as dBASE files for quantitative analysis in Excel. Under different scenarios, the growth rate of suitable habitat area for each province was calculated as the percentage increase relative to the current suitable habitat area. Venn diagrams were generated using Microbioinformatics (http://www.bioinformatics.com.cn/) to visualize provincial habitat distribution patterns (Tang et al., 2023).

2.7 Statistical correlation with climatic variables

To explore the potential drivers of observed habitat changes, provincial-level meteorological data for 2021, 2022, and 2024 (2023 data were unavailable) were obtained from the National Meteorological Science Data Center (https://data.cma.cn/; Supplementary Table S6). Spearman's rank correlation analysis was performed in Origin to quantify the relationships between provincial rates of habitat expansion or contraction and key climatic variables. The statistical significance of the correlations was evaluated using a p-value threshold of 0.05. The results were visualized as correlation heatmaps.

3 Results

3.1 Model accuracy analysis

The potential distribution of *H. dulcis* was predicted using the MaxEnt model. The model was run for 10 replicates, and the results were combined into an ensemble average. Model performance was assessed using the area under the receiver operating characteristic curve (AUC). To address potential overfitting issue that may caused by multicollinearity, we performed a Spearman's rank correlation analysis on all 33 environmental variables.

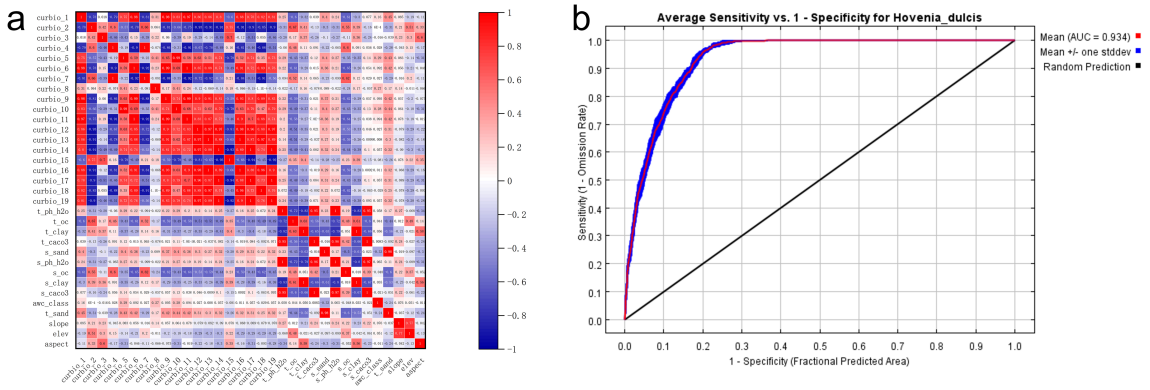

FIGURE 2
Prediction of the suitable habitat of *H. dulcis* based on the MaxEnt model and analysis of environmental variables. **(a)** Correlation heatmap related to environmental variables of *H. dulcis*; **(b)** ROC curve of the MaxEnt model.

In this study, the average training AUC for *H. dulcis* was 0.934 (Figure 2b), while the test AUC based on an independent subset of 25% of occurrence records was 0.921. Both values exceeded 0.9, indicating excellent predictive performance and strong model reliability. The approach applied in this study effectively identified key environmental variables shaping species distribution, which was in line with established methods of ecological modeling.

3.2 Identification of key environmental variables

Using the MaxEnt algorithm, the relative contributions of 15 environmental variables to the species distribution model were evaluated based on percentage contribution and permutation importance. In Table 2, Annual precipitation (Bio12) was the most influential factor (39.5%), followed by the minimum temperature of the coldest month (Bio06, 31.1%). Additional variables with measurable effects included slope (9.4%) and isothermality (Bio03, 5.8%), while the contributions of all remaining variables were minor (≤2.8%). Through the assessment of permutation importance, reflecting the sensitivity of the model, the primary influence of Bio06 (31.2%), elevation (16.9%), and Bio12 (16.6%) were confirmed, highlighting their critical roles in shaping the distribution of *H. dulcis*.

The Jackknife test further underscored the critical importance of these variables for mapping suitable habitats for *H. dulcis* across China. Specifically, Bio06 (Minimum Temperature of the Coldest Month), Bio02 (Mean Diurnal Range), and Bio12 (Annual Precipitation) emerged as the most influential variables governing its distribution (Figure 3a). Therefore, the distribution of the species was mainly driven by extreme temperatures, diurnal temperature variation, annual precipitation, and topography (elevation).

Response curve analysis (Figure 3b) identified the optimal ranges and threshold values of the key environmental variables that restrict the distribution of *H. dulcis*. The appropriate ranges and corresponding optimum values were: annual precipitation of 708.45–2956.80 mm (Bio12; optimum: 1985.02 mm), minimum temperature of the coldest month from –4.93 to 8.92°C (Bio06; optimum: 4.20°C), elevation between 273.85 and 1019.40 m (optimum: 681.21 m), and mean diurnal temperature range of 6.81–10.18 °C (Bio02; optimum: 8.13°C). Within these intervals, the probability of species occurrence increased toward the optimum value, whereas values beyond these thresholds resulted in a reduced probability of occurrence. Overall, temperature-related variables, precipitation, and elevation were the primary environmental driving factors affecting the distribution of *H. dulcis*.

3.3 Distribution prediction of *H. dulcis* under current climate conditions

The predicted distribution of suitable habitats for *H. dulcis* under current climate conditions was visually summarized in Figure 4. Habitat suitability was classified into four categories: unsuitable (gray), low-suitable (green), medium-suitable (yellow), and high-suitable (red). It is primarily distributed between 30°N–37°N latitude and 101°E–123°E longitude, delineating its overall suitable habitat range. The total suitable area was estimated at 147.70×10^4 km², accounting for 15.39% of China's land area, among which high-suitable habitats accounted for 35.23%. The total suitable habitat area of *H. dulcis* was relatively concentrated, primarily located at the intersection of central, southwestern, and northwestern China, as well as coastal regions of eastern and southern China. No suitable habitats were predicted in the northernmost parts of the country. Occurrence records further indicate that *H. dulcis* predominantly occupies low- to mid-elevation hilly terrain, particularly around the Sichuan Basin. This predicted distribution was consistent with the range of the species' native habitats recorded in the *Flora of China*, and also closely corresponded to the specimen records of the herbarium from 1950 to 2020. By contrast, unsuitable habitats were mostly located in northeastern, northern, and northwestern China, which might be due to the limitations of climatic factors.

10.3389/fpls.2025.1641811

TABLE 2 Percent contribution and permutation importance of the dominant environmental variables in the MaxEnt model.

Variable	Description	Percent contribution (%)	Permutation importance (%)
bio12	Annual precipitation	39.5	16.6
bio06	Min temperature of coldest month	31.1	31.2
slope	Slope	9.4	10.3
bio03	Isothermality ((Bio02/Bio07) * 100)	5.8	3.5
elev	Elevation	2.8	16.9
aspect	Aspect	2.5	2.2
bio02	Mean diurnal range (mean of monthly (max temp - min temp))	2.0	3.0
bio04	Temperature seasonality	1.5	4.5
s_clay	Substrate-soil clay content	1.5	2
s_caco3	Topsoil calcium Carbonate	1.3	2.7
bio08	Mean temperature of wettest quarter	1.1	1.4
s_sand	Sediment content in the subsoil	0.8	3.7
s_oc	Substrate-soil organic carbon	0.5	0.5
t_oc	Topsoil organic carbon	0.3	0.4
bio10	Mean temperature of warmest quarter	0.2	0.8

3.4 Distribution prediction under past and future climates

The past and future predicted distribution patterns of *H. dulcis* were summarized in Table 3 and Figures 5, 6. Under the LGM and MH scenarios, the total area of suitable habitat was markedly restricted, with most habitats classified as low suitability (Figures 6a, b). Although the MH scenario showed a wider range of suitable environments than the LGM scenario, no high-suitable habitats were detected, and medium-suitable habitats remained limited. This pattern was consistent with the key climatic variables identified to affect the distribution of *H. dulcis*, especially the minimum temperature of the coldest month and annual precipitation.

At present, the suitable habitat area of *H. dulcis* has expanded considerably. High-, medium-, and low-suitable habitats covered 52.04×10^4 km², 95.66×10^4 km², and 62.64×10^4 km² respectively (Figure 5). These findings indicated that contemporary climatic conditions are favorable for its survival. The core distribution area was in subtropical monsoon zones, with hot and humid summers

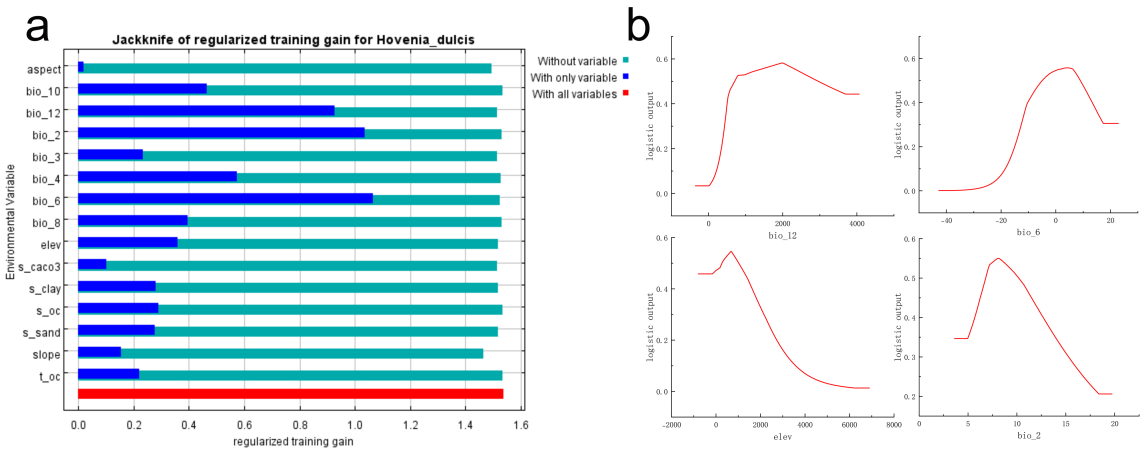

FIGURE 3
Prediction of the suitable habitat of *H. dulcis* based on the MaxEnt model. **(a)** Jackknife test of environmental variables; **(b)** Response curve of key influential variables.

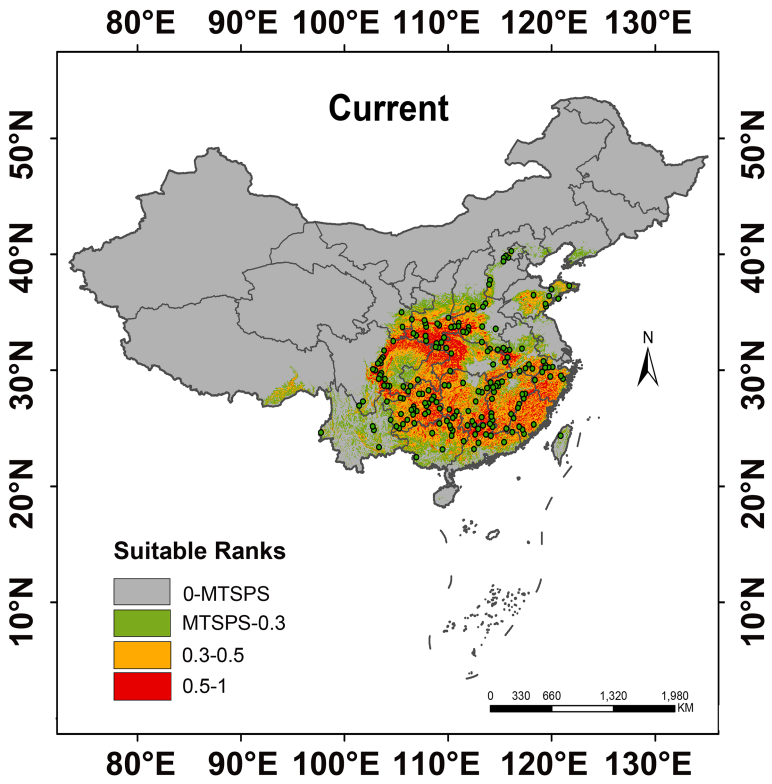

FIGURE 4
Distribution of suitable habitats for *H. dulcis* in the current scenario.

and mild and moist winters. Such climatic conditions were consistent with the key environmental variables identified in the response analysis.

Future projections indicated a general contraction of suitable habitats (Figures 6c-f). Under the SSP126 scenario, it was expected that the appropriate area will initially decrease and then rebound slightly, but it would still be lower than the current levels. Between 2041 and 2060, the total suitable area was expected to decline by 3.91% to 141.92 × 10^4 km^2. Medium-suitable habitats were projected to decrease by 8.69%, whereas low- and high-suitable habitats were expected to increase by 11.40% and 4.86% respectively.

From 2081 to 2100, the estimated total suitable area was 143.17 × 10^4 km^2, a decrease of 3.07% compared to current conditions. During this period, low- and high-suitable habitats were expected to increase by 13.68% and 2.00% respectively, whereas medium-suitable habitats were projected to decline by 5.82%. However, under the SSP585 scenario, the loss of suitable habitat was predicted to be more pronounced. Between 2041 and 2060, the total suitable area was projected to decline by 4.91% to 140.45 × 10^4 km^2. Low-suitable habitats were expected to increase by 20.18%, while medium- and high-suitable habitats decreased by 5.93% and 3.04% respectively. It was estimated that from 2081 to 2100, the total suitable area will decline sharply by 19.35% to 119.12 × 10^4 km^2. Among them, the low-suitable habitats increased by 44.46%, medium-suitable habitats decreased by 10.18%, and high-suitable habitats declined by 36.18%. Collectively, these projections indicated that global warming will substantially reduce the environmental suitability for *H. dulcis* survival.

3.5 Provincial distribution of suitable habitats for *H. dulcis* under current climate condition

Under current climatic conditions, the distribution of suitable habitats for *H. dulcis* varied considerably across Chinese provinces and was broadly spread across many regions (Supplementary Table S4). No suitable habitats were found in Heilongjiang, Shanghai, Xinjiang, or Macau SAR, while other provinces had suitable habitats to varying degrees. Medium-suitable habitats were concentrated in central and western China, while high-suitable habitats were distributed across western, central, and eastern regions. As shown in Table 1, Yunnan Province had the largest area of low-suitable habitat, covering 199,295.91 km^2. The Guangxi Zhuang Autonomous Region contained the largest extent of medium-suitable habitat (95,434.07 km^2), followed by Hunan (95,047.70 km^2), Sichuan (82,345.70 km^2), Guizhou (79,979.16 km^2), and Jiangxi (73,048.60 km^2). All other provinces contained less than 60,000 km^2 of medium-suitable habitat.

Hunan Province contained the largest area of high-suitable habitat, covering 85,364.23 km^2, followed by Guizhou (79,544.49 km^2), Sichuan (75,656.62 km^2), Hubei (74,714.83 km^2), Jiangxi (70,778.66 km^2), Shaanxi (65,079.66 km^2), and Fujian (62,495.80

10.3389/fpls.2025.1641811

TABLE 3 Statistics on the area of the suitable habitat of *H. dulcis* in different periods.

Period		Unsuitable habitat		Low-suitable habitat		Medium-suitable habitat		High-suitable habitat	
		Area (*10^4 km^2)	Percentage (%)	Area (*10^4 km^2)	Percentage (%)	Area (*10^4 km^2)	Percentage (%)	Area (*10^4 km^2)	Percentage (%)
LGM		927.45	96.61	31.04	3.23	1.51	0.16	0	0
MH		913.91	95.20	44.39	4.62	1.70	0.18	0	0
Current		749.66	78.09	62.64	6.53	95.66	9.96	52.04	5.42
2050s	SSP126	748.30	77.95	69.78	7.27	87.35	9.10	54.57	5.68
	SSP585	744.27	77.53	75.28	7.84	89.99	9.37	50.46	5.26
2090s	SSP126	745.62	77.67	71.21	7.42	90.09	9.38	53.08	5.53
	SSP585	750.38	78.16	90.49	9.43	85.92	8.95	33.21	3.46

km^2). Each of the remaining provinces has less than 60,000 km^2 of high-suitable habitat. Under the current climatic conditions, the combination of medium- and high-suitable habitats indicated that Hunan, Guizhou, Sichuan, and Jiangxi are the most suitable regions for the growth of *H. dulcis*.

3.6 Changes in the suitable habitat of *H. dulcis* under SSP126 and SSP585 scenarios

Further analysis of Figure 6 and Supplementary Table S5 illustrated changes in suitable habitats of *H. dulcis* under two future climate scenarios. Under the SSP126 scenario, suitable habitats across China were projected to expand in both the 2050s and the 2090s. Hebei, Liaoning, Ningxia, and Beijing exhibited continuous and significant expansion during both periods, with Hebei showing the greatest increase (216.93%) by the 2090s. In the 2050s, Shanxi and Gansu displayed the highest growth rates (70.03% and 33.67%, respectively), whereas Guangxi and Guangdong experienced declines of 23.40% and 17.70%. Among provinces with suitable habitat areas exceeding 15,000 km^2, more exhibited habitat loss than expansion, while those below this threshold showed more variable patterns. By the 2090s, the reductions in Guangxi and Guangdong intensified to 30.53% and 21.18% respectively. Chongqing shifted from habitat reduction in the 2050s to expansion in the 2090s, while Yunnan followed the opposite trend. Overall, the number of provinces experiencing habitat loss exceeded those with gains, and the spatial pattern of habitat expansion and contraction remained largely consistent throughout the two periods.

Under the SSP585 scenario, Liaoning Province exhibited an exceptionally high growth rate of 1,936.36% by the 2090s, mainly due to the small baseline habitat area under current conditions. Therefore, even a moderate absolute increase resulted in a disproportionately high relative growth rate. Hebei, Shanxi, and Gansu also witnessed substantial increases, reaching 284.98%, 147.01%, and 121.36%, respectively, whereas Shandong and Guangxi saw an accelerated declines of 58.79% and 51.13%. Guizhou and Yunnan displayed more dynamic trends, with initial increases in the 2050s followed by declines in the 2090s. Among provinces with suitable areas exceeding 15,000 km^2, the numbers of those gaining and losing habitats were roughly comparable, yet a net contraction was observed at the national scale. Both scenarios consistently revealed obvious north-south differences, with an increase in suitability in northern China and a decrease in suitability in southern regions.

According to statistical analysis, in both current and future scenarios, the suitable habitat in 17 provinces exceeded 15,000 km^2 (Figure 7a). Among them, it was expected under future climate conditions, the temperatures in six provinces including Hebei, Shanxi, Jiangxi, Hunan, Shaanxi, and Gansu will continue to exceed current habitat levels (Figures 7b, 8a). In contrast, Zhejiang, Anhui, Fujian, Shandong, Henan, Hubei, Guangdong, Guangxi, and Sichuan were expected to experience reductions in habitat suitability relative to current levels (Figure 8b). Guizhou, Yunnan, Chongqing, and Tibet maintained relatively

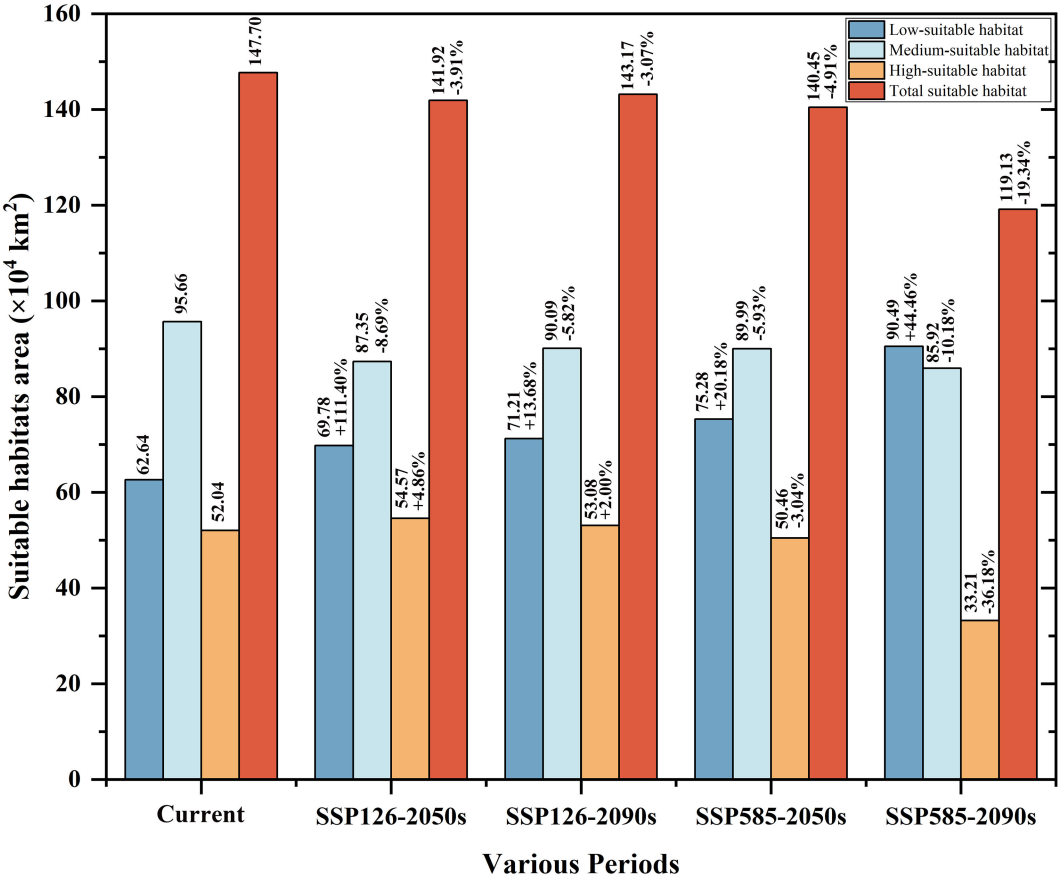

FIGURE 5
Suitable habitat area of *H. dulcis* under future climate conditions and the change in area compared to the current climate.

stable suitable habitat areas, with only minor fluctuations under both present and future conditions (Figure 8c). It was worth noting that Beijing, Hebei, Liaoning, and Ningxia are expected to see a significant increase, while Jilin, Heilongjiang, and Qinghai are expected to see new suitable habitats, indicating a northward and mid-latitude shift in the potential distribution of *H. dulcis* (Figure 8d). In all scenarios, Hunan remained the most suitable province, while Jiangxi also sustained a large and continuously expanding area of suitable habitats. Although Guizhou and Sichuan were projected to lose some suitable area, they still maintained a relatively high degree of suitability.

3.7 Relationship between provincial habitat change and climatic variables

Analysis of meteorological conditions across provinces revealed that the projected change (future/current) in suitable habitat area for *H. dulcis* correlated positively with temperature, which was consistent with the thermophilic nature of this species (Figure 9). In contrast, the change rate showed significant and negative correlations with both precipitation and air humidity. This suggested that excessive moisture inhibits its growth, which might explain its absence in coastal regions. A weak positive correlation with wind speed implied that moderate winds may enhance gas exchange and stimulate physiological activity. Elevation exerted an indirect influence on distribution by interacting with topography and wind speed. Terrain features such as slopes and valleys altered local wind patterns, thereby modifying microclimatic conditions (such as temperature and moisture retention), which are crucial for *H. dulcis* survival. These findings aligned with prior analysis of key environmental variables, reaffirming the critical roles of temperature, precipitation, and elevation in determining habitat suitability. Consequently, our results supported the prediction of an overall range contraction for *H. dulcis* under future climate warming scenarios.

In summary, the priority provinces for future cultivation of *H. dulcis* included Hunan, Jiangxi, Hebei, Liaoning and Beijing, where the suitable habitat areas continued to expand. Meanwhile, attention should be paid to provinces such as Guizhou and Sichuan, where the suitable area was decreasing but still maintained high suitability.

4 Discussion

4.1 Reliability of MaxEnt model prediction

Species distribution models serve as the significant tool for assessing the impacts of climatic and environmental changes on

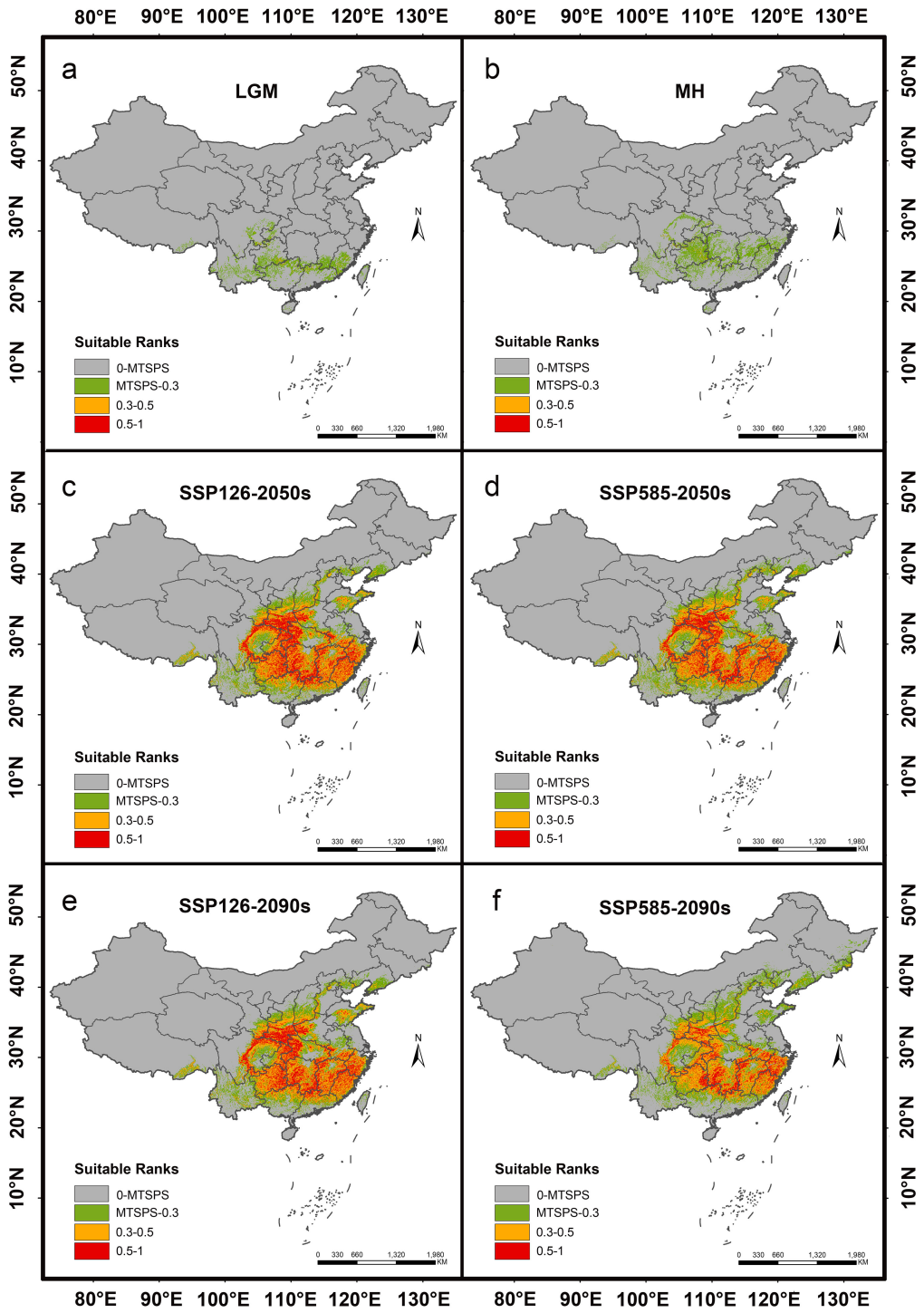

FIGURE 6
Distribution of suitable habitats for *H. dulcis* under different climate scenarios. **(a)** Last Glacial Maximum (LGM); **(b)** Mid-Holocene (MH); **(c)** 2041–2060 (2050s) average, SSP126; **(d)** 2041–2060 (2050s) average, SSP585; **(e)** 2081–2100 (2090s) average, SSP126; **(f)** 2081–2100 (2090s) average, SSP585.

habitat suitability (Wiens et al., 2009). Among them, MaxEnt model is regarded as one of the most frequently used ecological niche models in current studies, especially for presence-only data (Phillips and Dudík, 2008). This makes *H. dulcis* highly suitable for study, as a medicinal plant that has not received sufficient attention in biodiversity surveys. Our dataset contains 191 verified occurrence records. Although these records are spatially sparse, the robustness of the MaxEnt model effectively mitigates this limitation.

This study takes climatic conditions, edaphic properties, and topographical features as the main environmental variables and uses spatial modeling methods to predict the optimal habitat range of *H. dulcis*. However, the accuracy of the model predictions is

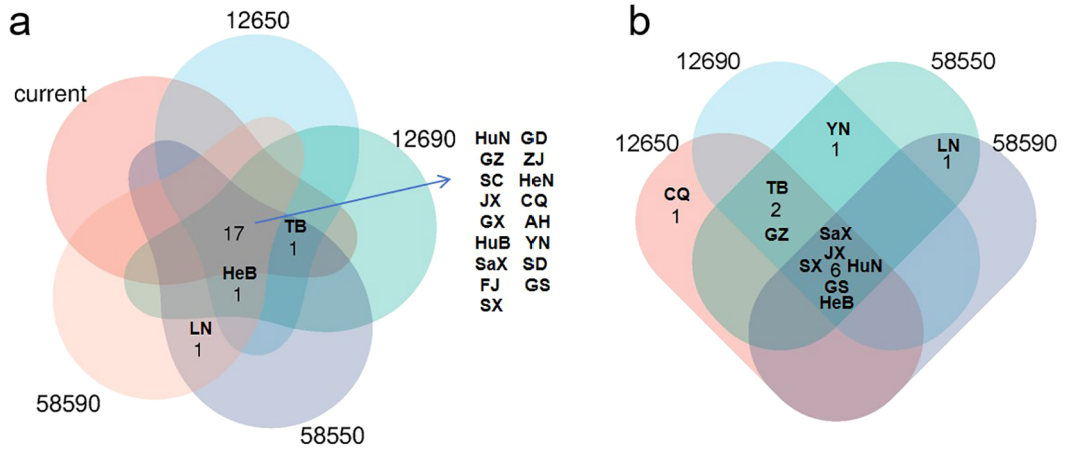

FIGURE 7
Provincial suitable habitat situation of *H. dulcis* under climate change scenarios. **(a)** Provinces where the area of suitable habitat remains above 15,000 km^2 throughout all periods and those expected to surpass 15,000 km^2 in future periods; **(b)** Provinces where suitable habitat area consistently surpasses current climatic suitable habitat area. (HuN, Hunan Province; GZ, Guizhou Province; SC, Sichuan Province; JX, Jiangxi Province; GX, Guangxi Zhuang Autonomous Region; HuB, Hubei Province; SaX, Shaanxi Province; FJ, Fujian Province; SX, Shanxi Province; GD, Guangdong Province; ZJ, Zhejiang Province; HeN, Henan Province; CQ, Chongqing; AH, Anhui Province; YN, Yunnan Province; SD, Shandong Province; GS, Gansu Province; HeB, Hebei Province; TB, Tibet Autonomous Region; LN, Liaoning Province).

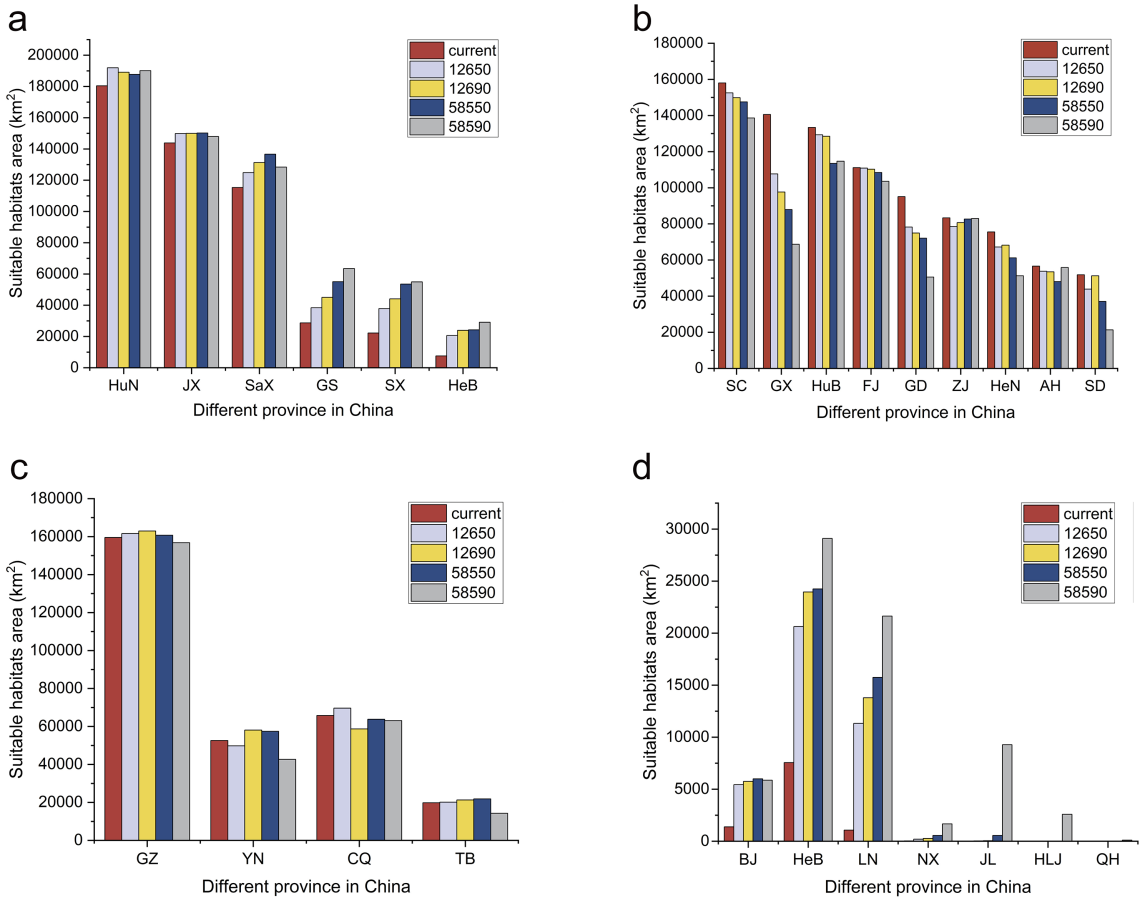

FIGURE 8
Area of suitable habitat in different provinces at different future climate scenarios. **(a)** The provinces with consistently larger suitable habitat areas than those under current climatic conditions; **(b)** Provinces with consistently smaller suitable habitat areas than under current climatic conditions; **(c)** Provinces where suitable habitat areas transiently exceed but ultimately remain smaller than current levels under future climate scenarios; **(d)** Provinces currently unsuitable but projected to become climatically suitable for *H. dulcis* under future climate scenarios.

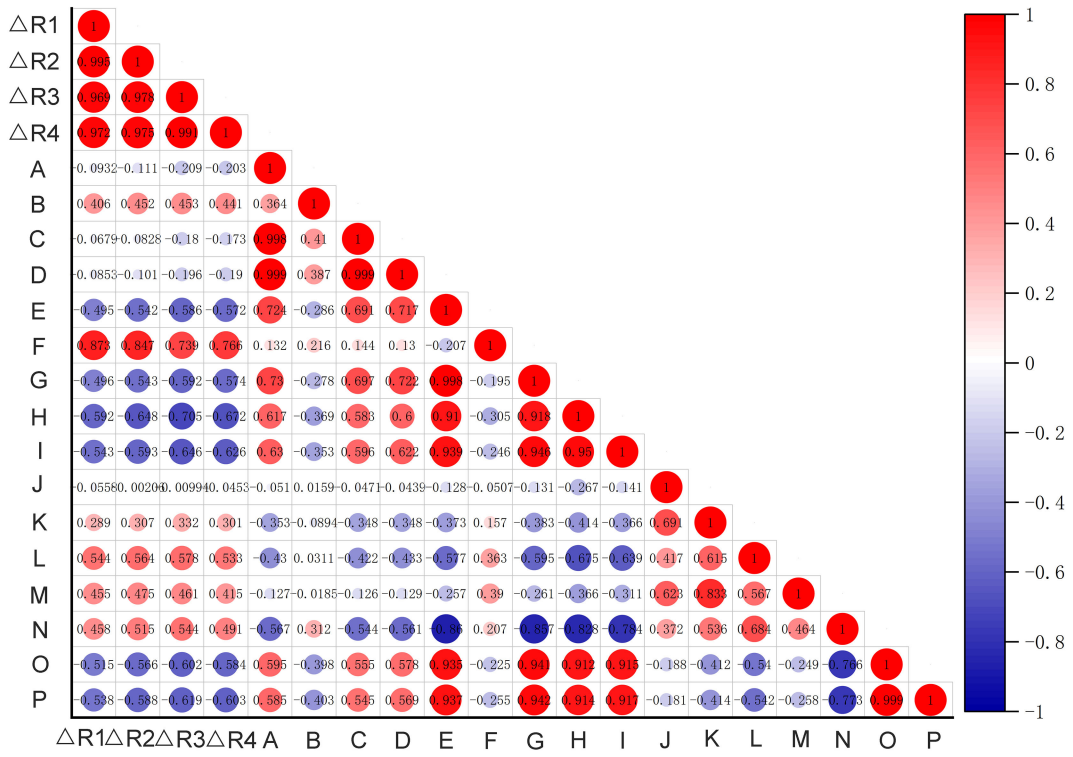

FIGURE 9
The correlation heatmap between the change rate of suitable habitat area in each province and climatic factors. (Hunan, Jiangxi, Shaanxi, Gansu, Shanxi, Hebei, Sichuan, Guangxi Zhuang Autonomous Region, Hubei, Fujian, Guangdong, Zhejiang, Henan, Anhui, Shandong)[△R1:△12650S/current; △R2:△12690S/current; △R3:△58550S/current; △R4:△58590S/current; (A) Atmospheric pressure (hPa); (B) Atmospheric pressure at sea level (hPa); (C) Maximum Pressure(hPa); (D) Minimum Pressure (hPa); (E) Temperature (°C); (F) Mean maximum temperature (°C); (G) Mean minimum temperature (°C); (H) Relative humidity (%); (I) Minimum Relative Humidity (%); (J) 2-Minute Mean Wind Speed (m/s); (K) Maximum Wind Speed (m/s); (L) Wind Direction (Angle) of Maximum Wind Speed (°); (M) Extreme Wind Speed (m/s); (N) Wind Direction of Extreme Wind Speed (°); (O) Annual 24-hour Precipitation (20:00-20:00 local time) (mm); (P) 24-hour Precipitation (08-08h) (mm)].

influenced by the degree of spatial aggregation of occurrence records. When these records display a high level of spatial correlation, the model is prone to overfitting, potentially introducing geographical biases. To reduce overfitting, variables with correlation coefficients exceeding an absolute value of 0.8 are excluded. A 10 km spatial thinning threshold is applied to improve the accuracy and reliability of the AUC output. Model performance is evaluated using the receiver operating characteristic (ROC) curve, and the MaxEnt model achieves an AUC value of 0.934 (Figure 2b). An AUC value approaching 1 indicates excellent model performance (Mahmoud et al., 2025), demonstrating that the model is both accurate and effective. Its strong predictive capability provides a valuable reference for developing conservation strategies and sustainable utilization plans for *H. dulcis*.

4.2 Environmental variables influencing the distribution of *H. dulcis* and corresponding planting strategies

The distribution of *H. dulcis* is highly sensitive to climate and constrained by multiple environmental factors. Studies indicate that its potential distribution is primarily driven by four key variables: annual precipitation, minimum temperature of the coldest month, elevation, and mean diurnal temperature range. The species thrives under conditions of annual precipitation ranging from 708.45 to 2956.80 mm, minimum coldest-month temperatures between -4.93 °C and 8.92 °C, mean diurnal temperature ranges of 6.81–10.18 °C, and elevations from 273.85 to 1019.40 m. Optimal growth occurs at a minimum coldest-month temperature of 4.20 °C and a mean diurnal range of 8.13 °C, suggesting that *H. dulcis* prefers environments with relatively limited temperature fluctuations. The probability of occurrence shows a unimodal response to annual mean temperature (Bio1), with peaks ranging from 5.80 to 11.33 °C (Rong et al., 2024). Elevation strongly modulates regional climate and hence shapes plant distributions (Zhang et al., 2024).

In Northeast and North China, seasonal temperature variations are significant and no suitable habitats have been found, confirming that extreme temperature fluctuations limit survival. *H. dulcis* prefers warm and humid climates, with optimal growth occurring at an annual precipitation of 1985.02 mm, consistent with humid regions where precipitation typically exceeds 800 mm. Its distribution is concentrated in subtropical monsoon climate zones, primarily at the junction of Central, Southwest, and Northwest China, as well as in the coastal areas of East and South

China. These regions are characterized by warm, moderately moist conditions and abundant rainfall, aligning closely with the model predictions and underscoring the dominant role of temperature and precipitation in shaping its distribution. Additionally, *H. dulcis* exhibits a strong preference for low- to mid-elevation hills ranging from 273.85 to 1019.40 m (Duan et al., 2025), consistent with its observed distribution (Figure 1). Therefore, conservation and cultivation efforts should give priority to warm, humid climates and mid-elevation areas to promote sustainable utilization.

4.3 Historical and future distribution evolution of the suitable habitat for *H. dulcis* under climate change

With global warming intensifying, the global surface temperature rose by 1.1°C during 2011–2020 compared with the baseline from 1850 to 1900, triggering significant redistributions and altered phenological timings that cascade into ecosystem-level reorganizations (Riahi et al., 2017). The frigid and arid conditions of the Last Glacial Maximum (LGM) are likely to have made the environment unsuitable for *H. dulcis* to survive. In contrast, the comparatively milder and wetter climate of the Mid-Holocene (MH) provided more favorable conditions for *H. dulcis.* (Berman et al., 2018). As a thermophilic and hydrophilic pioneer species, *H. dulcis* may have limited suitable habitats during both the LGM and MH scenarios, primarily constrained by extreme cold and unstable climate.

Under current climatic conditions, its potential distribution has expanded markedly, particularly across central, southwestern, and northwestern China, as well as in the eastern and southern coastal regions, consistent with its affinity for temperate and humid monsoon climates (Tiansawat et al., 2022). However, future projections under high-emission scenarios (e.g., SSP585) suggest substantial habitat loss, likely driven by temperatures exceeding the physiological tolerance of species, coupled with terrain and anthropogenic constraints (Gao et al., 2024). By the 2050s and 2090s, regions such as Guangxi and Shandong are projected to lose more than 50% of their suitable habitat, with the remaining areas shifting to higher elevations. On the contrary, climate warming may facilitate range expansion into new regions, including Beijing, Hebei, Liaoning, Ningxia, and Heilongjiang, indicating a pronounced northward shift in distribution. Hunan Province is expected to retain the largest and most climatically suitable habitats, owing to its stable hydrothermal conditions.

4.4 Conservation strategies and research implications for *H. dulcis*

To mitigate the adverse impacts of climate warming on the distribution of *H. dulcis*, it is necessary to formulate an integrated conservation strategy that combines habitat protection, climate adaptation, and public participation. In regions with extensive suitable habitats, such as Hunan Province, establishing nature reserves or ecological corridors is crucial to protect existing populations and habitats. At the same time, strengthening the monitoring and management of hydrological and thermal systems is essential to ensure environmental stability. In areas experiencing substantial habitat reduction, including Guangxi Zhuang Autonomous Region and Shandong Province, local intervention measures such as artificial irrigation and shading should be implemented to alleviate heat and drought stress by optimizing microclimates. Meanwhile, proactive efforts should aim to expand the species' range by establishing populations in newly identified suitable habitats in Beijing, Hebei, Liaoning, Ningxia, and Heilongjiang through artificial propagation and *ex situ* conservation. By taking advantage of the phenotypic plasticity of species at different environmental gradients and their inherent adaptability to diverse climatic zones, climate-adaptive breeding programs can focus on enhancing heat and drought tolerance to improve resilience in vulnerable regions (Nicotra et al., 2010). Furthermore, future studies should incorporate non-climatic factors, such as human interference and land use change, to improve the predictive models and develop effective and scientific management strategies, so as to preserve *H. dulcis* for a long time under changing environmental conditions.

5 Conclusion

This study employed a species distribution model to evaluate the impacts of climate change on the habitat suitability of *Hovenia dulcis* across China. The MaxEnt model demonstrated a high predictive accuracy (AUC = 0.934), and the species distribution is primarily affected by annual precipitation (Bio12), minimum temperature of the coldest month (Bio06), elevation, and mean diurnal temperature range (Bio02). Among them, annual precipitation (Bio12) and minimum temperature of the coldest month (Bio06) were the most influential, each contributing over 30% by percentage contribution and exceeding 16% by permutation importance, followed by elevation and diurnal temperature range. The results indicate that *H. dulcis* favors warm, humid subtropical monsoon climates, with optimal suitability occurring in mid-elevation hills of central, eastern, and southwestern China. Under future climate scenarios, its suitable range is expected to shift northward and upward in elevation. While regions such as Hunan, Jiangxi, Sichuan and Guizhou remain core suitable areas, northern provinces including Hebei, Liaoning, and Beijing are expected to become increasingly suitable. In contrast, habitats in Guangxi and Shandong may shrink significantly. These predicted shifts reflect the species' dependence on warm temperatures and adequate moisture, highlighting its vulnerability and adaptive potential under global warming. These findings provide a scientific foundation for targeted conservation and sustainable utilization of *H. dulcis*. Priority measures should include *in situ* protection of core habitats, assisted migration into new suitable regions, and *ex situ* conservation combined with breeding programs focused on climate-adaptive traits.

Data availability statement

The original contributions presented in the study are included in the article/Supplementary Material. Further inquiries can be directed to the corresponding author.

Author contributions

XL: Conceptualization, Data curation, Formal Analysis, Funding acquisition, Investigation, Methodology, Project administration, Resources, Software, Supervision, Validation, Visualization, Writing – original draft, Writing – review & editing. PL: Conceptualization, Data curation, Formal Analysis, Funding acquisition, Investigation, Methodology, Project administration, Resources, Software, Supervision, Validation, Visualization, Writing – original draft, Writing – review & editing. SL: Resources, Supervision, Writing – review & editing. MH: Supervision, Writing – review & editing. YaL: Investigation, Supervision, Validation, Writing – review & editing. YuL: Writing – review & editing, Investigation. SW: Project administration, Software, Writing – review & editing, Visualization. TS: Writing – review & editing, Project administration, Software. MY: Writing – review & editing, Validation. QC: Conceptualization, Data curation, Formal Analysis, Funding acquisition, Investigation, Methodology, Project administration, Resources, Software, Supervision, Validation, Visualization, Writing – original draft, Writing – review & editing.

Funding

The author(s) declare financial support was received for the research and/or publication of this article. This work was supported by the Natural Science Foundation of Hubei Province, China (No. 2024AFB502), the Nature Science Foundation of China (No. 82404795), Ph.D. Start-up Funding (No. BK202413) and Medical Fund (No. 2023YKY04) of Hubei University of Science and Technology.

Conflict of interest

The authors declare that the research was conducted in the absence of any commercial or financial relationships that could be construed as a potential conflict of interest.

Generative AI statement

The author(s) declare that Generative AI was used in the creation of this manuscript. During the preparation of this manuscript, the authors used Kimi to improve language. After using this tool, the authors reviewed and edited the content as needed and fully assume responsibility for the content of the publication.

Any alternative text (alt text) provided alongside figures in this article has been generated by Frontiers with the support of artificial intelligence and reasonable efforts have been made to ensure accuracy, including review by the authors wherever possible. If you identify any issues, please contact us.

Publisher's note

Supplementary material

The Supplementary Material for this article can be found online at: https://www.frontiersin.org/articles/10.3389/fpls.2025.1641811/full#supplementary-material

SUPPLEMENTARY TABLE 1
Distribution information of all *H. dulcis* sample points collected in this study (n = 479).

SUPPLEMENTARY TABLE 2
Distribution information of *H. dulcis* after excluding samples with unclear information (n = 254).

SUPPLEMENTARY TABLE 3
Distribution information of *H. dulcis* based on 191 valid occurrence points.

SUPPLEMENTARY TABLE 4
Area of different suitable habitat types in Chinese provinces.

SUPPLEMENTARY TABLE 5
Total suitable habitat area in various provinces of China across different periods (sum of medium and high suitable habitat areas).

SUPPLEMENTARY TABLE 6
Change rate of suitable habitats in some provinces and observed values of different meteorological factors.

References

Ahmadi, M., Hemami, M.-R., Kaboli, M., and Shabani, F. (2023). MaxEnt brings comparable results when the input data are being completed; Model parameterization of four species distribution models. *Ecol. Evol.* 13, e9827. doi: 10.1002/ece3.9827

Aligaz, M. A., Kufa, C. A., Ahmed, A. S., Argaw, H. T., Tamrat, M., Yihune, M., et al. (2024). Distribution and extent of suitable habitats of Ruspoli's Turaco (*Tauraco ruspolii*) and White-cheeked Turaco (*Tauraco leucotis*) under a changing climate in Ethiopia. *BMC Ecol. Evol.* 24, 83. doi: 10.1186/s12862-024-02245-y

Bergamin, R. S., Gama, M., Almerão, M., Hofmann, G. S., and Anastácio, P. M. (2022). Predicting current and future distribution of *Hovenia dulcis* Thunb. (Rhamnaceae) worldwide. *Biol. Invasions* 24, 2229–2243. doi: 10.1007/s10530-022-02771-0

Berman, A. L., Silvestri, G. E., and Tonello, M. S. (2018). On the differences between Last Glacial Maximum and Mid-Holocene climates in southern South America simulated by PMIP3 models. *Quat. Sci. Rev.* 185, 113–121. doi: 10.1016/j.quascirev.2018.02.003

Cao, Z., Zhang, L., Zhang, X., and Guo, Z. (2021). Predicting the Potential Distribution of *Hylomecon japonica* in China under Current and Future Climate Change Based on Maxent Model. *Sustainability* 13, 11253. doi: 10.3390/su132011253

De Godoi, R. S., Almerão, M. P., and Da Silva, F. R. (2021). In silico evaluation of the antidiabetic activity of natural compounds from *Hovenia dulcis* Thunberg. *J. Herb. Med.* 28, 100349. doi: 10.1016/j.hermed.2020.100349

Duan, Y., Bai, H., Du, Z., Liu, Y., Li, L., Lu, K., et al. (2025). Maxent modeling for predicting the potential distribution of *Hippophae Linn* species. *Trop. Ecol.* 66, 132–145. doi: 10.1007/s42965-025-00372-1

Elith, J., Phillips, S. J., Hastie, T., Dudík, M., Chee, Y. E., and Yates, C. J. (2011). A statistical explanation of MaxEnt for ecologists. *Divers. Distrib.* 17, 43–57. doi: 10.1111/j.1472-4642.2010.00725.x

Fan, J., Li, J., Xia, R., Hu, L., Wu, X., and Li, G. (2014). Assessing the impact of climate change on the habitat distribution of the giant panda in the Qinling Mountains of China. *Ecol. Model.* 274, 12–20. doi: 10.1016/j.ecolmodel.2013.11.023

Gao, H., Wei, X., Peng, Y., and Zhuo, Z. (2024). Predicting the impact of climate change on the future distribution of *Paederus fuscipes* Curtis 1826, in China based on the maxEnt model. *Insects* 15, 437. doi: 10.3390/insects15060437

Guisan, A., and Thuiller, W. (2005). Predicting species distribution: offering more than simple habitat models. *Ecol. Lett.* 8, 993–1009. doi: 10.1111/j.1461-0248.2005.00792.x

Guo, T., Yang, Q., Chen, D., Wang, X., Cheng, Q., Wang, S., et al. (2025). Assessment of Chinese suitable habitats of Amomum tsao-ko in different climatic conditions. *Front. Plant Sci.* 16. doi: 10.3389/fpls.2025.1561026

He, Y., Liu, M., Wang, Y., Wu, H., Wei, M., Xue, J., et al. (2024). *Hovenia dulcis*: a Chinese medicine that plays an essential role in alcohol-associated liver disease. *Front. Pharmacol.* 15. doi: 10.3389/fphar.2024.1337633

Hong, S. H., Lee, Y. H., Lee, G., Lee, D.-H., and Adhikari, P. (2021). Predicting impacts of climate change on northward range expansion of invasive weeds in South Korea. *Plants Basel Switz.* 10, 1604. doi: 10.3390/plants10081604

Huang, B., Chen, S., Xu, L., Jiang, H., Chen, X., He, H., et al. (2024). Predicting the potential geographical distribution of *Zingiber striolatum* Diels (Zingiberaceae), a medicine food homology plant in China. *Sci. Rep.* 14, 22206. doi: 10.1038/s41598-024-73202-4

Hyun, T., Eom, S., Yu, C., and Roitsch, T. (2010). *Hovenia dulcis* – an Asian traditional herb. *Planta Med.* 76, 943–949. doi: 10.1055/s-0030-1249776

Karuppaiah, V., Maruthadurai, R., Das, B., Soumia, P. S., Gadge, A. S., Thangasamy, A., et al. (2023). Predicting the potential geographical distribution of onion thrips, *Thrips tabaci* in India based on climate change projections using MaxEnt. *Sci. Rep.* 13, 7934. doi: 10.1038/s41598-023-35012-y

Khan, A. M., Li, Q., Saqib, Z., Khan, N., Habib, T., Khalid, N., et al. (2022). MaxEnt modelling and impact of climate change on habitat suitability variations of economically important chilgoza pine (*Pinus gerardiana* wall.) in south Asia. *Forests* 13, 715. doi: 10.3390/f13050715

Kumar, D., Pandey, A., Rawat, S., Joshi, M., Bajpai, R., Upreti, D. K., et al. (2022). Predicting the distributional range shifts of *Rhizocarpon geographicum* (L.) DC. @ in Indian Himalayan Region under future climate scenarios. *Environ. Sci. pollut. Res.* 29, 61579–61593. doi: 10.1007/s11356-021-15624-5

Li, S., Li, Y., Hu, M., Li, Y., Yang, M., Wang, S., et al. (2025). Ecological risk assessment of future suitable areas for *Piper kadsura* under the background of climate change. *Front. Plant Sci.* 15. doi: 10.3389/fpls.2024.1471706

Li, F., and Park, Y.-S. (2020). Habitat availability and environmental preference drive species range shifts in concordance with climate change. *Divers. Distrib.* 26, 1343–1356. doi: 10.1111/ddi.13126

Li, M., Xie, C., Meng, C., Zhang, Y., Gao, J., Wang, W., et al. (2021). Chemical constituents from *Hovenia dulcis* Thunb. and their chemotaxonomic significance. *Biochem. Syst. Ecol.* 94, 104214. doi: 10.1016/j.bse.2020.104214

Ma, C., Xu, X., Zhou, M., Hu, T., and Qi, C. (2024). A deep learning approach for chromium detection and characterization from soil hyperspectral data. *Toxics* 12, 357. doi: 10.3390/toxics12050357

Mahmoud, A. R., Farahat, E. A., Hassan, L. M., and Halmy, M. W. A. (2025). Remotely sensed data contribution in predicting the distribution of native Mediterranean species. *Sci. Rep.* 15, 12475. doi: 10.1038/s41598-025-94569-y

Mao, X., Zheng, H., Luo, G., Liao, S., Wang, R., Tang, M., et al. (2024). Climate change favors expansion of three Eucalyptus species in China. *Front. Plant Sci.* 15. doi: 10.3389/fpls.2024.1443134

Melo-Merino, S. M., Reyes-Bonilla, H., and Lira-Noriega, A. (2020). Ecological niche models and species distribution models in marine environments: A literature review and spatial analysis of evidence. *Ecol. Model.* 415, 108837. doi: 10.1016/j.ecolmodel.2019.108837

Meng, X., Tang, G., Zhao, C., Liu, Q., Xu, X., and Cao, S. (2020). Hepatoprotective effects of *Hovenia dulcis* seeds against alcoholic liver injury and related mechanisms investigated via network pharmacology. *World J. Gastroenterol.* 26, 3432–3446. doi: 10.3748/wjg.v26.i24.3432

Nicotra, A. B., Atkin, O. K., Bonser, S. P., Davidson, A. M., Finnegan, E. J., Mathesius, U., et al. (2010). Plant phenotypic plasticity in a changing climate. *Trends Plant Sci.* 15, 684–692. doi: 10.1016/j.tplants.2010.09.008

Niiya, M., Shimato, Y., Ohno, T., and Makino, T. (2024). Effects of *Hovenia dulcis* fruit and peduncle extract on alcohol metabolism. *J. Ethnopharmacol.* 321, 117541. doi: 10.1016/j.jep.2023.117541

Ottó, B., and Végvári, Z. (2022). Bioclimatic preferences of the great bustard in a steppe region. *Diversity* 14, 1138. doi: 10.3390/d14121138

Ouyang, X., Pan, J., Wu, Z., and Chen, A. (2022). Predicting the potential distribution of *Campsis grandiflora* in China under climate change. *Environ. Sci. pollut. Res.* 29, 63629–63639. doi: 10.1007/s11356-022-20256-4

Phillips, S. J., Anderson, R. P., and Schapire, R. E. (2006). Maximum entropy modeling of species geographic distributions. *Ecol. Model.* 190, 231–259. doi: 10.1016/j.ecolmodel.2005.03.026

Phillips, S. J., and Dudík, M. (2008). Modeling of species distributions with Maxent: new extensions and a comprehensive evaluation. *Ecography* 31, 161–175. doi: 10.1111/j.0906-7590.2008.5203.x

Pischl, P. H., Burke, S. V., Bach, E. M., and Duvall, M. R. (2020). Plastome phylogenomics and phylogenetic diversity of endangered and threatened grassland species (Poaceae) in a North American tallgrass prairie. *Ecol. Evol.* 10, 7602–7615. doi: 10.1002/ece3.6484

Pokharel, K. P., Ludwig, T., and Storch, I. (2016). Predicting potential distribution of poorly known species with small database: the case of four-horned antelope *Tetracerus quadricornis* on the Indian subcontinent. *Ecol. Evol.* 6, 2297–2307. doi: 10.1002/ece3.2037

Porfirio, L. L., Harris, R. M. B., Lefroy, E. C., Hugh, S., Gould, S. F., Lee, G., et al. (2014). Improving the use of species distribution models in conservation planning and management under climate change. *PLoS One* 9, e113749. doi: 10.1371/journal.pone.0113749

Riahi, K., van Vuuren, D. P., Kriegler, E., Edmonds, J., O'Neill, B. C., Fujimori, S., et al. (2017). The Shared Socioeconomic Pathways and their energy, land use, and greenhouse gas emissions implications: An overview. *Glob. Environ. Change* 42, 153–168. doi: 10.1016/j.gloenvcha.2016.05.009

Rong, W., Huang, X., Hu, S., Zhang, X., Jiang, P., Niu, P., et al. (2024). Impacts of climate change on the habitat suitability and natural product accumulation of the medicinal plant *Sophora alopecuroides* L. Based on the maxEnt model. *Plants* 13, 1424. doi: 10.3390/plants13111424

Sferrazza, G., Brusotti, G., Zonfrillo, M., Temporini, C., Tengattini, S., Bononi, M., et al. (2021). *Hovenia dulcis* thumberg: phytochemistry, pharmacology, toxicology and regulatory framework for its use in the European union. *Mol. Basel Switz.* 26, 903. doi: 10.3390/molecules26040903

Shen, L., Deng, H., Zhang, G., Ma, A., and Mo, X. (2023). Effect of climate change on the potentially suitable distribution pattern of *Castanopsis hystrix* miq. in China. *Plants* 12, 717. doi: 10.3390/plants12040717

Son, Y., Lee, D. H., Park, G. H., Jang, J.-H., Kim, J. A., Park, Y., et al. (2023). Comparison of Growth Characteristics and Active Compounds of Cultivated *Hovenia dulcis* under Different Environments in South Korea. *Diversity* 15, 905. doi: 10.3390/d15080905

Syfert, M. M., Smith, M. J., and Coomes, D. A. (2013). The effects of sampling bias and model complexity on the predictive performance of MaxEnt species distribution models. *PLoS One* 8, e55158. doi: 10.1371/journal.pone.0055158

Tang, D., Chen, M., Huang, X., Zhang, G., Zeng, L., Zhang, G., et al. (2023). SRplot: A free online platform for data visualization and graphing. *PLoS One* 18, e0294236. doi: 10.1371/journal.pone.0294236

Thomas, C. D., Cameron, A., Green, R. E., Bakkenes, M., Beaumont, L. J., Collingham, Y. C., et al. (2004). Extinction risk from climate change. *Nature* 427, 145–148. doi: 10.1038/nature02121

Tiansawat, P., Elliott, S. D., and Wangpakapattanawong, P. (2022). Climate niche modelling for mapping potential distributions of four framework tree species: implications for planning forest restoration in tropical and subtropical Asia. *Forests* 13, 993. doi: 10.3390/f13070993

Tomczyk, M., Zovko-Končić, M., and Chrostek, L. (2012). Phytotherapy of alcoholism. *Nat. Prod. Commun.* 7, 273–280. doi: 10.1177/1934578X1200700243

Wiens, J. A., Stralberg, D., Jongsomjit, D., Howell, C. A., and Snyder, M. A. (2009). Niches, models, and climate change: assessing the assumptions and uncertainties. *Proc. Natl. Acad. Sci. U.S.A.* 106 Suppl 2, 19729–19736. doi: 10.1073/pnas.0901639106

Yan, H., Feng, L., Zhao, Y., Feng, L., Wu, D., and Zhu, C. (2020). Prediction of the spatial distribution of *Alternanthera philoxeroides* in China based on ArcGIS and MaxEnt. *Glob. Ecol. Conserv.* 21, e00856. doi: 10.1016/j.gecco.2019.e00856

Yang, J., Jiang, X., Ma, Y., Liu, M., Shama, Z., Li, J., et al. (2024). Potential global distribution of *Setaria italica*, an important species for dryland agriculture in the context of climate change. *PLoS One* 19, e0301751. doi: 10.1371/journal.pone.0301751

Zhan, P., Wang, F., Xia, P., Zhao, G., Wei, M., Wei, F., et al. (2022). Assessment of suitable cultivation region for *Panax notoginseng* under different climatic conditions using MaxEnt model and high-performance liquid chromatography in China. *Ind. Crops Prod.* 176, 114416. doi: 10.1016/j.indcrop.2021.114416

Zhang, Y., Chen, S., Gao, Y., Yang, L., and Yu, H. (2023). Prediction of global potential suitable habitats of *Zanthoxylum bungeanum* Link et Otto based on MaxEnt model. *Sci. Rep.* 13, 4851. doi: 10.1038/s41598-023-29678-7

Zhang, K., Liu, H., Pan, H., Shi, W., Zhao, Y., Li, S., et al. (2020). Shifts in potential geographical distribution of *Pterocarya stenoptera* under climate change scenarios in China. *Ecol. Evol.* 10, 4828–4837. doi: 10.1002/ece3.6236

Zhang, M., Liu, Z., Yang, Z., Shen, H., Wang, J., and Wu, X. (2024). Altitudinal variation in species diversity, distribution, and regeneration status of a secondary *Picea* forest in Guandi mountain, northern China. *Forests* 15, 771. doi: 10.3390/f15050771

Zheng, T., Sun, J., Shi, X., Liu, D., Sun, B., Deng, Y., et al. (2022). Evaluation of climate factors affecting the quality of red huajiao (*Zanthoxylum bungeanum* maxim.) based on UPLC-MS/MS and MaxEnt model. *Food Chem. X* 16, 100522. doi: 10.1016/j.fochx.2022.100522

Zhou, Y., Newman, C., Xie, Z., and Macdonald, D. W. (2013). Peduncles elicit large-mammal endozoochory in a dry-fruited plant. *Ann. Bot.* 112, 85–93. doi: 10.1093/aob/mct096

frontiers | Frontiers in Plant Science

TYPE Original Research
PUBLISHED 22 October 2025
DOI 10.3389/fpls.2025.1662481

OPEN ACCESS

EDITED BY
Sumit Chakravarty,
Uttar Banga Krishi Viswavidyalaya, India

REVIEWED BY
Yuan Miao,
Henan University, China
Gao-Jian Huang,
Shanxi Agricultural University, China

*CORRESPONDENCE
Yang Zhenqi
yangzq@iwhr.com
Guo Jianying
guojy@iwhr.com

RECEIVED 09 July 2025
ACCEPTED 25 September 2025
PUBLISHED 22 October 2025

CITATION
Xin W, Zhenqi Y, Jianying G, Li Z and Fucang Q (2025) Effects of rainfall interception by sand-fixing vegetation on soil carbon and nitrogen distribution in a sand-covered hilly area.
Front. Plant Sci. 16:1662481.
doi: 10.3389/fpls.2025.1662481

Effects of rainfall interception by sand-fixing vegetation on soil carbon and nitrogen distribution in a sand-covered hilly area

Wang Xin[1,2], Yang Zhenqi[1,2]*, Guo Jianying[1,2]*, Zhen Li[3] and Qin Fucang[2,4]

[1]Ecological Conservation and Restoration Laboratory, Ministry of Water Resources Pastoral Area Water Conservancy Science Research Institute, Hohhot, Inner Mongolia, China, [2]College of Desert Control Science and Engineering, Inner Mongolia Agricultural University, Hohhot, Inner Mongolia, China, [3]Inner Mongolia Autonomous Region Forestry and Grassland Seedling Station, Hohhot, Inner Mongolia, China, [4]Inner Mongolia Academy of Forestry Sciences, Hohhot, Inner Mongolia, China

Aims: The landscape of sand-covered hilly areas has been reshaped by afforestation in these areas. Dynamic changes in soil moisture and nutrients in forests after afforestation have become evident. However, clear studies have not focused on whether rainfall interception in these plantations affects soil concentration or concentration.

Methods: This largely limits the development of effective management techniques for plantations and hinders the optimal utilization and management of water resources. In this study, an investigation was conducted on the plant community structure, rainfall interception characteristics, and soil organic carbon (SOC) and total nitrogen (N) concentrations or concentrations of three different plantations in the sand-covered hilly area of the Kuye River Basin. Grassland (Gl) was taken as the control.

Results: The critical throughfall values for *C. korshinskii* (Ck), *S. Cheilophila* (Sc) and *P. sylvestris* (Ps) were 0.28, 1.78 and 2.04 mm, respectively. Corresponding stemflow critical values measured were 2.93, 1.08, and 3.30 mm, respectively. Ps exhibited the highest interception capacity, which was attributable to its dense canopy and layered branch architecture. Sc ranked second due to its larger leaf area, while Ck showed the lowest interception because of wide branch angles and smaller leaf area. Post-rainfall ground-level soil moisture and litter deposition are regulated by vegetation canopy structure in a direct way. SOC and N concentrations are subsequently controlled by these ground-level parameters. SOC concentration under Ps was 1.54 compared to that under Gl, while N concentration was 1.50 times higher, respectively.

Conclusions: Thus, Ps demonstrates optimal effectiveness for improving soil quality in sandy hill restoration areas and merits continued implementation in this region.

KEYWORDS

sand fixed vegetation, community structure, rainfall redistribution, soil organic carbon, total nitrogen

1 Introduction

Sand-covered hilly areas are classified into arid and semi-arid regions. The precipitation level in such areas is low, and the frequency of extreme precipitation events has seen an increase owing to the impact of global climate change (Pei et al., 2023). Sand-covered hilly areas are the most typical and unique landscape in the dryland ecosystem. In these areas, sand-fixing vegetation plays a buffering role in breaking the wind, sand fixation and land degradation. Therefore, such vegetation is considered as an ecological barrier in this area (Liu and Du, 2022). In the past few decades, forest rehabilitation projects have been implemented as a part of slope agriculture in China, and numerous drought-tolerant trees and shrubs have been planted to reduce soil erosion (Bryan et al., 2018). These measures have significantly improved the vegetation coverage in this area and exerted a remarkable effect on soil and water conservation (Zhang et al., 2019a). Meanwhile, they have also resulted in changes to vegetation, soil properties and microbial community characteristics (Zhang et al., 2018). Nevertheless, the relationship between rainfall redistribution and soil organic carbon (SOC) and total nitrogen (N) during the construction of sand-fixing vegetation is unclear. Vegetation is an important factor affecting the SOC cycle. It participates in SOC cycling through root absorption and decomposition, as well as the reduction of litter and dead roots. Furthermore, different vegetation communities can form differing microtopographies, which causes differences in litter and decomposition rates (Tiessen et al., 1994). The community structure of plants exerts an influence on the rainfall interception process (Castro et al., 2006; Zhu et al., 2021). The change in soil nutrients is affected by vegetation (Li et al., 2021). To evaluate the effect of vegetation restoration and explore the resulting changes in soil composition, hence, it is necessary to comprehensively study and quantitatively characterize the process of rainfall interception (Lan et al., 2021).

The increased rainfall frequency with total unchanged rainfall amount increased SOC concentration, which mainly originated from increases in non-labile SOC concentration (Chen et al., 2020). The frequent occurrence of extreme rainfall events may greatly affect SOC fractions and carbon pool in the wet meadow of the Qinghai-Tibet Plateau (Wang et al., 2023). These studies have focused on the direct effects of rainfall on SOC, but the role of vegetation-mediated rainfall redistribution in regulating SOC and N remains underexplored. In forest ecosystems, the layers of canopy, herbaceous plants and litter intercept rainfall, divide it into interception, throughfall and stemflow, and influence soil moisture and nutrient dynamics (Gordon et al., 2020; de Queiroz et al., 2020). As a result, vegetation characteristics are key indicators for determining the amount of rainfall reaching soil (He et al., 2017; Wang et al., 2020). The characteristics of interception, stemflow, throughfall and litter interception have been described in extant studies (Ma et al., 2022). However, the effects of interception, stemflow, throughfall and litter interception of different sand-fixing vegetation types on SOC and N in forests need to be elucidated in more detail. In the process of artificial vegetation construction, the presence of different types of vegetation leads to differences in the composition of plant community and stand structure (Deng et al., 2018). Inevitably, this influences rainfall redistribution to varying degrees. The infiltration, storage and distribution of water in soil are deeply influenced by throughfall (Mei and Ma, 2022). This thus affects vegetation productivity and plant nutrient return (Yang et al., 2020), and furthermore soil nutrient characteristics (Liu et al., 2020). The effect of rainfall on SOC and N concentration characteristics is modulated by plant community and soil microbial decomposition (Fortier and Wright, 2021). Litter decomposition is a major factor that affects SOC and N concentration accumulation and cycling (Zhang et al., 2019b). The level of moisture entering different soil layers is different. Consequently, the nutrient concentration of each layer is different as well (Spyroglou et al., 2021; Simon et al., 2017). The effects of interception, stemflow, throughfall and litter interception on soil nutrient concentration and distribution after rainfall redistribution remain unclear despite their significance for elucidating the relationship between moisture and nutrient concentration during vegetation restoration.

Based on the above basic research, the association between rainfall redistribution and the dynamic changes in SOC and N for three kinds of sand-fixing vegetation in sand-covered hilly areas was examined in the present study. To address this gap, rainfall interception and the dynamic changes in SOC and N for three kinds of sand-fixing vegetation in sand-covered hilly areas were examined. The objective was to reveal the effects of rainfall redistribution on soil nutrient concentration, investigate the changes in nutrient levels under different sand-fixing vegetation types and clarify the coupling relationship between water and nutrients during vegetation restoration. The following research hypotheses were proposed: (1) Changes in vegetation structure lead to differences in the process of rainfall redistribution among sand-fixing vegetation types, and rainfall exerts a significant influence on throughfall, stemflow and canopy interception. (2) The cultivation of sand-fixing vegetation is beneficial to increasing SOC and N concentrations, with the most pronounced effects on the surface layer of soil. (3) The canopy characteristics of sand-fixing vegetation induce differences in the biomass and decomposition of the litter layer, which thereby substantially influences the concentrations of SOC and N in soil.

2 Materials and methods

2.1 Experimental site

A typical artificial forest sample plot near the soil and water conservation monitoring station in the Inner Mongolia section of the Kuye River Basin was selected as the study area (Figure 1). It is located on the right bank of the upper reaches of the four-level tributary of the Yellow River Basin (109° 31′ 30.97′′ E, 39° 39′ 2.89′′ N). The landform types of the area encompass Pisha sandstone, chestnut soil, aeolian sandy soil, as well as sand-covered hilly and gully areas. The Miaochuan Basin located within the study area, has an arid and semi-arid temperate continental climate. The

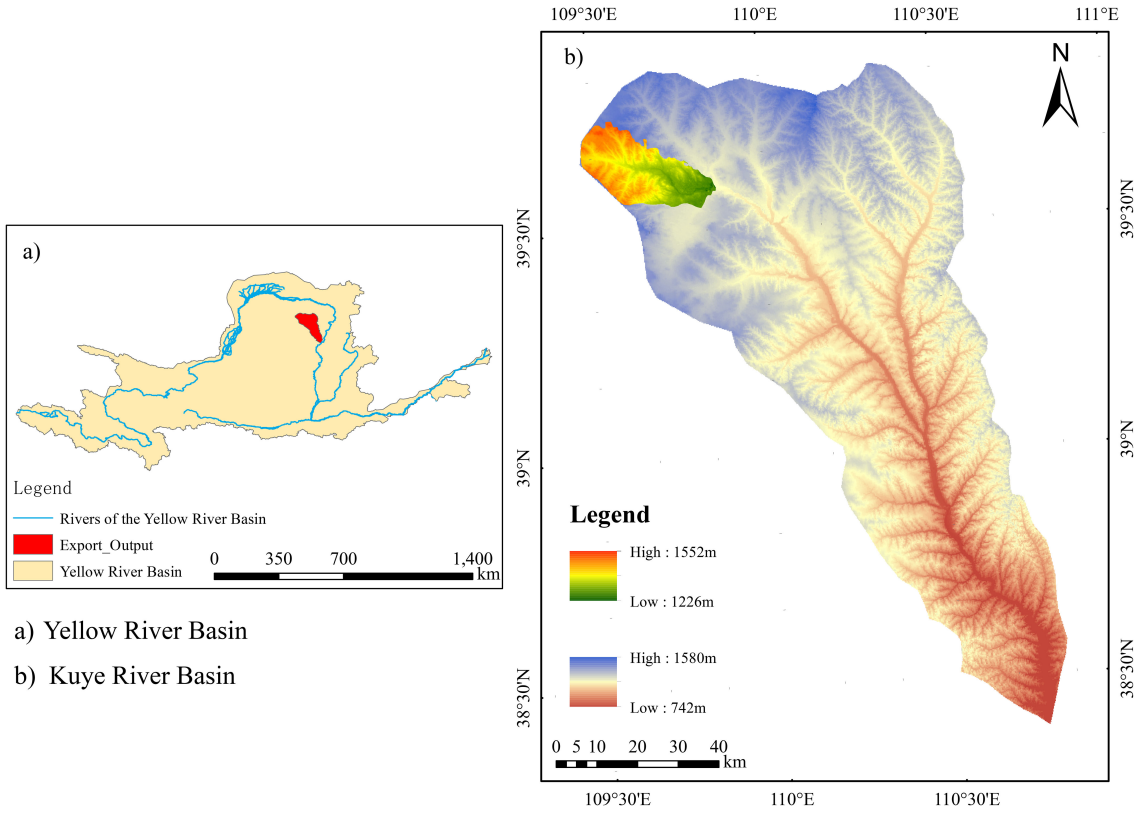

FIGURE 1
Map of the research region. **significant effects at p < 0.01 ,***significant effects at p < 0.001.

annual rainfall in the region averages 358.2 mm and ranges from 100.8 to 642.7 mm, with 2,900 sunshine hours annually. The effective accumulated temperature ≥10°C is 2,751.3°C and the mean annual evaporation is 2,563 mm. The prevailing wind in this area is northwesterly. Wind force varies from 5 to 8, with an annual wind speed of 3.6 m/s and a maximum instantaneous speed of 24 m/s.

2.2 Experimental design

The study area is situated in the Hetongchuanmiao section of the middle reaches of the Kuye River Basin. In June 2023, three common artificial sand-fixing vegetation types, namely Ck, Sc and Ps, were chosen as research objects. Sample plots of 20 m × 20 m and 15 m × 15 m were established for arboreal and shrub vegetations, respectively. Grassland (Gl) was used as a control. The characteristics of each stand were investigated and recorded (Table 1). Measurements were conducted for the average tree height, crown width, basal diameter, branch number, litter layer and biomass of trees and shrubs. The basal diameter of *C. korshinskii* (Ck) and *S. cheilophila* (Sc) is the total basal diameter obtained by adding the basal diameter of all branches on the ground (Luo et al., 2017). A field experiment was performed From July to October 2023. Nine standard trees were selected in each plot for the measurement of throughfall and stemflow.

TABLE 1 Characteristics of different types of vegetation in the study area.

Class	Vegetation	Height (m)	Average breast diameter (cm)	Average base diameter (cm)	Age (a)	CD (%)	HB ($t \cdot hm^{-2}$)	LB ($t \cdot hm^{-2}$)	LT (cm)
Shrub	*C.korshinskii*	2.9 ± 0.08b	–	20.7 ± 0.78	13	0.51 ± 0.03b	12.83 ± 0.53c	23.46 ± 1.61b	12.83 ± 0.02b
	S. cheilophila	3.02 ± 0.27b	–	28.66 ± 2.08	11	0.53 ± 0.03b	16.19 ± 0.61b	31.43 ± 3.74b	16.19 ± 0.57a
Arbor	*P. sylvestris*	4.17 ± 0.4a	38 ± 2.05	–	9	0.61 ± 0.01a	18.39 ± 1.18a	39.89 ± 3.80a	18.39 ± 0.12a

CD, Canopy density; HB, Herb biomass; LB, Litter biomass; LT, Litter thickness. Different lowercase letters in the same column indicate significant differences among different plantations, $p < 0.05$ level.

2.3 Investigation of vegetation characteristics

In June 2023, typical Ck, Sc and Ps forests near the contract temple soil and water conservation monitoring station in the contract temple basin of the Inner Mongolia section of the Kuye River Basin were selected for measurements. Later, sample sections of 20 m × 20 m and 15 m × 15 m were set up in each forest for the sampling of trees and shrubs, respectively. The space outside the field was used as a control. A measuring tape and a vernier caliper were utilized to measure the average height, diameter at breast height/basal diameter and biomass of trees and shrubs. Canopy density was determined on the basis of crown projection. The diameter at breast height of the tree refers to the diameter of the tree at a height of 1.1 meters from the ground. For Ck and Sc, the base diameter was used as the total base diameter obtained by adding the base diameter of all branches on the ground. The features of each stand were investigated and recorded (Table 1). The average value of each index was calculated. Standard plants were selected according to the average value. Nine standard plant vegetation types were chosen from each stand. Canopy density was the ratio of canopy projection area to forest area. Six 50 cm × 50 cm boxes were set up in each plot to collect litter. The thickness and weight of the litter layer were measured.

2.4 Investigation of soil characteristics

In the tree plot of 20 m × 20 m and the shrub plot of 15 m × 15 m, nine sampling points were selected. A soil sample from a depth of 0–150 cm was collected with a ring knife of 5 cm in diameter. Subsequently, soil samples from depths of 0-10, 10-20, 20-40, 40-60, 60-80, 80–100 and 100–150 cm were taken once. The collected soil was shade-dried, and its physical and chemical properties were determined. Soil samples were gathered in aluminum boxes to determine soil bulk density and soil mass water concentration (SMC, %). The method for determining SMC involved drying the sample in an oven at 105°C for 24 hours until it reached a constant weight. SOC ($g{\cdot}kg^{-1}$) was monitored by the dichromate titration-external heating method (Zhang et al., 2025). Soil N was determined by the Kjeldahl method (Cao et al., 2023).

The calculation formula for SOC density (SOCD) was as follows:

$$SOCDi = SOCi \times Bi \times di \times (1 - Gi) \quad (1)$$

$$SOCD = \sum_{i-1}^{n} SOCi \times Bi \times di \times (1 - Gi) \quad (2)$$

The formula for the calculation of soil N density (SND) was as follows:

$$SNDi = Ni \times Bi \times di \times (1 - Gi) \quad (3)$$

$$SND = \sum_{i=1}^{n} SNDi = Ni \times Bi \times di \times (1 - Gi) \quad (4)$$

In the formula, SOCDi represents the SOCD ($kg{\cdot}m^{-2}$) of a certain soil layer; SNDi stands for the SND of a certain soil layer ($kg{\cdot}m^{-2}$); SOCD denotes SOCD ($kg{\cdot}m^{-2}$); SND refers to SND ($kg{\cdot}m^{-2}$); SOCi means SOC concentration ($g{\cdot}kg^{-1)}$ in a certain soil layer; Ni is the N concentration of a soil layer ($g{\cdot}kg^{-1}$); Bi indicates the soil bulk density ($g{\cdot}cm^{-3}$) of a certain soil layer; di denotes the thickness of the soil layer (cm); Gi represents the percentage of the volume of gravel with a particle size greater than 2 mm. The soil particle size in this study is below 2 mm. As a result, Gi was ignored.

2.5 Observation of rainfall interception

Rainfall data were automatically collected by the long-term weather station. Rainwater was gathered in accordance with rainfall events, and six hours of rainfall were regarded as a rainfall event (Su et al., 2022). Rainfall was measured within 30 minutes after the end of the event (Zhang et al., 2021b). Ck, Sc and Ps plots were selected using a self-made rainfall collection device for forest throughfall observations (TF, mm). Nine standard plants were sampled from each plot. Within the projection areas of the selected standard plants, 12 self-made rain gauges were placed under each standard plant from the base to the four radiation directions. TF was calculated as follows:

$$TF = \frac{1}{n}\sum_{i=1}^{n}\frac{TF_i}{A_i} \quad (5)$$

where TF represents throughfall, mm; TF_i stands for the volume of throughfall in the i^{th} throughfall collector, mm^3; A_i refers to the rain area of the i^{th} throughfall collector, mm^2; n means the number of throughfall collectors.

A polyethylene hose was spirally wound on the trunk. The hose was fixed with iron nails. The gap between the hose and trunk was sealed with glass glue. The stemflow of a single tree was converted into stemflow at the plot scale using the following formula (Tu et al., 2021):

$$SF = \frac{N \times S_a}{A \times 10^3} \quad (6)$$

where SF represents stemflow, mm; N stands for the total tree in the sample plot; S_a refers to the mean stemflow of several standard trees, mL; A denotes plots (20 m × 20 m and 15 m × 15 m), m^2.

The interception was calculated with the water balance formula as follows:

$$Ic = P - TF - SF \quad (7)$$

where Ic represents interception, mm; P stands for rainfall, mm; TF is the amount of throughfall, mm; SF denotes stemflow, mm.

2.6 Statistical analysis

A normality test and a test for homogeneity of variance were carried out using IBM SPSS Statistics to ensure data validity. IBM SPSS Statistics 26.0 was applied to test the significance of the mean difference. Redundancy analysis was performed using CANOCO 5 software, followed by the implementation of partial least squares path modeling with the "plspm" package in R (v4.0.2).

10.3389/fpls.2025.1662481

3 Results and analysis

3.1 Rainfall redistribution characteristics of different forest stands

3.1.1 Characteristics of throughfall

In light of the rainfall redistribution data collected during the experiment in 2023, the total amount of throughfall for Ck, Sc and Ps was 140.02, 138.73 and 131.55 mm, respectively (Table 2). The total amount of throughfall (Equation 5) for each vegetation type accounted for 74.65%, 72.52%, and 69.96% of the total rainfall, respectively. A significant positive linear relationship was found between rainfall and throughfall for each vegetation type ($R^2 > 0.8$, $p < 0.01$) (Figure 2). The throughfall for each vegetation type increased with the increase in rainfall. It can be seen from the equation that the threshold of throughfall produced by Ck, Sc and Ps were 0.28, 1.78 and 2.04 mm, respectively. A logarithmic relationship was detected between rainfall and throughfall rate for each vegetation type. When the rainfall was low, the throughfall rate increased rapidly, and the increase in throughfall rate gradually slowed down with the increase in rainfall.

3.1.2 Characteristics of stemflow

During the experiment, the total stemflow of Ck, Sc and Ps was 3.5, 2.91 and 3.8 mm, respectively. The total stem runoff for each vegetation type occupied 1.88%, 1.56% and 2.04% of the total rainfall, respectively. A significant positive linear relationship was observed between the rainfall for each vegetation (Equation 6) type and stemflow ($R^2 > 0.9$, $p < 0.05$) (Figure 3). The stemflow for each vegetation type showed an increasing trend with the increase in rainfall, as indicated by the equation. The threshold for Ck, Sc and Ps to produce stemflow was 2.93, 1.08 and 3.30 mm, respectively. A logarithmic relationship existed between rainfall and stemflow rate for each vegetation type. When the rainfall was low, the stemflow rate increased rapidly, and the increase of stemflow rate gradually slowed down with the increase in rainfall.

3.1.3 Characteristics of interception

During the experiment, the total interception of Ck, Sc and Ps was 42.68, 44.56 and 49.85 mm, respectively (Equation 7). The total interception for each vegetation type took up 22.92%, 23.93% and 26.77% of the total rainfall, respectively (Figure 4). A significant positive exponential relationship was noticed between the rainfall for each vegetation type and the total interception ($R^2 > 0.70$, $p < 0.05$). The interception of each vegetation type rose with the increase in rainfall. A logarithmic relationship was noted between the rainfall and interception rate of each vegetation type. At the early stage of rainfall, the canopy was not saturated and the interception rate was high. With the increase in rainfall, a significant decrease occurred in the interception rate.

3.2 Changes in root biomass and soil bulk density in different vegetation types

Root biomass tends to rise before dropping with the increase of soil depth across different vegetation types. For all vegetation types,

TABLE 2 Statistical analysis of rainfall redistribution in different stands.

Vegetation	Throughfall			Stemflow			Interception			Rainfall (mm)
	Average (mm)	Total amount (mm)	Total throughfall rate	Average (mm)	Total amount (mm)	Total stemflow rate	Average (mm)	Total amount (mm)	Total interception rate	
C.korshinskii	14.00 ± 10.52a	140.02	74.65%	0.25 ± 0.12a	3.5	1.88%	4.27 ± 3.4a	42.68	22.92%	186.2
S. cheilophila	13.87 ± 11.69a	138.73	72.52%	0.29 ± 0.21a	2.91	1.56%	4.46 ± 2.4a	44.56	23.93%	
P. sylvestris	13.16 ± 11.26a	131.55	69.96%	0.28 ± 0.15a	3.8	2.04%	4.98 ± 2.7a	49.85	26.77%	

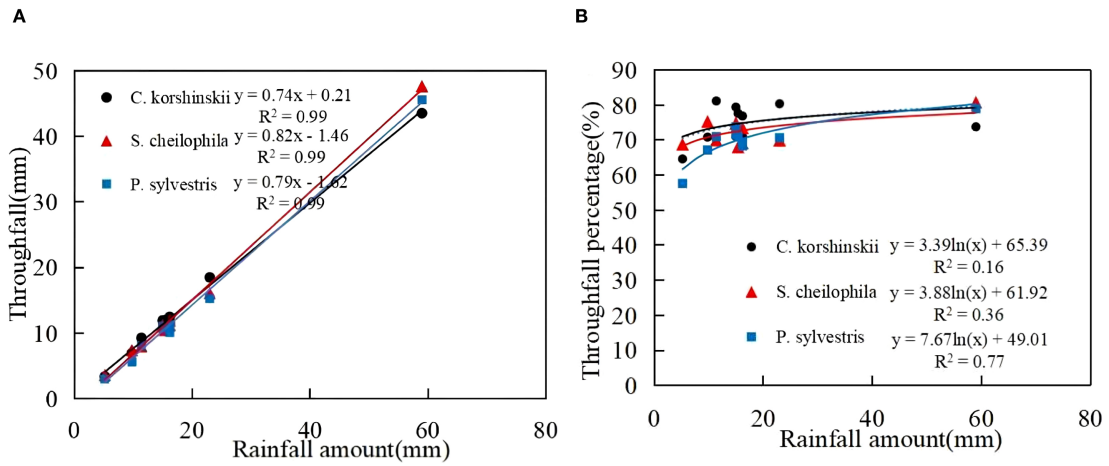

FIGURE 2
Characteristics of throughfall and its relationship with rainfall. **(A)** shows the throughfall characteristics of different sand-fixing vegetation types. **(B)** shows the throughfall percentage characteristics of different sand-fixing vegetation types.

root biomass in the soil layer of 0–40 cm was significantly higher than that below 40 cm. The root biomass of Sc in the soil layer of 0–80 cm was greatly higher than that of other vegetation types. The soil bulk density of arbor and shrub forests, and Gl showed significant changes in different soil layers (Figure 5). In the 0–40 cm soil layer, the soil bulk density of Ck was higher than that of Sc, Ps and Gl, and ranged from 1.41 to 1.81 g·cm^{-3}. In the 40–80 cm soil layer, the variation range of each vegetation type was 1.44 to 1.82 g·cm^{-3}. The soil bulk density of Ck was the highest, and that for each vegetation type was not significant in the range of 40–60 cm. In the range of 80–150 cm, a remarkable change took place in soil bulk density for each vegetation type. The soil bulk density of Ck was higher than that of Sc, Ps and Gl, and the variation range was 1.12 to 1.71 g·cm^{-3}.

3.3 Soil organic carbon and nitrogen distribution

3.3.1 Distribution of soil organic carbon and total nitrogen

Two-way analysis of variance (ANOVA) showed that SOC and N were strongly affected by soil depth and vegetation type (Table 3). In general, the trend in the variation of SOC and N concentrations decreased with the increase in soil depth (Figure 6). The trend in the variation of SOC and N concentrations for each vegetation type was Ps > Sc > Ck > Gl. The SOC concentrations of Sc, Ps and Ck were 1.37, 1.54 and 1.23 times higher than that of Gl, respectively. The N concentration was 1.34, 1.50 and 1.04 times higher, respectively ($p <$

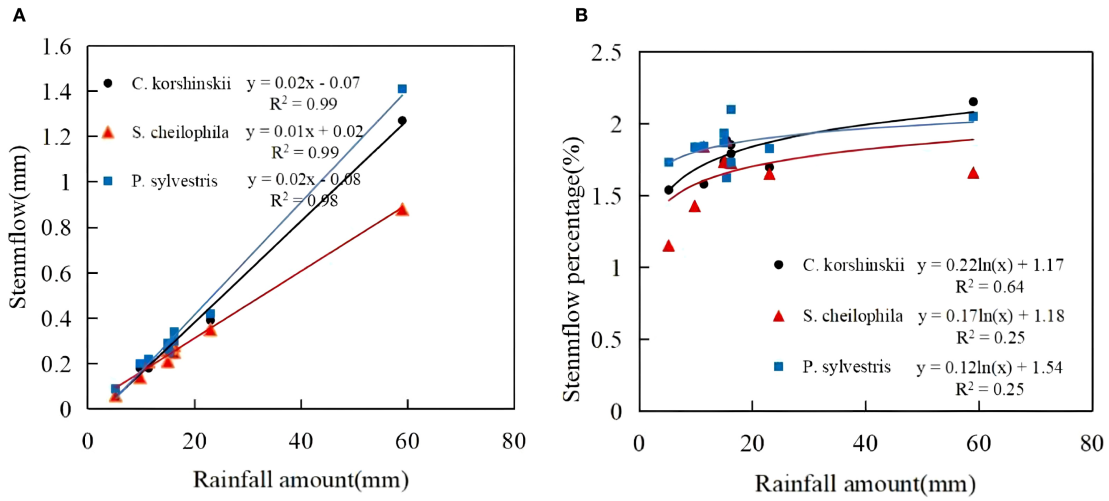

FIGURE 3
Characteristics of stemflow and its relationship with rainfall. **(A)** shows the stemflow characteristics of different sand-fixing vegetation types. **(B)** shows the stemflow percentage characteristics of different sand-fixing vegetation types.

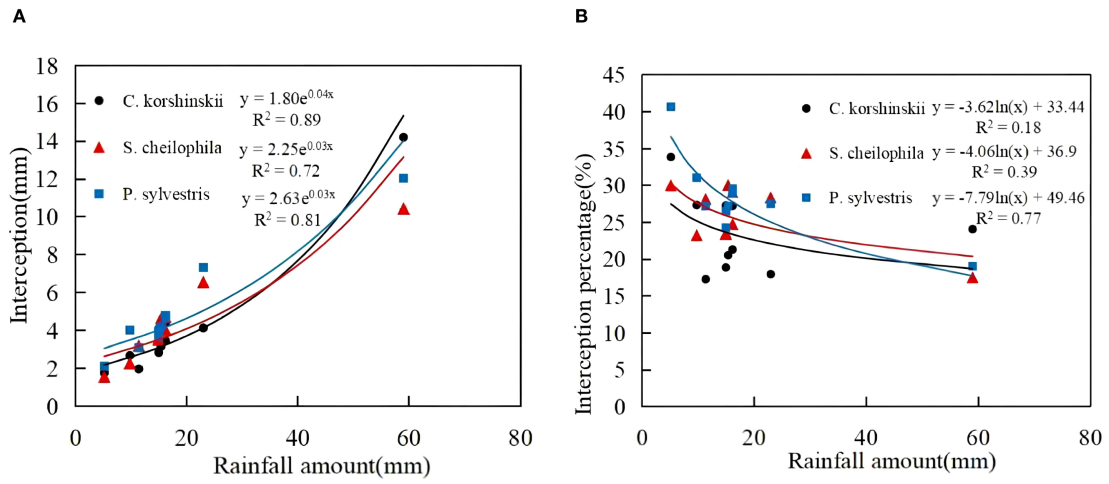

FIGURE 4
Characteristics of interception and its relationship with rainfall. **(A)** shows the canopy interception characteristics of different sand-fixing vegetation types. **(B)** shows the canopy interception percentage characteristics of different sand-fixing vegetation types.

0.05). In the soil layer of 0–80 cm, the SOC concentration of Ps was significantly higher than that of Gl ($p < 0.05$). In the soil layer of 80–150 cm, the SOC concentrations of Sc and Ps were substantially higher than that of Gl ($p < 0.05$). Across all soil layers, the N concentrations of both Sc and Ps were largely higher than that of Gl ($p < 0.05$). In the soil layer of 0–40 cm, the SOC concentration of Ps was far above that of Gl. In the soil layer of 40–80 cm, the range of difference in SOC and N for Gl was not obvious, but a large fluctuation took place for Sc, Ps and Ck. The concentrations of SOC and N in Gl were significantly lower than those in sand-fixing vegetation.

3.3.2 Distribution characteristics of soil organic carbon and nitrogen density in different vegetation types

As shown in Figure 7, the SOCD (Equations 1, 2) of different vegetation types in the 0–150 cm soil layer fluctuated in the range of 137.76 to 101.73 kg·m^{-2}. The SOCD and SND (Equations 3, 4) of Sc, Ps and Ck were significantly higher than that of Gl. The SOCD of Sc, Ps and Ck was 26.84%, 62.29% and 19.84% higher than that of Gl, respectively. The SND at a depth of 0–150 cm for different vegetation types fluctuated in the range of 13.57-10.30 kg·m^{-2}. The SND of Sc, Ps and Ck was 22.41%, 55.72% and 18.22% higher than

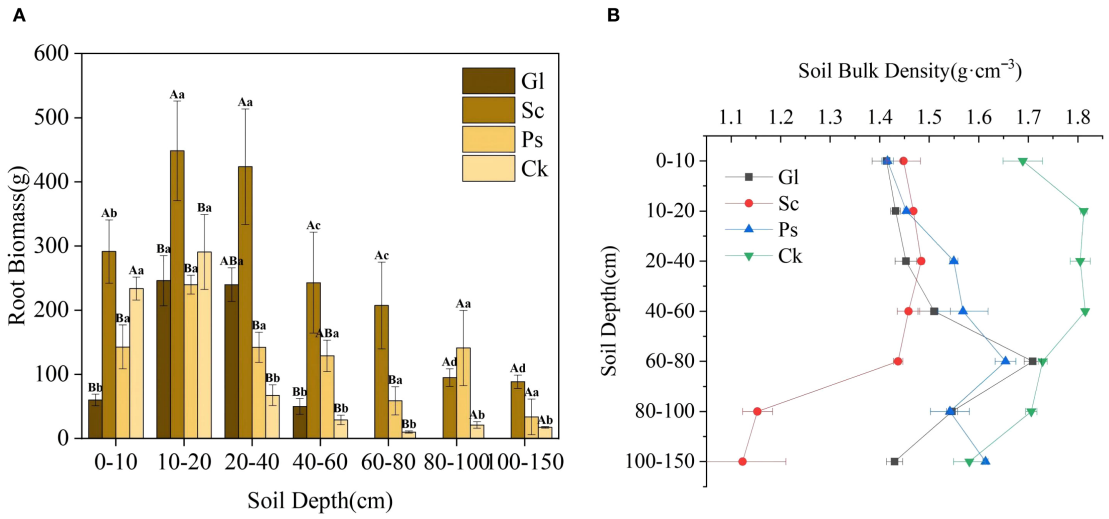

FIGURE 5
Root biomass and soil bulk density of each vegetation type. Gl, grassland; Sc, *S. cheilophila*; Ps, *P. sylvestris*; Ck, *C. korshinskii*. In Figure 5A, the capitalized letters stand for the significance of difference between different vegetation types on the same soil horizons, while small letters stand for the significance of difference between different soil horizons with the same plants. **(A)** shows the root biomass characteristics of different soil layers under different sand-fixing vegetation types. **(B)** shows the soil bulk density characteristics of different soil layers under different sand-fixing vegetation types.

TABLE 3 F values of two-way ANOVA.

Parameter	Soil depth	Vegetation	Soil depth×vegetation
SOC	22.64***	15.67***	7.25***
N	52.02***	15.72***	2.93***

***, significant effects at p<0.001.

that of Gl, respectively. Compared with Gl, the establishment of sand-fixing vegetation significantly increased SOC and N density, especially in Ps.

3.4 Relationship between vegetation, soil and rainfall interception

The redundancy analysis of vegetation and SOC and N revealed that the contribution rates of RDA1 and RDA2 were 90.58% and 9.37%, respectively (Figure 8). Evidently, height, RB, LT, LB, Ic and HB were correlated with SOC and N, while the correlation between SOCD and SND was relatively low. The RDA results showed that LB significantly influenced SOC, N, SOCD and SND ($p < 0.01$). Pearson's correlation analysis indicated significant positive influences of height, LT, LB, HB and RB on SOC and N ($p < 0.05$) (Figure 9). Both Q and BD had a significant negative influence on SOC and N ($p<0.05$).

A structural equation model was developed, which demonstrated a good fit to the data (good of fitness (GoF) = 0.71). Based on the structural equation model, the direct or indirect effects of different sand-fixing vegetation types on SOC and N and their concentration or concentration through vegetation, interception and the litter layer, and SOC and N distribution were determined (Figure 10).

Finally, the results showed that the composition and structure of the litter layer were closely related to vegetation characteristics. LB was in turn a significant factor affecting SOC, SOCD, N and SND of vegetation areas (Table 4).

4 Discussion

4.1 Response of rainfall redistribution to different vegetation types

Due to the influence of canopy characteristics, different vegetation types use rainfall after rainfall in different ways. When rainfall was redistributed by the vegetation canopy, the largest proportion was throughfall, followed by interception and stemflow in succession (Zheng et al., 2020; Guo et al., 2023). In this study area, the throughfall rate of the shrub forest was higher than that of the arbor forest, and the stemflow and interception rates of the shrub forest were lower than those of the arbor forest. More than 65% of the rainfall in the three stands fell in the form of throughfall. The total interception occupied 22.92%-26.77% of the total rainfall (Levia and Herwitz, 2005). The connection between throughfall and rainfall may be affected by vegetation types and canopy morphological characteristics. Vegetation characteristics such as stand density, canopy density, branch roughness and branch length also have a bearing on rainfall redistribution (Liu et al., 2017). The throughfall and throughfall rate of *Ps* were substantially lower than those of other stands. Because the branches grew in layers and canopy density was high, the canopy had strong rainfall interception ability, which resulted in less throughfall (Guo et al., 2023). In this study, it was shown that the stemflow and stemflow rate of the Ps forest were the highest at 1.85%. This conclusion was basically consistent with the findings of Fan et al. (2019) that the stemflow of the Ps forest accounted for 2.54% of rainfall. This study found that Ps had the highest interception capacity, which was ascribed to its layered branch structure and high density. With its larger leaf area, Sc ranked second. Ck had the lowest interception on account of its wide branch angles and smaller leaf area. In summary, rainfall redistribution characteristics vary considerably among different forest types and are primarily influenced by leaf area, branch angle, branch roughness, crown width and other vegetation characteristics.

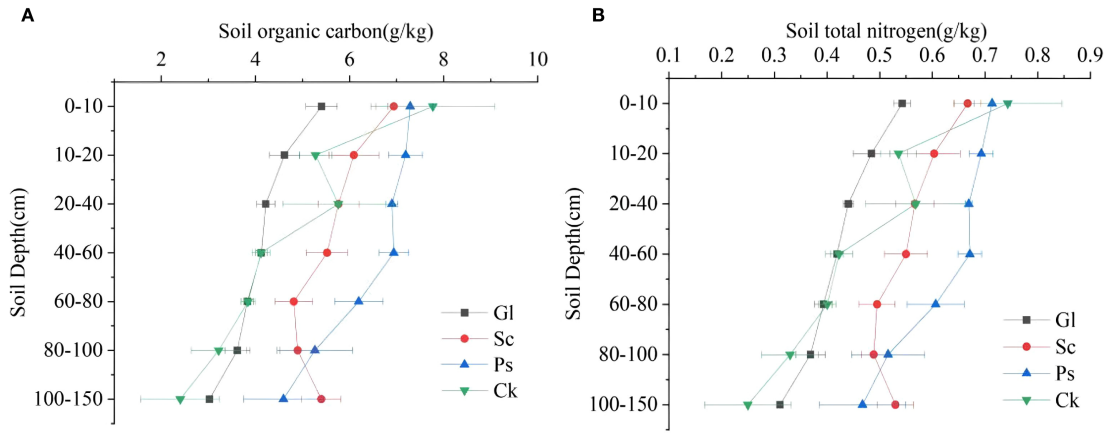

FIGURE 6
Distribution of soil organic carbon and total nitrogen in different vegetation types in different soil layers. **(A)** shows the soil organic carbon characteristics of different soil layers under different sand-fixing vegetation types. **(B)** shows the soil organic nitrogen characteristics of different soil layers under different sand-fixing vegetation types.

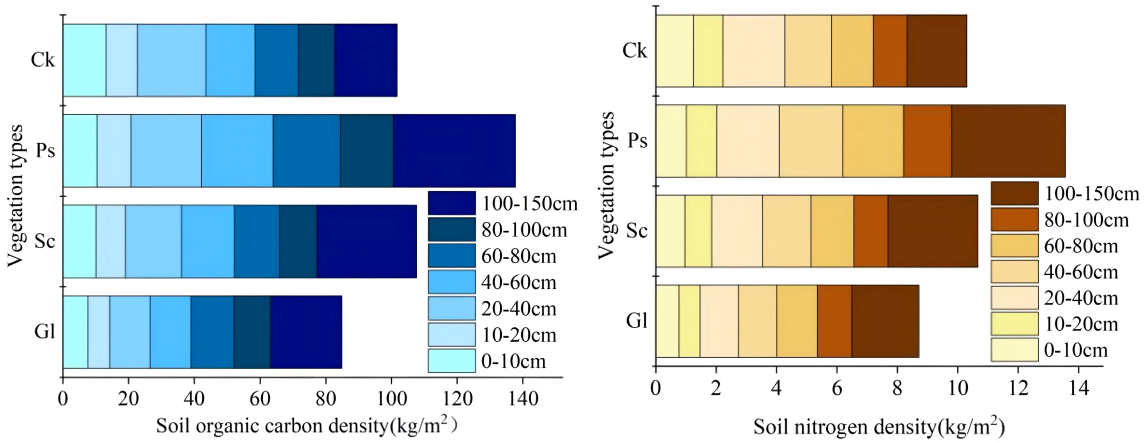

FIGURE 7
Carbon and nitrogen density distribution map of different vegetation types in different soil layers.

4.2 Response of soil characteristics to different vegetation types

4.2.1 Response of root biomass and soil bulk density to different vegetation types

Soil bulk density, a basic physical property of soil, is affected by soil parent material, climate and biological disturbances, which significantly affects soil nutrients (Yu et al., 2019). Soil bulk density varied with soil depth across different artificial sand-fixing vegetation plots. It was found that bulk density increased gradually with increasing depth in Gl and Ps, whereas it increased initially and then decreased with depth in Sc and Ck. This variation was likely put down to the considerable differences in vegetation root distribution among these sand-fixing vegetation types (Wang et al., 2008). In the current study, soil bulk density was lower in the surface layer (0–20 cm), which was likely due to the higher density of plant roots in this zone (Wu et al., 2024). The root characterized by high plasticity can perceive and adapt to complex soil environmental factors (Zhang et al., 2021a). For example, roots were primarily distributed within the 0–40 cm soil layer in the Gl plot (Xiao et al., 2023), which resulted in the lowest bulk density at these depths. In contrast, Sc, Ck and Ps plots exhibited a greater concentration of primary roots in the upper soil layer. Land use types can have a significant influence on soil bulk density. In particular, shrubs have been shown to effectively reduce bulk density (Han et al., 2010). This is a finding aligned with the results of this study. Therefore, shrubs can be effective in improving the soil texture of sandy land (Han et al., 2010). Among the three artificial sand-fixing vegetation types studied, Sc demonstrated the lowest soil bulk density. This is primarily attributable to its extensive root system and dense branching structure, which promote litter accumulation. The subsequent microbial decomposition and synthesis of this litter generate

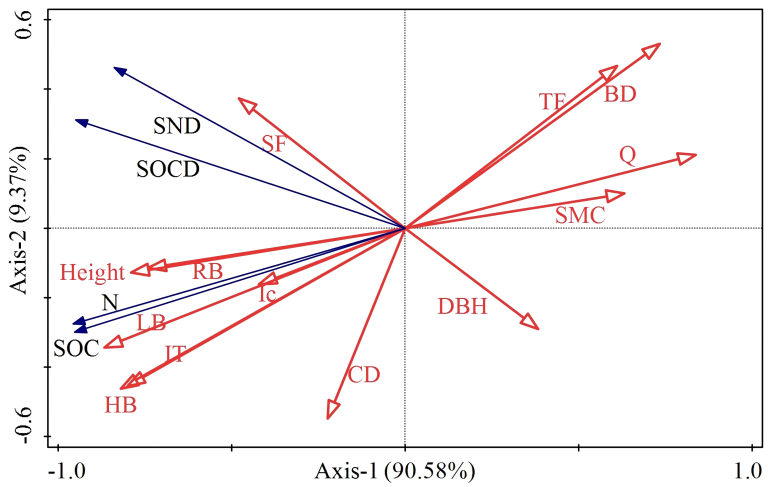

FIGURE 8
Redundancy analysis diagram. HB, Herbaceous biomass; LB, Litter biomass; LT, Litter thickness; CD, Canopy density; DBH, Diameter at breast height; Q, Vegetation Quantity; SMC, Soil mass water concentration; BD, Bulk Density; RB, Root biomass; Ic, Interception; SF, Stemflow; TF, Throughfall; SOC, Soil organic carbon; SOCD, Soil organic carbon density; SND, Soil nitrogen density; N, Soil total nitrogen.

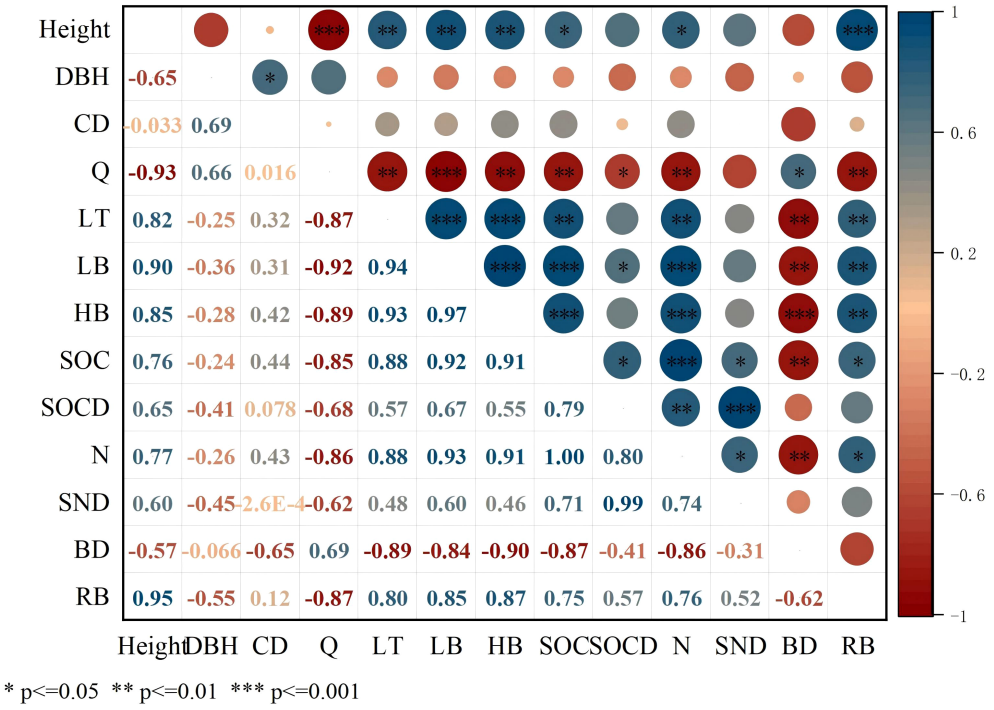

FIGURE 9
Pearson's rank correlation coefficients. HB, Herbaceous biomass; LB, Litter biomass; LT, Litter thickness; CD, Canopy density; DBH, Diameter at breast height; Q, Vegetation Quantity; BD, Bulk Density; RB, Root Biomass; SOC, Soil organic carbon; SOCD, Soil organic carbon density; SND, Soil nitrogen density; N, Soil total nitrogen.

substantial humus, and foster a loose, porous soil structure. This process reduces bulk density and consequently enhances the soil structure of sandy land.

4.2.2 Response of soil organic carbon and nitrogen distribution to different vegetation types

ANOVA revealed that soil depth, vegetation type and their interaction (depth × vegetation) exerted significant effects on SOC and N concentrations. These findings are in line with those reported by Sun (2018). Vegetation is a major factor influencing the distribution and fixation of SOC. Chen et al. (1998) suggested that different types of plants have differential efficiency in forming plant residues and litter. Moreover, the spatial pattern of vegetation and the soil microenvironment created also differ. This will also affect the concentration and distribution of SOC (Liu, 2017), which thus affects SOC accumulation and distribution (Batzal et al., 2015). In this study, it was discovered that the concentrations of SOC and N in different soil layers of different sand-fixing vegetation forests were in the following order: Ps > Sc > Ck > Gl. Trees have complex litter, which can sustainably input SOC to soil. In the meantime, Gl litter is easy to decompose, and the input of SOC is not as good as that of trees, followed by shrubs. Thus, the SOC concentration of Gl was significantly lower than that of the other three vegetation types (Samuel et al., 2024). Chen (2020) pointed out that the standing biomass of Ps plantations is directly proportional to their carbon fixation capacity in northern China. In the present study, it was found that these plantations have remarkably higher biomass than other vegetation types and, consequently, the highest levels of SOC. The N concentration of tree and shrub soil was substantially higher than that of Gl soil. This may be because the presence of sand-fixing plant litter can effectively retain N in soil (Wang, 2017). The biomass of Gl was lower than that of the other three kinds of sand-fixing vegetation. Sand-fixing vegetation is rich in species, particularly litter species, and high in species diversity. As a result, the microbial biomass in soil is high and microbial activity is strong. This is conducive to decomposing organic matter on the soil surface (Singh et al., 2022). The vertical distribution of SOC is influenced by multiple factors, including litter input, soil leaching, microbial characteristics and plant root distribution (Zhang et al., 2023). Zhang (2023) stated that litter on the forest floor is the primary source of SOC. The contributions of litter and root systems to SOC vary with soil depth because of differences in SOC formation mechanisms (like leaching and microbial activities) and the vertical distribution of litter and roots. The results are in consistency with those of the present study. SOC concentration typically decreases with increasing soil depth. However, the specific vertical distribution patterns vary among different vegetation types (Wang et al., 2014). The mass fraction of carbon and N in the soil is therefore increased. Chen (2020) studied the Mu Us Sandy Land and noted that the carbon fixation capacity of 0-0.4 m soil was higher for Ps than for Gl. This was consistent with the conclusions of this study. In this study, SOC and N concentrations in different artificial sand-fixing vegetation plots decreased with the increase in soil depth. This indicates that SOC was positively affected by the accumulation and decomposition of

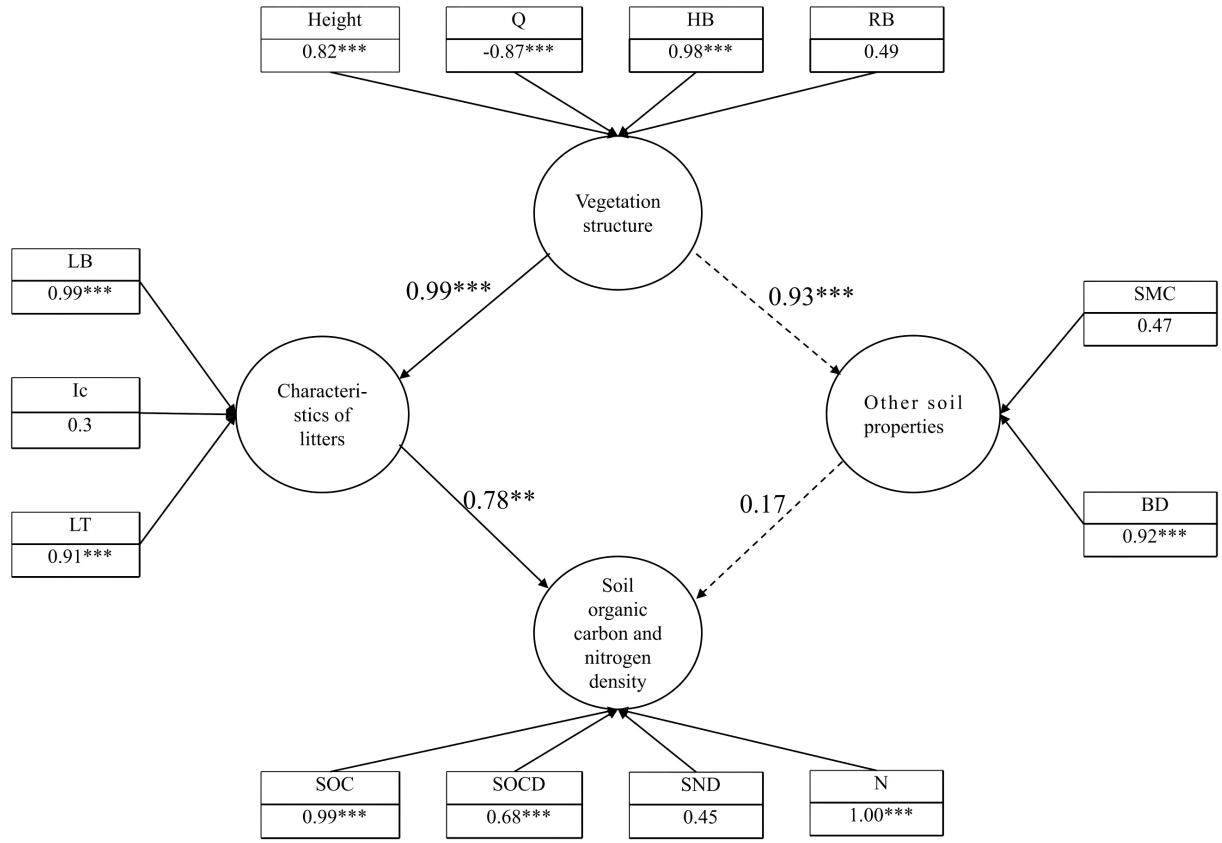

FIGURE 10
Structural equation model. **significant effects at p < 0.01 ,***significant effects at p < 0.001.

litter in the surface layer of soil. This resulted in the obvious surface accumulation of SOC in different artificial sand-fixing vegetation plots, which was aligned with previous research findings (Wang et al., 2002). SOC is a vital factor affecting N level, and N concentration mainly depends on the accumulation of SOC (Gao et al., 2017). Therefore, the variation in N concentration for sand-fixing vegetation is basically in line with that of SOC concentration. The same results were obtained in this study.

4.3 Effects of rainfall interception by vegetation on soil organic carbon and nitrogen

Rainfall influences the concentration of active SOC in soil (Rasmussen et al., 1998; Kelleway et al., 2016; Franzluebbers et al., 2001). Litter is also a key factor of soil carbon sequestration (Liu et al., 2023). In addition, rainfall can change its chemical properties to a large extent (Ma et al., 2023). The concentration of compounds in litter, like lignin, tends to vary with rainfall, which can affect the degradability of SOC in soil (Yu et al., 2024). A drastic increase in rainfall influences the decomposition rate of litter to a great degree. Hence, the rainfall redistribution attributed to vegetation restoration can affect the distribution of carbon and N in soil (Victor et al, 2020). Wang et al. (2025) argued out that the increase in rainfall input can alleviate aridity and boost the growth and carbon input of plants. The present study showed that vegetation structure and rainfall redistribution directly influence litter. Litter is decomposed into organic and inorganic compounds—sources of SOC and N of soil (Zhang et al., 2018). LB promoted the increase of biomass in an indirect way (de Queiroz et al., 2020). The decomposition of plants increased N concentration, which thereby increased SOC, SOCD and SND concentrations. Wang (2023) studied Mediterranean ecosystems and noticed that long-term increased precipitation induced SOC loss via changes in microbial community composition, functional traits, root production and soil moisture. This study revealed that Ps exhibited the highest SOC concentration in spite of intercepting the most rainfall (resulting in the least reaching soil). This contrast demonstrates that SOC concentration is not solely determined by rainfall volume. Other critical factors include functional traits, root production, litter decomposition, microbial community composition and vegetation-specific

TABLE 4 F values of two-way ANOVA.

Parameter	Soil depth	Vegetation	Soil depth×vegetation
SOCD	403.92***	248.71***	7.96***
SND	345.26***	17.92***	2.93***

***, significant effects at $p<0.001$.

redistribution patterns. Thus, future research should prioritize investigating these complex interactions. In this study, the impact of sand-fixing vegetation on soil nutrient concentration was explored by analyzing rainfall, canopy interception, and litter and soil layers. The findings offer valuable insights for vegetation restoration and plant species selection. The results also provide constructive advice on assessing the restoration of sand-fixing vegetation. Notably, the study highlights the significant role of litter in enhancing soil nutrients. Nevertheless, it does not include experiments on microbial activity or litter decomposition-key processes for the understanding of the mechanisms behind nutrient improvement. Thus, it is recommended that further research address these aspects.

5 Conclusions

This study elucidates how rainfall redistribution influences soil nutrient dynamics based on the distinct characteristics of different sand-fixing vegetation species. These findings provide critical guidance for selecting optimal vegetation species to restore ecosystems in sandy hills. Additionally, they clarify the essential coupling relationship between water redistribution and nutrient cycling during vegetation restoration.

1. Calculation shows that Ps, with the layered structure of its branches and large canopy cover, has the highest canopy interception. It is followed by Sc with broad leaves. Ck has the lowest canopy interception owing to its widely separated branches and small leaves.
2. The present study shows that the SOC and N concentrations in the understory soil of different sand-fixing vegetations drop with the increase of depth. In the depth between 0 and 150 cm, the concentrations of SOC and N in the soil of Gl, willow sand Ps and Ck decrease with the increase of depth. Various types of vegetation considered exhibit higher concentrations of SOC and N compared with Gl. Ps has the best performance in improving SOC and N in sand-covered hilly areas.
3. Redundancy and correlation analyses, and structural equation modeling indicate that the canopy structure of sand-fixing plants directly affects factors such as Ic, LB and LT. Furthermore, increases in LB and LT significantly enhance SOC, SOCD, N and SND.

Data availability statement

The raw data supporting the conclusions of this article will be made available by the authors, without undue reservation.

Author contributions

WX: Conceptualization, Methodology, Investigation, Writing – review & editing, Visualization, Writing – original draft, Formal analysis. ZY: Investigation, Writing – original draft. GJ: Methodology, Writing – original draft, Investigation, Visualization, Data curation, Formal analysis. ZL: Writing – review & editing. FQ: Writing – original draft, Investigation, Formal analysis, Visualization, Methodology.

Funding

The author(s) declare financial support was received for the research and/or publication of this article. This research was supported by the National Key Research and Development Program of China (No. 2023YFF1305104), National Natural Science Foundation project (42307463), Open Project of the Key Laboratory of Soil and Water Conservation on Loess Plateau, Inner Mongolia Autonomous Region Science and Technology Plan Project (2021GG0052), Inner Mongolia Autonomous Region "Science and Technology to Prosper Mongolia" Action Key Project (2022EEDSKJXM003), and the Ordos City Science and Technology Plan Project "Research on Intelligent Soil and Water Conservation Technology in the Typical Watershed of the Pisha Sandstone Area in the Upper Reaches of Kuye River". Inner Mongolia Autonomous Region 's " Talented Mongolia " Project Young Top Talents Special Training Program Project. Inner Mongolia Autonomous Region 's " Talented Mongolia " Project Young Top Talents Special Training Program Project.

Conflict of interest

The authors declare that the research was conducted in the absence of any commercial or financial relationships that could be construed as a potential conflict of interest.

Generative AI statement

The author(s) declare that no Generative AI was used in the creation of this manuscript.

Any alternative text (alt text) provided alongside figures in this article has been generated by Frontiers with the support of artificial intelligence and reasonable efforts have been made to ensure accuracy, including review by the authors wherever possible. If you identify any issues, please contact us.

Publisher's note

References

Batzal, N., Verrecchia, P. E., Veterdal, L., and Lane, S. N. (2015). Organic matter processing and soil evolution in a river system. *Catena* 126, 86–97. doi: 10.1016/j.catena.2014.10.013

Bryan, B. A., Gao, L., Ye, Y., Sun, X., Connor, J. D., Crossman, N. D., et al. (2018). China's response to a national land-system sustainability emergency. *Nature* 559, 193–204. doi: 10.1038/s41586-018-0280-2

Cao, L., Xu, M. P., Liu, Y. S., Yu, Z. C., Sun, L., Tian, X. F., et al. (2023). Response of soil nitrogen concentration or content and its vertical distribution to rainfall redistribution during Robinia pseudoacacia forest restoration on the Loess Plateau. *Ecol. Indicators.* 155, 111036. doi: 10.1016/j.ecolind.2023.111036

Castro, G., Romero, P., Gomez, J. A., and Fereres, E. (2006). Rainfall redistribution beneath an olive orchard. *Agric. Water Manage.* 86, 249–258. doi: 10.1016/j.agwat.2006.05.011

Chen, Z. Z., Wang, Y. F., and Tieszen, T. (1998). Distribution of soil organic carbon in the major grasslands of xilinguole, inner Mongolia, China. *Chin. J. Plant Ecology.* 22, 545–551.

Chen, W., Yang, J. J., Yuan, Y., Zhang, H., and Han, F. P. (2020). Effects of artificial sand-fixing vegetation on soil nutrientsin Mu Us Sandy Land. *Arid Zone Res.* 37, 1447–1456. doi: 10.13866/j.azr.2020.06.09

Deng, L., Wang, K. B., Zhu, G. Y., Liu, Y. L., Chen, L., and Shang, Z. P. (2018). Changes of soil carbon in five land use stages following 10 years of vegetation succession on the Loess Plateau, China. *Catena* 171, 185–192. doi: 10.1016/j.catena.2018.07.014

Fan, G. H., Han, C., Sun, Y. T., Ge, B., and Zhuang, J. Y. (2019). Rainfall redistribution in Pinus massoniana forest of Yangtze River Delta. *Southwest China J. Agric. Sci.* 32, 422–428. doi: 10.16213/j.cnki.scjas.2019.2.032

Fortier, R., and Wright, S. J. (2021). Nutrient limitation of plant reproduction in a tropical moist forest. *Ecology* 102 (10), e03469. doi: 10.1002/ecy.3469

Franzluebbers, A. J., Haney, R. L., Honeycutt, C. W., Arshad, M. A., Schomberg, H. H., and Hons, F. M. (2001). Climatic influences on active fractions of soil organic matter. *Soil Biology&Biochemistry* 33, 1103–1111. doi: 10.1016/s0038-0717(01)00016-5

Gao, Y., Peng, D., Zhao, Q. X., Liu, J. L., and Liu, J. B. (2017). Effects of vegetation rehabilitation on soil organic and inorganic carbon stocks in the Mu Us Desert, Northwest China. *Land Degradation Dev.* 29, 1031–1040. doi: 10.1002/ldr.2832

Gordon, D. A. R., Coenders-Gerrits, M., Sellers, B. A., Sadeghi, S. M. M., and Van Stan, J. T. (2020). Rainfall interception and redistribution by a common North American understory and pasture forb, Eupatorium capillifolium (Lam. dogfennel). *Hydrol. Earth Syst. Sci.* 24, 4587–4599. doi: 10.5194/hess-24-4587-2020

Guo, B., Yang, H., Li, J. C., Zhu, C. Y., Zhao, Y. H., Cao, J. S., et al. (2023). Rainfall partitioning measurements for Pinus tabulaeformis forest in Taihang Mountains. *Chin. J. Eco-Agriculture.* 31 (12), 2011-2021. doi: 10.12357/cjea.20230172

Han, F. P., Hu, W., Zheng, J., Du, F., and Zhang, X. C. (2010). Estimating soil organic carbon storage and distribution in a catchment of Loess Plateau, China. *Geoderma* 154, 261–266. doi: 10.1016/j.geoderma.2009.10.011

He, Z., Xiao, P., Hao, S., and Yang, C. (2017). Research progress on influence factors and models of rainfall redistribution under the action of vegetation. *IOP Conf. Ser. Earth Environ.* 69, 12034. doi: 10.1088/1755-1315/69/1/012034

Kelleway, J. J., Saintilan, N., Macreadie, P. I., Skilbeck, C. G., Zawadzki, A., and Ralph, P. J. (2016). Seventy years of continuous encroachment substantially increase blue carbon capacity as mangroves replace intertidal salt marshes. *Global Change Biol.* 22, 1097–1109. doi: 10.1111/gcb.13158

Lan, Z. L., Zhao, Y., Zhang, J. G., Jiao, R., Khan, M. N., Sial, T. A., et al. (2021). Long-term vegetation restoration increases deep soil carbon storage in the Northern Loess Plateau. *Sci. Rep.* 11, 13758. doi: 10.1038/s41598-021-93157-0

Levia, D. F., and Herwitz, S. R. (2005). Interspecific variation of bark water storage capacity of three deciduous tree species in relation to stemflow yield and solute flux to forest soils. *Catena* 64, 117–137. doi: 10.1016/j.catena.2005.08.001

Li, D. J., Wen, L., Xiao, K. C., Song, T. Q., and Wang, K. L. (2021). Responses of soil gross nitrogen transformations to three vegetation restoration strategies in a subtropical karst region. *Land Degrad. Dev.* 32, 2520–2527. doi: 10.1002/ldr.3907

Liu, X. D. (2017). *Characteristics of soil labile organic carbon fractions in different communities of desert steppe* (Ningxia University).

Liu, X., and Du, H. (2022). Effects of different cropland reclamation periods on soil particle size and nutrients from the perspective of wind erosion in the mu us sandy land. *Front. Environ. Sci.* 10. doi: 10.3389/fenvs.2022.861273

Liu, Z. B., Wang, Y. H., Deng, X. X., Liu, Y., Zhang, T., Zuo, H. J., et al. (2017). Spatial variations of throughfall in a Larix principis-ruprechtii plantation of Liupan Mountains, Ningxia, China. *Acta Ecologica Sinica.* 37, 3471–3481. doi: 10.5846/stxb201602210305

Liu, Y., Wang, K., Dong, L., Li, J., Wang, X., Shangguan, Z., et al. (2023). Dynamics of litter decomposition rate and soil organic carbon sequestration following vegetation succession on the Loess Plateau, China. *Catena* 229, 107225. doi: 10.1016/j.catena.2023.107225

Liu, Y., Zhu, G., Hai, X., Li, J., Shangguan, Z. P., Peng, C. H., et al. (2020). Long-term forest succession improves plant diversity and soil quality but not significantly increase soil microbial diversity: Evidence from the Loess Plateau. *Ecol. Eng.* 142, 105631. doi: 10.1016/j.ecoleng.2019.105631

Luo, Y. K., Fang, J. Y., and Hu, H. F. (2017). Biomass estimation models and allocation patterns of 14 shrub species in Mountain Luya, Shanxi, China. *Chin. J. Acta Phytoecological Sin.* 41, 115–125. doi: CNKI:SUN:ZWSB.0.2017-01-013

Ma, N., Ji, Y., Yue, K., Peng, Y., Li, C., Zhang, H., et al. (2023). Effect of the seasonal precipitation regime on shrub litter decomposition in a subtropical forest. *For. Ecol. Management.* 548, 121423. doi: 10.1016/j.foreco.2023.121423

Ma, C. K., Luo, Y., Shao, M. A., and Jia, X. X. (2022). Estimation and testing of linkages between forest structure and rainfall interception characteristics of a Robinia pseudoacacia plantation on China's Loess Plateau. *J. Forestry Res.* 33, 529–542. doi: 10.1007/s11676-021-01324-w

Mei, X. M., and Ma, L. (2022). Effect of afforestation on soil water dynamics and water uptake under different rainfall types on the Loess hillslope. *Catena* 213, 106216. doi: 10.1016/j.catena.2022.106216

Pei, Y., Huang, L., Shao, M., Wang, J., and Zhang, Y. (2023). Patterns and drivers of seasonal water sources of artificial sand-fixing plants in the northeastern Mu Us Sandy Land. *Pedosphere*. 34 (01), 63-77. doi: 10.1016/j.pedsph.2023.03.007

de Queiroz, M. G., Silva, T. G., Zolnier, S., Souza, C. A., Souza, L. S., Araújo, G. N., et al. (2020). Partitioning of rainfall in a seasonal dry tropical forest. *Ecohydrol. Hydrobiol.* 20, 230–242. doi: 10.1016/j.ecohyd.2020.02.001

Rasmussen, P. E., Albrecht, S. L., and Smiley, R. W. (1998). Soil C and N changes under tillage and cropping systems in semi-arid pacific northwest agrivulture. *Soil&Tillage Res.* 47, 197–205. doi: 10.1016/S0167-1987(98)00106-8

Samuel, J., Liang, G., Savannah, A., Karen, F., Jessica, M., and Bonnie, W. (2024). Land use drives the distribution of free, physically protected, and chemically protected soil organic carbon storage at a global scale. *Global Change Biol.* 30, e17507. doi: 10.1111/gcb.17507

Simon, J., Dannenmann, M., Pena, R., Gessler, A., and Rennenberg, H. (2017). Nitrogen nutrition of beech forests in a changing climate: importance of plant-soil-microbe water, carbon, and nitrogen interactions. *Plant Soil.* 418, 89–114. doi: 10.1007/s11104-017-3293-y

Singh, G., Mishra, D., Singh, K., Shukla, S., and Choudhary, G. R. (2022). Geographical settings and tree diversity influenced soil carbon storage in different forest types in Rajasthan, India. *Catena* 209, 105856. doi: 10.1016/j.catena.2021.105856

Spyroglou, G., Fotelli, M., Nanos, N., and Radoglou, K. (2021). Assessing black locust biomass accumulation in restoration plantations. *Forests* 12, 1477. doi: 10.3390/f12111477

Su, L., Yang, J., Zhao, X., and Miao, Y. (2022). Effects of fire on interception loss in a coniferous and broadleaved mixed forest. *J. Hydrology.* 613, 128425. doi: 10.1016/j.jhydrol.2022.128425

Sun, L. (2018). *The Dynamics of Soil Organic Carbon Fractions in Different Vegetation Types of Tianshan Forest* (China: Xinjiang University).

Tiessen, H., Cuevas, E., and Chacon, P. (1994). The role of soil organic matter in sustaining soil fertility. *Nature* 371, 783–785. doi: 10.1038/371783a0

Tu, L., Xiong, W., Wang, Y., Yu, P., Liu, Z., Han, X., et al. (2021). Integrated effects of rainfall regime and canopy structure on interception loss: A comparative modelling analysis for an artificial larch forest. *Ecohydrology* 14, e2283. doi: 10.1002/eco.2283

Victor, A., Valery, N., Boris, N., Aimé, V., and Louis, Z. (2020). Carbon storage in cashew plantations in Central Africa: case of Cameroon. *Carbon Management.* 12, 25–35. doi: 10.1080/17583004.2020.1858682

Wang, D. (2017). *Relationship Between Soil Carbon and Plant Communities In TheYellow River Delta* (China: LiaoCheng University).

Wang, S., Huang, M., Shao, X., Mickler, R. A., Li, K. R., and Ji, J. J. (2014). Vertical distribution of soil organic carbon in China. *Environ. Management.* 33, 200–209. doi: 10.1007/s00267-003-9130-5

Wang, Y. W., Liao, C. Y., Sun, C. Z., and Xu, H. (2008). Soil physical properties of sand-fixing forestsin Maowusu Sandland. *J. Northwest Forestry University.* 23, 36–39. doi: 10.19336/j.cnki.trtb.2009.04.013

Wang, G. L., Liu, G. B., and Xu, M. X. (2002). Effect of vegetation restoration on soil nutrient changes in Zhifanggou watershed of Loess Hilly Region. *Bull. Soil Water Conserv.* 22, 1–5. doi: 10.13961/j.cnki.stbctb.2002.01.001

Wang, F., Pan, X. B., Gerlein-Safdi, C., Cao, X. M., Wang, S., Gu, L. H., et al. (2020). Vegetation restoration in N orthern China: A contrasted picture. *Land Degrad Land Degrad. Dev.* 31, 669–676. doi: 10.1002/ldr.3314

Wang, M. M., Sun, X., Cao, B. C., Chiariello, N. R., Docherty, K. M., Field, C. B., et al. (2023). Long-term elevated precipitation induces grassland soil carbon loss via microbe-plant–soil interplay. *Global Change Biol.* 29, 5429–5444. doi: 10.1111/gcb.16811

Wang, M. M., Zhang, S., Guo, X. W., Wang, G. C., Xia, L. J., Xiao, L. J., et al. (2025). Whole-profile soil carbon responses to concurrent warming and precipitation changes across global biomes. *Global Change Biol.* 31, e70105. doi: 10.1111/gcb.70105

Wu, Z., Xu, C., Li, R., Xu, Y., Hua, J., Sun, S., et al. (2024). Full-field straw mulching and fertilizer application improved the soybean seed yield through optimization of the root and canopy structure: A study case in Huang-Huai-Hai region. *Eur. J. Agronomy.* 159, 127280. doi: 10.1016/j.eja.2024.127280

Xiao, L., Leng, M., Greenwood, P., Zhao, R., Xie, Z., You, Z., et al. (2023). Temporal and vertical dynamics of carbon accumulation potential under grazing-excluded grasslands in China: The role of soil bulk density. *J. Environ. Management.* 351, 119696. doi: 10.1016/j.jenvman.2023.119696

Yang, B., Zhang, W. J., Meng, X. J., Singh, A. K., Zakari, S., Song, L., et al. (2020). Effects of a funnel-shaped canopy on rainfall redistribution and plant water acquisition in a banana (Musa spp.) plantation. *Soil Tillage Res.* 203, 104686. doi: 10.1016/j.still.2020.104686

Yu, D. X., Jia, X. X., Huang, L. M., Shao, M. A., and Wang, J. (2019). Spatial variation of soil bulk density in different soil layers in the Loess area and simulation. *Acta Pedologica Sin.* 56, 55–64. doi: 10.11766/trxb201802040086

Yu, W., Wang, C., Cornelissen, J., Ye, X., Yang, X., Cui, Q., et al. (2024). Precipitation and diameter affect wood decomposition both directly and indirectly via deadwood traits and position. *Soil Biol. Biochem.* 199, 109604. doi: 10.1016/j.soilbio.2024.109604

Zhang, W., Gao, D. X., Chen, Z. X., Li, H., Deng, J., Qiao, W. J., et al. (2018). Substrate quality and soil environmental conditions predict litter decomposition and drive soil nutrient dynamics following afforestation on the Loess Plateau of China. *Geoderma* 325, 152–161. doi: 10.1016/j.geoderma.2018.03.027

Zhang, W., Liu, W. C., Xu, M. P., Deng, J., Han, X. H., Yang, G. H., et al. (2019a). Response of forest growth to C:N: P stoichiometry in plants and soils during Robinia pseudoacacia afforestation on the Loess Plateau, China. *Geoderma* 337, 280–289. doi: 10.1016/j.geoderma.2018.09.042

Zhang, F., Hou, Y., Ao, Y., Shen, J., and Jin, K. (2021a). Root-soil interaction under soil compaction. *J. Plant Nutr. Fertilizers.* 27, 531–543. doi: 10.11674/zwyf.20318

Zhang, Y., Tang, Z., You, Y., Guo, X., Wu, C., Liu, S., et al. (2023). Differential effects of forest-floor litter and roots on soil organic carbon formation in a temperate oak forest. *Soil Biol. Biochem.* 180, 109017. doi: 10.1016/j.soilbio.2023.109017

Zhang, J., Wang, T., Wang, J., Shen, H., Li, Y., Wu, W. J., et al. (2025). Nutrient availability drives the ecological linkage between microbial functional diversity and soil organic matter molecular complexity during forest restoration. *J. Environ. Management.* 390, 126312. doi: 10.1016/j.jenvman.2025.126312

Zhang, W., Xu, Y. D., Gao, D. X., Wang, X., Liu, W. C., Deng, J., et al. (2019b). Ecoenzymatic stoichiometry and nutrient dynamics along a revegetation chronosequence in the soils of abandoned land and Robinia pseudoacacia plantation on the Loess Plateau, China. *Soil Biol. Biochem.* 134, 1–14. doi: 10.1016/j.soilbio.2019.03.017

Zhang, X., Zhao, J., Lei, L., and Wang, D. (2021b). Characteristics of rainfall redistribution of six shrubs in Eastern Qilian Mountain. *Chin. J. Grassl* 43 (01), 83–89. doi: 10.16742/j.zgcdxb.20190327

Zheng, C. L., and Jia, L. (2020). Global canopy rainfall interception loss derived from satellite earth observations. *Ecohydrology* 13, e2186. doi: 10.1002/eco.2186

Zhu, X. R., Liu, H. Y., Li, Y. Y., and Liang, B. Y. (2021). Quantifying the role of soil in local precipitation redistribution to vegetation growth. *Ecol. Indicators.* 124, 107355. doi: 10.1016/j.ecolind.2021.107355

Frontiers in
Plant Science

Cultivates the science of plant biology and its applications

The most cited plant science journal, which advances our understanding of plant biology for sustainable food security, functional ecosystems and human health.

Discover the latest Research Topics

See more →

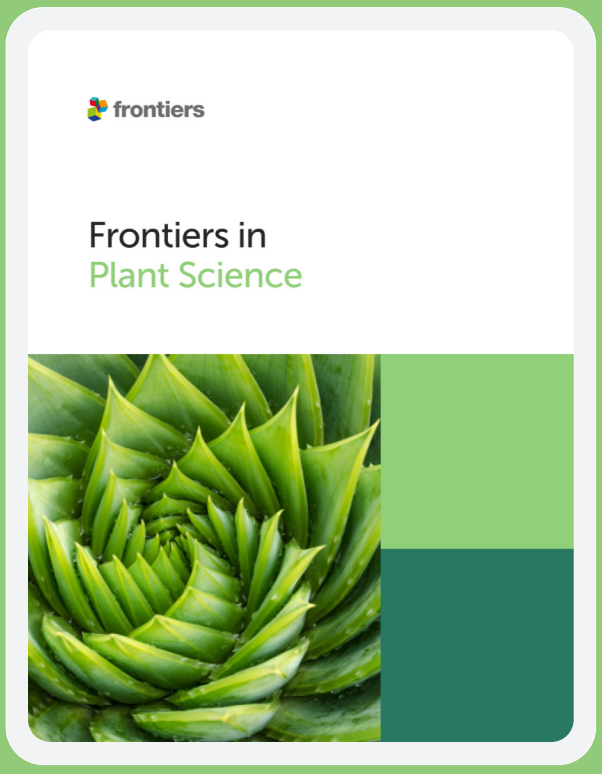

Frontiers

Avenue du Tribunal-Fédéral 34
1005 Lausanne, Switzerland
frontiersin.org

Contact us

+41 (0)21 510 17 00
frontiersin.org/about/contact